



Institute for Glycomics

Queensland, Australia

Glyconanoparticles for targeting macrophages to deliver therapeutic agents

Tamim Mosaib

B.Sc. (Hons), M.Sc., MPH

Institute for Glycomics

Griffith University

A thesis submitted in fulfilment of the requirements of the degree of

Doctor of Philosophy

November 2018



Dedication

This thesis is dedicated to my lovely parents and my beautiful wife. I do highly appreciate all of yours' great care, love and endless support.

Statement of Originality

This work has not previously been submitted for a degree or diploma in any university. To the best of my knowledge and belief, the thesis contains no material previously published or written by another person except where due reference is made in the thesis itself.

(Signed) _____

Tamim Mosaiab

November 2018

Abstract

Bacterial infection is still one of the leading causes of hospitalization and mortality, although antibiotics are used comprehensively to treat the infectious diseases. The clinical failure of antibiotic therapy is associated with low bioavailability, poor penetration capacity to bacterial infection sites, the side effect of antibiotics, and the antibiotic resistance properties of bacteria. Moreover, many deadly infectious diseases are produced by microorganisms that are able to survive in macrophages. The intracellular location of these pathogens protects them from the host defence systems and from some antibiotics with poor penetration into macrophages. Therefore, the use of non-viral nanoparticulate systems for the delivery of therapeutic agents is receiving considerable attention to improve the penetration of drugs into macrophages as well as the use of specific target molecules onto the nanocarrier systems that deliver these drugs directly to the target cell. These systems can be designed to meet specific physicochemical requirements, and they exhibit low toxic and immunogenic effects.

This thesis attempts to rationally design and synthesise antibiotic-encapsulated glyconanoparticles (GNPs) and glyco-coated liposomes for active targeting of macrophages to treat a range of infectious diseases. Macrophages are a promising target for carbohydrate-based therapeutics as they express carbohydrate binding receptors which internalize bound material *via* receptor-mediated endocytosis. Therefore, we targeted the lectin receptors presented on the macrophage cell membrane by coupling many monomeric sugar moieties onto appropriate scaffolds such as polymers or liposomal systems to create multivalent targeting carriers and improve the activity, stability and lower cytotoxicity. The natural cationic polysaccharide chitosan was selected to conjugate specific carbohydrate sequences on the polymer backbone to target macrophages. Moreover, a variety of liposomal formulations with multivalent targeting ligands were considered as potential therapeutic carriers to macrophages.

The hydrophobic antibacterial agents *N*-alkylsulphonylacetamide and hydrophilic aminoglycoside were loaded into the artificial nanocarrier system to explore their ability to inhibit bacterial growth. The antibiotic carrier was also modified *via* different monosaccharides including mannose and galactose to promote the interaction of the

nanovehicle with macrophages and enhance drug concentration into the infected immune cells.

Glycolipids from *Mycobacterium tuberculosis* have a profound impact on the innate immune response of the host. Macrophage inducible C-type Lectin (Mincle) is a pattern recognition receptor that has been shown to bind trehalose dimycolate (TDM) from the mycobacteria and instigate intracellular signaling in the immune cell. There are structural similarities between TDM and phosphatidyl inositol mannoside (PIM) structures and these latter structures may also bind Mincle. To test this, we have successfully synthesized and characterized a series of novel mannose derivatives modified with fatty esters at the 6-position to explore their ability to interact with macrophages. The results showed that the amount of two major cytokines such as tumor necrosis factor (TNF)- α and interleukin (IL)-6 released from LPS stimulated U937 cells decreased significantly when compared to control upon treatment with the prepared glycolipids indicating the reduction of cytokines production by macrophages. (Chapter 2)

Antibiotic loaded [amikacin and *n*-decanesulphonylacetamide (DSA)] cationic dimethyldioctadecylammonium bromide (DDAB) with fatty acyl and fatty amido α -D-benzylmannoside liposomes were prepared by the thin film hydration method and characterized *via* DLS (Chapter 3). The antibiotic loading efficiency and the release profile in the prepared glyco-coated liposomes were also determined. The efficiencies of the drug loaded liposomes were tested against *S. aureus* infected macrophages and results showed significant intracellular bacterial growth inhibition (Chapter 3).

In Chapter 4, mannose precursors have been synthesized with carboxyl group at the anomeric position and fatty amides at the 6-position. The lactose and mannose derivatives were prepared after conjugating these sugar molecules onto the chitosan backbone to produce mannose and lactose grafted chitosan (Chitmannolac). The engineered chitosan derivatives were utilized to make GNPs *via* nanoprecipitation method and characterized using NMR spectroscopy, FT-IR spectroscopy, UV-vis spectroscopy, fluorescence spectroscopy and DLS. The intracellular bacterial killing efficiency was determined using the artificial GNPs and result showed promising antimicrobial inhibition upon incubating with these GNPs.

Overall this PhD thesis implements modern synthetic strategies to discover novel drug carriers for biomedical application. This thesis work develops a macrophage targeted drug delivery system from the ground up through: (i) designing novel glycolipids that can mimic various naturally occurring glycolipids; (ii) providing step by step synthesis of glycolipids and their characterization; (iii) preparation of liposomes and micelles using the similar glycolipids moieties and compare their target ability to mammalian cells; and (iv) demonstrating the intracellular bacterial inhibition using liposomes and GNPs that encapsulate both hydrophobic and hydrophilic drugs in the same carrier.

Publications and Conference Presentations

Mosaiab, T, Farr, D. C.; Wei, M. Q.; Kiefel, M. J.; Houston, T. A., *Glyco-coated nanoliposomes for efficient targeting of macrophages and delivering antimicrobial agents.* Manuscript in preparation

Mosaiab, T, Farr, D. C.; Kiefel, M. J.; Houston, T. A., *Carbohydrate-based nanocarriers to target macrophages and deliver antimicrobial agents.* Manuscript in preparation.

Mosaiab, T.; Boiteux, S.; Zulfiker, A. H. M.; Wei, M. Q.; Kiefel, M. J.; Houston, T. A., A Simple Glycolipid Mimic of the Phosphatidylinositol Mannoside Core from *Mycobacterium tuberculosis* Inhibits Macrophage Cytokine Production. *Chembiochem* **2018**, *19* (14), 1476-1481.

Sun, H.-K.; Pang, A.; Farr, D. C.; **Mosaiab, T.;** Britton, W. J.; Anoopkumar-Dukie, S.; Grice, I. D.; Kiefel, M. J.; West, N. P.; Grant, G. D.; Houston, T. A., Thioamide Derivative of the Potent Antitubercular 2-(Decylsulfonyl)acetamide is Less Active Against *Mycobacterium tuberculosis*, but a More Potent Antistaphylococcal Agent. *Aust J Chem* **2018**, *71* (9), 716-719.

Conference Presentations

Mosaiab, T, Wei, M. Q.; Kiefel, M. J.; Houston, T. A., *Antibiotics Loaded Liposomes and Micelles for Intra-Cellular Infections.* Glycomics Week Student Forum, 9-12 October 2017, Institute for Glycomics, Gold Coast campus, Griffith University, Queensland, Australia. **(Oral Presentation)**

Mosaiab, T, Wei, M. Q.; Kiefel, M. J.; Houston, T. A., *Glyco-coated Micelles and Liposomes to Treat Intracellular Infections.* RACI Centenary Congress, 23-28 July 2017, Melbourne Convention and Exhibition Centre, Melbourne, Victoria, Australia. **(Oral Presentation)**

Mosaiab, T, Wei, M. Q.; Kiefel, M. J.; Houston, T. A., *Glycolipids coated liposomal adjuvant system for targeting macrophages to deliver antibiotics.* Queensland Annual Chemistry Symposium (QACS 2016), 25th November 2016,

The Physiology Building, The University of Queensland, St Lucia Campus, Brisbane, Queensland, Australia. (**Oral Presentation**)

Mosaiab, T, Wei, M. Q.; Kiefel, M. J.; Houston, T. A., *Synthesis and evaluation of glycolipids for active targeting of macrophages*. Glycomics Week Student Forum, 10-13 October 2016, Institute for Glycomics, Gold Coast campus, Griffith University, Queensland, Australia. (**Poster Presentation**)

Mosaiab, T, Kiefel, M. J.; Houston, T. A., *Antibiotic loaded chitosan-derivatives for targeting macrophages to cure tuberculosis*. Drug Delivery Australia (DDA 2015), 19-20 November 2015, St Leo's College, The University of Queensland. Brisbane, Queensland, Australia. (**Poster Presentation**)

Mosaiab, T, Wei, M. Q.; Kiefel, M. J.; Houston, T. A., *Chitosan derivatives for targeting Macrophages to deliver antibiotics*. Glycomics Week Student Forum, 12-15 October 2015, Institute for Glycomics, Gold Coast campus, Griffith University, Queensland, Australia. (**Oral Presentation**)

Mosaiab, T, Kiefel, M. J.; Houston, T. A., *Polysaccharide derivatives for targeting macrophages*. Medicinal Chemistry and Chemical Biology Symposium (MCCB 2015), 25th September 2015, The Ship Inn Function Room, Southbank Brisbane, Queensland, Australia. (**Oral Presentation**)

Mosaiab, T, Kiefel, M. J.; Houston, T. A., *Synthesis and Characterization of Mannose and Lactose-Conjugated Polysaccharides to Target Macrophages*. 35th Australian Polymer Symposium (35APS), 12-15 July 2015, QT Hotel, Gold Coast, Queensland, Australia. (**Poster Presentation**)

Mosaiab, T, Kiefel, M. J.; Houston, T. A., *Glyconanoparticles: A Versatile Nanocarrier of Therapeutics to Macrophages*. Glycomics Week Student Forum, 7-10 October 2014, Institute for Glycomics, Gold Coast campus, Griffith University, Queensland, Australia. (**Poster Presentation**)

Acknowledgements

I have made great efforts in my PhD project, which would not have been possible without the kind support and help of many individuals and organizations. I would like to extend my sincere thanks to all of them.

I am highly indebted to my principal supervisor, Dr. Todd A. Houston for his guidance, advice, encouragement and patience over the last four years of my PhD journey. Thank you so much for giving me the opportunity to work in freedom, to look at research in different ways and overall to grow as an independent researcher. I feel very privilege to have had such an excellent supervisor. The accomplishment of this thesis would not have happened without his enlightening ideas and professional knowledge.

My sincere gratitude to my associate supervisor, Dr. Milton J. Kiefel for his indispensable advice, support, constant supervision and direction regarding the project. I would like to extend my sincere to his immense support for proof reading of documents including manuscript and thesis dissertation, which has helped me to improve my writing ability. I also thank him for teaching me a range of laboratory experiments including chemical synthesis, purification, and characterization. All the scientific suggestions from him were invaluable on some extent of my PhD project.

I would like to extend my sincere gratitude to Professor Ming Q. Wei, for his kind approval to work in his laboratory for last four years in the Menzies Health Institute Queensland (MIHQ), Griffith University to perform *in vitro* experiment for my PhD project and made important contributions in the collaborated publication during my PhD work. My special thanks to Dr. Bassam Elgamoudi helping me to plan and perform antibacterial activity.

I am very thankful to Dr. Robin Thomson for her great support to organize laboratory experiments and reagents. Her suggestions, motivations and inspirations were incredible for me to keep up with my work. I would like to thank Dr. Darren Grice for his invaluable advice and offering me organic chemistry lab demonstration for his course which helps me a lot in terms of learning and teaching. To Dr. Catherine Tindal, thank you for your help and advice for the NMR and mass spectroscopy. I highly thank you

for the high temperature NMR for Chitosan and teach me to learn NMR and mass spectroscopy operating and maintenance.

My appreciation also goes to my laboratory colleagues especially Brigid Pappin, Dylan Farr, Matt Hugo, Sandra Boiteux, and James Carter those gave me much support during my PhD journey. It was a great pleasure to work with them. I would like to extend my sincerest thanks to all the colleagues and members of the Institute for Glycomics including Faith Rose, Dr. Anil Kumar Glore, Dr. Taha Taha.

I would like to recognize Griffith University, Griffith Graduate Research School, and Institute for Glycomics for awarding me the scholarship as tuition and living allowance, without which this work would not have happened.

To all my friends, I would like to say thank you, particularly those are working with me in the Institute for Glycomics including Aloysious Ssemaganda, Sanjesh Singh, Amar-Al-Kass, Dr. Rahul Mishra, Dr. Mohammad Bohari and many more. I specially thanks to my childhood friend Tanim Ahamed, Ajgar Ali, Shorif Sumon those gave me huge motivation and inspiration during my PhD work.

I would like to express my gratitude towards my parents specially my mother. Without her motivation, it was impossible to enrol my PhD and reach this destination. Dad, you were amazing at all times to inspire me over phone. I would also extend my greatest thanks to my family members, my brother and sister, mother-in-law, and their family for the endless support, inspiration and care throughout my life.

Finally, I would like to extend my greatest thanks to my wife, for her love, caring, understanding, patience and friendship. Without her support, this work would not have been possible. I also thank her to gift me three lovely kids, two boys, Tyaaf & Tyaad, and a girl, Shuhad, during my PhD candidature.

Also, I would like to thank to all the people whom I unintentionally forgot mention here.

Table of contents

Statement of Originality	II
Abstract	III
Publications and Conference Presentation.....	VI
Acknowledgment	VIII
Table of Contents	X
List of Figures	XIV
List of Tables	XVII
Abbreviations	XVIII
Chapter 1.....	1
1. Introduction	2
1.1 General background.....	2
1.2 Nanocarriers used in drug delivery systems.....	3
1.2.1 Advantages of nanoparticle-based DDS.....	4
1.2.2 Preparation and application of nanoparticles in DDS.....	5
1.3 Polysaccharides-based nanoparticles and their advantages	6
1.4 Preparation of glyconanoparticles (GNPs).....	10
1.4.1 Covalently crosslinked glyconanoparticles.....	10
1.4.2 Ionically crosslinked glyconanoparticles.....	13
1.4.3 GNPs by polyelectrolyte complexation.....	15
1.4.4 Self-assembled glyconanoparticles.....	18
1.4.5 Limitations of prepared glyconanoparticles.....	19
1.5 Macrophage targeting.....	20
1.5.1 Phagocytosis and nanoparticles uptake by macrophages	21
1.5.2 Physicochemical properties of nanoparticles to penetrate macrophages.....	24
1.5.2.1 Nanoparticle Size.....	25
1.5.2.2 Nanoparticle Shape.....	26
1.5.2.3 Nanoparticle Surface Charge.....	28
1.5.2.4 Surface composition and hydrophobicity.....	30
1.5.2.5 Targeting ligand.....	31
1.5.2.6 Mechanical properties and elasticity.....	34

1.5.3	Nanoparticles-induced cytotoxicity of macrophages.....	34
1.5.3.1	Biodegradability.....	34
1.5.3.2	Biocompatibility.....	35
1.6	Glyconanoparticles for macrophage-mediated therapies.....	35
1.6.1	Bacterial infectious diseases.....	35
1.6.1.1	Infection due to mycobacteria.....	36
1.6.1.2	Salmonellosis.....	38
1.6.1.3	<i>Staphylococcus aureus</i>	39
1.6.2	Protozoan infectious diseases.....	40
1.6.3	Viral infectious diseases.....	41
1.6.4	Fungal infections.....	42
1.1	PhD program synopsis.....	45
1.7.1	Significance of the project.....	45
1.7.2	Aims and objectives of the program.....	46
	Chapter 2.....	49
	Statement of contribution to co-authored published paper.....	50
	A Simple Glycolipid Mimic of the Phosphatidylinositol Mannoside Core from Mycobacterium tuberculosis Inhibits Macrophage Cytokine Production.....	56
	Chapter 3.....	70
	Glyco-coated nanoliposomes for intracellular delivery of antimicrobial agents.....	71
	3.1. Introduction.....	71
	3.2. Experimental Section.....	76
3.2.1.	Materials and chemical reagents.....	76
3.2.2.	Preparation of cationic liposomes.....	76
3.2.3.	Size, polydispersity and Zeta-potential of cationic liposomes.....	77
3.2.4.	The colloidal stability of prepared liposomes.....	77
3.2.5.	Drug loading in liposomes.....	77
3.2.6.	Encapsulation efficiency.....	78
3.2.7.	<i>In vitro</i> drug release studies.....	79
3.2.8.	Bacteria Strains and cell lines.....	79

3.2.9. ELISA (Detection of TNF-a and IL-6).....	80
3.2.10. Macrophage infection and intracellular bacterial inhibition assays.....	81
3.2.11. Statistics.....	81
3.3. Results and Discussions.....	82
3.4. Conclusion.....	94
Chapter 4.....	96
4.1.Introduction.....	97
4.2.Experimental Sections.....	101
4.2.1. General.....	101
4.2.2. Materials.....	102
4.2.3. Synthesis of Allyl 2,3,4,6-tetra-acetyl- α -D-mannoside.....	102
4.2.4. Synthesis of 3-Thia-heptanoic acid-2,3,4,6-tetra- <i>O</i> -acetyl- α -D-mannoside....	103
4.2.5. Synthesis of 3-Thia-heptanoic acid- α -D-mannoside	104
4.2.6. Synthesis of Allyl 6-azido α -D-mannoside	104
4.2.7. Synthesis of Allyl 6-amino α -D-mannoside	105
4.2.8. Synthesis of allyl 6-fatty amido- α -D-mannoside: General Procedures.....	105
4.2.9. Synthesis of 3-thio-heptanoic acid-2,3,4-tri- <i>O</i> -acetyl -6-fatty amido- α -D- mannoside: General Procedures.....	107
4.2.10. Synthesis of 3-thio-heptanoic acid-6-fatty amido- α -D-mannoside: General Procedures	110
4.2.11. Digestion and purification of commercially available chitosan	112
4.2.12. Synthesis of lactose grafted chitosan (Chitlac): General procedure....	112
4.2.13. Synthesis of lactose and mannose conjugated chitosan (Chitmannolac): General procedure.....	113
4.2.14. Synthesis of palmitoyl amido mannoside-g- Chitmannolac (PAM-g- Chitmannolac)	114
4.2.15. Synthesis of stearoyl amido mannoside-g- Chitmannolac (SAM-g- Chitmannolac).....	114
4.2.16. Synthesis of fluorescein and glycolipid grafted chitosan.....	115
4.2.17. Preparation of DSA encapsulated chitosan based glyconanoparticles..	115
4.2.18. Immobilization of amikacin into the DSA/PAM-GNP _{5k} and DSA/SAM- GNP _{5k}	116

4.2.19.	<i>In vitro</i> amikacin release studies.....	116
4.2.20.	Characterization of the prepared GNPs.....	117
4.2.21.	Macrophage cell culture.....	118
4.2.22.	Determination of cellular toxicity using MTT Assays.....	118
4.2.23.	Enzyme-linked immunosorbent assay (ELISA): Determination of the TNF- α and IL-6 Release.....	118
4.2.24.	Confocal images.....	119
4.2.25.	Macrophage infection and intracellular bacterial inhibition assays.....	120
4.2.26.	Statistical Analysis.....	120
4.3.	Results and Discussions.....	121
4.4.	Conclusions	139
Chapter 5.....		140
5.1.	Conclusions and future directions.....	140
References		145

List of Figures

Figure 1.1: The important features of nanoparticles for intracellular drug delivery applications.....	4
Figure 1.2: Schematic representation of preparation method of chitosan based nanocarrier and intracellular drug release triggered by pH and UV light.	11
Figure 1.3: A schematic representation of prepared amoxicillin-loaded genipin-crosslinked fucose-chitosan/heparin nanoparticles.....	12
Figure 1.4: Schematic representation of the synthesis of CS-TPP/IL-12 nanoparticle system.....	14
Figure 1.5: Schematic illustration of the formation and the phosphatase-induced degradation of the polymeric supra-amphiphiles and the spherical aggregates.....	15
Figure 1.6: Diagram illustrating the preparation process for LbL-coated SLNs containing DOX/DS complexes.....	16
Figure 1.7: Schematic diagram of the formation of siRNA loaded PEG-CMCS/CaP hybrid anionic nanoparticles (NPPEG-CMCS/CaP/siRNA).....	18
Figure 1.8: (a) Schematic representation of phagocytosis of microorganisms within the macrophages and (b) upon phagocytosis, bacteria reside in phagosome and not interact with lysosomes.....	22
Figure 1.9: Factors affecting the intracellular activity of antibiotics and mechanism of glyconanoparticles as a carrier of antibiotics in macrophages.....	23
Figure 1.10: The local geometry of nanoparticles at the contact point between cell and nanoparticles.....	27
Figure 1.11: Effect of surface properties on nanoparticle internalization.....	29
Figure 1.12: (A) Schematic illustration of vancomycin-loaded mannosylated nanogels (MNG-V) and the bacteria-responsive drug release; (B) Schematic illustration of targeted uptake of MNG-V, transport, degradation, drug release and bacteria inhibition.....	32

Figure 1.13: The binding and subsequent endocytosis of fluorescent mannose glycopolymers by the macrophage mannose receptor.....	33
Figure 1.14: Schematic illustration of Amp B conjugated arabinogalactan.....	44
Figure 3.1: Chemical structure of amikacin (a) and DSA (b).....	73
Figure 3.2: Schematic illustration of amikacin and DSA encapsulated glyco-coated DDAB liposomes.....	74
Figure 3.3: Average vesicle size of glyco-coated DDAB liposomes.....	84
Figure 3.4: Average vesicle size of glyco-coated DDAB liposomes.....	85
Figure 3.5: Secretion of IL-6 and TNF- α upon treatment with glyco-coated DDAB liposomes in RAW 264.7 cells.....	86
Figure 3.6: The <i>in vitro</i> release of amikacin from glyco-coated DDAB liposomes at 37°C in PBS buffer at pH 7.4.....	89
Figure 3.7: Intracellular growth of <i>S. aureus</i> inside RAW264.7 macrophages at different time points.....	90
Figure 3.8: Intracellular growth of <i>S. aureus</i> inside RAW264.7 macrophages at different time points upon treatment with different antibiotic loaded DDAB liposomal formulation and incubated for 1, 3, 12 and 24 h, respectively.....	92
Figure 4.1: Schematic representation of self-assembled antibiotic loaded chitosan based GNPs.....	100
Figure 4.2. Synthesis route of 3-thio-heptanoic acid- α -D-mannoside.....	121
Figure 4.3. Synthesis route of 3-thio-heptanoic acid- α -D-mannoside.....	122
Figure 4.4. Synthesis of lactose grafted chitosan (Chitlac) via <i>N</i> -alkylation of chitosan with lactose and the synthesis pathway of mannose and lactose grafted chitosan (Chitmannolac) using EDC-NHS coupling.....	123
Figure 4.5: ¹ H NMR spectra of chitosan, Chitlac, Chitmannolac and PAM-g-Chitmannolac _{5k} at 298K in D ₂ O.....	125

Figure 4.6: ^1H NMR spectra of Chitlac with increasing degree of lactosylation at 343 K, in $\text{D}_2\text{O}/\text{CD}_3\text{COOD}$	126
Figure 4.7: Comparison of solubility of chitosan and its derivatives (a) Chitosan _{5k} derivatives and (b) Chitosan _{2k} derivatives at different pH values as determined by light transmittance at a fixed wavelength of 600 nm. UV-vis (c) and fluorescence spectra (Ex: 440 nm) of the prepared fluorescein conjugated GNPs (d).....	127
Figure 4.8: Average particle size of the prepared DSA loaded GNPs before and after amikacin encapsulation.....	130
Figure 4.9. Effects of antibiotic loaded GNPs on RAW264.7 macrophage cell viability.....	134
Figure 4.10. Production of proinflammatory (TNF- α and IL-6) cytokines upon 12, 24 and 48 h treatment with DSA/PAM-GNPs _{5k} (a and b) and DSA/SAM-GNP _{5k} (c and d) against RAW264.7 macrophage cells.....	135
Figure 4.11. Confocal laser scanning microscope (CLSM) of Flu-c-Chitosan and DSA/Flu-c-PAM-GNP _{5k} using RAW264.7 macrophage cell after 4 h incubation to describe the intracellular uptake characteristic.....	137
Figure 4.12: Intracellular growth of <i>S. aureus</i> inside RAW264.7 macrophages against various concentrations of DSA/PAM-GNP _{5k} (a) and amikacin/DSA/PAM-GNP _{5k} (b) nanoparticles.....	138

List of Tables

Table 1.1: Chemical structures of mono-, oligo-, and polysaccharides that are used in the development glyconanoparticle drug delivery systems.....	7
Table 1.2: Polysaccharides based nanoparticles tested for drug delivery to bacteria infected macrophages.....	37
Table 3.1: Lipid composition and physical characterization of DDAB/glycolipids liposomes.....	82
Table 3.2: Physicochemical characterization of DSA and amikacin encapsulated DDAB/glycolipids (80:20, mol%) liposomes and patterns of the amikacin loading and <i>in vitro</i> release.....	87
Table 4.1: Reaction conditions by altering the amount of lactose molecule to synthesize Chitlac A, Chitlac B, Chitlac C, Chitlac D, Chitlac _{5k} , and Chitlac.....	113
Table 4.2: Reaction conditions to synthesize Chitmannolac, Chitmannolac _{5k} and Chitmannolac _{2k}	114
Table 4.3: Reaction conditions to synthesize palmitoyl amido mannoside-g-Chitmannolac (PAM-g-Chitmannolac).....	114
Table 4.4: Reaction conditions to synthesize stearyl amido mannoside-g-Chitmannolac (SAM-g-Chitmannolac).....	115
Table 4.5: Reaction conditions to synthesize fluorescein-c-palmitoyl amido mannoside-g-Chitmannolac (Fluorescein-c-PAM-g-Chitmannolac) and fluorescein-c-stearyl amido mannoside-g-Chitmannolac (Fluorescein-c-SAM-g-Chitmannolac).....	115
Table 4.6: Preparation and structural parameters of lactose modified chitosan	124

Abbreviations

Ac	Acetyl	DS	Degree of substitution
AcOH	Acetic acid	DSA	<i>n</i> -Decanesulphonylacetamide
Ac ₂ O	Acetic anhydride	DSPC	1,2-Distearoyl- <i>sn</i> -glycero-3-phosphocholine
AFM	Atomic force microscopy	DTT	Dithiothreitol
AG	Aminoglycosides	EDC	1-Ethyl-3-[3-imethylaminopropyl]carbodiimide hydrochloride
AIDS	Acquired immunodeficiency syndrome	EDS	Energy-dispersive X-ray spectroscopy
AmB	Amphotericin B	EE	Encapsulation efficacy
ANOVA	Analysis of variance	ELISA	Enzyme-linked immunosorbent assay
APCs	Antigen presenting cells	ESI	Electro spray ionization
ATP	Adenosine-5'-triphosphate	EtOAc	Ethyl acetate
ATRP	Atom transfer radical polymerization	FACS	Fluorescence activated cell sorters
BMM	Bone marrow-derived macrophages	FcR γ	Fc receptor γ -chain
BSA	Bovine serum albumin	FTIR	Fourier transform infra-red
CFU	Colony forming unit	FBS	Fetal bovine serum
Chitlac	Lactose modified chitosan	g	grams
Chitmannolac	Lactose and mannose modified chitosan	GC	Glycol chitosan
CLR	C-type lectin receptor	GNPs	Glyconanoparticles
CMC	Carboxymethyl cellulose	GS	Gentamycin sulphate
CMCs	Critical micelle concentrations	HA	Hyaluronic acid
Chol	Cholesterol	HIV	Human immunodeficiency virus
CMCS	Carboxymethyl chitosan	IC ₅₀	50% inhibitory concentration
CPT	Camptothecin	IL	Interleukin
CTX	Ceftriaxone sodium	ITAM	Immunoreceptor tyrosine-based activation motif
d	Doublet	<i>J</i>	Coupling constant (NMR)
dd	Doublet of doublets	kDa	Kilo Dalton
DDA	Degree of deacetylation	LB media	Luria-Bertani media
DDAB	Dimethyldioctadecylammonium bromide	LBL	Layer-by-layer
DDS	Drug delivery system	LE	Loading efficiency
DLS	Dynamic light scattering	LMWC	Low molecular weight chitosan
DMEM	Dulbecco's modified eagle medium	LPS	Lipopolysaccharide
DMF	<i>N,N</i> -Dimethyl formamide	m	Multiplet
DNA	Deoxyribonucleic acid	<i>m/z</i>	Mass/charge ratio (MS)
DOX	Doxorubicin	MCL	Macrophage C-type lectin

MIC	Minimum inhibitory concentration	TB	Tuberculosis
mg	Milligram	TBDMS	<i>tert</i> -Butyldimethylsilyl
MGL	Macrophage galactose-type lectin	TBDMSCl	<i>tert</i> -Butyldimethylsilyl chloride
Mincle	Macrophage inducible C-type Lectin	TDM	Trehalose dimycolate
MMR	Macrophage mannose receptor	TEM	Transmission electron microscopy
mL	Millilitre	TLC	Thin layer chromatography
mV	Millivolt	TMB	Tetramethylbenzidine
MTT	3-(4,5-dimethylthiazol-2-yl)2,5-diphenyltetrazolium bromide	TNF	Tumour necrosis factor
MWCO	Molecular weight cut-off	TPP	Tripolyphosphate
NMR	Nuclear magnetic resonance	TsCl	p-Toluenesulfonyl chloride (tosyl chloride)
OPA	<i>o</i> -Phalaldialdehyde	UV-vis	Ultra-violet visible spectroscopy
PAA	Poly(acrylic acid)	XPS	X-ray photoelectron spectroscopy
PABM	Benzyl 6-palmitylamido- α -D-mannoside		
PAM	Palmitoyl amido mannoside		
PBM	Benzyl 6-palmityl- α -D-mannoside		
PCL	Poly(ϵ -caprolactone)		
PDI	Polydispersity index		
PEC	Polyelectrolyte complex		
PEG	Poly(ethylene glycol)		
PEI	Polyethyleneimine		
PIM	Phosphatidylinositol mannoside		
PLL	Poly-L-lysine		
PLM	Phospholipomannan		
PVA	Poly(vinyl alcohol)		
RAFT	Reversible addition-fragmentation chain-transfer		
RES	Reticuloendothelial system		
RNA	Ribonucleic acid		
RT	Room temperature		
SABM	Benzyl 6-stearoylamido- α -D-mannoside		
SAM	Stearoyl amido mannoside		
SBM	Benzyl 6-stearoyl- α -D-mannoside		
SEM	Scanning electron microscopy		
SLN	Solid lipid nanoparticles		
STM	Scanning tunnelling microscopy		
TB	Tuberculosis		
t	Triplet		

Chapter 1

1. Introduction:

1.1 General Background

Recent developments in medicine and biotechnology have fortified the requirement to improve nanoengineered non-viral delivery systems that can encapsulate a wide variety of novel therapeutics such as proteins, nucleic acids, and chemo-therapeutics.¹⁻⁴ In addition, these delivery systems should be designed and prepared in an intelligent way such that they can deliver their encapsulated therapeutics at a well-defined time, place, or in response to a specific stimulus with minimum cytotoxicity in comparison with viral systems. Delivery of therapeutic agents to the target site is still a major concern in the treatment of many diseases. Conventional application of many potential drugs is often characterized by limited effectiveness, poor biodistribution, and lack of selectivity. These limitations and draw-backs can be overcome by controlling drug delivery.⁵ In drug delivery systems (DDS), the therapeutic is transported to the specific target site such that it influences the maximum absorption of the drug as well as minimizes the undesirable side effects. Moreover, DDS protect the therapeutic from quick degradation or clearance, thereby increasing the amount of drug in target tissues, and hence lowering the effective dose.^{6,7}

The emergence of glycobiology, glycotecnology and glycomics and their continual adaptation by pharmaceutical scientists have highlighted the enormous potential of carbohydrates for medicinal applications.⁸ It has been recognized that carbohydrates represent the third class of informational biomolecules after proteins and nucleic acids and play vital roles in both physiological and pathological events including cell-cell communication, proliferation and differentiation, tumor metastasis, inflammatory response, or viral infection.⁸ A carbohydrate-based non-viral nanoparticulate system is commonly known as glyconanoparticles (GNPs).⁹ GNPs have gained considerable attention such as studies of carbohydrate-carbohydrate and carbohydrate-protein interaction as well as in the fields of targeted drug and gene delivery system. With recent advances in polymerization techniques and glycoscience, the design and preparation of carbohydrate-based biomaterials has become the subject of intense research in the last few decades. For example, polysaccharides have been exploited for designing and preparing GNPs for clinical application because of their versatile traits,

including biocompatibility, biodegradability, and low immunogenicity. Moreover, the targeting efficacies of the GNPs toward certain organs can be modulated either by incorporating specific ligands on the surface of the GNPs or by increasing the densities of carbohydrates.

In general, drugs can be targeted to particular cells by using specific targeting ligands (active targeting) or can be targeted to particular organs or cells based on their own or their drug carrier's size and physicochemical properties (passive targeting).⁸ Among potential cellular targets by drug-loaded nanoparticles, macrophages are considered vital as they play a crucial role in inflammation and act as reservoirs of microorganisms which are involved with deadly infectious diseases. When the most common and potent drugs are applied in free form to treat macrophage-mediated disease this often prompts undesirable side effects because of lower bioavailability at the desired site. Therefore, it necessitates high drug doses to induce a therapeutic effect to overcome systemic dilution. For this, the application of drug-loaded nanoparticles offer a useful alternative to avoid, or at least reduce side effects and increase efficacy.¹⁰ This review summarizes the synthetic strategies for the preparation of various glyconanomaterials and its application in the delivery of bioactive molecules to macrophages.

1.2 Nanocarriers used in drug delivery systems

In recent decades, nanotechnology has been used extensively by researchers in the arena of improved therapeutics and is considered one of the most promising drug delivery strategies. Nanoparticle DDS are nanometric carriers used as a delivery vector of different drugs and biomolecules. According to the National Nanotechnology Initiative of the United States, nanotechnology is the research and development of technology at the atomic, molecular, or macromolecular levels to provide a fundamental understanding of materials and phenomena on the nanometer scale and creation of structure, devices or systems that have novel properties and functions.^{11,12} Recent nanotechnology research and development shows that nanoparticles smaller than 100 nm in at least one dimension have great potential as drug transporters. Due to their small sizes and large surface areas, the nanostructures provide unique biological and physicochemical properties that make them a favourable material in healthcare

management including nanotherapeutics, nanodiagnostics, and nanomaterials for pharmaceutical applications.



Figure 1.1: The important features of nanoparticles for intracellular drug delivery applications.

1.2.1 Advantages of nanoparticle-based DDS

Nanotechnology has opened a new field in DDS by the wide spread utilization of nanocarriers including nanospheres, nanocapsules, nanovesicles, nanoemulsions, nanoliposomes, nanosuspensions, nanocrystals, virosomes, solid-lipid nanoparticles (SLN), protein-based nanoparticles and polymeric nanosystems, (e.g., polymeric nanoparticles, polymer micelles, polymersomes, dendrimers and niosomes). The application of nanoparticles as a drug delivery tool has outstanding benefits¹²⁻¹⁴: (a) they possess the ability of targeting the drug to the site of action and enhancing the drug uptake that enables it to reduce toxic side effects; (b) they can exhibit controlled drug

release properties against different physicochemical and metabolic responses such as pH, temperature, ionic strength, and biodegradability; (c) they can cross the blood-brain barrier and also penetrate cells and tissue gaps to accumulate at target organs such as brain, lung, liver, spleen, lymph and spinal cord; (d) they are able to encapsulate drugs or biomolecules into their interior structures or absorb onto their exterior surfaces and therefore improve the stability of the pharmaceutical agents.

1.2.2 Preparation and application of nanoparticles in DDS

At present, nanoparticles have been comprehensively used to deliver drugs, vaccines, proteins, polypeptides, genes, nucleic acids, photo/fluorophores, photo-responsive molecules, photo-thermal agents. However, the potential application of nanoparticles is continually expanding, and some of these new areas are summarise in Figure 1.1.^{15,16} Recently, the preparation of nanoparticles for DDS depends on the selective combination of the carrier materials to attain suitable release properties and the surface modification of the nanoparticles to enhance their targeting capability.^{17,18} Researchers also investigated *in vivo* dynamic processes to reveal the interaction of nanoparticles with blood and targeting tissues and organs.¹⁹⁻²¹ Furthermore, the development of the nanocarriers focuses on their application in clinics and the possibility of industrial production.^{22,23}

Polymeric nanoparticles prepared from natural and synthetic polymers have been studied extensively by researchers because of their stability and simplicity of surface modification. It is highly desirable that polymeric nanocarriers for DDS be biocompatible as well as biodegradable. For this reason, many synthetic and natural polymeric materials have been applied such as poly(ethylene glycol), poly(glycolic acid), Pluronic, poly(vinyl pyrrolidone), poly(ϵ -caprolactone), poly(lactic acid), poly(lactic-co-glycolic acid), poly(acrylic acid) family, poly(trimethylenecarbonate), polysaccharides (i.e., chitosan, alginate, heparin, hyaluronic acid, dextran, cyclodextrin, and amylose), proteins or polypeptide (i.e., gelatin).²⁴⁻²⁶ Among natural polymers, proteins and polysaccharides tend to be internalized and degraded rapidly enabling a moderate intracellular release of the drug or biomolecules. Nonetheless, polysaccharides have been frequently applied in the preparation of DDS among polymeric materials due

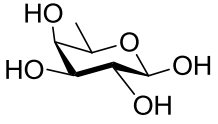
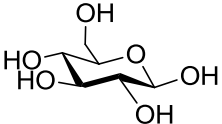
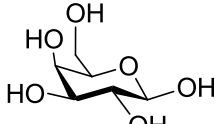
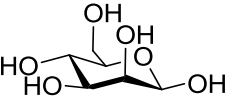
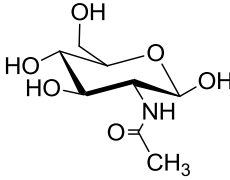
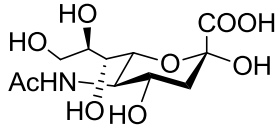
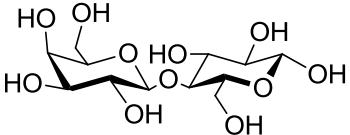
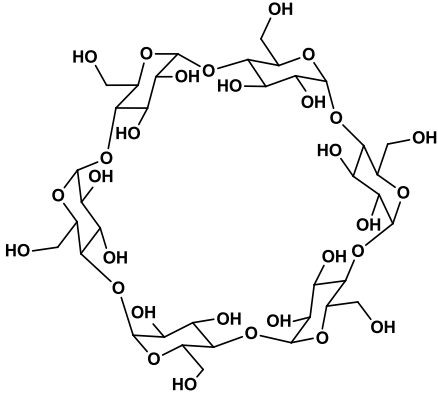
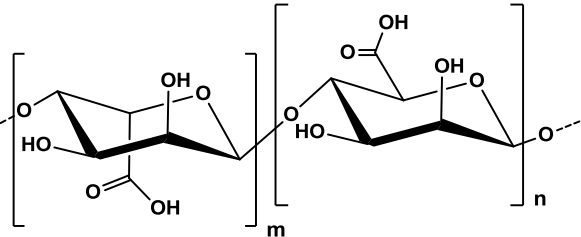
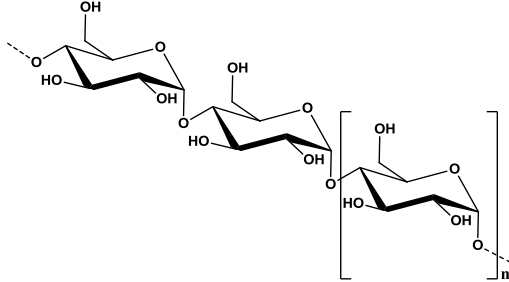
to their biodegradability, high stability, high biocompatibility, and low immunogenicity.²⁷

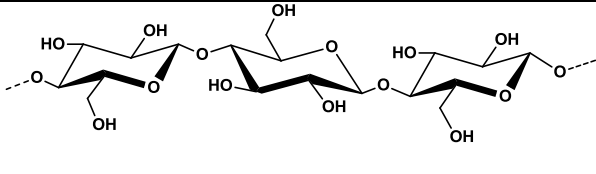
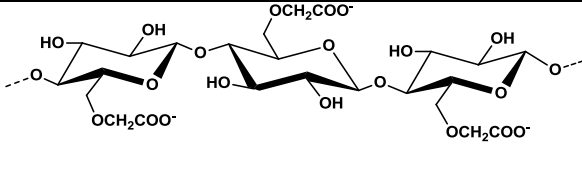
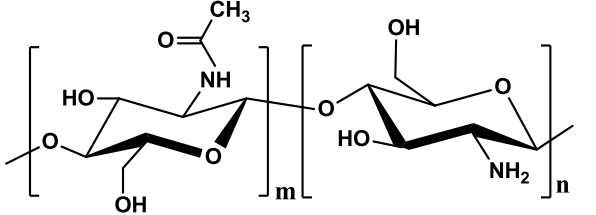
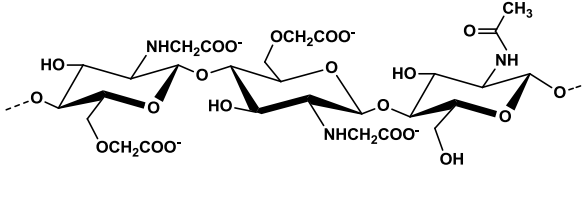
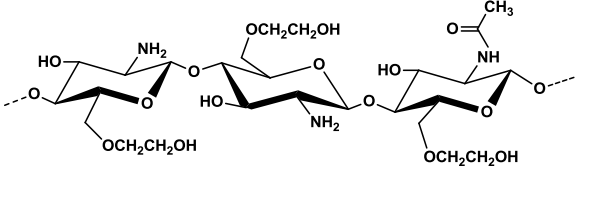
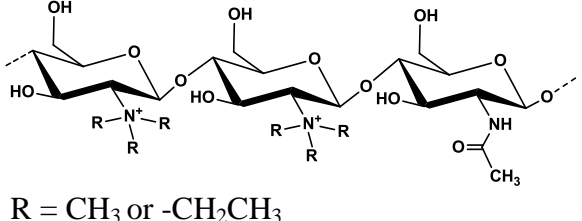
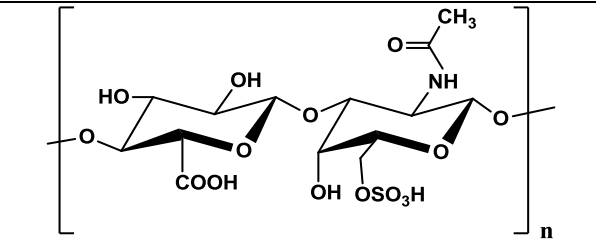
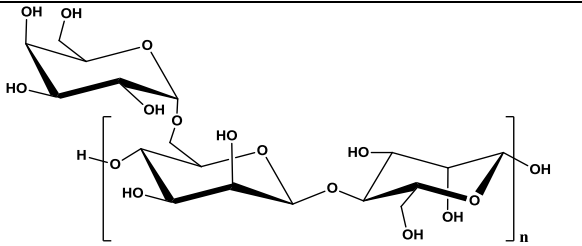
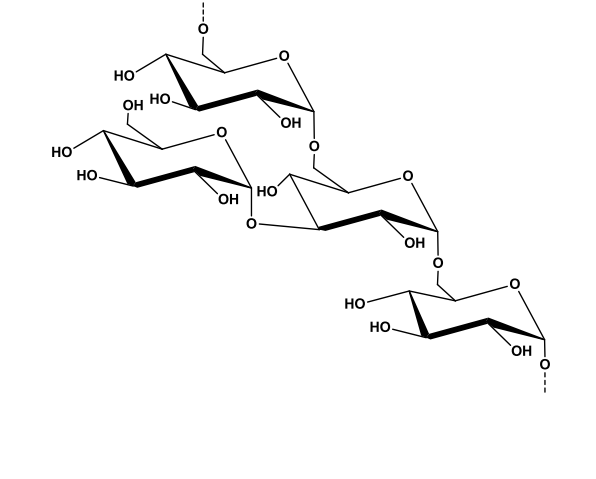
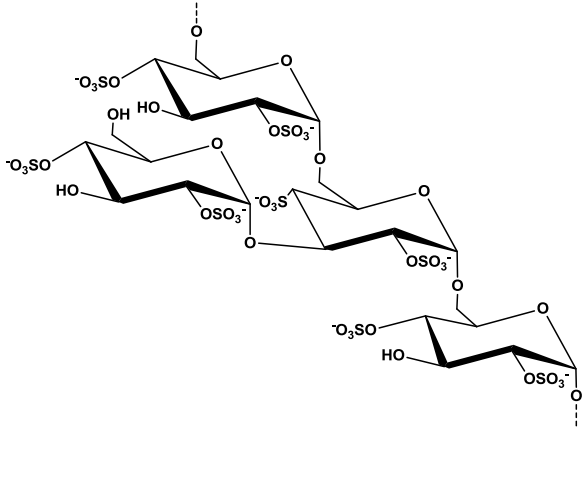
1.3 Polysaccharides-based nanoparticles and their advantages

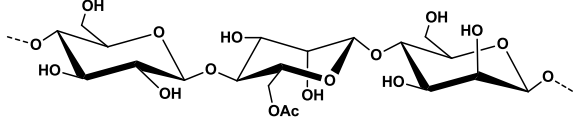
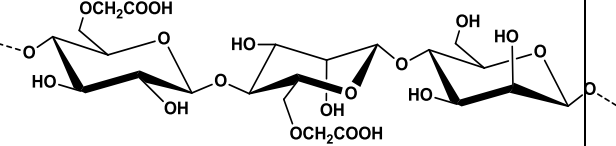
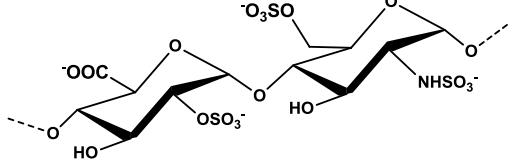
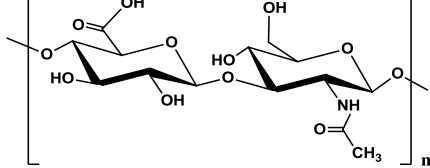
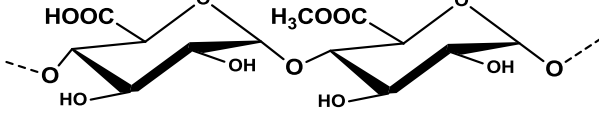
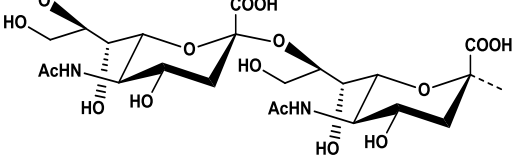
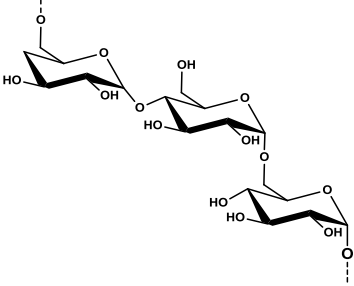
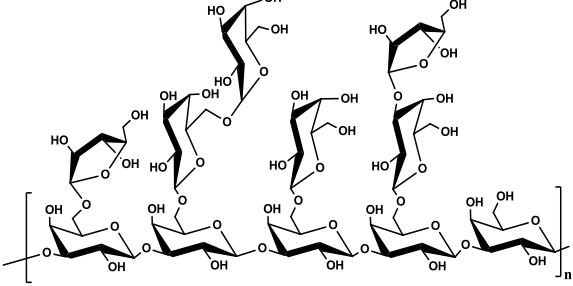
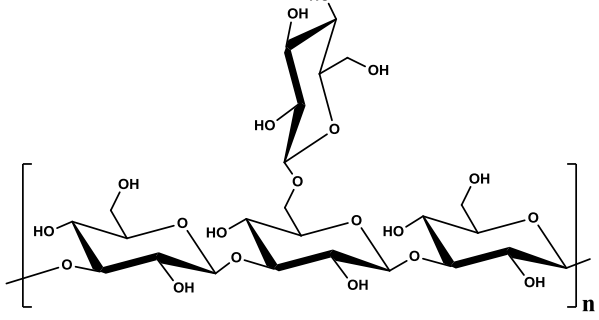
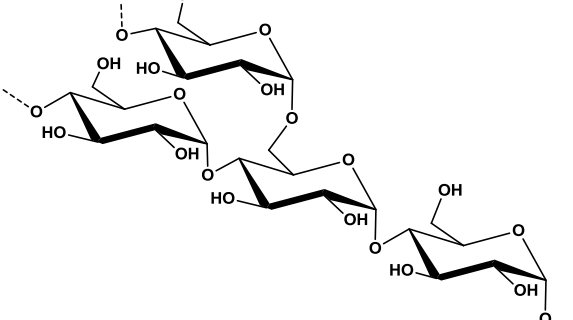
Polysaccharides are a diverse class of natural (plant, animal, algal, microbial) polymeric materials formed *via* a glycosidic linkage between monosaccharides. Polysaccharides can have a linear or branched chemical structure depending on the nature of the monosaccharides. In addition to structural diversity, polysaccharides have a large number of reactive groups, (including hydroxyl, amino, and carboxylic acid groups) typically yielding high aqueous solubility with the possibility for chemical modification. Moreover, polysaccharide molecular weight can vary between hundreds and thousands of Daltons, further increasing diversity.

Polysaccharides can be readily modified and exist in positive, negative, and neutral charge states.²⁸ In addition, some polysaccharides are bio-active and can be applied to enhance the therapeutic efficacy of an associated drug and/or can improve the targeting ability of the carrier system. Also, the presence of hydrophilic groups in their structure, imparting non-covalent bioadhesion with biological tissue like epithelia and mucous membranes, is a useful strategy to improve bioavailability of drugs included in DDS. In contrast to many synthetic polymers, polysaccharides have very low toxicity and high biocompatibility.²⁹ Also owing to their native presence within the body, most polysaccharides are subject to enzymatic degradation. Polysaccharides can be broken down to their monomer or oligomer building blocks through enzyme catalysis and recycled for use as storage, structural support, or even cell signalling applications.³⁰ Finally, polysaccharides are abundant resources in nature and have low cost associated with their processing. All of these advantages support polysaccharides as an effective carrier platform for drug delivery. A list of polysaccharides used for macrophage targeted drug delivery is shown in **Table 1.1**.

Table 1.1: Chemical structures of mono-, oligo-, and polysaccharides that are used in the development glyconanoparticle drug delivery systems are shown in the Table below.

Monosaccharides		
Fucose ^{31,32}	Glucose ^{33,34}	Galactose ^{35,36}
		
Mannose ^{18,37,38}	N-acetyl glucosamine ^{39,40}	Sialic acid ^{41,42}
		
Di- or Oligosaccharides		
Lactose ^{35,43}	α -Cyclodextrin ⁴⁴⁻⁴⁶	
		
Polysaccharides		
Alginate ^{22,47,48}	Amylose ^{24,49}	
		

Cellulose ^{50,51}	Carboxymethyl cellulose ^{52,53}
	
Chitosan ^{54,55}	Carboxymethyl chitosan ^{56,57}
	
Glycol chitosan ^{58,59}	N-trimethyl or triethyl chitosan ^{60,61}
	 <p>R = CH₃ or -CH₂CH₃</p>
Chondroitin sulphate ^{18,62}	Guar gum (guaran) ^{63,64}
	
Dextran ^{65,66}	Dextran sulphate ^{67,68}
	

<p style="text-align: center;">Glucomanan^{69,70}</p>	<p style="text-align: center;">Carboxymethyl konjac glucomanan^{69,71}</p>
	
<p style="text-align: center;">Heparin^{31,72}</p>	<p style="text-align: center;">Hyaluronic acid⁷³⁻⁷⁵</p>
	
<p style="text-align: center;">Pectin^{76,77}</p>	<p style="text-align: center;">Poly(sialic acid)^{78,79}</p>
	
<p style="text-align: center;">Pullulan^{80,81}</p>	<p style="text-align: center;">Arabinogalactan^{82,83}</p>
	
<p style="text-align: center;">Schizophyllan^{84,85}</p>	<p style="text-align: center;">Starch^{86,87}</p>
	

1.4 Preparation methods of glyconanoparticles (GNPs)

In recent years, a large number of studies have been conducted on glyconanoparticles focusing on the preparation and their potential application as drug delivery systems. As time goes on, more glyconanoparticles emerge, which significantly improves their importance and versatility in terms of category and function. Early studies suggest that GNPs should be designed and developed with careful attention towards material selection, potential modification, structural features and the techniques carried out to prepare GNPs. According to the literature and structural features, GNPs are mainly prepared *via* covalent crosslinking, ionic crosslinking, polyelectrolyte complexation, self-assembly of hydrophobically modified polysaccharides, copolymerization of saccharides molecules, and nanoprecipitation.

1.4.1 Covalently crosslinked glyconanoparticles

Initially, preparation of GNPs was by means of covalent crosslinking. Covalently crosslinked GNPs enable the network structure to be permanent since irreversible chemical links are formed unless biodegradable or stimuli-responsive crosslinkers are employed. The rigid network permits absorption of water and bioactive molecules without dissolution of the GNPs even when the pH is significantly changed.^{88,89}

The most commonly used polysaccharide for nanoparticle fabrication is chitosan. Chitosan is a linear polysaccharide, composed of glucosamine and *N*-acetyl glucosamine units *via* β -(1 \rightarrow 4) linkages, randomly or block distributed throughout the biopolymer chain. Chitosan, the *N*-deacetylation product of chitin, is hydrophilic and soluble in acidic solution by protonation of amine groups, and degraded by enzymes such as lysozymes, some lipases and proteases.⁹⁰ Chemical crosslinking of chitosan has been achieved by forming covalent bonds between polysaccharide main chains and crosslinkers such as glutaraldehyde, dopamine, genipin, and low toxic natural di- and tricarboxylic acids including citric acid, malic acid, succinic acid, tartaric acid.⁹¹⁻⁹⁴ Glutaraldehyde has been usually used as cross-linker to obtain nanoparticles by emulsion cross-linking methods where free amino group of chitosan conjugates with glutaraldehyde through the formation of imines.⁹¹ Particle size can be controlled by varying the amount of glutaraldehyde which changes the degree of cross-linking. 5-

Fluorouracil loaded chitosan nanoparticles were prepared by a water-in-oil (w/o) emulsion method followed by glutaraldehyde crosslinking of the chitosan amino groups.¹⁴ However, the cytotoxicity of glutaraldehyde limits its application in nanocarrier drug delivery systems. Recently, Meng and co-workers have synthesized dual pH-/light-responsive crosslinked nanocarriers by using amphiphilic glycol chitosan-*o*-nitrobenzyl succinate (GC-NBSCs) conjugates to crosslink with glutaraldehyde.⁹⁵ In this case, hydrophobic light-sensitive *o*-nitrobenzyl succinate was covalently conjugated onto the main chain of hydrophilic glycol chitosan (GC). Then, the nanosized micelles were prepared by the self-assembly of GC-NBSCs in water and further stabilized by cross-linking their GC shells with glutaraldehyde to form dual responsive nanocarriers (Figure 1.2).

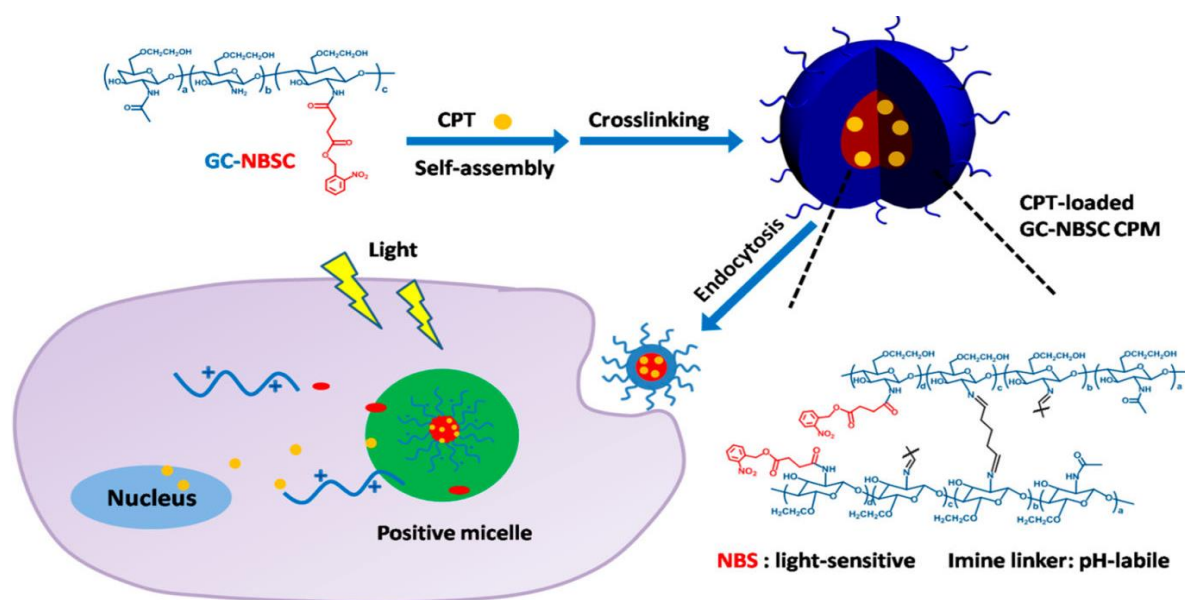


Figure 1.2: Scheme represents the preparation of chitosan based camptothecin (CPT) encapsulated nanocarrier and the intracellular drug release triggered by pH and UV light.⁹⁵

Genipin, a naturally occurring crosslinking agent, has been used as cross-linkers of amino groups on chitosan backbones using w/o microemulsion method and also provided significantly less cell cytotoxicity compared with glutaraldehyde in crosslinking amine group containing biomaterials. For instance, multifunctional genipin-crosslinked fucose-chitosan/heparin nanoparticles have been developed by Yu-Hsin and co-workers.³¹ In this study, they combined fucose-conjugated chitosan and

genipin crosslinking technologies in preparing pH-responsive chitosan/heparin nanoparticles. The particle sizes of the prepared GNPs were in range of 180 to 230 nm (Figure 1.3).

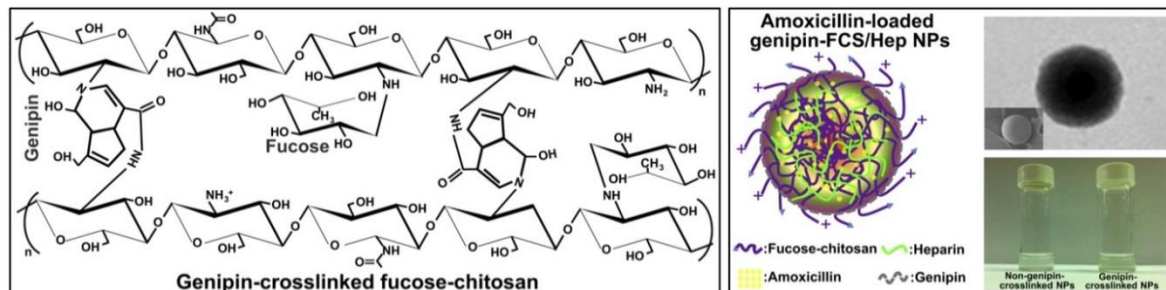


Figure 1.3: A schematic representation of prepared amoxicillin-loaded genipin-crosslinked fucose-chitosan/heparin nanoparticles.³¹

Hyaluronic acid (HA) is another common natural polysaccharide employed in the preparation of GNPs through carbodiimide chemistry due to its non-toxic, biocompatible and biodegradable properties. The chemical composition of HA consists of nonsulfated glycosaminoglycan containing repeating units of disaccharide, β -1,4-D-glucuronic acid and β -1,3-N-acetyl-D-glucosamine with a molecular weight ranging from 100 kDa - 8000 kDa. The preparation of GNPs based on HA takes place by covalently cross-linking *via* carboxyl groups of the HA main chain. Bondar and co-workers have prepared spherical GNPs by covalently cross-linking carboxyl groups of the HA chain with a diamine in aqueous media at room temperature using carbodiimide techniques. An injectable hydrogel showing excellent tissue adhesion was developed using catechol-thiol reactions between the two biocompatible copolymers of HA and pluronic copolymer. HA-dopamine conjugates and thiol terminated Pluronic F127 copolymers were mixed to produce HA/Pluronic hybrid hydrogels using catechol-thiol reactions.⁹⁶ Rolf and co-workers have obtained covalently stabilized trimethyl chitosan-hyaluronic acid nanoparticles with sizes of about 200-300 nm for nasal and intradermal vaccination.⁹⁷ Recently, robust nanohybrids were designed by conjugating HA and branched polyethyleneimine (bPEI) using carbodiimide chemistry and subsequently functionalized with mannose at the terminal end of the copolymer.⁹⁸

1.4.2 Ionically crosslinked glyconanoparticles

Physical crosslinking of polysaccharides is based on ionic interactions between charged polysaccharides and ionic cross-linkers. This method provides GNPs with reversibility and is considered biocompatible due to the lack of complex preparation conditions or toxic cross-linkers. Ionically-crosslinked GNPs are generally pH sensitive, thus suitable for stimuli-responsive controlled release. Nanoparticles can be obtained from aqueous solutions of charged polysaccharide and small ions of opposite charges. Thus, polycations and polyanions could act as crosslinkers with polyanionic and polycationic polysaccharides, respectively. In this process, very dilute solutions of the polysaccharide are used as the chain of the polymer can react with the crosslinkers to form small clusters. These clusters are finally stabilized by forming complex with oppositely charged electrolytes.⁹⁹

To date, tripolyphosphate (TPP), a non-toxic and multivalent anionic molecule, is the most widely used polyanion crosslinker for the preparation of crosslinked chitosan nanoparticles.^{100,101} The cationic nature of chitosan, in an acidic aqueous solution (pH 4-6) can be exploited to form nanoparticles by adding small amounts of TPP in an alkaline phase (pH 7-9). After mixing of the two phases, inter- and intra-molecular linkages are created between chitosan amino groups and the TPP phosphates.¹⁰² A slightly modified ionotropic gelation technique was employed by Domaratzki and Ghanemin to obtain smooth, spherical GNPs based on chitosan and TPP crosslinker.¹⁰¹ Their results showed that nanoparticle size depends on degree of hydration, and crosslinking conditions, with the smallest nanoparticles in the size range of 160-270 nm. TPP crosslinked chitosan nanoparticles have been used for delivering protein, DNA, siRNA, doxorubicin, cladribine, and some antibiotics (such as aminoglycosides, rifampicin, ceftriaxone, ciprofloxacin) due to their high physical stability and encapsulation efficiencies.^{66,103-106}

Depending on pH and ionic strength of the dispersing medium, these nanoparticles are capable of swelling and shrinking, thus facilitating the release of the encapsulated drug in the nanoparticles upon the action of various stimuli including pH and ion concentration. Recently, Xu *et al.* have developed chitosan-TPP/IL-12 nanoparticles to deliver therapeutic proteins and genes.¹⁰⁷ In this case, they utilized encapsulated IL-12 by incorporation using TPP as the coacervated crosslinking agents to form chitosan

nanoparticles (Figure 1.4). The modified chitosan with TPP shows the mean diameter of the nanoparticles ranges from 178 to 372 nm along with an increasing in the chitosan/TPP weight ratio. They also measured the zeta potential of the nanoparticles ranges between 24 and 53 mV depending on the feeding ratio of chitosan and TPP.¹⁰⁷

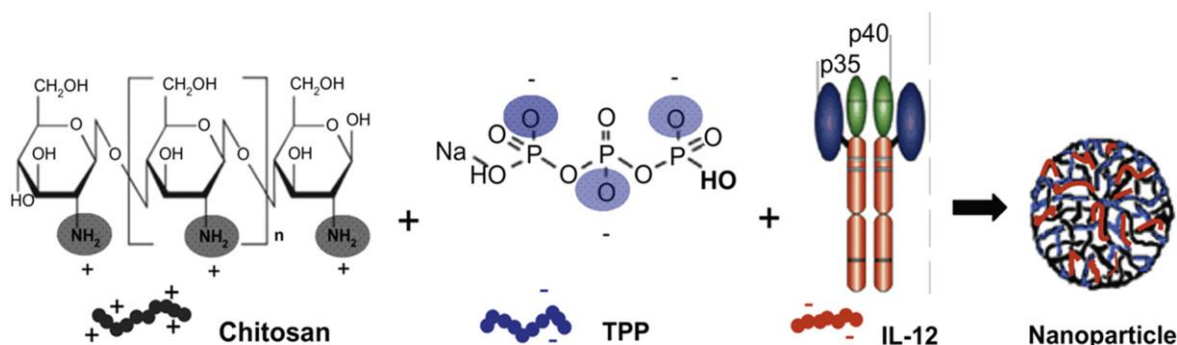


Figure 1.4: Schematic representation of the synthesis of CS-TPP/IL-12 nanoparticle system.¹⁰⁷

TPP is not the only material used as a crosslinker to prepare chitosan nanoparticles by the ionic gelation method. Some researchers have obtained chitosan-based nanoparticles *via* physical crosslinking using the encapsulated drug as a cross-linker, forming electrostatic interactions between an amine group of chitosan and hydroxyl group of the drug such as retinol, cladribine, or glabridine.¹⁰⁸ For example, Kim and co-workers encapsulated retinol in chitosan nanoparticles for pharmaceutical and cosmetic applications *via* forming an ionic complex from the interaction between the amine group of chitosan and the hydroxyl group of retinol.¹⁰⁹ The authors claimed the electrostatic interaction was confirmed by FT-IR spectra generating a specific semi-doublet peak of chitosan at 1590 cm^{-1} . Recently, chitosan and adenosine-5'-triphosphate (ATP) were employed as building blocks to form spherical aggregates based on electrostatic interactions (Figure 1.5).¹¹⁰ Since the ratio between ATP and chitosan varies during physical interaction, part of the chitosan is associated with ATP and rest of the chitosan remains cationic and hydrophilic. In this way, a polymeric supra-amphiphile is fabricated and is responsible for chitosan-ATP aggregated by self-assembly with sizes between 50 and 68 nm. Among negatively charged polysaccharides, alginate is widely used to obtain GNPs by ionic gelation. Alginate is a water soluble polysaccharide consisting of alternating blocks of 1-4 linked α -L-guluronic (G-block) and β -D-

mannuronic acid (M-block) residues, which are generally arranged in an irregular blockwise pattern of varying proportions of G-G, M-G, and M-M blocks. Carboxylic groups on the main chain of alginate structure can be crosslinked through small cations like bivalent calcium, strontium, zinc, or barium ions to form GNPs.⁵⁴ However, monovalent cations and magnesium ions cannot form gelation with alginates.¹¹¹

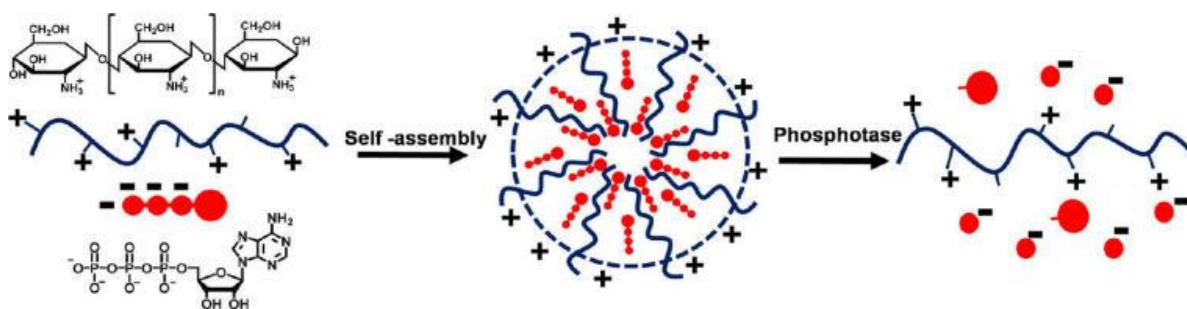


Figure 1.5: Schematic illustration of the formation and the phosphatase-induced degradation of the polymeric supra-amphiphiles and the spherical aggregates.¹¹⁰

1.4.3 Glyconanoparticles by polyelectrolyte complexation (PEC)

GNPs are also prepared by direct interactions of oppositely charged polysaccharides in solution without any chemical covalent cross-linker. The major interaction between two polyelectrolyte polysaccharides includes the strong but reversible electrostatic and dipole-dipole association, as well as hydrogen bond and hydrophobic interactions. The stability of polyelectrolyte complexes (PEC) is determined by the degree of interaction of the polyelectrolytes, which is affected by the charge density and distribution, chemical environment such as pH, temperature, ionic strength, mixing ratio, and the molecular weight of the polyelectrolytes. Compared to chemically crosslinked complexes, PEC derived GNPs are generally non-toxic, biocompatible and well-tolerated due to ease of preparation and modification as well as fewer steps required for PEC. Positively or negatively charged GNPs with a core/shell structure can be obtained according to the nature of the polyelectrolyte which is used in excess. The hydrophobic core is composed of the complexed segments whereas the excess component is not incorporated in the PEC, and thus is segregated in the outer shell ensuring the colloidal stabilization of the GNPs against coagulation and conferring the charge of the nanoparticle surface.⁹⁹

Although any polyelectrolyte could interact with polysaccharides to prepare PEC nanoparticles, only water soluble and biocompatible polymers are used as polyelectrolytes to form GNPs. Among the existing polyanionic and polycationic polysaccharides used to develop PEC based GNPs, chitosan is extensively utilized because it satisfies the requirements of safety and solubility. Due to the protonation of amino groups on the backbone in acidic medium, chitosan becomes a cationic polyelectrolyte which can form PEC with negatively charged polyelectrolytes.⁵⁴ It can be seen throughout the literature that much research has been carried out on PEC with chitosan and many polyanions from different categories such as alginate, pectin, carboxymethyl cellulose (CMC), heparin, dextran sulphate, hyaluronic acid, carrageenan, collagen, xanthum gum, carboxymethyl pachyman, poly(acrylic acid) (PAA), or nucleic acids.^{54,76,112-114}

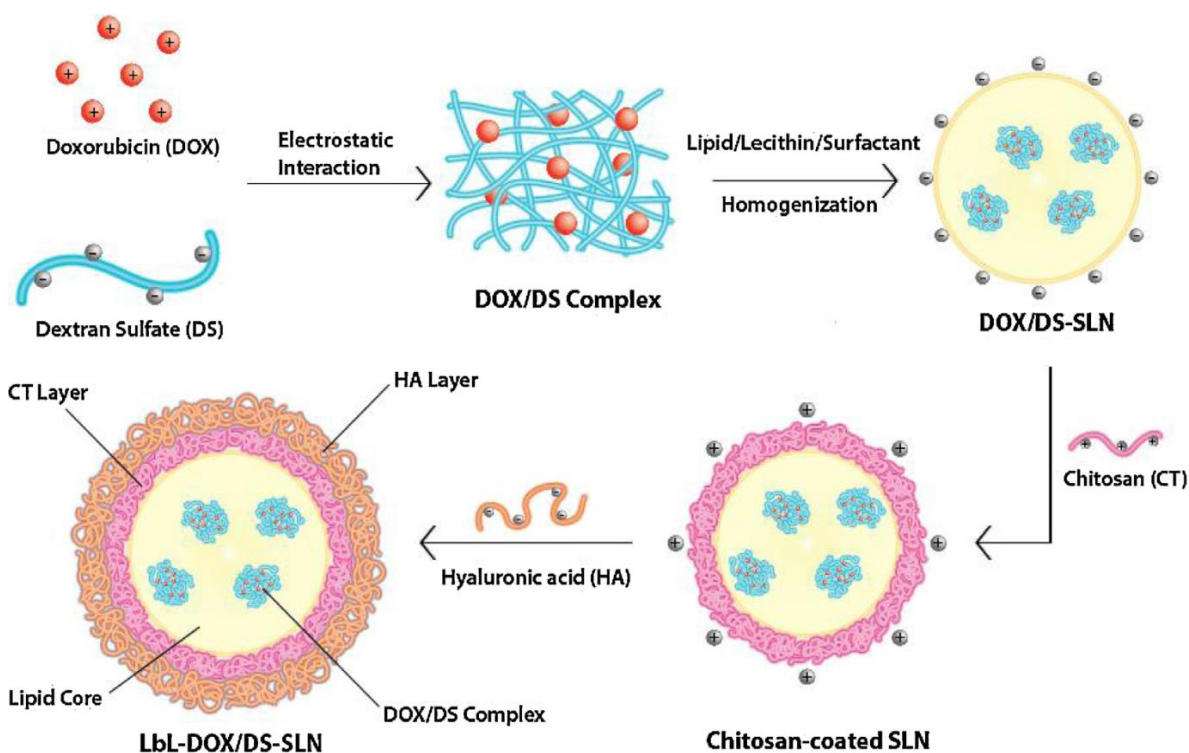


Figure 1.6: Diagram illustrating the preparation process for LbL-coated SLNs containing DOX/DS complexes. LBL: Layer-by-layer, SLN: Solid-Lipid Nanoparticles.¹¹⁵

Ramasamy and co-workers developed layer-by-layer (LbL) coated core-shell lipid-polymer hybrid nanoparticles for anticancer drug delivery by step-wise deposition of

chitosan and hyaluronic acid on negatively charged hybrid solid lipid nanoparticles (SLNs).¹¹⁵ Furthermore, a doxorubicin/dextran sulphate complex was incorporated into the SLNs (Figure 1.6). The resulted spherical GNPs were about 265 nm in diameter, with a zeta potential of approximately -12 mV. The nanoparticles were physically stable and exhibited controlled drug release kinetics.

The formation of the complex between chitosan and poly(acrylic acid) (PAA) has been widely studied. The influence of molecular weights of chitosan and PAA, the ratio of the initial polyelectrolyte concentrations, dropping temperature, pH of the initial solutions and purification process are considered to form PEC. For instant, Chen and co-workers developed chitosan/PAA GNPs *via* complexation between chitosan and PAA.¹¹⁶ When polyanion PAA was added into polycation chitosan solution dropwise, chitosan/PAA nanoparticles were formed with diverse microstructure under different experimental conditions. Ronald *et al.* developed PEC based GNPs from chitosan and PAA homopolymers and polystyrene-block-PAA diblock copolymers.¹¹⁷ They also investigated nanoparticles size and found the particles sizes were smaller than 100 and 200 nm for complexes of chitosan with the homopolymer and copolymer, respectively.

Tang *et al.* obtained a thermoresponsive chitosan/poly(vinyl alcohol) (PVA) hydrogel containing nanoparticles with different charges for drug delivery through the electrostatic effect of the quaternary amine $-N^+(CH_3)_3$ and $-COO^-$ by forming *N*-(2-hydroxy)propyl-3-trimethylammonium chitosan chloride and carboxymethyl chitosan.¹¹⁸ Additionally nanoparticles with different charges were reported by different ratio of $-[N(CH_3)_3]^+$ and $-COO^-$, which were suitable for drug delivery with opposite charges. They also found the release of the positive or negative drugs were the slowest with the hydrogels containing negative or positive nanoparticles, respectively. Davidenko and co-workers reported chitosan/PAA PEC nanoparticles which were prepared by coacervation under mild experimental conditions without the use of any organic solvent or surfactants.¹¹⁹ They found that it was possible to obtain suspensions of GNPs for solution concentration 0.1 wt%. They also established that the pH values of the reactant solutions had a great influence on both the yield of the complex and the particle that was formed. They observed the most convenient pH values for obtaining

chitosan/PAA nanoparticles with optimum yield near 90% were 4.5-5.5 for chitosan and 3.2 for PAA.

1.4.4 Self-assembled glyconanoparticles

Amphiphilic polymers are generated when hydrophobic segments are grafted to chains of hydrophilic polymers. Amphiphilic polymers can self-assemble in solution to form micelles or vesicles. Therefore, introduction of hydrophobic segments into hydrophilic polysaccharide backbones enables them to form self-assembled structures such as micelles, particles, and hydrogels *via* undergoing intra- or intermolecular associations to achieve a state of minimum free energy. Nanoparticles can be formed by maintaining the lengths and molar ratios of both polysaccharides and hydrophobic segments. Hydrophobic segments on polysaccharides are obtained by grafting hydrophobic molecules from hydroxyl, amino, or carboxylic groups of the polysaccharides main chain. In general, self-assembled GNPs can serve as reservoirs for various hydrophobic drugs because their hydrophobic domain is surrounded by a hydrophilic outer shell. The drugs are then released from the inner core of the nanoparticles *via* alteration of external stimuli including pH, ionic strength, and temperature. There are various hydrophobic molecules that can be attached to polysaccharides in order to obtain self-assembled nanostructures such as pluronic copolymers, poly(ϵ -caprolactone), cholesterol, deoxycholic acid, long-chain fatty acids, and other carboxylic acids.

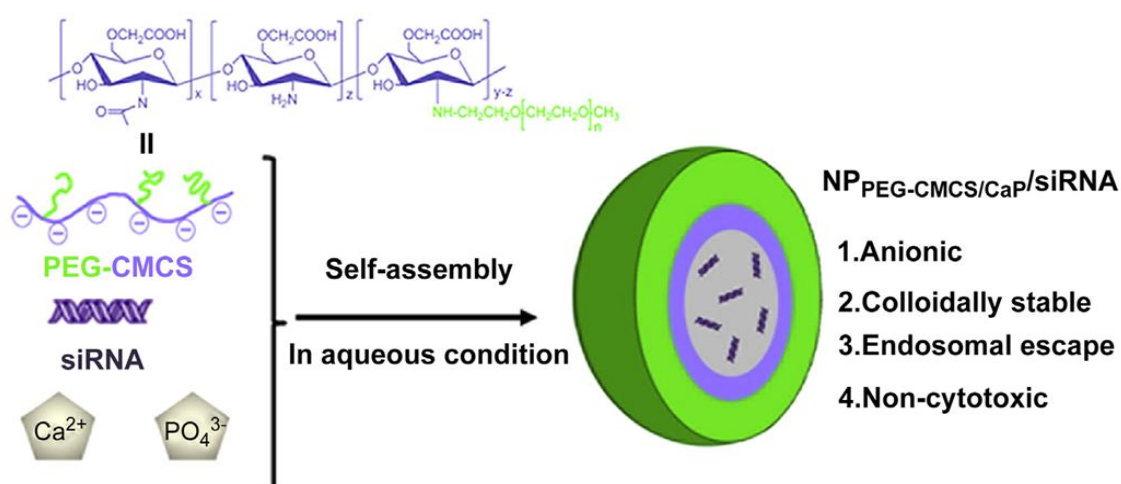


Figure 1.7: Schematic diagram of the formation of siRNA loaded PEG-CMCS/CaP hybrid anionic nanoparticles (NPPEG-CMCS/CaP/siRNA).¹¹⁴

Poly(ethylene glycol) (PEG) has been extensively employed in pharmaceutical and biomedical fields because of its outstanding physico-chemical and biological properties such as high hydrophilicity, solubility, non-toxicity, biodegradability, ease of chemical modification and absence of antigenicity. It is ideal for prevention of bacterial surface growth, decrease of plasma protein binding and erythrocyte aggregation, and prevention of recognition by the immune system (stealth effect). PEG and its derivatives can be attached to the structure to form micelles directly in an aqueous medium by adjusting the hydrophilicity /hydrophobicity of the polysaccharide chain. Xie *et al.* synthesized a pH-sensitive polymer of PEG grafted carboxymethyl chitosan (PEG-CMCS) and prepared anionic-charged hybrid nanoparticles of PEG-CMCS and calcium phosphate for siRNA delivery for anticancer therapy through a single-step self-assembly method in aqueous condition (Figure 1.7).¹¹⁴

Among different cyclic hydrophobic molecules, cholesterol is one of the most utilized to give hydrophobic character to polysaccharide structures and self-assembled GNPs in aqueous solution. Yuan *et al.* developed cholesterol-modified chitosan self-aggregated nanoparticles containing 1.7-4.7 cholesterol groups per 100 anhydroglucosamine units of chitosan by an EDC mediated coupling reactions for delivery of drugs to ocular surface.¹²⁰ The mean diameters of the self-assembled nanoparticles were less than 230 nm. Self-assembled cholesterol-modified *o*-carboxymethyl nanoparticles were prepared with different degree of substitution (DS) of cholesterol moiety in water by a probe sonication method and reported spherical nanoparticles size ranging from 100.1 to 234.9 nm which could be controlled by DS of cholesterol moiety.¹²¹

1.4.5 Limitations of prepared GNPs

The physical and chemical stabilities of the synthesized GNPs are of great importance during preparation. This issue brings unexpected difficulties to carbohydrate chemists. For instance, the acetyl protecting group is the most commonly used protective group in carbohydrate chemistry. It is useful to synthesize the sugar modified acrylate monomeric families and these are widely used as glycomonomer during polymerization *via* atom transfer radical polymerization (ATRP) and reversible addition-fragmentation chain-transfer (RAFT) before preparing GNPs. However, it is possible to hydrolyze the ester bond of acrylate monomer unavoidably during deacetylation step, which might be

a significant uncertainty at the stage of glycopolymer because of the difficulty in characterization. Therefore, the correct type of glycoside linkage and definite stereochemistry are significant requirements of glycopolymers.

1.5 Macrophage targeting

Macrophages are an essential component of the immune system and their principal function is to ingest and destroy microorganisms. However, pathogenic microorganisms are sometimes able to survive and reproduce after they have been ingested by macrophages, which impede the treatment of this type of infection. The intracellular location of these microorganisms protects them from the host defense mechanisms, such as antibodies or complement, and from the action of antibiotics that are unable to penetrate the cell. This results in difficulties to treat infections caused by obligate intracellular microorganisms and the pathological importance of intracellular reservoirs of infections caused by facultative microorganisms. Furthermore, these reservoirs may lead to chronic disease or delayed onset through latency. Since microorganisms can prevent the action of antibiotic by surviving in cells and leaving the host cell when the level of antibiotic is low enough, this causes further relapses. Consequently, the accumulation of antibiotics inside macrophages is of great therapeutic interest for fighting this type of infection.

Macrophages are an attractive therapeutic target due to the fact that they play an important role in the inflammatory response and wound healing. A number of macrophage subsets have been described that are associated with distinct phenotypes. Classically activated macrophages (M1 macrophages) are critical for host defense from a variety of bacteria, protozoa and viruses and have roles in antitumor immunity whereas alternatively activated macrophages (M2 macrophages) are important in injury resolution and wound healing.¹²² However, dysregulated macrophage function is associated with a wide range of conditions including allergic asthma, atherosclerosis, chronic ulcers, autoimmune disorders, and fibrotic diseases.¹²² The antibiotics mainly used today in the treatment of this type of infections belong to different groups including aminoglycosides, macrolides, fluoroquinolones, beta-lactams and glycopeptides. These drugs are characterized by having varying ability to penetrate macrophages, which may limit their efficacy in the treatment of intracellular infections.

Therefore, the use of antibiotic delivery systems capable of directly targeting and modulating macrophages as well as possessing the ability for selective distribution in macrophages is an important resource in improving antibiotic therapy against intracellular infections.

1.5.1 Phagocytosis and nanoparticles uptake by macrophages

Macrophages are known to play important roles in an organism's protection against infectious agents through the phagocytotic process. Phagocytosis consists of the ingestion of microorganisms by the macrophages and their subsequent destruction and elimination. The cellular uptake of the microorganism occurs *via* surface receptors; a process mediated by antibodies, and internalizes it, forming a vesicle or phagosome, which then fuses with lysosomes to form a phagolysosome. Macrophages also produce a series of antibactericidal agents that contribute to this action such as nitric oxide and cationic proteins (Figure 1.8a). In some diseases macrophages are rendered incapable of destroying the germs responsible for an infection either by the microorganism preventing fusion of the lysosome and phagosome or by resisting the microbiocidal mechanisms in the phagolysosome. As a result, pathogens can survive and even multiply inside different intracellular compartments of macrophages including the phagosome, phagolysosome, and/or cytosol and therefore have the ability to continue to evade the immune system (Figure 1.8b).

In recent times, macrophage-mediated therapies constitute many well-proven and new promising approaches to treating diseases. It is well known that macrophages are mainly involved in the uptake of nanoparticles, leading to their degradation and clearance from blood stream.¹²³ However, cellular uptake is highly challenging, especially for hydrophilic drugs and macromolecules. Interaction of nanoparticles with components of the outer surface of cells and cellular membranes followed by internalization into vesicles (invagination of the plasma membrane surrounds the nanoparticle) are the initial steps for the endocytosis process.²³ These vesicles are then pinched off to form membrane-bound vesicles of different sizes, compositions and internal environments, to form endosomes, phagosomes, or macropinosomes, depending on the internalization pathway. Currently, there are five recognized mechanisms for the uptake of nanoparticles depending on the proteins assisting in the endocytosis process including

phagocytosis, macropinocytosis, clathrin-mediated, caveolin-mediated, and clathrin/caveolin-independent endocytosis.¹²⁴

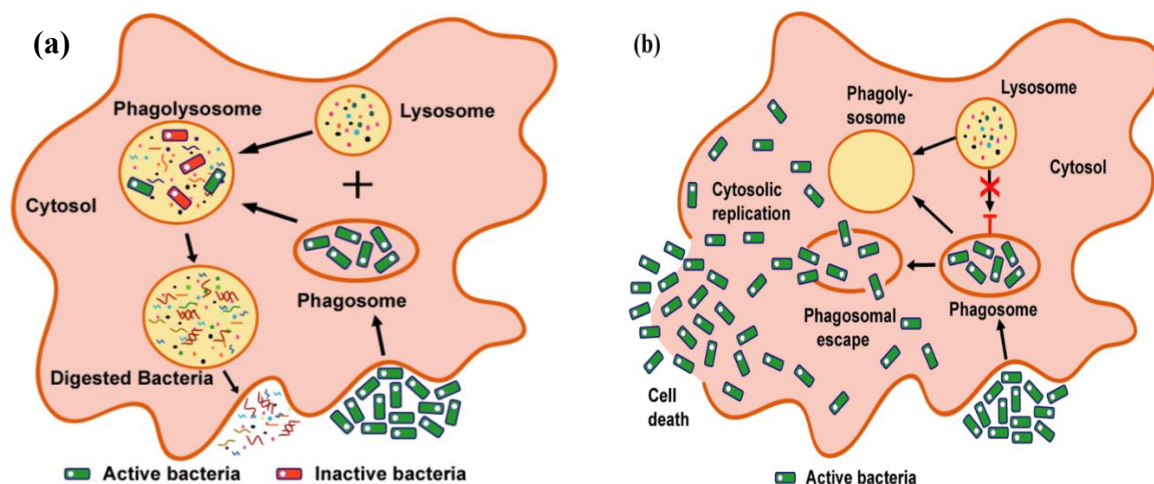


Figure 1.8: (a) Schematic representation of phagocytosis of microorganisms within the macrophages and (b) upon phagocytosis, bacteria reside in phagosome and not interact with lysosomes. Bacteria then rapidly disrupt the phagosome membrane and reach the cytosol where they undergo extensive replication, followed by cell death and bacterial release.

Generally, the uptake of nanoparticles by macrophages can be viewed as a two-step process: first, a binding step on the cell membrane and second, the internalization step. The attachment of the particles to the cell membrane as the first step seems to be greatly affected by the surface charge of nanoparticles. After the adsorption of nanoparticles on the cellular membrane, the uptake of nanoparticles is energy dependent and occurs *via* several possible mechanisms such as pinocytosis, non-specific or receptor-mediated endocytosis and different mechanisms are involved in the uptake of nanoparticles with different surface properties and in different cell types.¹²⁵ Furthermore, direct translocation of nanoparticles across the plasma membrane is another suggested endocytic pathway that does not depend on the metabolic activity of the cells.¹²⁶ This pathway is known as “energy independent”, “receptor-independent” uptake or “transduction”. The interesting feature of this pathway is that nanoparticles have a direct and quick access to the cytoplasm after crossing the membrane, which could simplify the design of nanoparticles by eliminating the need for additional features to be built into the nanoparticle framework for the purpose of disrupting the endocytic vesicles.

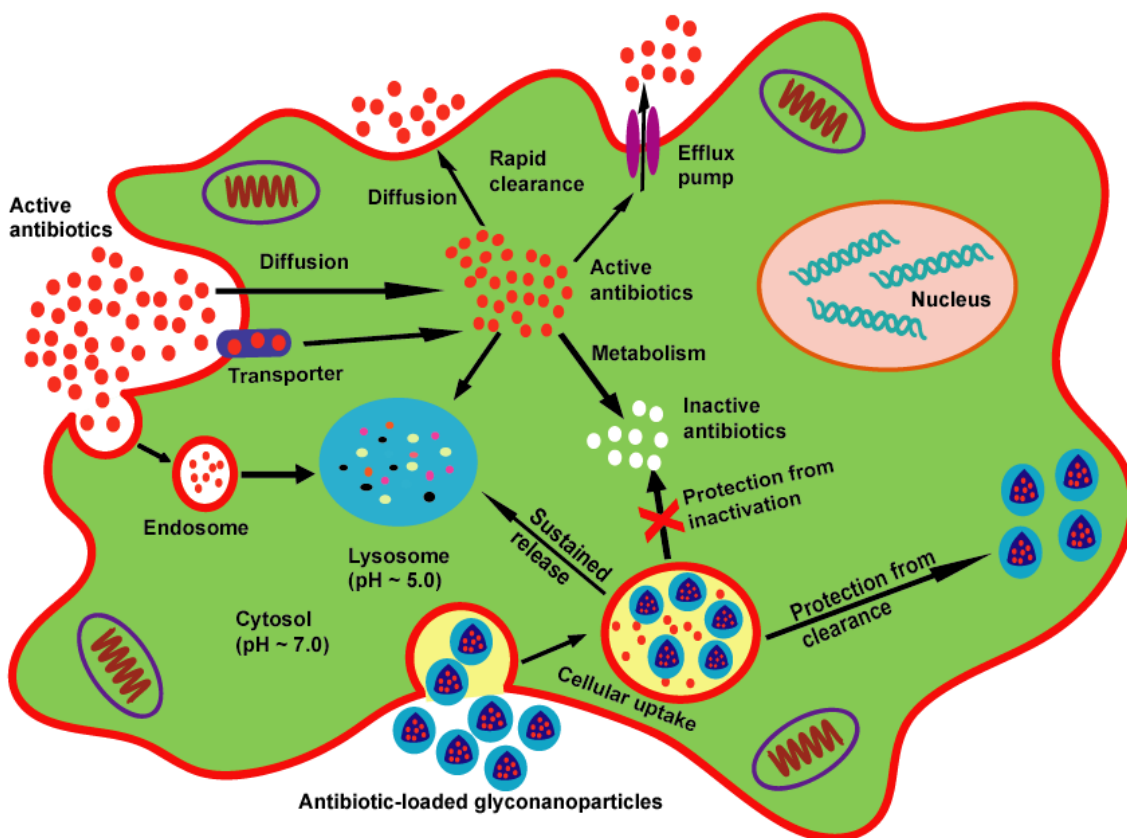


Figure 1.9: Factors affecting the intracellular activity of antibiotics and mechanism of glyconanoparticles as a carrier of antibiotics in macrophages.

Nanocarrier systems permit antibiotics to be delivered selectively to macrophages and enhance their cellular uptake in order to treat intracellular infections, especially those active antibiotics that have a low intracellular penetration capacity and can only be taken through the process of pinocytosis.¹⁵ Moreover, administration of encapsulated nanoparticles containing antibiotics alters the tissue distribution and plasma pharmacokinetics of the drug and increases the concentration of antibiotics at the site of infection, thus increasing drug bioavailability.^{13,127} Nanocarrier systems also provide a protective coat for bioactive antibiotics against environmental degradation and deactivation and protect them from the body's metabolic clearing mechanisms, so that sustained therapeutic concentrations can be maintained in the body.¹²⁸ In addition, antibiotic-loaded nanoparticles can maintain the proper drug concentration for a relatively long time by means of slow and sustained release of drug, thus reducing the dosing frequency and the dosage, while administration of free antibiotics often demonstrates a rapid and short effect and requires several doses per day.¹⁵ Antibiotic

treatment is usually complicated by the rapid clearance of antibiotics from organs, the inactivation of the drug and the barriers of tissues. Glyconanoparticles are able to protect the drug against degradation and the body's clearing mechanisms as well as facilitate transport across critical and specific barriers, thus drugs are sustained in their released to maintain a proper drug concentration for a longer time (Figure 1.9).

1.5.2 Physicochemical properties of nanoparticles to penetrate macrophages

The phagocytic uptake of nanoparticles is also influenced by physicochemical properties such as physical characteristics and morphology (particle size and shape), chemical structure and functionality, surface charge, hydrophobicity and hydrophilicity, interaction with plasma protein (opsonins), biodistribution and targeted delivery of payload to the intended target as well as cells the ability for cells to sense and respond to nanoparticles for endocytosis.¹⁰ The binding and activation of membrane receptors and subsequent protein expression strongly depend on nanoparticle size. The surface charge of the nanoparticles can significantly influence their stability, opsonization, phagocytosis, circulation in the blood and interaction with cells. The hydrophobicity/hydrophilicity of the surface regulates the adsorption of plasma proteins on the nanoparticles and is expected to influence macrophage uptake. Improved hydrophobicity of the nanocarrier is known to increase the uptake by forming hydrophobic interactions with the macrophage cell surface.¹²⁹ In addition to particle size and surface characteristics, the shape of the nanoparticle is another crucial property that plays important role in various biological processes including cellular uptake and efficient delivery of therapeutics.

1.5.2.1 Nanoparticle Size

Particle size plays an important role in the mode of endocytosis, cellular uptake, and the efficiency of particle processing in the endocytic pathway.^{130,131} For effective delivery of therapeutics to diseased cells, nanoparticles must avoid clearance by reticuloendothelial system (RES) or filtration by liver, lung, or spleen. The size of the nanoparticles has been found to have a strong influence on opsonin absorption and therefore phagocytosis. Although all nanoparticles within 2-100 nm size range were found to alter signalling process for basic cell functions (including cell death), 40-50 nm

particles demonstrated the greatest effect.^{132,133} Furthermore, polymeric nanoparticles of intermediate size (20-100 nm) are believed to be internalized easily by cells, in comparison to smaller or larger particles.¹³⁴ Macrophage uptake is heavily dependent upon the particle size, which can affect the efficiency, subcellular distribution, and pathway of cellular uptake of nanoparticles by the interaction of nanoparticles with cells.^{132,135}

Generally, small particles are less likely to be taken up by macrophages than large ones because the proper geometric configuration for efficient complement activation is achieved less easily on the more highly curved surfaces of the smaller particles than on larger ones.¹³⁶ For example, the uptake kinetics of rhodamin B labelled carboxymethyl chitosan-based GNPs in murine macrophages vary with size, and GNPs with 300 and 500 nm showed greater uptakes by cells when compared with 150 nm GNPs, which indicates that the phagocytic cells favoured the uptake of larger particles.¹³⁰ The size of particles themselves can determine the pathway of endocytosis.¹³⁷ Internalization of nanoparticles with a diameter < 200 nm involves clathrin-coated pits. Particles with 500 nm size are internalized by cells *via* an energy-dependent process. With increasing size, a shift to a mechanism that relies on coaveolae-mediated internalization becomes apparent, which is the predominant pathway of entry for particles of 500 nm in size.¹³⁷ There are also some established rules of thumb with respect to particle internalization into cells; particles > 1 μm are taken up by phagocytosis, and those are diameter between 0.2 and 1 μm are internalized by endocytosis. Nonetheless, it has been reported that particles as large as 5 μm can be endocytosed through receptor-mediated endocytosis, which may open new applications in targeted delivery to the vasculature.^{131,138}

1.5.2.2 Nanoparticle Shape

Shape is one of the essential characteristics of nanoparticles that play an important role in their internalization *via* macrophages. A wide variety of nanoparticles with non-spherical shapes have been reported such as cones, cubes, cylinders, discs, ellipsoids, hemispheres, urchins, and other complex shapes. These include red blood cell-like biconcave discoids, and filovirus-mimicking filamentous particles have been designed using a variety of fabrication techniques.^{139,140} Experimental studies of different shapes

of nanoparticles have shown that phagocytosis by macrophages display a strong dependence on shape.^{141,142} Recent studies have shown that endocytosis by macrophages including phagocytosis follow similar shape dependence and not only ingest larger particles but also engulf highly curved targets.¹⁴³

The local geometry of nanoparticles at the contact point with the cell, not the overall particle shape, can determine whether macrophages initiate internalization or simply spread on nanoparticles (Figure 1.10).¹⁴¹ For instance, a macrophage attached to an elliptical disc at the pointed end fully internalized the particle in a few minutes, while a macrophages attached to a flat region of the same ellipse did not internalize it for over 12 h.¹⁴¹ As shown in Figure 1.10, the internalization velocity of the nanoparticles changes as a function of omega (Ω), which is defined as the angle between average of tangential angles (T) from 0° to $\pi/2$ and the membrane normal at the site of attachment (N). Nanoparticles can be internalized successfully *via* actin-cup and ring formation when $\Omega \leq 45^\circ$ where phagocytosis velocity is inversely correlated to Ω (up to 45°). In contrast, macrophage can spread on nanoparticles, but the internalization is inhibited in case of $\Omega > 45^\circ$.¹⁴¹ Therefore, the local particle shape on the internalization propensity of macrophages indicates that nanoparticles with higher aspect ratios which are more likely to contact with macrophages at $\Omega > 45^\circ$ are less likely to undergo phagocytosis and can be used as stealth nanoparticles that evade the immune system.¹⁴⁴

Increasing the aspect ratios of particles leads to reduced phagocytosis by human macrophage cells with the longest particles showing almost no phagocytosis. For example, worm-like particles possessing very high aspect ratios show reduced phagocytosis compared with spherical one of the same volume.¹⁴⁵ Moreover, there are reports that nanoparticles with low aspect ratios are more easily internalized than those with high aspect ratios. On the contrary, some studies have reported that nanoparticles with larger aspect ratios are internalized into the cell line to a higher extent and have faster uptake rates.^{131,146} For example, nanoparticles with an aspect ratio of 3 are internalized about four times faster than their spherical counterparts of the same volumes.¹³¹ Furthermore, the internalization of nanoparticles has an optimum aspect ratio and nanoparticles with 2.1 – 2.5 aspect ratio are taken up in larger quantities compared to shorter or longer-length rods.¹⁴⁷ It has also been reported that the geometry

does not play a vital role in the internalization of nanoparticles *via* macrophages.¹⁴⁸ These contradictory results may be due to the fact that internalization is not only determined by the nanoparticles' geometry and shape but also other physicochemical properties including the composition, size and surface properties.

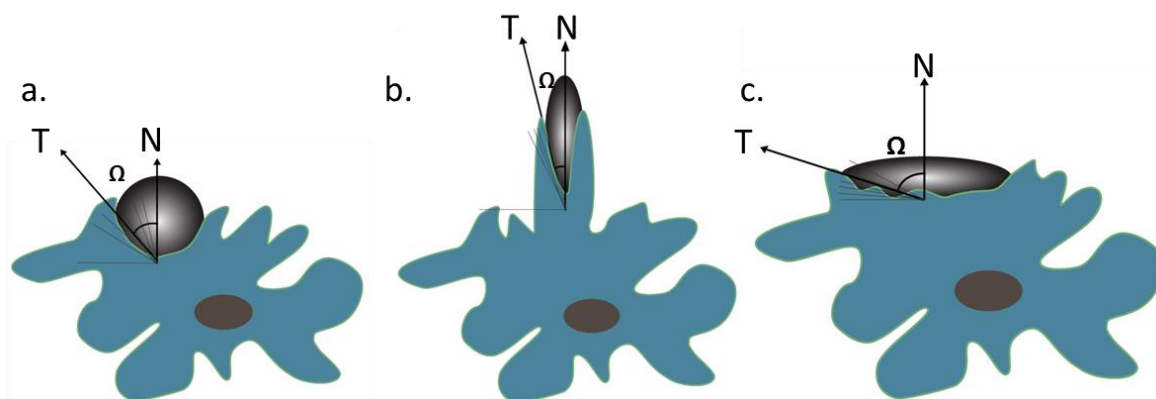


Figure 1.10: The local geometry of nanoparticles at the contact point between cell and nanoparticles. The shape indicates whether macrophages initiate internalization or spread on particles. Ω is defined as the angle between the average of tangential angles (T) from 0° to $\pi/2$ and the membrane normal at the site of attachment. When $\Omega \leq 45^\circ$, particles are internalized successfully (a. and b.); when $\Omega > 45^\circ$, cells can spread on the particle, but internalization is inhibited (c.).

1.5.2.3 Nanoparticle Surface charge

The surface charge of the nanoparticles influences the recognition and adsorption of nanoparticles by macrophages, followed by phagocytosis and elimination, which further affect their biodistribution.¹⁴⁹ It has been reported that negatively charged nanoparticles exhibit a low phagocytic uptake, thereby contributing to the elongation of blood circulation time. In contrast, positively charged nanoparticles will lead to increased phagocytosis, presumably because of better interaction of nanoparticles with the anionic cell membrane. For instance, nanoparticles with the positive zeta potential have been found to be more phagocytatable through the proton sponge effect in comparison with non-charged nanoparticles.¹⁵⁰

Vadakkan *et al.* reported the first step cellular uptake of the cationic nanocarriers was postulated to be the fusion with the plasma membrane and direct entry into the

cytosol.¹⁵¹ Another study demonstrated a linear relationship between the zeta potential of the nanoparticles and their uptake by macrophages.¹⁵² Chitosan-based GNPs with a positive surface charge showed a higher cellular internalization rate, compared to negatively or neutrally charged ones.^{153,154} The rhodamine B labelled chitosan-based GNPs with positive zeta potential (25 mV) have been found to increase the phagocytic uptake by nearly 1.3-fold when compared to negatively charged GNPs with the similar absolute value of zeta potential (-25 mV).¹³⁰ A possible reason for this phenomenon is that the positive charge of these nanoparticles can trigger the concurrent influx of chloride ions to maintain charge neutrality, thus leading to osmotic internalization which is known as the ‘proton-sponge’ effect. However, other researchers have demonstrated that neutral and cationic nanoparticles can reduce the macrophage uptake by reticuloendothelial system (RES), while negatively charged nanoparticles can potentially bind to available cationic sites on the macrophages surface and be recognized by scavenger receptors, thus facilitating uptake by RES.¹⁵⁵

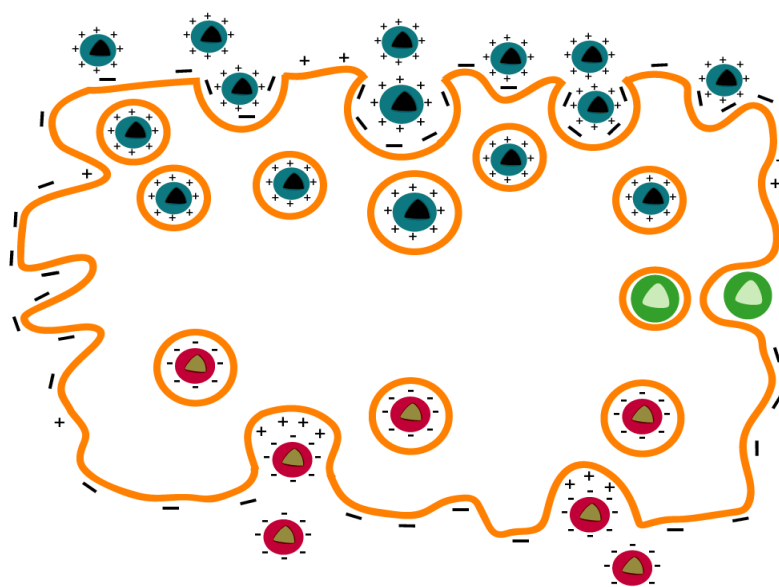


Figure 1.11: Effect of surface properties on nanoparticle internalization. Charged nanoparticles can lead to high internalization, presumably because of better interactions with the cationic and/or anionic domains of the cell surfaces. In contrast, coating with hydrophilic polymers (e.g., PEG) will form a ‘cloud’ of hydrophilic steric barrier for non-charged nanoparticles, which prevents interactions with cells, resulting in less internalization.

In addition to this, nanoparticles with negative zeta potential have greater affinity for cell membranes and can bind at the cationic site in the form of clusters because of their repulsive interactions with the large negatively charged domains of the cell surface; therefore anionic nanoparticles are highly captured by cells compared to the ones with positive zeta potentials.¹⁵⁶⁻¹⁵⁸ The inconsistent results from the above studies may be due to the difference of nanoparticles types, the nature of charged groups, variation in stability of nanoparticles resulting from surface charge, surface hydrophobicity or composition, other confounding factors such as inhomogeneous particle sizes, and the variation of cell type under investigation. In particular, the absolute value of zeta potential may be the most important factor for phagocytosis of nanoparticles. Macrophage uptake increases with the surface charge increasing (either positive or negative), and the nanoparticles with the lowest absolute value of zeta potential can effectively avoid the uptake by macrophages.^{130,159} In addition to this, positive nanoparticles may be more effective for internalization by proliferating cells, whereas negative nanoparticles with less cellular uptake and faster diffusion may perform better when delivering drugs deep into the tissues.¹⁶⁰ However, excess positive charge can induce toxicity and initiate immunological reactions.

1.5.2.4 Surface composition and hydrophobicity

Chemical composition of the surface of nanoparticles will alter the kinetics, the amount and even the route of nanoparticle uptake in cells.¹⁶¹ Generally, the surface properties of nanoparticles are mainly responsible for the number and type of biomolecules (e.g., proteins, aptamers, and antibodies) which are adsorbed onto the nanoparticle surface through electrostatic or hydrophobic/hydrophilic forces to achieve the targeted delivery of therapeutic agents.¹⁶²⁻¹⁶⁵ The chemical composition and the thickness of the adsorbed bio-layer will further promote or suppress adhesion of the nanoparticles to the cell membrane, thus influencing cellular uptake.^{166,167}

Hydrophobic nanoparticles, which have an affinity for the lipid bilayer of the cell surfaces, can facilitate the cellular internalization. Many nanoparticles have been coated with polyethylene glycol (PEG) and its analogue (such as poloxamers and ploxamines series, block copolymers of PEO and PPO) to prolong the surface circulation half-life and effective tissue accumulation. PEG chains on the surface of nanoparticles can form

a ‘cloud’ of hydrophilic stearic barrier, probably due to its high hydrophilicity, chain flexibility, electrical neutrality, and absence of functional groups, which prevent interaction with macrophages or plasma protein, thereby resulting in less RES uptake and prolonged circulation time.^{136,168} PEGylated nanoparticles can effectively suppress the macrophage uptake *in vitro* and prolong the circulation half-life *in vivo*, thus decreasing the accumulation of nanoparticles in the liver.¹⁶⁹⁻¹⁷¹ For example, the multilayered polyelectrolyte nanoshells have been modified with PEG of varying molecular weight (either MW 2000, 5000, or 20000 Da) to form a hydrophilic and long-circulating nanoparticle to determine how the hydrophilicity and the charge on the nanoshell can promote or reduce uptake.¹⁶⁸ Results showed that after 24 h uptake was decreased 3-fold when PEGs of 2000 and 20 000 Da when compared with either positively or negatively charged nanoshell.¹⁶⁸

1.5.2.5 Targeting ligand

The surface modification of nanoparticles is a crucial issue in terms of their uptake by cells and targeted tissue. Surface modifications in the carriers develop an affinity for recognizing and specifically interacting with target cells. This can be accomplished by binding of ligands on the surface of nanoparticles, which are recognized by specific receptors of macrophages and enhance the binding capability as well as facilitate their internalization *via* receptor mediated endocytosis.¹⁷² In this sense a restricted number of macrophage phagocytic receptors are involved including the mannosyl, fucosyl, scavenger, Fc (fragment, crystallizable) receptors those are involved in the recognition of conserved motifs on pathogens.^{31,173} A general practice is to apply polysaccharides or glycoproteins ending in mannose or fucose residues for the affinity of macrophage receptors.¹⁸

Multivalent carbohydrate ligands have proven to yield high-avidity interactions with lectins due to proximity of glycans in space generating a “cluster glycoside effect”.¹⁷⁴ Unlike other glycoprotein receptors, the mannose receptor has the ability to mediate the phagocytosis of saccharide-coated nanoparticles and the pinocytosis of soluble glycoconjugates.¹⁷⁵ This characteristic is exploited in nanocarrier systems for macrophage-mediated therapies by incorporating specific ligands that facilitate their entry into the cells.¹⁸ Furthermore, the availability of macrophage receptors, in terms of

number and nature, are dependent of the differentiation and activation states of the cells. These parameters are essential to consider when designing nanoparticles for macrophage targeting.

Xiong and co-workers reported a strategy for targeted antibiotic delivery to macrophages to treat bacterial infections utilizing a mannosylated nanogel as the drug carrier that undergoes degradation by bacterial enzymes (Figure 1.12).¹⁷⁶ In this approach, the nanogel contains mannosyl ligands conjugated to the shell of PEG arms and core-crosslinked polyphosphoester, thus offering advantages of potentially targeted antibiotic delivery to macrophages that express high level of the mannose receptor as well as drug accumulation at bacterial infection sites through macrophage transport. At the infection site, macrophages further ingest bacteria which trigger the degradation of the drug containing polyphosphoester core by the active phosphatase or phospholipase produced by the bacteria. Jiang *et al.* developed mannosylated chitosan-graft-polyethyleneimine copolymer for targeting into antigen presenting cells having mannose receptors.¹⁷⁷

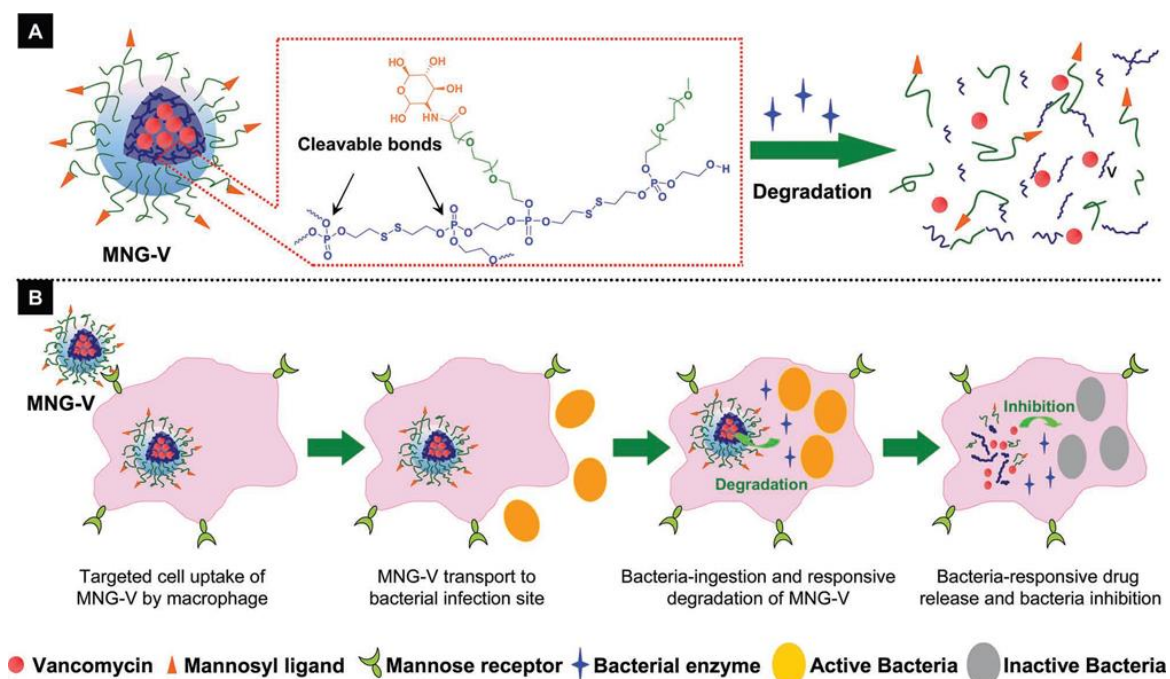


Figure 1.12: (A) Schematic illustration of vancomycin-loaded mannosylated nanogels (MNG-V) and the bacteria-responsive drug release; (B) Schematic illustration of targeted uptake of MNG-V, transport, degradation, drug release and bacteria inhibition.¹⁷⁶ Mannose is incorrectly presented in this published Figure 1.12.

Recently, Ratner and co-workers reported that the glycopolymers with mannose or *N*-acetylglucosamine showed increased uptake by macrophages both *in vitro* and *in vivo* compared to galactose-containing glycopolymers.¹⁷⁸ To determine the macrophage-specific targeting, various glycopolymers displaying pendent carbohydrate moieties were fluorescently labelled. They found that mannose- and *N*-acetylglucosamine containing glycopolymers were able to specifically target mouse bone marrow-derived macrophages (BMDMs) *in vitro* in a dose-dependent manner as compared to a galactose-containing glycopolymer (30- and 90-fold higher uptake, respectively). The *in vivo* experiment using alveolar macrophages also demonstrated the similar results where 6-fold higher internalization of mannose glycopolymer were reported as compared to galactose by following intratracheal administration in mice (Figure 1.13).^{178,179}

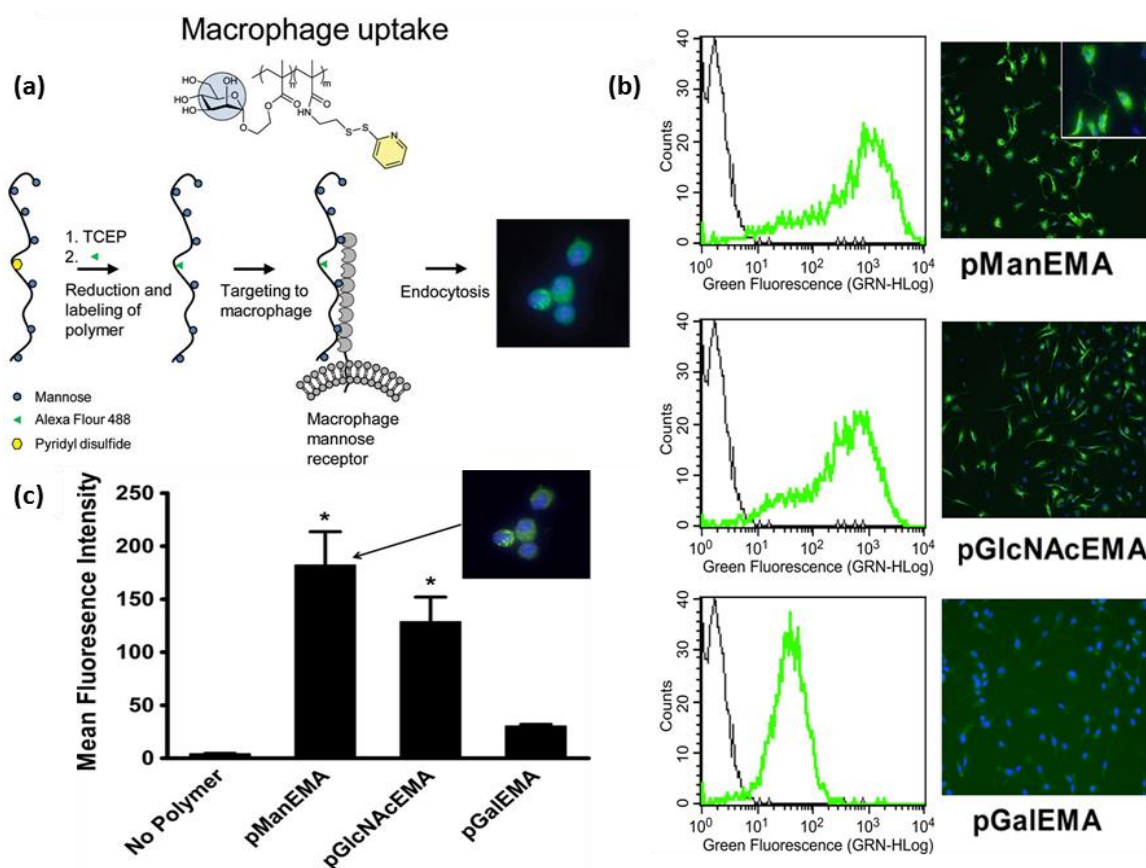


Figure 1.13: (a) The binding and subsequent endocytosis of fluorescent mannose glycopolymers by the macrophage mannose receptor.¹⁷⁹ (b) *in vitro* BMDM glycopolymer uptake. Inset shows a higher magnification image of the AF488-pManEMA treated cells. (c) internalization of glycopolymers by alveolar macrophages *in vivo*. Mice were given 10 mM AF488-glycopolymers intratracheally.

Bronchoalveolar lavage (BAL) was performed after 30 min and BAL cells were analyzed by flow cytometry.¹⁷⁸

Therefore, nanoparticles of different surface properties may be internalized *via* various endocytic mechanisms. For example, folic acid, albumin or cholesterol decorated nanoparticles favour caveolin-mediated endocytosis, which avoids the lysosomal degradation pathways. Alternatively, transferring and cell penetrating peptides encourage the uptake by clathrin-mediated endocytosis and macropinocytosis, respectively. It is still challenging to design nanoparticles for specific endocytic pathways.¹⁸⁰ The endocytosis process depends on the composition, size, surface charge, shape and geometry of nanoparticles and both cell density and type. It is complicated to determine the main contributing factor due to the fact that changing one of these factors can affect other characteristics. For example, increasing the positive or negative charge ratio of nanoparticles to impart higher positive charge can affect the size, stability, and morphology of the formed particles. Furthermore, each mechanism relies on the cell type and treatment conditions. Finally, these endocytic pathways can be interchangeable, which means blocking the uptake through a specific pathway may enhance uptake *via* other endocytic pathways.²³ Excellent reviews on the effect of nanoparticle size, shape and surface chemistry on nanoparticle function have been published elsewhere.^{23,136,181}

1.5.2.6 Mechanical properties and elasticity

Recently, there have been several studies which emphasize the importance of mechanical properties in biological functions.^{182,183} It has been shown that macrophages engulf rigid particles to a significantly higher extent compared to soft particles.¹⁸³ The energy involved in winding up a nanoparticle by the cell membrane decreases as a function of increased stiffness resulting rigid nanoparticles favourable for cellular uptake.¹⁸⁴ However, rigid nanoparticles are easily excreted during *in vivo* administration compared to the elastic nanoparticles which could be simply deformed to squeeze through blood vessels even narrower than their diameter.¹⁸⁵ Therefore, improving the elasticity of the nanoparticles might be an option for enhancing the circulation of the nanoparticles.

1.5.3 Nanoparticles-induced cytotoxicity of macrophages

1.5.3.1 Biodegradability

Biodegradability is an important consideration for designing nanoparticles to target macrophages from the perspective of drug release efficacy and toxicity. It requires degradation or disassociation of the nanoparticle to release the drug efficiently after arriving at its destination. For this, degradation could be triggered by functional moieties that is responsive to specific signal generated from cellular environment including chemical stimulus i.e. enzymes, pH etc.

1.5.3.2 Biocompatibility

Biocompatibility is another crucial characteristic of nanoparticles which prefers to use materials degraded into nontoxic products. The biocompatible glycopolymer with the ability to breakdown into biologically tolerable molecules that are easily metabolized and removed from the body *via* normal metabolic pathways should be used to prepare GNPs by an organic solvent free process.

1.6 Glyconanoparticles for macrophage-mediated therapies

As stated previously, macrophage-specific delivery systems are particularly attractive because macrophages act as host cells for many pathogenic bacteria and parasites that can produce outbreaks of many deadly diseases. In the design of drug carriers for macrophage-mediated infections, issues of safety, toxicity, and bioavailability have to be considered, and the application of GNPs simplifies some of these issues. Therefore, GNPs are emerging as new promising materials to be applied in the design of drug delivery systems upon macrophage targeting. Some recent examples of GNPs based drug delivery system have been described below in terms of bacterial, protozoan, and viral infectious diseases.

1.6.1 Bacterial infectious diseases

In the field of antibiotic therapy, intracellular infections remain difficult to eradicate mainly due to the poor intracellular penetration of most of the commonly used antibiotics. Moreover, bacteria have adapted such that their intracellular localization allows them to be protected from the host immune system as well as the actions of

antimicrobial agents. Thus, new strategies have to be considered in order to counteract these problems, and GNPs loaded with antibiotics represent a promising approach. As shown in previous sections, it is possible to encapsulate, incorporate, or even conjugate therapeutic molecules into different GNPs in order to deliver their payloads intracellularly and hence to treat infections. Several studies have reported the potential application of GNP systems to enhance the selectivity of antibiotics for macrophages and improve therapeutic efficiency in the treatment of intracellular infections.

1.6.1.1 Infection due to mycobacteria

Infections due to mycobacteria are an important global health problem since these microorganisms are responsible for severe diseases including tuberculosis, leprosy, and are in turn responsible for opportunistic infection in immunodepressed patients, such as individuals with AIDS. Tuberculosis (TB) is a common lung infection caused by *Mycobacterium tuberculosis* and is the second most deadly infectious disease which is widely endemic in certain regions.¹⁸⁶ Furthermore, the incidence of tuberculosis has increased recently due to its association with AIDS. The current treatment of pulmonary TB involves prolonged oral administration of high systemic doses of combined antibiotics, with a cocktail of four “front line” drugs: rifampicin, isoniazid, pyrazinamide, and ethambutol, given daily for 6-8 months or longer by oral route, thus it develops undesired side-effects and poor compliance. Moreover, most antibiotics are relatively ineffective for the treatment of intra-macrophage infections of TB owing to the low macrophage permeability and rapid degradation of many drugs used to treat other infections. Therefore, the use of antibiotic delivery systems facilitates the selective shuttling of antibiotics to the site of infections and such systems can provide slow and sustained drug release, which permits administration over longer intervals of time while lowering the systemic doses and shortening the treatment time.

The encapsulation of different antibiotics in GNPs has shown good antibacterial efficacy in both macrophage cell lines and in animal models.¹⁸⁷⁻¹⁹² The aminoglycoside (AG) antibiotics including amikacin, apramycin, gentamycin, kanamycin, neomycin, netilmicin, paromomycin, streptomycin, and tobramycin, are very efficacious against mycobacterium infections, but they are not highly membrane permeable, thus causing a whole range of side effects, particularly nephro- and ototoxicity. Aminoglycoside-

loaded chitosan nanoparticles have been prepared by Lu *et al.* with high drug incorporation efficiency to test for *in vivo* oral efficacy of AG loaded GNPs in a *M. tuberculosis* chronic infection mouse model.⁶⁶

Table 1.2: Polysaccharides based nanoparticles tested for drug delivery to bacteria infected macrophages

Nanocarrier Composition	Targeted microbes	Encapsulated Drug (s)	Targeted cells	Advantages	Ref.
Alginate	<i>Mycobacterium tuberculosis</i>	isoniazid, rifampicin, Pyrazinamide			192
Chitosan	<i>Salmonella typhimurium</i>	Ceftriaxone sodium	J744.2 cells	Inhibits the growth of intracellular <i>S. typhimurium</i>	104
Mannosylated dendrimers	<i>Mycobacterium tuberculosis</i>	Rifampicin	Alveolar macrophages	Enhanced macrophages uptakes of rifampicin	193
Chitosan and Galactomannan	<i>Mycobacterium tuberculosis</i>	Rifampicin	RAW 264.7 cells	Increase intracellular concentration of rifampicin	194
Chitosan	<i>Mycobacterium tuberculosis</i>	siRNA (targeting luciferase)	Murine Alveolar macrophages	Inhalable dry siRNA powders have the possibility of effective pulmonary gene silencing	195
Dextran	<i>Mycobacterium tuberculosis</i>	siRNA (targeting CD45)	Murine Alveolar macrophages	effective siRNA delivery to Resident alveolar macrophages	196,197
Chitosan	<i>Mycobacterium tuberculosis</i>	isoniazid, rifampicin	Murine Alveolar macrophages	Drug loaded nanoparticles are effective against the mycobacterium than free drugs.	198
Chitin	<i>Escherichia coli, S. aureus</i>	rifampicin	human monocytes	exhibits sustained release of antibiotics until 72 hours	199
O-carboxymethyl chitosan	<i>S. aureus</i>	tetracycline	HEK-293 and THP-1 macrophages	Bacterial inhibition increased sixfold compared to free drug	200
chondroitin sulfate and dextran sulfate	<i>Salmonella Paratyphi A</i>	chloramphenicol	RAW 264.7 cells	enhanced intracellular uptake and effectively killed intracellular microbes both <i>in vitro</i> and <i>ex vivo</i>	201
Fucodian coated chitosan	<i>Salmonella Paratyphi A</i>	ciprofloxacin	RAW 264.7 cells	Effective in eradicating <i>Sal²⁰²monella</i> infections and effective in dispersing <i>Salmonella</i> gallstone biofilms.	202

Dextran sulphate was used to shield the positive charge of AG and increase the drug incorporation in the chitosan nanoparticles. They incorporated three amino glycosides: streptomycin, gentamycin, and tobramycin molecules into the GNPs and obtained drug incorporation efficiency 60, 63, and 38%, respectively. The *in vivo* results indicated that oral drug loaded GNPs were effective in killing intracellular *M. tuberculosis* with one log 10 reduction in growth of the bacilli growth for both treated groups, AG loaded GNPs Vs. free AG, at the same concentration of 100 mg Kg⁻¹.⁶⁶ Recently, Grumezescu and co-workers reported water dispersible cross-linked magnetic chitosan nanoparticles for increasing the antimicrobial efficiency of AG antibiotics (kanamycin and neomycin) and reported the AG loaded GNPs reduced the amount of antibiotics necessary for their antimicrobial effect.²⁰³ Hombach *et al.* studied *in vitro* evaluation of an oral tobramycin sulphate delivery system using thiolated chitosan and observed almost 90% of the tobramycin was released within 4 h.²⁰⁴

Saraogi *et al.* described mannosylated gelatin nanoparticles for the selective delivery of antitubercular drug, isoniazid, to alveolar macrophages.¹⁸⁷ They reported the size of the nanoparticles were in range of 260-380 nm where maximum drug payload was found to be 40-55%. The J774 macrophage cell lines were used to evaluate the macrophage targeting efficacy of prepared nanoparticles using fluorescence activated cell sorters (FACS) and found a gradual increase of nanoparticles in macrophage cell lines. The organ distribution studies also demonstrated the efficiency of nanoparticles for spatial delivery of isoniazid to alveolar tissues and significant reduction of bacterial counts in the lungs and spleen of TB-infected mice as well as reduction of hepatotoxicity of the drug.¹⁸⁷ The same group previously studied mannosylated solid lipid nanoparticulate carriers of rifabutin for alveolar macrophages and reported promising *in vitro*, *in vivo* and *ex vivo* alveolar macrophage uptake, drug releases, and haematological studies.¹⁹⁰ Kumar *et al.* reported intracellular macrophage uptake of rifampicin-loaded mannosylated dendrimers and found the dendrimer reduced release rate of drug at pH 7.4, and lowered haemolytic toxicity and cytotoxicity; whereas they observed that the mannosylated dendritic system stimulate significant alveolar macrophage uptake and enhanced drug release at pH 5.0.²⁰⁵

1.6.1.2 Salmonellosis

Salmonella infections occur after ingestion of contaminated food or after contact with another person with the infection. Salmonellosis is caused by the bacteria named as salmonella. Salmonella bacteria are also the reason for typhoid fever when they enter the lymphatic system, which makes treatment more difficult. Salmonella infections and their gallstone associated biofilm infections are challenging to treat due to poor penetration of bioactive molecules into the intracellular sections of macrophages and within biofilms.²⁰²

Dipshikha *et al.* prepared chitosan-dextran sulphate nanocapsule (CD) for efficient targeting and killing intracellular *Salmonella* infection after successfully loading ciprofloxacin into the nanocapsule.¹¹³ Both *in vitro* and *in vivo* experiment displayed significant inhibition of *Salmonella* infections in time-dependent manner upon treatment with antibiotic loaded CD compared to free drug. Noha and Mohamed developed ceftriaxone sodium (CTX)-loaded chitosan nanoparticles for the intracellular delivery of the poorly cell-penetrating antibiotics CTX against *Salmonella typhimurium*.¹⁰⁴ The prepared CTX-chitosan nanoparticles exhibited considerable reduction of *S. typhimurium* in cano-2 and macrophages J774.2 cells compared to placebo nanoparticles.¹⁰⁴

1.6.1.3 Staphylococcus aureus

Staphylococcus aureus (*S. aureus*) is a major cause of infectious morbidity and mortality in community and hospital settings and the causative agent of a wide variety of illness such as skin infections, meningitis, pneumonia, osteomyelitis, endocarditis and sepsis. *S. aureus* occasionally causes intracellular infections by invading phagocytes like monocytes, macrophages, and polymorphonuclear leukocytes and can survive intracellularly for 4-7 days without affecting host cell viability.²⁰⁶

Maya *et al.* reported tetracycline encapsulated *O*-carboxymethyl chitosan nanoparticles (Tet-*O*-CMC Nps) *via* ionic gelation for its sustained delivery of Tet into macrophages.²⁰⁶ They described sixfold effective killing of intracellular *S. aureus* compared to tetracycline alone upon treatment in HEK-293 and differentiated THP1 macrophage cells.²⁰⁶ Zhongwei co-workers developed gentamycin sulfate (GS)-loaded

carboxymethyl-chitosan (CM-chitosan) formulation to achieve superb inhibition on bacterial growth and biofilm formation of *S. aureus*.²⁰⁷ They also reported the loading GS was beneficial for the osteoblastic MC3T3-E1 cell responses as well as enhance the antibacterial efficiency. The biocompatibility of the prepared CM-chitosan could be altered by the concentrations of crosslinker and GS.²⁰⁷

1.6.2 Protozoan infectious diseases

Leishmania is a parasite that causes various infectious diseases and is transmitted through vector insects (sandflies). It can spread to the visceral organs including liver and spleen, resulting in visceral leishmaniasis, or to mucous membranes of the mouth and nose. This disease is endemic to many countries and causes death if not treated appropriately. Currently, the number of infected patients has increased owing to co-infection with HIV.²¹ *Leishmania* are obligate intracellular parasites that cause infection only in the phagolysosome of host macrophages. The localization of these parasites within the lysosomal vacuoles of reticuloendothelial macrophages hampers the access and bioavailability of antileishmanial drugs.¹⁰ Thus, it is necessary to design nanocarriers for targeting antileishmanial drugs to macrophages to increase their bioavailability. Furthermore, the encapsulation of antileishmanial drugs is desirable to overcome their adverse side effects.

There are many drugs available with antileishmanial activity, but their use is limited because of their toxicity or the appearance of resistance. The drugs of choice are pentavalent antimonials including meglumine antimonials, or sodium stibogluconate, but these are toxic for both liver and skin. Amphotericin B and pentamidines are also used as antileishmanial drugs, but these are toxic to the liver and heart. Other antileishmanial drugs include aphidicolin, atovaquone, primaquine, cytotoxic drugs, such as doxorubicin and methotrexate, and plant substances such as amarogentin and andrographolide.²¹

Recently, lectin-functionalized lipo-polymersome encapsulated Amphotericin B (AmB) has been designed for specific internalization *via* lectin receptors overexpressed on infected macrophages in treatment of visceral leishmaniasis.²⁰⁸ Chaubey *et al.* studied curcumin-loaded mannosylated chitosan nanoparticles for the treatment of visceral

leishmaniasis with particle size of 215 nm and drug entrapment efficiency of 82.12%.¹⁰² They also performed drug release behaviours and cellular uptake *in vitro* and *in vivo* by using J774A.1 macrophage cell line with parasite strain *Leishmania donovani*. The pharmacokinetic study of the drug-loaded GNPs showed significant improvement in the value of mean resident time compared to free drug. An *in vivo* uptake study indicated that endocytosis took place effectively within the macrophages of reticuloendothelial system.¹⁰² This group also studied rifampicin loaded mannose-conjugated chitosan nanoparticles for the treatment of visceral leishmaniasis.¹⁷³ Astana and co-workers reported Amphotericin B-encapsulated nanoemulsion template-based chitosan nanocapsules for visceral leishmaniasis on the J774A model cell line and the *in vitro* result showed 50% inhibitory concentration (IC₅₀) of 0.2 µg AmB/ml compare to free drug. *In vivo* experiments in conjunction with effective internalization by macrophages illustrated the efficacy of AmB loaded GNPs at augmenting antileishmanial characteristics.²⁰⁹

1.6.3 Viral infectious diseases

Human immunodeficiency virus (HIV) is a Lentivirus that causes acquired immunodeficiency syndrome (AIDS), a condition in humans in which the immune system begins to fail leading to life-threatening infections.²¹⁰ The joint United Nations Programme on HIV and AIDS (UNAIDS) reported that around 2.1 million new cases with 1.1 million AIDS-related death just in 2015.²¹¹ Although two viral types of HIV (HIV-1 and HIV-2, share ~30-60% genetic similarity) are responsible for AIDS, type 1 (HIV-1) exhibits most of the global burden of AIDS because of its greater transmission rates and more rapid clinical progression.²¹² The monocyte-macrophage system is the first to be infected by HIV and can interact non-specifically with cell surface receptors and other lectins, heparan-sulfate moieties, or natural receptors with cellular host proteins present in the viral envelop.²¹³ Generally infection involves initial binding of the viral envelop glycoprotein gp 120 to the CD4 receptor on the extra-cellular side, which undergoes conformational changes leading to further interaction with other co-receptors, thereby delivering the viral core to the cytoplasm where there is reverse-transcription the viral RNA genome into DNA.^{213,214} It supports the intracellular replication of the virus prior to integration into the host genome by viral integrase in the

cell nucleus where the infected host cell acts as a reservoir, thus favouring the dissemination of the infection and protects the virus against antiretroviral treatment.²¹⁵

Stavudine is active against HIV, but has insufficient macrophage penetration capacities and low bioavailability, which rise to appearance of resistance and toxic effects due to accumulation in other organs.²¹⁶ The application of nanocarrier systems allows doses to be lowered and convey the drug into the site of infection because macrophage infected by HIV show greater phagocytic activity than healthy cells.

The encapsulation of Stavudine in various nanoparticles enhances the penetration into human macrophages in all cases.²¹⁰ Recently, Stavudine loaded chitosan nanoparticles have been developed for treating AIDS.^{216,217} Dev *et al.* designed poly(lactic acid)/chitosan nanoparticles for anti-HIV drug lamivudine delivery.²¹⁸ Stearate-g-chitosan oligosaccharide polymeric micelles were used to deliver antiviral drug lamivudine and showed high cellular uptake percentage with low cytotoxicity against viral transfected tumor cells.²¹⁹ Azidothymidine-triphosphate, the active form of Zidovudine, displays an important pharmacological activity for the treatment of HIV. Chitosan nanoparticles have been synthesized for the intracellular delivery of triphosphate analogues, Zidovudine, for the treatment of HIV with minimal particle size of 200 nm and encapsulation efficiency of 70%.²²⁰ More recently, the saquinavir-loaded chitosan nanoparticles have been reported as potent anti-HIV therapeutic systems with drug encapsulation efficiency of 75% and cell targeting efficiency greater than 92%.²²¹ As compared to soluble free drug control, the saquinavir-loaded chitosan carriers caused superior arresting of viral proliferation as measured by using NL4-3 and Indie-C1 viral strains and different target T-cells.²²¹

1.6.4 Fungal infections

Fungal infections are global public health problem especially in management of individuals who have weakened immune system such as those who have HIV/AIDS or cancer. Candidiasis, aspergillosis and cryptococcosis are one of the major causes of morbidity and mortality in immunocompromised patients. For example, invasive candida infections are the third most common cause of hospital acquired infection.²²² Once the fungus reaches the bloodstream, phagocytosing cells of the innate immune

system play a vital role to restrain the fungus or allow it to spread to different organs including brain, lungs and kidneys.²²³ The presence of any fungal infection in patients commonly indicates that the host defence systems have been compromised to some extent. Thus, the intracellular location of the pathogens requires high doses to reach therapeutic levels inside the cell which leads to toxic effects. The clinical effect of the fungal disease in the immunocompromised host depends on the nature of the underlying disorder and the types of the fungus involved. In general, fungal diseases are very likely to be progressive in nature, and often disseminated, ultimately becoming life threatening.²²⁴

There are many drugs that can be used to combat all systemic and superficial fungal infections in humans. Management of fungal infections includes oral or topical antibiotics and/or antifungal creams or similar medications. Various effective antifungal agents available include polyenes, azoles, allylamines, flucytosine, morpholines, griseofulvin, hydroxyl-stibamine, triphenylmethanes, iodides and imidazole classes of drugs.^{225,226} Among them, polyene antibiotics are the most widely used in clinical practice because of their broad spectrum antifungal activity. Amphotericin B (Amp B) is the drug of choice against systemic infections including candidiasis, aspergillosis or histoplasmosis and pulmonary aspergillosis. The drug is accumulated in phagocytic cells and enhances the antifungal activity of macrophages and PMNs. The major side effects associated with Amp B are its dose-dependent toxicity to the host, particularly in kidneys. Other side effect of Amp B includes fever to severe haemolytic anaemia, headache, chills, hypotension, thrombophlebitis, dyspnoea, nausea and acute nephritis, limiting its complete exploitation as a suitable therapeutic measure.²²⁷

Chemical analogues of Amp B have been prepared to improve the biodistribution and reduce the toxic side effects, but have not led to the success anticipated. Therefore, different drug delivery systems have been demonstrated to deliver Amp B while eliminating its toxic side reactions as well as increasing its therapeutic index. The use of the liposomes, lipid complexes and colloidal dispersions as vehicles for Amp B has been demonstrated against a broad range of fungal diseases, such as candidiasis, histoplasmosis and cryptococcosis, allowing the selective administration of Amp B to

phagocytes with higher doses to achieve a sustained drug distribution and systemic trafficking to the sites of active disease, reducing the potential nephrotoxicity of Amp B.

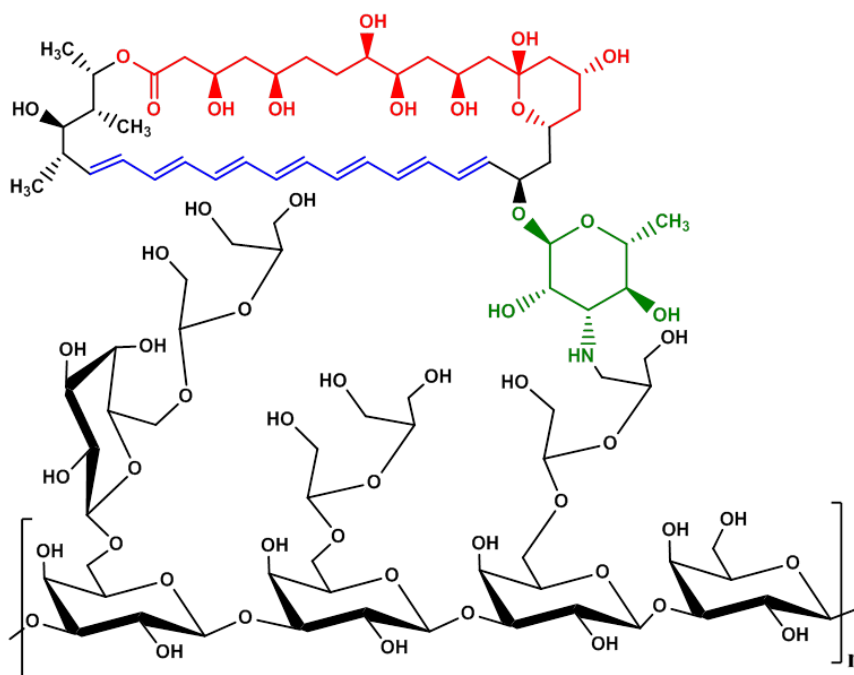


Figure 1.14: Schematic illustration of Amp B conjugated arabinogalactan.^{228,229}

Apart from Amp B delivery, chitosan-tailored cubic nanoparticles were developed by thin film hydration method with Pluronic F127 to deliver clotrimazole antifungal agents to improve the mucoadhesion properties.²³⁰ The concentration of chitosan influences the particle size and mucin binding of cubic nanoparticles while Pluronic F127 only responsible the mucin binding. The optimum concentration of the polymer mixture in the cubic nanoparticles loaded with clotrimazole showed significantly higher antifungal activity than conventional clotrimazole suspension against *C. albicans*.²³⁰ Low-methoxy amidated pectin (LMAP) and carboxymethylcellulose based formulation was prepared to obtain prolonged residence and controlled release of econazole nitrate against *C. albicans* and *C. krusei*.²³¹ Saraf and his group reported cellulose based mucoadhesive gel of novel ternary mixture of miconazole nitrate with efficient killing of *C. albicans*, *Cryptococcus neoformans* and *Sporothrix schenckii*.²³²

1.7 PhD program synopsis

1.7.1 Significance of the project

Protein-carbohydrate interactions are wide spread in living systems and critical in many biological processes including immune response, cellular recognition, and infection. Glyco-ligands targeting proteins have vital role for diseases diagnosis, treatment, and prevention, however the major disadvantage is the low-affinity of interactions between the biomolecules and carbohydrates. The binding strength may be improved by exploiting multivalency such as multivalent glycoligands bind simultaneously to the proteins of interest. By coupling many monomeric ligands or drugs onto appropriate scaffolds such as polymers can create multivalent systems to enhance the activity and stability and lowered toxicity. Therefore, the natural cationic polysaccharide chitosan was selected to conjugate specific carbohydrate sequences on their backbones to target macrophages. Moreover, a variety of liposomal formulation with multivalent targeting ligands was considered as potential therapeutic carrier to macrophages.

It is well known that mannose receptors that are used for phagocytosis and endocytosis of antigens are predominantly expressed on antigen presenting cells (APCs) such as macrophages and dendritic cells.²³³ Macrophages are a promising target for carbohydrate-based therapeutics as they express carbohydrate binding receptors which internalize bound material *via* receptor-mediated endocytosis.¹⁷⁸ Mannose can also recognize the cell-surface mannose receptors by specific ligand-receptor interactions such as macrophage mannose receptor (MMR; CD206) bind oligosaccharides containing terminal mannose residues on infectious agents and transport them into endocytotic pathways. For selective drug delivery to infected cells, we target the MMR of macrophages for a higher affinity of simple mannoside than the corresponding glucosides. We also modify mannoside at the anomeric and C-6 positions with various moieties to furnish a diverse suite of compounds that will be tested against MMR.

On the other hand, macrophage galactose-type lectin (MGL) is expressed at high levels by activated macrophages under inflammatory conditions. Therefore, to develop the GNPs, different target ligands such as mannose and galactose were grafted onto the chitosan main chain to enhance the internalization of the therapeutics. It was the objective to maintain the particle size of the prepared GNPs in the range of 100-200 nm

to obtain better cellular uptake. Finally, amikacin as therapeutic agent was encapsulated into the synthesized GNPs with various loading contents to find the *in vitro* efficacy of the encapsulated drug.

1.7.2 Aims and objectives of the program:

The aim of this program is to design and develop antibiotic encapsulated glyconanoparticles and glyco-coated liposomes for active targeting of macrophages to treat a range of infectious diseases. In order to accomplish this, a series of the following aims to synthesize and testing of the nanoparticles and liposomal delivery systems has been chosen.

Aim 1: Synthesis of glycolipids and study of their potential biological activity against macrophages (Chapter 2 and 4)

Objective 1: It has been hypothesized that the chain length of the glycolipid analogue is important for the physicochemical properties and adjuvant activity upon incorporation into DDAB liposomes. The direct synthesis of 6-fatty acyl and amido mannosides with varying lipid lengths were synthesized to determine the optimal chain length to balance maximal affinity and minimal activation. We have targeted benzyl mannoside derivatives as the aromatic ring is expected to mimic the hydrophobic face of inositol of phosphatidylinositol mannoside (PIM). The cellular toxicity and secretion of pro-inflammatory cytokines of the synthesized glycolipids were determined to explore their possible capabilities to activate macrophages (Chapter 2).

We also synthesized the allyl mannoside derivatives to conjugate the mannose precursor onto the chitosan backbone. To compare stability with analogous of fatty ester derivatives in the cellular environment, 6-fatty acyl and amido mannoside with varying lipid lengths were synthesized (Chapter 4).

Aim 2: Antibiotic loaded glyco-coated liposomal formulation for active targeting of macrophages and their killing efficiency of intracellular bacteria (Chapter 3)

Objective 2: It has also been hypothesized that the poor intracellular penetration of standard amikacin or DSA solutions could be overcome through introducing a targeted delivery system based on a glyco-coated liposomal carrier as an efficient “Trojan

horse". Antibiotic loaded (amikacin and DSA) cationic dimethyldioctadecylammonium bromide (DDAB) with fatty acyl and fatty amido α -D-benzylmannoside liposomes were prepared by the thin film hydration method and characterized *via* DLS (Chapter 3). The efficiency of the drug loaded liposomes was tested against *S. aureus* infected macrophages.

Aim 3: Synthesis and characterization of carbohydrate modified polysaccharides derivatives and preparation and characterization of antibiotic loaded glyconanoparticles (GNPs) (Chapter 4)

Objective 3: A reductive amination reaction (*N*-alkylation) has been performed to exploit the aldehyde group of lactose and the amino group of the glucosamine residues of chitosan to obtain a highly soluble engineered chitosan molecule. The mannose precursors were grafted to the chitosan backbone using carbodiimide chemistry and characterized *via* $^1\text{H-NMR}$ and FT-IR spectroscopy. Finally, the GNPs have been prepared by self-assembling of the modified chitosan where the long lipid chain from glycolipids assembled into the core of the micelles in aqueous environment. Average particle size, polydispersity index (PDI), and critical micelles concentration of the GNPs were determined by the laser diffraction method (DLS). Further, a fluorescence molecule will be attached to the GNPs to trace the cellular uptake of prepared GNPs.

Aim 4: Therapeutic efficiency and *in vitro* activity of the drug loaded GNPs (Chapter 4)

Objective 4: Finally, it was hypothesized that the surface functionalization of prepared GNPs with multivalent lectin binding sugar molecules including mannose, galactose and glycolipids combined with the advantageous properties of GNPs would improve the potential interaction to specific receptors of macrophages. This would control the targeted release of drug at the site of infection as well as improve the stability, rigidity, solubility and pharmacokinetic profile of the GNPs. The loading efficiency (LE) and encapsulation efficacy (EE) of the antibiotic-loaded GNPs were determined using UV-vis spectroscopy. The *in vitro* release profiles of antibiotic from the GNPs were studied at 37°C at pH 5.5 and pH 7.4 to mimic the endosomal and body fluid environment,

respectively. Then the percentage of cumulative amount of released drug was determined by a standard calibration curve.

The U937 (human myelomonocytic leukemia cell line) and RAW 264.7 (a mouse macrophage-like cell line) were used to evaluate the cytotoxicity and macrophage uptake potential of prepared GNPs. The macrophage activation against the prepared GNPs was also determined from the secreted proinflammatory cytokines. Finally, antibacterial activity of drug loaded GNPs were evaluated against *S. aureus* infected macrophages as model biological system to explore the GNPs as efficient drug vehicle.

Chapter 2

STATEMENT OF CONTRIBUTION TO CO-AUTHORED PUBLISHED PAPER

Mosaiab T, Boiteux S, Zulfiker AHM, Wei MQ, Kiefel MJ, Houston TA (2018).

A Simple Glycolipid Mimic of the Phosphatidylinositol Mannoside Core from Mycobacterium tuberculosis Inhibits Macrophage Cytokine Production.

Published in ChemBioChem, 2018, DOI: 10.1002/cbic.201800150.

Publication link: <https://onlinelibrary.wiley.com/doi/abs/10.1002/cbic.201800150>


This chapter includes a co-authored paper. The bibliographic details (published)/status of the co-authored paper, including all authors, are: **Tamim Mosaiab**, Sandra Boiteux, Abu Hasanat Md Zulfiker, Ming Q. Wei, Milton J. Kiefel, and Todd A. Houston.

My contribution to the paper involved:

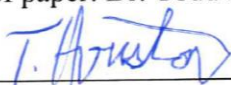
Compounds synthesis, purification and characterization. Experimental design and implementation. Data collection and analysis. Preparation of manuscript and then edited and truncated by my supervisors to develop the final copy of the published journal article.

(Signed)  (Date) 9/11/2018

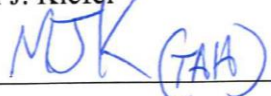
Tamim Mosaiab

(Countersigned)  (Date) 9/11/18

Corresponding author of paper: Dr. Todd A. Houston

(Countersigned)  (Date) 9/11/18

Supervisor: Dr. Milton J. Kiefel

(Countersigned)  (Date) 9/11/18

Supervisor: Dr. Todd A. Houston

JOHN WILEY AND SONS LICENSE
TERMS AND CONDITIONS
Jun 22, 2018

This Agreement between Griffith University -- Tamim Mosaiab ("You") and John Wiley and Sons ("John Wiley and Sons") consists of your license details and the terms and conditions provided by John Wiley and Sons and Copyright Clearance Center.

License Number	4374081172272
License date	Jun 22, 2018
Licensed Content Publisher	John Wiley and Sons
Licensed Content Publication	ChemBioChem
Licensed Content Title	A Simple Glycolipid Mimic of the Phosphatidylinositol Mannoside Core from Mycobacterium tuberculosis Inhibits Macrophage Cytokine Production
Licensed Content Date	Jun 6, 2018
Licensed Content Pages	1
Type of use	Dissertation/Thesis
Requestor type	Author of this Wiley article
Format	Print and electronic
Portion	Full article
Will you be translating?	No
Title of your thesis / dissertation	Glyconanoparticles for targeting macrophages to deliver thereapeutic agents
Expected completion date	August 2018
Expected size (number of pages)	250
Requestor Location	Griffith University G26, Parkland Drive Southport, Queensland 4217 Australia Attn: Griffith University
Publisher Tax ID	EU826007151

Total 0.00 USD

Terms and Conditions

TERMS AND CONDITIONS

This copyrighted material is owned by or exclusively licensed to John Wiley & Sons, Inc. or one of its group companies (each a "Wiley Company") or handled on behalf of a society with which a Wiley Company has exclusive publishing rights in relation to a particular work (collectively "WILEY"). By clicking "accept" in connection with completing this licensing transaction, you agree that the following terms and conditions apply to this transaction (along with the billing and payment terms and conditions established by the Copyright Clearance Center Inc., ("CCC's Billing and Payment terms and conditions"), at the time that you opened your RightsLink account (these are available at any time at <http://myaccount.copyright.com>).

Terms and Conditions

- The materials you have requested permission to reproduce or reuse (the "Wiley Materials") are protected by copyright.
- You are hereby granted a personal, non-exclusive, non-sub licensable (on a stand-alone basis), non-transferable, worldwide, limited license to reproduce the Wiley Materials for the purpose specified in the licensing process. This license, **and any CONTENT (PDF or image file) purchased as part of your order**, is for a one-time use only and limited to any maximum distribution number specified in the license. The first instance of republication or reuse granted by this license must be completed within two years of the date of the grant of this license (although copies prepared before the end date may be distributed thereafter). The Wiley Materials shall not be used in any other manner or for any other purpose, beyond what is granted in the license. Permission is granted subject to an appropriate acknowledgement given to the author, title of the material/book/journal and the publisher. You shall also duplicate the copyright notice that appears in the Wiley publication in your use of the Wiley Material. Permission is also granted on the understanding that nowhere in the text is a previously published source acknowledged for all or part of this Wiley Material. Any third party content is expressly excluded from this permission.
- With respect to the Wiley Materials, all rights are reserved. Except as expressly granted by the terms of the license, no part of the Wiley Materials may be copied, modified, adapted (except for minor reformatting required by the new Publication), translated, reproduced, transferred or distributed, in any form or by any means, and no derivative works may be made based on the Wiley Materials without the prior permission of the respective copyright owner. **For STM Signatory Publishers clearing permission under the terms of the STM Permissions Guidelines only, the terms of the license are extended to include subsequent editions and for editions in other languages, provided such editions are for the work as a whole in situ and does not involve the separate exploitation of the permitted figures or extracts**, You may not alter, remove or suppress in any manner any copyright, trademark or other notices displayed by the Wiley Materials. You may not license, rent, sell, loan, lease, pledge, offer as security, transfer or assign the Wiley Materials on a stand-alone basis, or any of the rights granted to you hereunder to any other person.

- The Wiley Materials and all of the intellectual property rights therein shall at all times remain the exclusive property of John Wiley & Sons Inc, the Wiley Companies, or their respective licensors, and your interest therein is only that of having possession of and the right to reproduce the Wiley Materials pursuant to Section 2 herein during the continuance of this Agreement. You agree that you own no right, title or interest in or to the Wiley Materials or any of the intellectual property rights therein. You shall have no rights hereunder other than the license as provided for above in Section 2. No right, license or interest to any trademark, trade name, service mark or other branding ("Marks") of WILEY or its licensors is granted hereunder, and you agree that you shall not assert any such right, license or interest with respect thereto
- NEITHER WILEY NOR ITS LICENSORS MAKES ANY WARRANTY OR REPRESENTATION OF ANY KIND TO YOU OR ANY THIRD PARTY, EXPRESS, IMPLIED OR STATUTORY, WITH RESPECT TO THE MATERIALS OR THE ACCURACY OF ANY INFORMATION CONTAINED IN THE MATERIALS, INCLUDING, WITHOUT LIMITATION, ANY IMPLIED WARRANTY OF MERCHANTABILITY, ACCURACY, SATISFACTORY QUALITY, FITNESS FOR A PARTICULAR PURPOSE, USABILITY, INTEGRATION OR NON-INFRINGEMENT AND ALL SUCH WARRANTIES ARE HEREBY EXCLUDED BY WILEY AND ITS LICENSORS AND WAIVED BY YOU.
- WILEY shall have the right to terminate this Agreement immediately upon breach of this Agreement by you.
- You shall indemnify, defend and hold harmless WILEY, its Licensors and their respective directors, officers, agents and employees, from and against any actual or threatened claims, demands, causes of action or proceedings arising from any breach of this Agreement by you.
- IN NO EVENT SHALL WILEY OR ITS LICENSORS BE LIABLE TO YOU OR ANY OTHER PARTY OR ANY OTHER PERSON OR ENTITY FOR ANY SPECIAL, CONSEQUENTIAL, INCIDENTAL, INDIRECT, EXEMPLARY OR PUNITIVE DAMAGES, HOWEVER CAUSED, ARISING OUT OF OR IN CONNECTION WITH THE DOWNLOADING, PROVISIONING, VIEWING OR USE OF THE MATERIALS REGARDLESS OF THE FORM OF ACTION, WHETHER FOR BREACH OF CONTRACT, BREACH OF WARRANTY, TORT, NEGLIGENCE, INFRINGEMENT OR OTHERWISE (INCLUDING, WITHOUT LIMITATION, DAMAGES BASED ON LOSS OF PROFITS, DATA, FILES, USE, BUSINESS OPPORTUNITY OR CLAIMS OF THIRD PARTIES), AND WHETHER OR NOT THE PARTY HAS BEEN ADVISED OF THE POSSIBILITY OF SUCH DAMAGES. THIS LIMITATION SHALL APPLY NOTWITHSTANDING ANY FAILURE OF ESSENTIAL PURPOSE OF ANY LIMITED REMEDY PROVIDED HEREIN.
- Should any provision of this Agreement be held by a court of competent jurisdiction to be illegal, invalid, or unenforceable, that provision shall be deemed amended to achieve as nearly as possible the same economic effect as the original provision, and the legality, validity and enforceability of the remaining provisions of this Agreement shall not be affected or impaired thereby.
- The failure of either party to enforce any term or condition of this Agreement shall not constitute a waiver of either party's right to enforce each and every term and condition of this Agreement. No breach under this agreement shall be deemed waived or excused by either party unless such waiver or consent is in writing signed by the party granting such

waiver or consent. The waiver by or consent of a party to a breach of any provision of this Agreement shall not operate or be construed as a waiver of or consent to any other or subsequent breach by such other party.

- This Agreement may not be assigned (including by operation of law or otherwise) by you without WILEY's prior written consent.
- Any fee required for this permission shall be non-refundable after thirty (30) days from receipt by the CCC.
- These terms and conditions together with CCC's Billing and Payment terms and conditions (which are incorporated herein) form the entire agreement between you and WILEY concerning this licensing transaction and (in the absence of fraud) supersedes all prior agreements and representations of the parties, oral or written. This Agreement may not be amended except in writing signed by both parties. This Agreement shall be binding upon and inure to the benefit of the parties' successors, legal representatives, and authorized assigns.
- In the event of any conflict between your obligations established by these terms and conditions and those established by CCC's Billing and Payment terms and conditions, these terms and conditions shall prevail.
- WILEY expressly reserves all rights not specifically granted in the combination of (i) the license details provided by you and accepted in the course of this licensing transaction, (ii) these terms and conditions and (iii) CCC's Billing and Payment terms and conditions.
- This Agreement will be void if the Type of Use, Format, Circulation, or Requestor Type was misrepresented during the licensing process.
- This Agreement shall be governed by and construed in accordance with the laws of the State of New York, USA, without regards to such state's conflict of law rules. Any legal action, suit or proceeding arising out of or relating to these Terms and Conditions or the breach thereof shall be instituted in a court of competent jurisdiction in New York County in the State of New York in the United States of America and each party hereby consents and submits to the personal jurisdiction of such court, waives any objection to venue in such court and consents to service of process by registered or certified mail, return receipt requested, at the last known address of such party.

WILEY OPEN ACCESS TERMS AND CONDITIONS

Wiley Publishes Open Access Articles in fully Open Access Journals and in Subscription journals offering Online Open. Although most of the fully Open Access journals publish open access articles under the terms of the Creative Commons Attribution (CC BY) License only, the subscription journals and a few of the Open Access Journals offer a choice of Creative Commons Licenses. The license type is clearly identified on the article.

The Creative Commons Attribution License

The Creative Commons Attribution License (CC-BY) allows users to copy, distribute and transmit an article, adapt the article and make commercial use of the article. The CC-BY

license permits commercial and non-

Creative Commons Attribution Non-Commercial License

The Creative Commons Attribution Non-Commercial (CC-BY-NC) License permits use, distribution and reproduction in any medium, provided the original work is properly cited and is not used for commercial purposes.(see below)

Creative Commons Attribution-Non-Commercial-NoDerivs License

The Creative Commons Attribution Non-Commercial-NoDerivs License (CC-BY-NC-ND) permits use, distribution and reproduction in any medium, provided the original work is properly cited, is not used for commercial purposes and no modifications or adaptations are made. (see below)

Use by commercial "for-profit" organizations

Use of Wiley Open Access articles for commercial, promotional, or marketing purposes requires further explicit permission from Wiley and will be subject to a fee.

Further details can be found on Wiley Online Library
<http://olabout.wiley.com/WileyCDA/Section/id-410895.html>

Other Terms and Conditions:

v1.10 Last updated September 2015

Questions? customercare@copyright.com or +1-855-239-3415 (toll free in the US) or +1-978-646-2777.

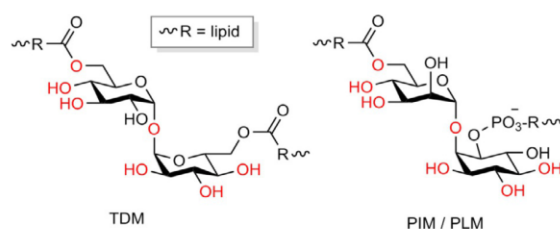
A Simple Glycolipid Mimic of the Phosphatidylinositol Mannoside Core from *Mycobacterium tuberculosis* Inhibits Macrophage Cytokine Production

Tamim Mosaiab,^[a] Sandra Boiteux,^[a] Abu Hasanat Md Zufiker,^[b, c] Ming Q. Wei,^[b] Milton J. Kiefel,^{*[a]} and Todd A. Houston^{*[a]}

Glycolipids from *Mycobacterium tuberculosis* have a profound impact on the innate immune response of the host. Macrophage-inducible C-type lectin (Mincle) is a pattern-recognition receptor that has been shown to bind trehalose dimycolate (TDM) from the mycobacterium and instigate intracellular signalling in the immune cell. There are structural similarities between the structures of TDM and phosphatidyl inositol mannoside (PIM). We thus hypothesized that these latter structures might also modulate an immune response in a similar manner. To test this, we synthesized a series of new mannoside derivatives modified with fatty esters at the 6-position and assessed the release of inflammatory cytokines in human U937 macrophages under the induction of lipopolysaccharides (LPS) after glycolipid treatment. The results showed that the amount of two major cytokines—tumour necrosis factor (TNF)- α and interleukin (IL)-6—released from LPS-stimulated U937 cells decreased significantly when compared to a control upon treatment with the prepared glycolipids, thus indicating a reduction in cytokine production by the macrophages.

Introduction

Glycolipids from *Mycobacterium tuberculosis* (MTB) have a profound impact on the immune response of a human host, allowing the microorganism to survive intracellularly upon capture by macrophages. An important core structure common to several complex glycolipids is the phosphatidylinositol mannoside (PIM; Scheme 1). Importantly, it contains a mannoside at the 2-position of inositol, a position that is unsubstituted in human phosphatidylinositol (PI) species. It is likely that such



Scheme 1. Structural similarity between the core structures of trehalose dimycolate (TDM) and phosphatidylinositol mannoside (PIM) from *Mycobacterium tuberculosis* and phospholipomannan (PLM) from *Candida* (note: PLM contains a phosphodiester in place of the ester at the C6 position of mannose in PIM).

substitution would identify it as “non-self” to pattern-recognition receptors (PPRs) of the innate immune system. A second mannoside is added to the 6-position of inositol, and this PIM2 core can be further decorated with additional mannoside (PIM3–PIM6).^[1] This core is also the starting point for the biosynthesis of the large polysaccharide derivatives, the lipoarabinomannans (LAMs).^[2] Both PIMs and LAMs contain additional lipid modifications at various positions, including the 6-position of the mannose attached directly to the PI anchor.

These two families possess different immunomodulatory activity; whereas PIM facilitates early endosome–phagosome fusion, LAM inhibits the phagosome’s maturation and late endosome–lysosome fusion.^[3] This is in one sense a holding pattern that might allow access to nutrients during MTB latency while avoiding lysosome destruction. LAM from MTB also plays a role in intracellular survival by promoting phosphorylation of the proapoptotic protein Bad from the Bcl-2 family.^[4] Based on the diverse structural features and varied immune modulation profiles of these glycolipids, it is certain that they interact with multiple targets. For example, the mannose trisaccharide caps found on LAM from pathogenic mycobacteria bind the lectin DC-SIGN and dampen IL-12 production in macrophages through a TLR2-dependent (TLR = toll-like receptor) mechanism.^[5] To investigate the role of the PIM core on macrophage cytokine production, we have created a simple monosaccharide mimic of this structure (Scheme 2).

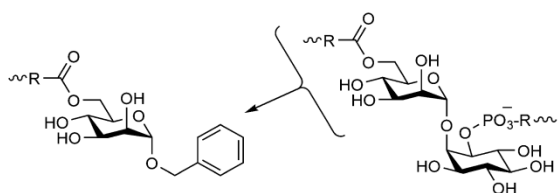
One PRR that might bind the PIM core is macrophage-inducible C-type lectin (Mincle), an important element of the innate immune response to both mycobacterial and fungal infections.^[6] It was initially discovered to play a role in identifying damaged or dead cells by responding to spliceosome-associated protein 130.^[7] Several carbohydrate ligands have been identified—trehalose dimycolate (TDM) from mycobacteria^[8] and

[a] T. Mosaiab, S. Boiteux, Dr. M. J. Kiefel, Dr. T. A. Houston
Institute for Glycomics, Griffith University
Gold Coast Campus, Parklands Drive
Southport, Queensland, 4215 (Australia)
E-mail: m.kiefel@griffith.edu.au
t.houston@griffith.edu.au

[b] Dr. A. H. M. Zufiker, Dr. M. Q. Wei
Menzies Health Institute Queensland and School of Medical Science
Griffith University, Gold Coast Campus
Parklands Drive, Southport, Queensland 4215 (Australia)

[c] Dr. A. H. M. Zufiker
Department of Biomedical Sciences
John C. Edwards School of Medicine, Marshall University
1 John Marshall Drive, Huntington, WV 25701 (USA)

Supporting information and the ORCID identification numbers for the authors of this article can be found under: <https://doi.org/10.1002/cbic.201800150>.



Scheme 2. Fatty acylated mannose derivatives as mimics of the PIM structure.

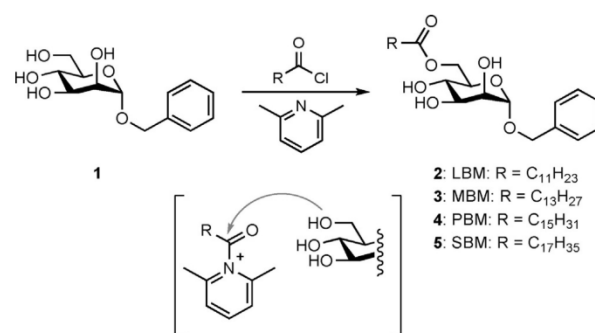
glycolipids from *Malessezia pachydermatis*[9]—and undoubtedly many more will be discovered for this critical component of immune surveillance. We have noted the close structural similarity between TDM and both phosphatidylinositol mannosides (PIMs)^[10] from mycobacteria and phospholipomannan (PLM)^[11] from *Candida albicans*, and believe that this motif (2-mannosyl-inositol) is likely to be recognized by Mincle. As inositol modified at the 2-position has not been identified in mammalian cell-surface components, it is reasonable to assume that Mincle, as a pattern-recognition receptor scouting for pathogen-associated molecular patterns, might have evolved to identify this motif in macrophage-resident microorganisms such as *M. tuberculosis* and *C. albicans*. In fact, Lee and colleagues have shown that Mincle has a higher affinity for simple mannosides than for the corresponding glucosides.^[12] Thus, it is possible that TDM might not be the only cell-surface glycoconjugate on mycobacteria recognized by this lectin, especially as *M. tuberculosis* is replete with mannose conjugates on its exterior. The structures of trehalose and 2-mannosylated inositol are quite similar (Scheme 1), particularly along the sides of both rings *opposite* the lipid anchors of TDM and PIM/PLM. It is important to note that these structures have identical stereochemistry in eight out of nine contiguous stereocentres as highlighted by the red oxygen atoms in Scheme 1. The difference between PIM and PLM occurs at the C6-position of mannose where some PIM derivatives contain fatty esters and PLM extends a large oligosaccharide (mannan).

We are interested in novel methods of drug delivery to treat macrophage infections^[13] and are seeking to identify targeting ligands for this purpose. As Mincle appears to be up-regulated in response to these infections, it could be a target for selective drug delivery to infected cells. Ideally, we require a Mincle ligand that binds the lectin with some avidity but does not activate an inflammatory response in uninfected macrophages. It is important to note that the dimeric structure of TDM is important to both Mincle affinity and its subsequent activation, and glucose monoesters do not activate the Mincle signalling cascade.^[8] Herein, we report the direct synthesis of 6-acyl and 6-amido mannosides with various lipid lengths in order to determine the optimal chain length to balance maximal affinity and minimal activation. Ainge, et al., have reported evidence showing that inositol is responsible for TLR agonist activity,^[10b] whereas more complex, natural PIM₆ structures negatively regulate TLR-4.^[10a] Thus, we targeted benzyl mannoside derivatives, as the aromatic ring is expected to mimic the hydrophobic face of inositol that contains three axial hydrogens

(Scheme 2). In addition, inositol groups often bind aromatic groups on proteins or synthetic receptors,^[14] and the benzyl group might also have π -cation interactions with cationic side chains. Moreover, mannose and its derivatives are widely used to target the macrophage mannose receptor (MMR), a pattern-recognition receptor that is involved in host defence, innate immunity, triggering cytokine production, and modulating cell surface receptors.

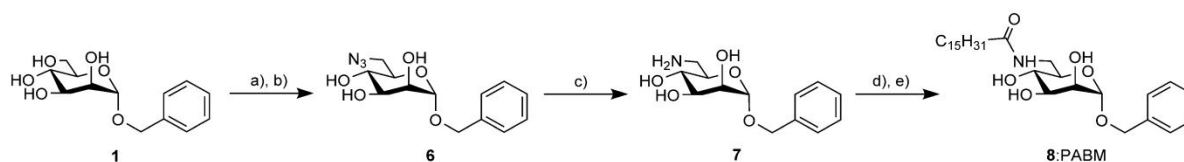
Results and Discussion

Several methods are available for the selective introduction of an ester linkage at the C6 primary hydroxy group of a hexopyranoside.^[15] Previously, we have investigated esterification under Mitsunobu activation to facilitate similar transformations.^[16] However, alkanolic acids tend to be less reactive partners than aryl carboxylic acids in these reactions. Yamamoto and co-workers have shown that the C6 primary alcohol of hexopyranosides can be selectively esterified by using 2,4,6-trimethylpyridine activation of acid chlorides.^[17] 2,6-Dimethylpyridine also contains methyl substituents on the carbons adjacent to the pyridine nitrogen. The pyridinium intermediate shown in Scheme 3 is more reactive toward primary than toward secondary alcohols due to steric shielding of the carbonyl carbon by the *ortho*-type methyl groups on trimethylpyridine. We chose to compare 2,4,6-trimethylpyridine and 2,6-dimethylpyridine for selective esterification of benzyl α -D-mannoside (**1**; Scheme 3).



Scheme 3. Synthesis of C6-esterified benzyl α -D-mannosides. a) **1**, corresponding fatty acid chloride, 2,6-dimethylpyridine, 0 °C, 3 h, RT, 1 h.

Progenitor **1** was synthesized, according to Zunk's method,^[18] in 98% yield. Selective esterification of this monosaccharide was attempted with a range of fatty acid chlorides and either 2,4,6-trimethylpyridine or 2,6-dimethylpyridine as promoter. 2,6-Dimethylpyridine required higher temperatures than 2,4,6-trimethylpyridine (−40 vs. 0–20 °C, respectively) and led to small amounts of diesters being formed. However, these undesired compounds were easily removed by flash column chromatography. The higher reaction temperature used with 2,6-dimethylpyridine allowed conversion to the desired monoesters in a shorter time frame and thus was the preferred method. Four novel compounds—benzyl 6-lauroyl- α -D-manno-



Scheme 4. Synthesis of **8** from **1**. a) *p*-TsCl, pyridine, 0 °C, 12 h; b) NaN_3 , DMF, 100 °C, 24 h; c) $\text{Zn}/\text{NH}_4\text{Cl}$, methanol/water (9:1), RT, 1 h; d) Palmitoyl chloride, pyridine, 0 °C, 12 h; e) Na, MeOH, RT, 24 h.

side (LBM, **2**), benzyl 6-myristoyl- α -D-mannoside (MBM, **3**), benzyl 6-palmitoyl- α -D-mannoside (PBM, **4**), benzyl 6-stearoyl- α -D-mannoside (SBM, **5**)—were synthesized by this protocol in reasonable yields (65–75%). Of particular note is compound **4**, which is derived from palmitoyl chloride, as its lipid matches the chain length common in some PIM structures.^[10]

Because these esters might be subject to cleavage by lipases, we synthesized an amide derivative as a control. To synthesize benzyl palmitoylamido- α -D-mannoside (PABM, **8**), benzyl 6-azido-6-deoxy- α -D-mannoside (**6**) was obtained by following the published protocol of Wang and co-workers, omitting the acetylation/deacetylation sequence (Scheme 4).^[19] The azido group was reduced to amino (compound **7**) by using zinc and ammonium chloride under mild conditions.^[20] This primary amine was then treated with palmitoyl chloride to give PABM with small amounts of acylation at the C3 and C4 positions (confirmed by NMR spectroscopy, data not shown). Deacylation of the esters by using sodium in methanol provided pure PABM.

Having successfully prepared the acyl and amido benzyl α -D-mannosides, the toxicity of these compounds was investigated against human U937 macrophages at different concentrations by MTT assay, so as to allow nonspecific cellular toxicity to be excluded as a credible explanation for any altered cytokine output. As shown in Figure 1, the glycolipids displayed little cytotoxicity on the differentiated U937 cells at concentrations up to 40 μM . These results show that the mannosides are relatively nontoxic, even at fairly high concentrations, and are thus suitable for interrogating macrophage cytokine output.

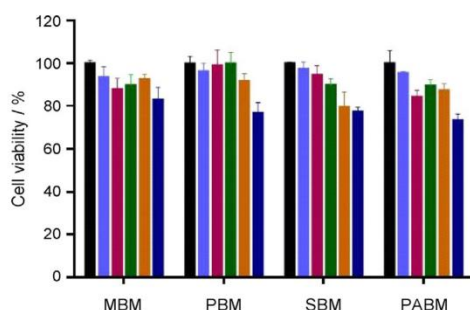


Figure 1. Effects of glycolipids on U937 cell viability. A MTT assay was performed to detect any *in vitro* cytotoxic effects of MBM, PBM, SBM, and PABM against U937 cells after 24 h of incubation. Cells were treated with 0 (■, i.e., DMSO), 5 (■), 10 (■), 20 (■), 40 (■), or 80 μM (■) of corresponding glycolipids, and results were expressed as mean \pm s.d. ($n = 6$) of three independent experiments.

Macrophages play a critical role in the initiation, maintenance, and resolution of inflammation. Stimulated by bacterial endotoxins, such as lipopolysaccharide (LPS), macrophages can secrete large amounts of inflammatory cytokines, such as TNF- α and IL-6, and these inflammatory cytokines further activate macrophages, thus creating a vicious feedback cycle increasing the inflammatory response.^[21] To explore the abilities of our glycolipids to interact with macrophages, we determined the proinflammatory cytokine (TNF- α and IL-6) secretion after incubation with the glycolipids by ELISA. Interestingly, all the glycolipids significantly inhibited cytokine production compared to a control in a dose-dependent manner in LPS-primed macrophages; this inhibition was greater for compounds with longer lipid chains (C_{16}/C_{18}). For instance, the secretions of IL-6 and TNF- α were significantly lower at higher concentration (20 μM) of PBM compared to those in untreated macrophages (Figure 2A). Similar results were observed with SBM, which has an extended steroyl group at the 6-OH position of the mannose (Figure 2B). The levels of TNF- α were not significantly altered by treatment with PBM and SBM in the cells not treated with LPS. To explore the variation of cytokine production by the amide-linked chain at the 6-OH position of mannose, PABM was tested in a similar manner. Upon treatment with PABM, both IL-6 and TNF- α secretions decreased in the LPS-treated cells (Figure 2C). However, the amount of IL-6 was enhanced with 40 μM of PABM; this is the opposite to what was observed with the related ester PBM.

Macrophage phagocytosis of virulent MTB involves MMR, and our results are consistent with previously published results showing that simple mannose can inhibit the secretion of proinflammatory cytokines by upregulated expression of MMR.^[22] The MMR inhibitor mannan (1 mg mL^{-1}) was used to block mannose receptors by treating the differentiated U937 macrophages with it for 1 h. The cells were then treated with the synthesized glycolipids to determine the cytokine production after 24 h at a fixed concentration (20 μM). We still observed significant inhibition of IL-6 and TNF- α secretion in LPS-treated cells (Figure 3A and B); however, there was no considerable amount of cytokines secreted from the LPS-untreated cells. This indicates that these glycolipids exert their anti-inflammatory potential through receptors other than the MMR.

Conclusion

We have successfully synthesized novel mannose derivatives and tested whether they affect the secretion of pro-inflammatory cytokines in human macrophages. The results showed sig-

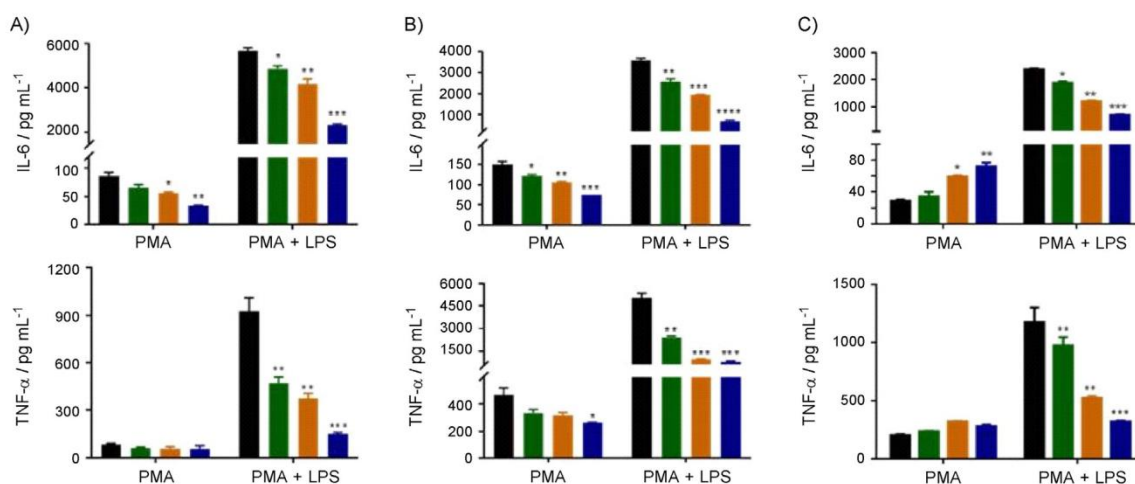


Figure 2. Production of proinflammatory (IL-6 and TNF- α) cytokines after LPS-treated (10 nm) and untreated U937 cells had been treated with DMSO (■), or 10 (■), 20 (■), or 40 μM (■) A) PBM, B) SBM or C) PABM for 24 h. The supernatants were analysed for IL-6 (centre) and TNF- α (right) production by ELISA. For all graphs, the means \pm s.d. of triplicate samples from representative experiments performed in duplicate are shown. * $p < 0.05$, ** $p < 0.01$, *** $p < 0.001$ vs. blank control group.

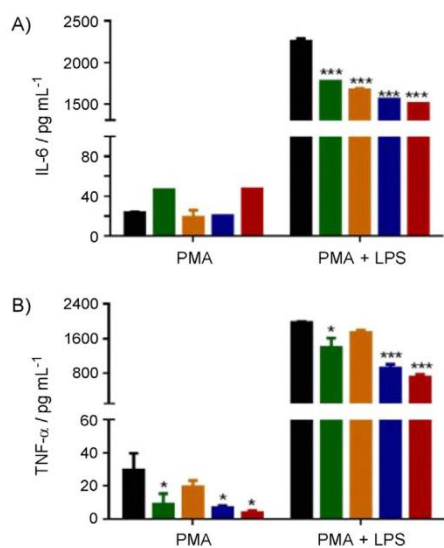


Figure 3. Following treatment with 1 mg mL^{-1} mannan for 1 h (■), LPS-treated (10 nm) and untreated cells were incubated for 24 h with 20 μM of MBM (■), PBM (■), SBM (■), or PABM (■). The supernatants were analysed for A) IL-6 and B) TNF- α production by ELISA. For all graphs, the means \pm s.d. of triplicate samples from representative experiment performed in duplicate are shown. * $p < 0.05$, ** $p < 0.01$, *** $p < 0.001$ vs. blank control group.

nificant reduction in cytokine production in LPS-stimulated macrophages. Our mannose derivatives follow the same trend of activity as monoacylated trehalose derivatives, for which decreasing affinity to Mincle based on fatty ester lipid chain length has been observed.^[23] Further work is necessary to verify the immune cell target(s) of the compounds presented here. These derivatives could be used in liposome preparations

or as components in nanoparticle drug-delivery systems for the treatment of macrophage-resident infections. In addition, one report suggests that compounds of this type (e.g., the methyl mannose analogous to **2**) might have antimicrobial activity as well.^[24]

Experimental Section

Preparation of acylated benzyl α -D-mannopyranosides

General procedure: A solution of benzyl α -D-mannoside (0.2 g, 0.75 mmol) in 2,6-dimethylpyridine (5 mL, 43.2 mmol) at 0 $^{\circ}\text{C}$ was prepared under nitrogen, and a solution of the desired fatty acid chloride (≈ 1.0 mmol) in CH_2Cl_2 (3 mL) was added dropwise. The resulting mixture was stirred vigorously at that temperature for 3 h, then at room temperature (20 $^{\circ}\text{C}$) for 1 h. The reaction was monitored by TLC, which was visualized by UV fluorescence and by charring plates with 5% H_2SO_4 in ethanol. Afterwards, methanol (2 mL) was poured into the suspension, and the mixture was concentrated under reduced pressure. The solid residue was purified by column chromatography on silica gel ($\text{CH}_2\text{Cl}_2/\text{MeOH}$ 10:1) to yield the desired fatty acylated benzyl α -D-mannoside (≈ 65 –70%) as a colourless oil.

Benzyl 6-lauroyl- α -D-mannopyranoside (LBM, **2):** Mannopyranoside **2** was obtained from benzyl α -D-mannopyranoside in 70% yield. $^1\text{H NMR}$ (400 MHz, CDCl_3): $\delta = 0.81$ (t, $J = 6.9$ Hz, 3H; RCH_3), 1.13–1.24 (m, 16H; RCH_2R), 1.54–1.61 (m, 2H; RCH_2R), 2.31–2.35 (m, 2H; $-\text{COCH}_2\text{R}$), 3.51 (t, $J = 9.6$ Hz, 1H; H-4), 3.66–3.70 (m, 1H; H-5), 3.83 (dd, $J = 9.3$, 3.4 Hz, 1H; H-3), 3.93 (d, $J = 1.9$ Hz, 1H; H-2), 4.07 (dd, $J = 12.3$, 2.2 Hz, 1H; H-6a), 4.46 (d, $J = 11.9$ Hz, 1H; $-\text{OCH}_2\text{Ph}$), 4.54 (dd, $J = 12.3$, 4.0 Hz, 1H; H-6b), 4.64 (d, $J = 11.9$ Hz, 1H; $-\text{OCH}_2\text{Ph}$), 4.88 (d, $J = 1.1$ Hz, 1H; H-1), 7.24–7.29 ppm (m, 5H; Ar-H); $^{13}\text{C NMR}$ (CDCl_3): $\delta = 14.13$ (RCH_3), 22.69 (RCH_2R), 24.77 (RCH_2R), 24.96 (RCH_2R), 29.18 (RCH_2R), 29.31 (RCH_2R), 29.35 (RCH_2R), 29.49 (RCH_2R), 29.62 (RCH_2R), 29.63 (RCH_2R), 31.92 (RCH_2R), 34.24 ($-\text{COCH}_2\text{R}$), 63.53 (C6), 67.72 (C4), 69.9 (OCH_2Ph), 70.54 (C2), 70.72 (C5), 71.44 (C3), 99.01 (C1), 128.02, 2×128.05 , 2×128.52 (Ar-H),

136.93 (*ipso*-Ar), 175.0 ppm (-COCH₂R); ES-MS: *m/z* 475.3 [M+Na]⁺, HRMS (ESI): *m/z* calcd for [C₂₅H₄₀O₇+Na]⁺: 475.2666; found: 475.2676.

Benzyl 6-myristoyl- α -D-mannopyranoside (MBM, 3): Mannopyranoside **3** was obtained from benzyl- α -D-mannopyranoside in 72% yield. ¹H NMR (400 MHz, CDCl₃): δ =0.9 (t, *J*=6.8 Hz, 3H; RCH₃), 1.27–1.31 (m, 20H; RCH₂R), 1.67 (dt, *J*=14.8, 7.4 Hz, 2H; RCH₂R), 2.34–2.46 (m, 2H; -COCH₂R), 3.61 (t, *J*=9.6 Hz, 1H; H-4), 3.75–3.79 (m, 1H; H-5), 3.92 (dd, *J*=9.3, 3.4 Hz, 1H; H-3), 4.02 (dd, *J*=3.3, 1.4 Hz, 1H; H-2), 4.17 (dd, *J*=12.3, 2.2 Hz, 1H; H-6a), 4.55 (d, *J*=11.9 Hz, 1H; -OCH₂Ph), 4.62 (dd, *J*=12.3, 4.0 Hz, 1H; H-6b), 4.73 (d, *J*=11.9 Hz, 1H; -OCH₂Ph), 4.97 (s, 1H; H-1), 7.31–7.40 ppm (m, 5H; Ar-H); ¹³C NMR (CDCl₃): δ =14.13 (RCH₃), 22.70 (RCH₂R), 24.77 (RCH₂R), 24.96 (RCH₂R), 29.13 (RCH₂R), 29.20 (RCH₂R), 29.33 (RCH₂R), 29.37 (RCH₂R), 29.51 (RCH₂R), 29.67 (RCH₂R), 29.68 (RCH₂R), 29.71 (RCH₂R), 31.94 (RCH₂R), 34.25 (-COCH₂R), 63.69 (C6), 67.75 (C4), 69.2 (OCH₂Ph), 70.58 (C2), 70.72 (C5), 71.50 (C3), 98.99 (C1), 128.01, 2 \times 128.06, 2 \times 128.52 (Ar-H), 136.93 (*ipso*-Ar), 174.87 ppm (-COCH₂R); ES-MS: *m/z* 503.3 [M+Na]⁺, HRMS (ESI): *m/z* calcd for [C₂₇H₄₄O₇+Na]⁺: 503.2979; found: 503.2985.

Benzyl 6-palmitoyl-benzyl- α -D-mannopyranoside (PBM, 4): Mannopyranoside **4** was obtained from α -D-benzylmannopyranoside in 68% yield. ¹H NMR (400 MHz, CDCl₃): δ =0.9 (t, *J*=6.9 Hz, 3H; RCH₃), 1.27–1.31 (m, 20H; RCH₂R), 1.67 (dt, *J*=12.3, 2.3 Hz, 2H; RCH₂R), 2.37–2.49 (m, 2H; -COCH₂R), 3.60 (t, *J*=9.6 Hz, 1H; H-4), 3.77 (ddd, *J*=9.8, 3.7, 2.3 Hz, 1H; H-3), 3.92 (dd, *J*=9.2, 3.1 Hz, 1H; H-2), 4.02 (dd, *J*=3.4, 1.5 Hz, 1H; H-5), 4.16 (dd, *J*=12.3, 2.3 Hz, 1H; H-6), 4.56 (d, *J*=11.9 Hz, 1H; -OCH₂Ph), 4.64 (dd, *J*=12.3, 3.9 Hz, 1H; H-6a), 4.73 (d, *J*=11.9 Hz, 1H; -OCH₂Ph), 4.97 (d, *J*=1.1 Hz, 1H; H-1), 7.31–7.40 ppm (m, 5H; Ar-H); ¹³C NMR (CDCl₃): δ =14.14 (RCH₃), 22.71 (RCH₂R), 24.97 (RCH₂R), 29.19 (RCH₂R), 29.33 (RCH₂R), 29.38 (RCH₂R), 29.51 (RCH₂R), 29.66 (RCH₂R), 29.68 (RCH₂R), 29.72 (RCH₂R), 31.94 (RCH₂R), 34.25 (-COCH₂R), 63.62 (C6), 67.74 (C4), 69.24 (OCH₂Ph), 70.55 (C2), 70.73 (C5), 71.46 (C3), 99.05 (C1), 128.02, 2 \times 128.06, 2 \times 128.52 (Ar-H), 136.93 (*ipso*-Ar), 174.93 ppm (-COCH₂R); ES-MS: *m/z* 531.1 [M+Na]⁺, HRMS (ESI): *m/z* calcd for [C₂₉H₄₈O₇+Na]⁺: 531.3292; found: 531.3302.

Benzyl 6-stearoyl- α -D-mannopyranoside (SBM, 5): Mannopyranoside **5** was obtained from benzyl α -D-mannopyranoside in 65% yield. ¹H NMR (400 MHz, CDCl₃): δ =0.81 (t, *J*=6.6 Hz, 3H; RCH₃), 1.17–1.18 (m, 28H; RCH₂R), 1.53 (dd, *J*=14.0, 6.9 Hz, 2H; RCH₂R), 2.27–2.31 (m, 2H; -COCH₂R), 3.56 (t, *J*=9.4 Hz, 1H; H-4), 3.69–3.72 (m, 1H; H-5), 3.79 (d, *J*=7.1 Hz, 1H; H-3), 3.89 (s, 1H; H-2), 4.19 (d, *J*=11.6 Hz, 1H; H-6a), 4.36 (d, *J*=5.5 Hz, 1H; -OCH₂Ph), 4.41 (d, *J*=11.7 Hz, 1H; H-6b), 4.62 (d, *J*=11.8 Hz, 1H; -OCH₂Ph), 4.82 (s, 1H; H-1), 7.21–7.28 ppm (m, 5H; Ar-H); ¹³C NMR (CDCl₃): δ =14.13 (RCH₃), 22.71 (RCH₂R), 24.97 (RCH₂R), 29.20 (RCH₂R), 29.33 (RCH₂R), 29.38 (RCH₂R), 29.52 (RCH₂R), 29.68 (RCH₂R), 29.69 (RCH₂R), 29.73 (RCH₂R), 31.94 (RCH₂R), 34.25 (-COCH₂R), 63.63 (C6), 67.74 (C4), 69.23 (OCH₂Ph), 70.56 (C2), 70.72 (C5), 71.47 (C3), 99.0 (C1), 128.01, 2 \times 128.06, 2 \times 128.52 (Ar-H), 136.93 (*ipso*-Ar), 174.91 ppm (-COCH₂R); ES-MS: *m/z* 559.4 [M+Na]⁺; HRMS (ESI): *m/z* calcd for [C₃₁H₅₂O₇+Na]⁺: 559.3605; found: 559.3618.

Synthesis of benzyl palmitoylamido- α -D-mannopyranoside

General procedure: Mannopyranoside **6** was synthesized according to the procedure by Wang et al.^[19] Reduction of **6** by using zinc and ammonium chloride in methanol/water (9:1) produced the desired product benzyl 6-amino-6-deoxy- α -D-mannopyranoside (**7**, 92.5% yield). Palmitoyl chloride (4.5 mm) was added dropwise to a solution of **7** (1 g, 3.7 mmol) in dry pyridine (20 mL) at 0 °C under nitrogen. The reaction was monitored by TLC; the starting

material was consumed completely after 12 h. After the reaction had been quenched with methanol, the solvent was evaporated under vacuum. The crude compound was then dissolved in CH₂Cl₂ (50 mL) and washed with HCl (1 M, 3 \times 50 mL), NaHCO₃ (50 mL), and brine (50 mL), dried over Na₂SO₄, filtered, and concentrated to yield a yellowish solid. The residues were purified by flash chromatography with hexane/EtOAc (5:1) as eluent and a mixture of acylated benzyl palmitoylamido- α -D-mannopyranosides was obtained as a white solid (confirmed by ¹H and ¹³C NMR spectroscopy and mass spectroscopy, data not shown).

To deacylate this mixture, 0.1 mmol was dissolved in dry methanol (50 mL), and sodium metal (0.023 g, 1.0 mmol) was added slowly at 0 °C. The ice bath was removed when the sodium was completely dissolved, and the solution was stirred for 24 h at room temperature. Afterwards, the solution was neutralized on ion-exchange resin (Dowex 50 WX 8–400 ion-exchange resin, Sigma–Aldrich), filtered, and concentrated under reduced pressure to give a yellowish solid. The residue was purified by flash chromatography with EtOAc/hexane (2:3–3:2) to obtain the desired benzyl palmitoylamido- α -D-mannopyranoside as a white solid with yields between 30 and 55%.

Benzyl 6-palmitoylamido- α -D-mannopyranoside (PABM, 9): Mannopyranoside **9** was obtained from benzyl 6-amino-6-deoxy- α -D-mannopyranoside (**7**) in 40% yield. ¹H NMR (400 MHz, CDCl₃/methanol 9:1): δ =0.81 (t, *J*=6.8 Hz, 3H; RCH₃), 1.09–1.25 (m, 24H; RCH₂R), 1.51–1.59 (m, 2H; RCH₂R), 2.14–2.21 (m, 2H; -COCH₂R), 2.95 (d, *J*=14.8 Hz, 1H; H-4), 3.40 (dd, *J*=11.5, 7.7 Hz, 1H; H-3), 3.54 (d, *J*=9.7 Hz, 1H; H-2), 3.92 (s, 1H; H-5), 4.44 (d, *J*=11.9, 1H; H-6), 4.60 (d, *J*=11.9 Hz, 1H; -OCH₂Ph), 4.81 (d, *J*=1.1 Hz, 1H; H-1), 7.27 ppm (dt, *J*=13.5, 4.6 Hz, 5H; Ar-H); ¹³C NMR (CDCl₃): δ =13.96 (RCH₃), 22.59 (RCH₂R), 25.78 (RCH₂R), 29.27 (RCH₂R), 29.42 (RCH₂R), 29.56 (RCH₂R), 29.59 (RCH₂R), 29.66 (RCH₂R), 29.68 (RCH₂R), 31.83 (RCH₂R), 36.23 (RCH₂R), 39.65 (-COCH₂R), 67.42 (C6), 69.25 (C4), 70.37 (OCH₂Ph), 71.21 (C2), 76.78 (C5), 77.30 (C3), 99.26 (C1), 127.80, 2 \times 127.87, 2 \times 128.39 (Ar-H), 137.01 (*ipso*-Ar), 175.95 ppm (-COCH₂R); ES-MS: *m/z* 530.4 [M+Na]⁺.

Cell culture, differentiation, and sample collection for ELISA:

Human leukemic monocyte lymphoma cells U937 were obtained from American Type Culture Collection (ATCC, Manassas, VA, USA) and cultured according to the ATCC procedure. Briefly, cells were cultured in RPMI 1640 (Sigma–Aldrich) medium supplemented with 10% heat-inactivated foetal bovine serum (FBS), penicillin (100 U mL⁻¹), and streptomycin (100 μ g mL⁻¹, Sigma–Aldrich) in a humidified atmosphere of 5% CO₂ at 37 °C and used for experiments between passages 12 and 16. To differentiate the cell line into macrophage-like cells, phorbol 12-myristate 13-acetate (PMA, 50 ng mL⁻¹, Sigma–Aldrich) was added to 5 \times 10⁵ cells in RPMI 1640 medium (1 mL) for 2 days in a 12-well plate. After differentiation, the adherent cells were washed with PBS to remove PMA and non-adherent cells. The adherent cells, referred to as U937 macrophages, were treated with various concentrations of fatty acylated and amido mannose derivatives with or without further stimulation by the lipopolysaccharide (LPS, 100 ng mL⁻¹, Sigma–Aldrich, USA) in fresh culture medium for 6, 12, and 24 h. Then, aliquots (500 μ L) were taken from the supernatant and stored at –80 °C until they were used for measurements by sandwich ELISA assays.

Cell viability

MTT assays: Cell proliferation was evaluated in the MTT assay. U937 cells with PMA (50 ng mL⁻¹) in RPMI 1640 medium (100 μ L) were seeded into a 96-well plate (5 \times 10³ cells/well) for 48 h, washed, and treated with different glycolipids (10, 20, 40, and 80 μ M) for

24 h at 37 °C. After 24 h of treatment, cells were washed with PBS, and MTT stock solution (5 mg mL⁻¹) was then added to each well, and the plate was incubated for an additional 4 h. At the end of the experiment, the medium was replaced with DMSO (100 µL) to dissolve the formazan crystals, and the absorbance was measured at 540 nm by using Polarstar Omega 96-well microplate reader (BMG Labtech GmbH, Germany). The cell viability was calculated from the following formula: Cell viability [%] = (OD_{exp} - OD_{blank}) / (OD_{control} - OD_{blank}) × 100%.

ELISA: Determination of the TNF-α and IL-6 release: Both cytokines were quantified by enzyme-linked immunosorbent assay (ELISA) obtained from elisakit.com, and performed according to producer's instructions. Briefly, supernatants diluted 1:5 in RPMI 1640 (for U937) were incubated in antibody-coated 96-well plates to facilitate the binding of released cytokines. The plates were incubated with a biotinylated primary antibody, then with streptavidin-horse radish peroxidase. All incubation steps were followed by washing, which guarantees the removal of unbound molecules. Horseradish peroxidase is capable of oxidizing its substrate tetramethylbenzidine (TMB) to give a stable staining complex with sulfuric acid that can be detected at 450 nm by a plate reader. The limits of sensitivity for detecting TNF-α and IL-6 were <5 and <1 pg mL⁻¹, respectively, with both intra-assay and inter-assay variability < 10%.

Statistical analysis: Data from all samples within each group were combined and are given as means ± S.E.M. Data were averaged from three independent experiments each containing at least four replicates. Statistical significant was determined by one-way analysis of variance (ANOVA), and a Dunnett's multiple comparison was used to compare the effects among groups by using GraphPad Prism software (v. 6.01, La Jolla, CA). Values with *p* < 0.05 were considered significant.

Acknowledgements

The authors wish to thank the Institute for Glycomics and Griffith University for financial support through a PhD scholarship to T.M. and infrastructure funding within the Institute.

Conflict of Interest

The authors declare no conflict of interest.

Keywords: inflammation · lectins · macrophages · mannose · Mincle

- [1] V. Briken, S. A. Porcelli, G. S. Besra, L. Kremer, *Mol. Microbiol.* **2004**, *53*, 391–403.
- [2] J. Nigou, M. Gilleron, G. Puzo, *Biochimie* **2003**, *85*, 153–166.
- [3] R. A. Fratti, J. Chua, I. Vergne, V. Deretic, *Proc. Natl. Acad. Sci. USA* **2003**, *100*, 5437–5442.
- [4] D. Maiti, A. Bhattacharyya, J. Basu, *J. Biol. Chem.* **2001**, *276*, 329–333.
- [5] E. H. Song, A. O. Osanya, C. A. Petersen, N. L. Pohl, *J. Am. Chem. Soc.* **2010**, *132*, 11428–11430; mannose caps may not dominate LAM interactions with the host, see: B. J. Appelmelk, J. Den Dunnen, N. N. Driesen, R. Ummels, M. Pak, J. Nigou, G. Larrouy Maumus, S. S. Gurcha, F. Movahedzadeh, J. Geurtsen, et al., *Cell. Microbiol.* **2008**, *10*, 930–944.
- [6] M. B. Richardson, S. J. Williams, *Front. Immunol.* **2014**, *5*, 1–9.
- [7] S. Yamasaki, E. Ishikawa, M. Sakuma, H. Hara, K. Ogata, T. Saito, *Nat. Immunol.* **2008**, *9*, 1179–1188.
- [8] E. Ishikawa, T. Ishikawa, Y. S. Morita, K. Toyonaga, H. Yamada, O. Takeuchi, T. Kinoshita, S. Akira, Y. Yoshikai, S. Yamasaki, *J. Exp. Med.* **2009**, *206*, 2879–2888.
- [9] T. Ishikawa, F. Itoh, S. Yoshida, S. Saijo, T. Matsuzawa, T. Gono, T. Saito, Y. Okawa, N. Shibata, T. Miyamoto, S. Yamasaki, *Cell Host Microbe* **2013**, *13*, 477–488.
- [10] a) E. Doz, S. Rose, N. Court, S. Front, V. Vasseur, S. Charron, M. Gilleron, G. Puzo, I. Fremaux, Y. Delneste, F. Erard, B. Ryffel, O. R. Martin, V. F. J. Quesniaux, *J. Biol. Chem.* **2009**, *284*, 23187–23196; b) G. D. Ainge, W. J. Martin, B. J. Compton, C. M. Hayman, D. S. Larsen, G. F. Painter, S. Yoon, I. A. Wilson, J. L. Harper, *J. Med. Chem.* **2011**, *54*, 7268–7279; c) G. M. Rankin, B. J. Compton, K. A. Johnston, C. M. Hayman, G. F. Painter, D. S. Larsen, *J. Org. Chem.* **2012**, *77*, 6743–6759.
- [11] P. A. Trinel, E. Maes, J. P. Zanetta, F. Delplace, B. Coddeville, T. Jouault, G. Strecker, D. Poulain, *J. Biol. Chem.* **2002**, *277*, 37260–37271.
- [12] R. T. Lee, T. L. Hsu, S. K. Huang, S. L. Hsieh, C. H. Wong, Y. C. Lee, *Glycobiology* **2011**, *21*, 512–520.
- [13] a) C. W. Gray, Jr., B. T. Walker, R. A. Foley, T. A. Houston, *Tetrahedron Lett.* **2003**, *44*, 3309–3312; b) K. L. Kramp, K. DeWitt, J. W. Flora, D. C. Muddiman, K. M. Slunt, T. A. Houston, *Tetrahedron Lett.* **2005**, *46*, 695–698; c) T. A. Houston, *Curr. Drug Delivery* **2007**, *4*, 264–268; d) B. T. Walker, T. A. Houston, *Tuberculosis* **2013**, *93*, 102–103.
- [14] a) D. W. Heinz, M. Ryan, T. L. Bullock, O. H. Griffith, *EMBO J.* **1995**, *14*, 3855–3860; b) K. Niikura, A. Metzger, E. V. Anslin, *J. Am. Chem. Soc.* **1998**, *120*, 8533–8534; c) C. W. Gray, K. Barry, E. J. Lindberg, T. A. Houston, *Tetrahedron Lett.* **2007**, *48*, 2683–2686.
- [15] M. Therisod, A. M. Klibanov, *J. Am. Chem. Soc.* **1986**, *108*, 5638–5640.
- [16] a) S. Quader, S. E. Boyd, I. D. Jenkins, T. A. Houston, *Org. Biomol. Chem.* **2006**, *4*, 36–37; b) S. Quader, S. E. Boyd, I. D. Jenkins, T. A. Houston, *J. Org. Chem.* **2007**, *72*, 1962–1979; c) S. Quader, S. E. Boyd, I. D. Jenkins, T. A. Houston, *Carbohydr. Res.* **2015**, *413*, 16–21.
- [17] K. Ishihara, H. Kurihara, H. Yamamoto, *J. Org. Chem.* **1993**, *58*, 3791–3793.
- [18] M. Zunk, M. J. Kiefel, *Tetrahedron Lett.* **2011**, *52*, 1296–1299.
- [19] P. Wang, G. J. Shen, Y. F. Wang, Y. Ichikawa, C. H. Wong, *J. Org. Chem.* **1993**, *58*, 3985–3990.
- [20] W. Lin, X. Zhang, Z. He, Y. Jin, L. Gong, A. Mi, *Synth. Commun.* **2002**, *32*, 3279–3284.
- [21] X. He, J. Shu, L. Xu, C. Lu, A. Lu, *Molecules* **2012**, *17*, 3155–3164.
- [22] a) L. S. Schlesinger, *J. Immunol.* **1993**, *150*, 2920–2930; b) X.-L. Xu, P. Zhang, Y.-H. Shen, H.-Q. Li, Y.-H. Wang, G.-H. Lu, J.-Y. Zhou, *Int. J. Clin. Exp. Pathol.* **2015**, *8*, 6214–6224.
- [23] B. L. Stocker, A. A. Khan, S. H. Chee, F. Kamena, M. S. M. Timmer, *ChemBioChem* **2014**, *15*, 382–388.
- [24] A. Smith, P. Nobmann, G. Henehan, P. Bourke, J. Dunne, *Carbohydr. Res.* **2008**, *343*, 2557–2566.

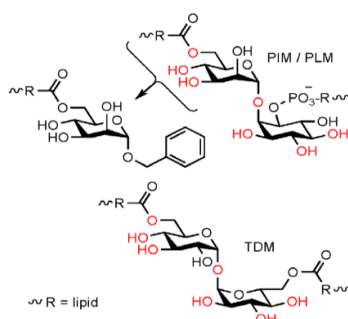
Manuscript received: March 18, 2018

Accepted manuscript online: April 25, 2018

Version of record online: June 6, 2018

COMMUNICATIONS

Inflammatory remarks: New mannose derivatives modified with fatty esters at the C6-position reduce the release of inflammatory cytokines in human U937 macrophages under the induction of lipopolysaccharides (LPS) after synthetic glycolipid treatment.



T. Mosaiab, S. Boiteux, A. H. M. Zulfiker,
M. Q. Wei, M. J. Kiefel,* T. A. Houston*

■ ■ - ■ ■

**A Simple Glycolipid Mimic of the
Phosphatidylinositol Mannoside Core
from *Mycobacterium tuberculosis*
Inhibits Macrophage Cytokine
Production**



CHEMBIOCHEM

Supporting Information

A Simple Glycolipid Mimic of the Phosphatidylinositol Mannoside Core from *Mycobacterium tuberculosis* Inhibits Macrophage Cytokine Production

Tamim Mosaib,^[a] Sandra Boiteux,^[a] Abu Hasanat Md Zulfiker,^[b, c] Ming Q. Wei,^[b] Milton J. Kiefel,^{*[a]} and Todd A. Houston^{*[a]}

cbic_201800150_sm_miscellaneous_information.pdf

Experimental Section

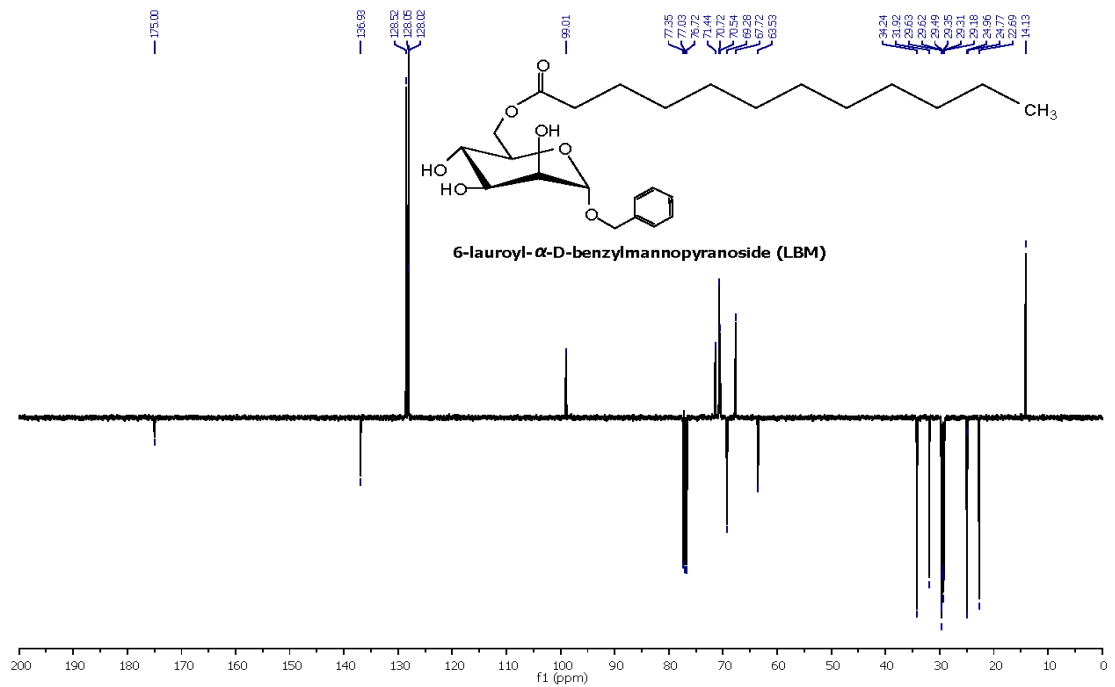
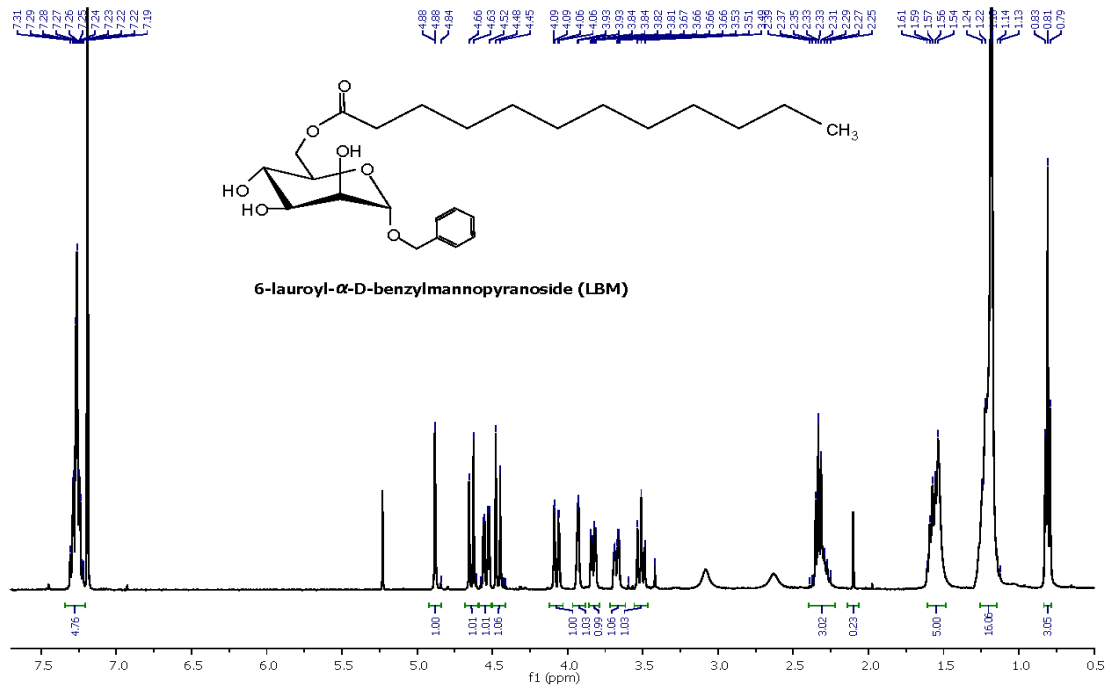
1. General Information

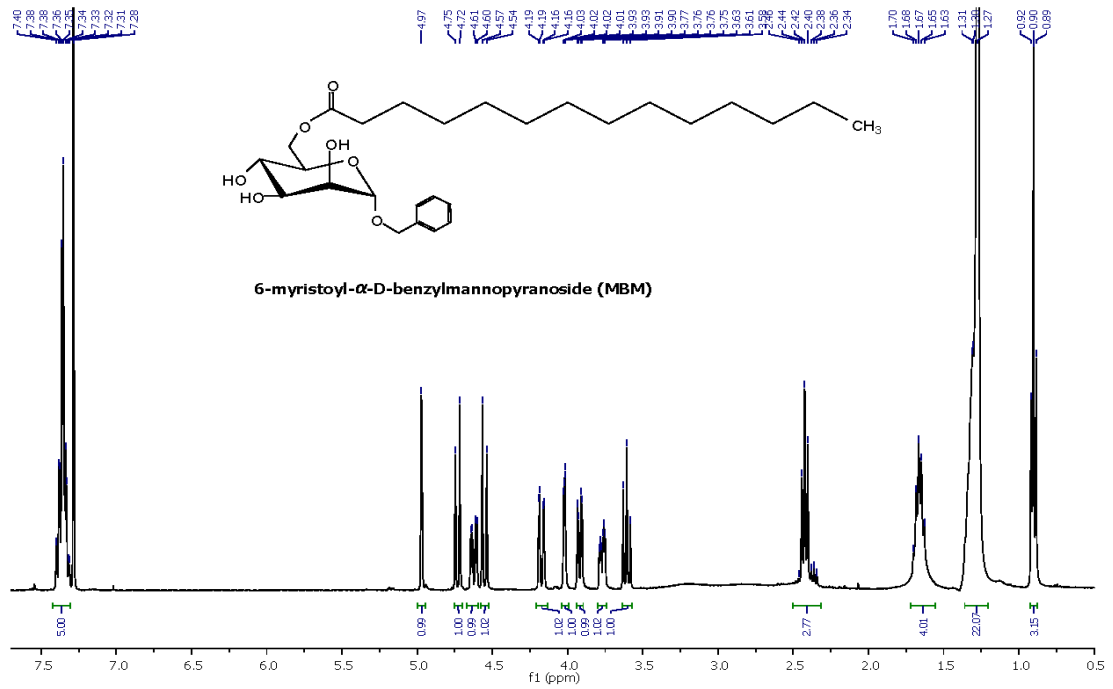
All solvents and reagents used were of analytical grade or distilled prior to use. All reactions were performed under an inert atmosphere of dry argon or nitrogen using distilled dry solvent. α -D-mannopyranoside, benzyl alcohol, acetyl chloride, tosyl chloride, zinc powder, ammonium chloride, sodium azide, 2,6-lutidine, lauroyl chloride, myristoyl chloride, palmitoyl chloride, stearoyl chloride, anhydrous dichloromethane, pyridine and DMF were purchased from Sigma Aldrich Australia. The 2,4,6-collidine was obtained from Alfa-Aesar, Australia and α -D-benzylmannoside was prepared according the literature reported by Zunk et al.^[1]

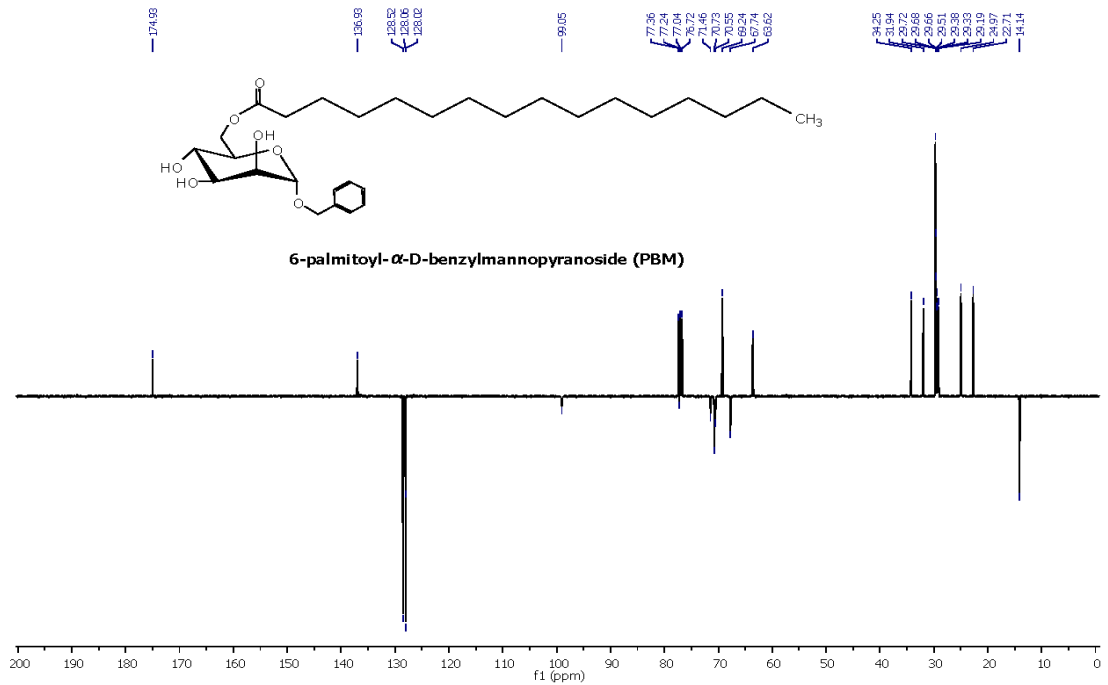
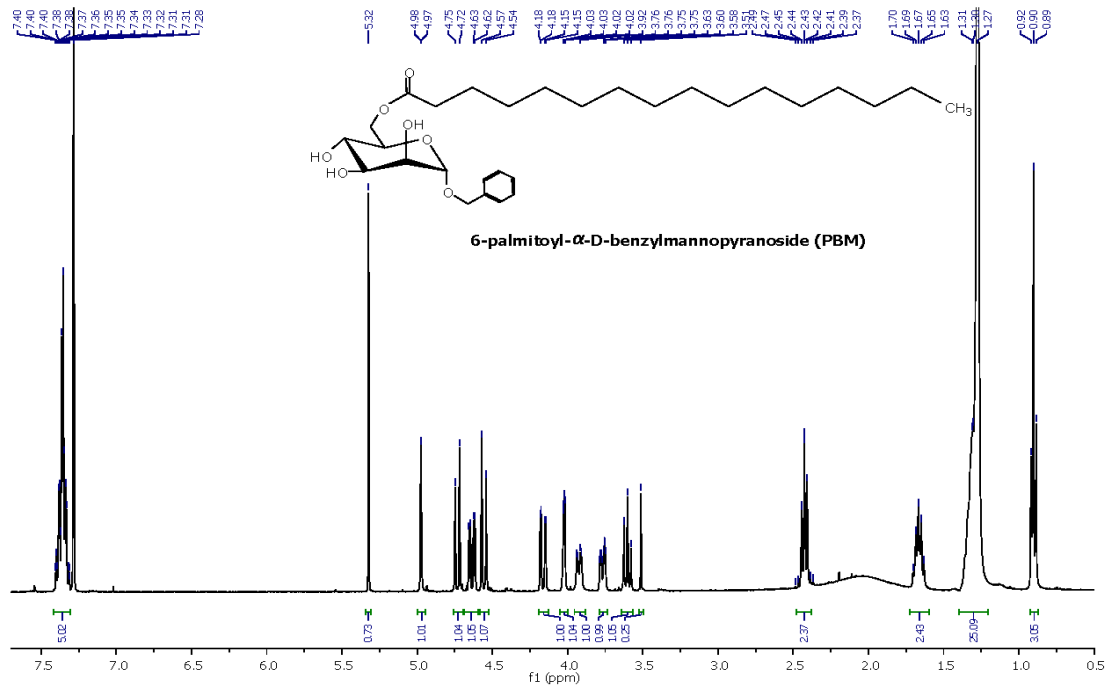
2. Characterization

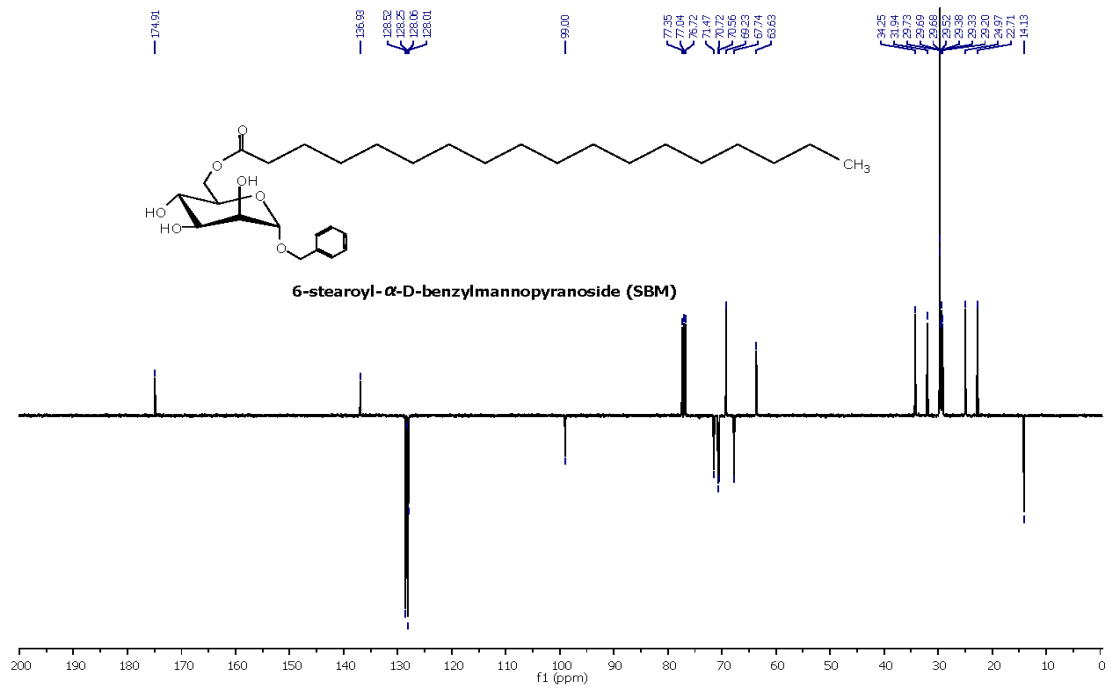
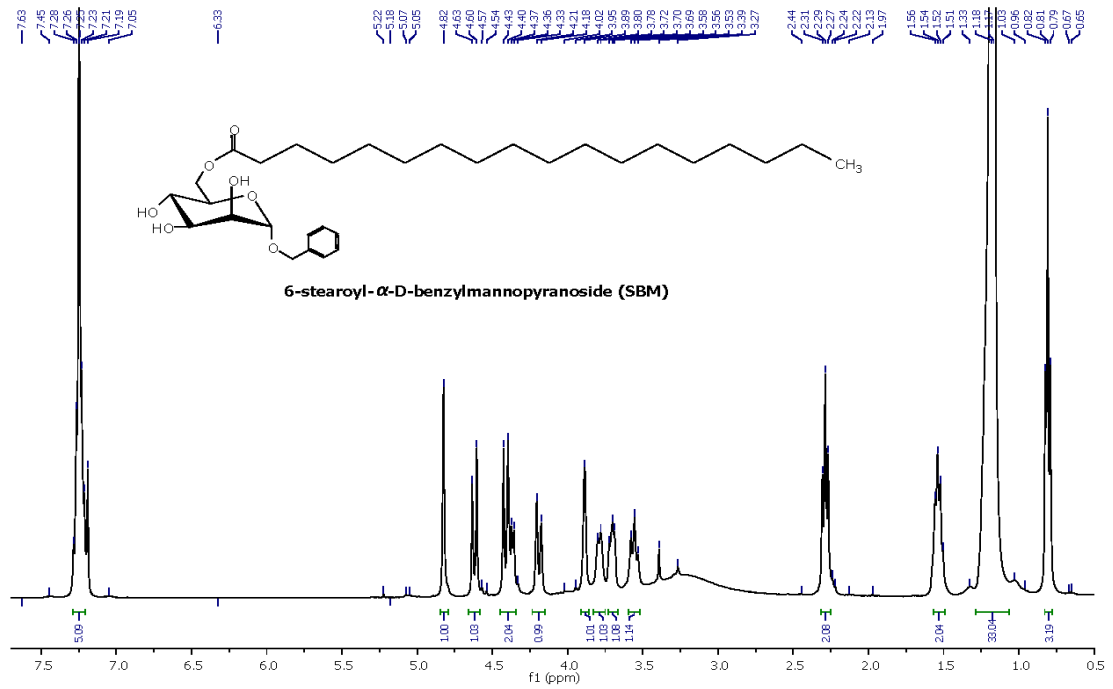
The ^1H and ^{13}C NMR were recorded in the designated solvents on a Bruker Assend 400 MHz spectrometer using tetramethylsilane (TMS) as internal standard. Signals are reported in terms of their chemical shift (δ in ppm) relative to CDCl_3 . Electrospray ionization mass spectra (ESI-MS) were obtained on a Bruker Esquire 3000 Spectrometer. Pre-coated silica gel (0.25 mm thick layer over Al sheet, Merck, Darmstadt, Germany) TLC plates were used to monitor the reactions. Plates were observed under UV light at 254 nm and then visualized after charring using H_2SO_4 . Flash column chromatography was performed using Merck 230-400 mesh silica gel for purification.

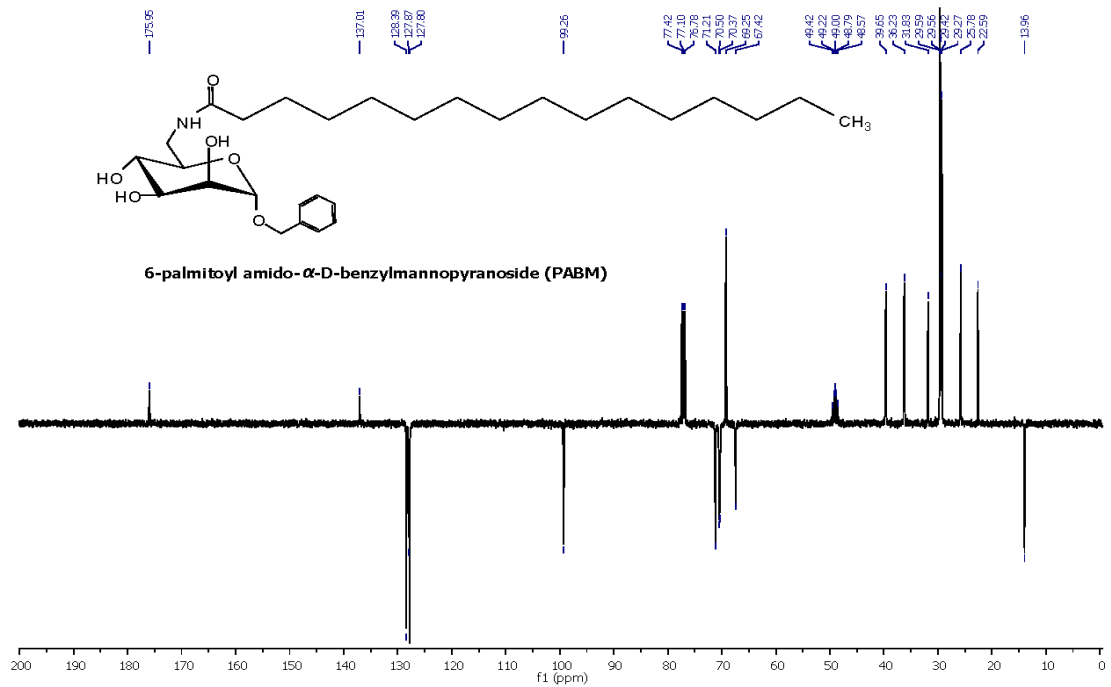
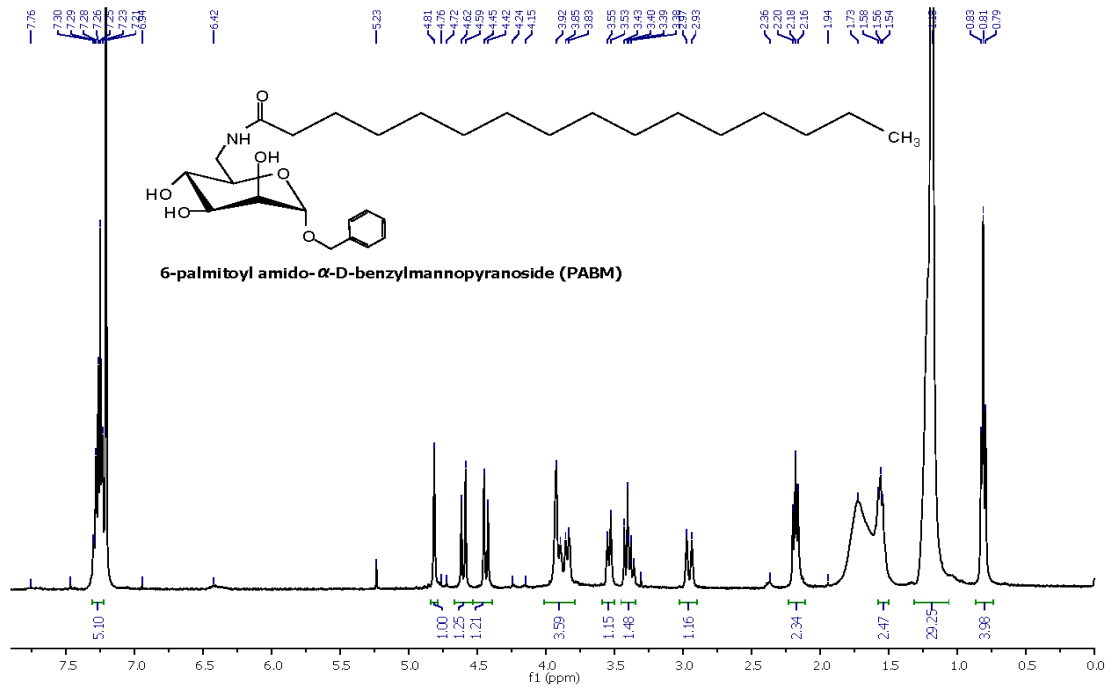
[1] M. Zunk, M. J. Kiefel, *Tetrahedron Lett* **2011**, *52*, 1296-1299.











Chapter 3

Glyco-coated nanoliposomes for intracellular delivery of antimicrobial agents

3.1 Introduction

Intracellular infections including *Mycobacterium* spp., *Salmonella* spp., *Brucella* Spp., *S. aureus*, *Listeria monocytogenes* etc. have developed the ability to generate a number of serious diseases worldwide.^{3,234,235} These intracellular bacteria evolve a number of indigenous mechanisms to take shelter, multiply and spread without damaging the host cells.^{236,237} The intracellular location provides a preferential habitation for microorganisms because they are protected from the host immune system, and are difficult to eradicate, mainly due to the poor cellular penetration, limited intracellular retention and unsatisfactory subcellular distribution of most of the commonly used antibiotics.^{3,238} Moreover, the activity of antibiotics might be influenced by physical and chemical factors such as temperature, pH, enzymes etc.^{239,240} Therefore, the resulting lower intracellular concentration of antibiotics is often ineffective against intracellular pathogens, and results in drug resistance.²³⁶ Additionally, high doses of therapeutics are often necessary to avoid the problems of antibiotic resistance, thus generating many side effects and increased toxicity.²⁴¹

Receptor-mediated targeted drug delivery has been extensively investigated to deliver therapeutics in a safe, efficient and more selective manner.²⁴² Targeted drug delivery is also a promising approach to deliver drugs to the diseased tissue *via* specific interaction over a long period of time. One particular method exploits the interactions of sugars with carbohydrate-binding proteins (lectins) as these are an extremely important factor for specific cellular recognition processes including immune functions, enzyme trafficking, cellular migration, and cancer metastasis.^{39,242} Based on the highly specific carbohydrate-lectin interaction, carbohydrate ligands and their mimetics have been used for targeting drug delivery vehicles to site-specific carbohydrate-binding receptors.^{243,244} Particularly, the efficiency of mannosylated nanocarrier drug delivery systems can be described to their potential ability to target mannose receptors, which are highly expressed in the immune cells such as macrophages and dendritic cells.^{48,245-247}

Liposomes, the most extensively studied class of nanocarriers, form small lipid-bilayer(s) membrane vesicles surrounding an aqueous core that can be prepared with different lipid compositions in various particle sizes and charges.^{248,249} Liposomes are made from natural and biodegradable non-toxic lipid molecules (mostly phospholipids) and can bind or encapsulate drug molecules onto or into their membranes.⁴ The ease of design and preparation of liposomes allows formulation of optimal therapeutic loading and drug delivery to target specific cells or tissues.^{250,251} Moreover, active targeting of liposomes enhances the pharmacological effect of drugs as well as reduces their potential side-effects during therapy.²⁵² Active targeting methods employ ligands that specifically interact with receptors presented on the cell surface of interest to encourage liposomes binding and internalization.²⁵³ As mentioned, promising route to achieve this goal is by targeting lectin receptors presented on the surface of immune cells to maximize selectivity and therapeutic efficiency. Furthermore, multivalency of a targeting moiety can be introduced to the liposome's surface to enhance binding. However, high ligand density may increase immunogenicity and promote nonspecific interaction with normal cells including endothelial and other non-immune cells, resulting in a reduction of cell selectivity and/or in opsonization-mediated clearance of liposomes.^{18,49,224}

Aminoglycoside antibiotics, including amikacin, gentamicin, streptomycin, neomycin, and tobramycin are extremely potent antimicrobial agents that are broadly active against both Gram positive and gram-negative bacteria.^{15,254,255} However, these antibiotics penetrate eukaryotic cell membranes very slowly and their high polarity reduces the bactericidal activity by the acidic endosomal pH when they reach the cytoplasm, resulting poorly activity against strictly intracellular bacteria.²⁵⁶ Additionally, it is necessary to maintain a narrow range of plasma concentrations of aminoglycosides to minimize the nephro- and ototoxicity.²⁵⁷ To overcome this impediment, encapsulation of aminoglycosides in the aqueous cavity of liposomes may promote the therapeutic index and achieve effective intracellular delivery by increasing the concentration of the antibiotic at the site of infection. This increases specific subcellular distribution of aminoglycosides, as has been demonstrated for amikacin.^{237,256,258,259}

Amikacin consists of multiple amino groups attached to the various saccharide rings (Figure 3.1a) which makes it basic, strongly polar and cationic in nature at physiological pH making it highly soluble in water. The chemical structure of amikacin is less susceptible to enzymatic inactivation which promotes its efficiency in long-term clinical treatment.²⁶⁰ Amikacin is active against a range of intracellular bacteria such as *S. aureus*, *Pseudomonas aeruginosa*, *Mycobacterium tuberculosis*.^{257-259,261} Therefore, we chose amikacin as model therapeutic to eradicate intracellular bacteria upon loading into a liposomal formulation.

N-Alkylsulphonylacetamide compounds can potentially target fatty acid synthesis and have been found to have potent antimicrobial properties.²⁶²⁻²⁶⁵ Our group previously reported the synthesis and antitubercular activity of *n*-decanesulphonylacetamide (DSA, Figure 3.1b) with a minimum inhibitory concentration (MIC) of 2.85-5.69 μ M (BACTEC radiometric growth assay, *M. tuberculosis* H37Rv).²⁶² This result is comparable to first line drugs used to treat tuberculosis. DSA can inhibit the synthesis of mycolic acids which is a clinically effective method due to its importance in *Mycobacterium* survival used by a number of antitubercular agents including the frontline drug isoniazid.^{264,266} Recently, we found that DSA can also prevent *S. aureus* growth as well (unpublished data).

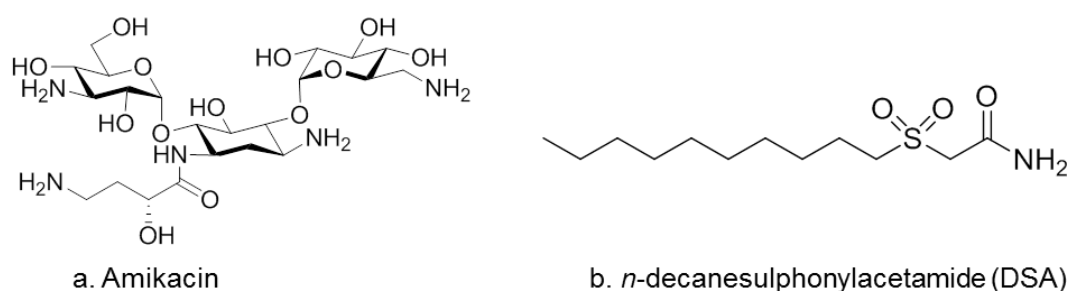


Figure 3.1: Chemical structure of amikacin (a) and DSA (b).

In Chapter 2, we have reported various low-molecular-weight glycolipids to introduce the sugar moieties on the exposed liposomal surfaces for targeting of macrophages to deliver antibiotics.²⁶⁷ Briefly, the direct synthesis of benzyl 6-acyl mannoside and benzyl 6-amido mannoside with palmitoyl (C16) and stearoyl (C18) chain length were

reported as the mimic of the phosphatidylinositol mannoside (PIM) core from *Mycobacterium tuberculosis*. It has been hypothesized that these synthetic glycolipid-coated liposomes may promote the interaction with a variety of mannose binding receptors at the cellular level. More importantly, the mannosylated ligands with high affinity and specificity for macrophage mannose receptor (MMR) or dendritic cell-specific intercellular adhesion molecule-3 grabbing non-integrin (DC-SIGN) receptor and macrophage inducible C-type lectins (Mincle) receptor provide a novel approach for a C-type lectin receptor (CLR)-targeted system that play a central role in innate and adaptive immune responses.²⁶⁷ Moreover, mannosylated drug carrier could be a potential adjuvant delivery system to macrophages by enhancing immune-stimulating activities.³⁸

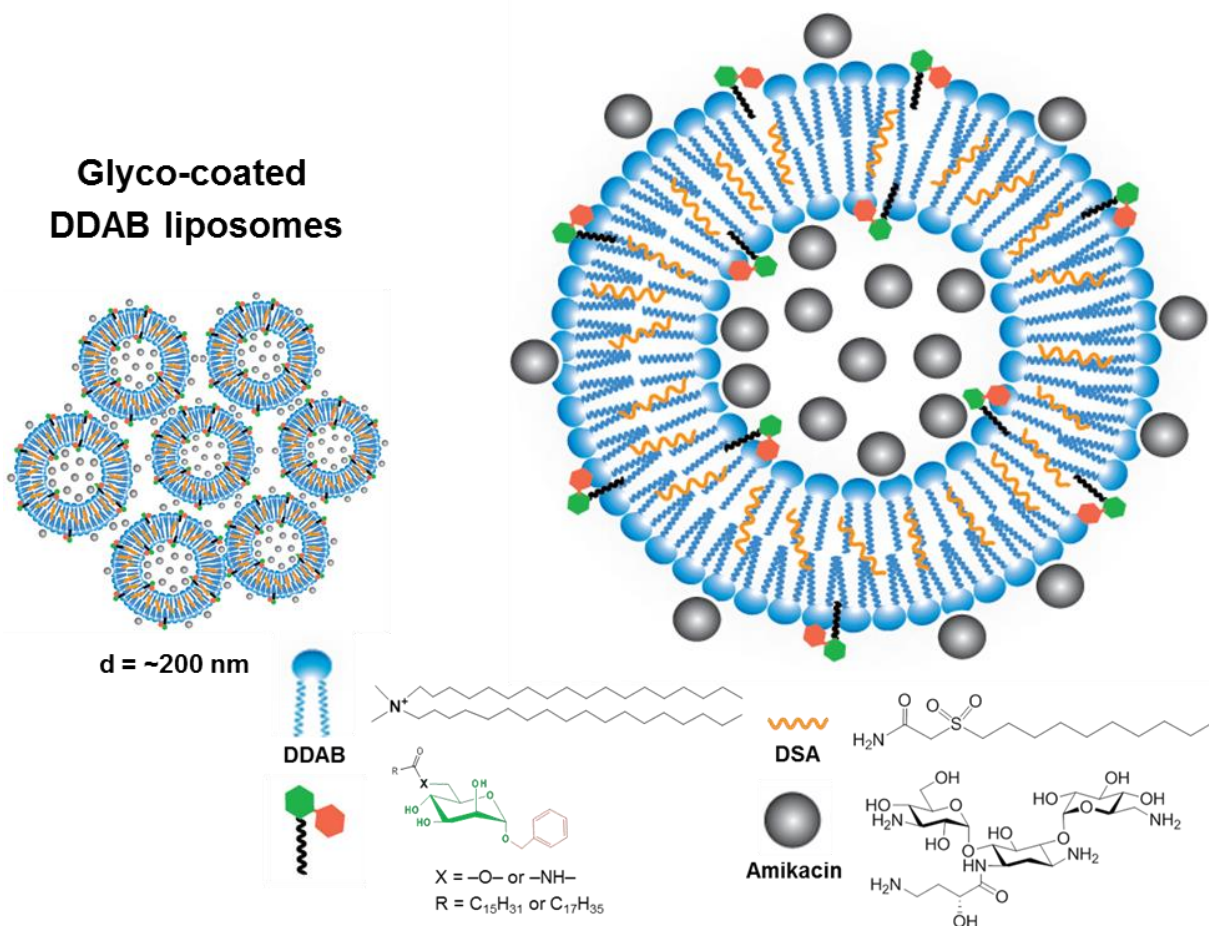


Figure 3.2: Schematic illustration of amikacin and DSA encapsulated glyco-coated DDAB liposomes.

To test our delivery system against an intracellular pathogen *in vitro*, we selected *S. aureus* to infect macrophages. *S. aureus* is a major cause of infectious morbidity and mortality in community and hospital settings and the causative agent of a wide variety of illness such as skin infections, meningitis, pneumonia, osteomyelitis, endocarditis and sepsis. *S. aureus* occasionally causes intracellular infections by invading phagocytes like monocytes, macrophages, and polymorphonuclear leukocytes. Andrew *et al.* reported the intracellular killing of methicillin-resistant *S. aureus* (MRSA) by formulating conventional and PEGylated liposomal vancomycin (lacking of any targeting ligand) to immune cells.²⁶⁸ Raja and co-workers developed an efficient nanomedicine prepared by tetracycline encapsulated *O*-carboxymethyl chitosan and confirmed sixfold increased killing of intracellular *S. aureus* compared to tetracycline alone.²⁰⁶

In the present study, novel glyco-coated liposomal antibiotic delivery systems have been investigated to eradicate intracellular bacteria. Initially, we have synthesized a family of glycolipid analogues using benzyl mannoside with conjugated to a fatty acid chain at C6 position of mannose. To decorate the liposomes, dimethyldioctadecylammonium bromide (DDAB) was used with varying concentrations of glycolipids. We hypothesized that the chain length of the glycolipid analogues is important for the physicochemical properties and adjuvant activity upon incorporation into DDAB liposomes. We therefore evaluated the physicochemical properties and *in vitro* adjuvant effect of the prepared glyco-coated DDAB liposomes in macrophages. Finally, we investigated the intracellular antibiotic efficiency of amikacin and/or DSA loaded glyco-coated DDAB liposomes against *S. aureus*-infected murine macrophages. We hypothesized that the poor intracellular penetration of standard amikacin or DSA solutions could be overcome through introducing a targeted delivery system based on glyco-coated liposomal carrier as an efficient “Trojan horse”.

3.2 Experimental Section

3.2.1 Materials and chemical reagents

Dimethyldioctadecylammonium bromide (DDAB), cholesterol (Chol), amikacin sulphate was purchased from Sigma Aldrich Australia. 1,2-Distearoyl-sn-glycero-3-phosphocholine (DSPC) was obtained from Avanti Polar Lipids (Alabaster, AL, USA). All the glycolipids used to prepare liposomes were synthesized in our previous work (Chapter 2). Among them, four glycolipids namely benzyl 6-palmitoyl- α -D-mannoside (PBM), benzyl 6-stearoyl- α -D-mannoside (SBM), benzyl 6-palmitoylamido- α -D-mannoside (PABM), and benzyl 6-stearoylamido- α -D-mannoside (SABM), were employed. All other solvents and reagents were obtained commercially at analytical grade or distilled prior to use.

3.2.2 Preparation of cationic liposomes

The glyco-coated dimethyldioctadecylammonium bromide (DDAB) liposomes containing increasing amount of glycolipids were prepared by using the thin film hydration method followed by probe sonication and extrusion step to ensure lower particle size with a narrow size distribution as described elsewhere.^{243,269} Briefly, weighed amount of DDAB (1.25 mg/mL; 2.0 mM) and glycolipids (0, 0.125, 0.25, and 0.5 mg/ml) were dissolved in chloroform: methanol (9:1, v/v) and mixed in a 50 mL round-bottom flask to give the appropriate compositions. The organic solvent was removed by rotary evaporation at 40°C and a thin film of dry lipid was deposited on the inner wall of the flask. The film was dried overnight under high vacuum to remove the residual organic solvents. The resultant dry lipid film was rehydrated in 2.5 mL by adding Tris buffer (10 mM, pH 7.4) with the final lipid concentration of DDAB and glycolipids of 2.5 mg/mL and 0.25/0.5/1.0 mM, respectively, corresponding to the DDAB:glycolipid molar ratio of 90:10/80:20/70:30. The lipid mixtures were hydrated at 60°C (10°C above main phase transition temperature of DDAB ($T_m \sim 47^\circ\text{C}$)) for 30 min with 2 min of vigorous vortex mixing every tenth min to ensure complete hydration. After hydration, the dispersion was sonicated in a bath-type sonicator for 10 min at 60°C, followed by a tip-type sonicator (Branson, Danbury, CT, USA) for 3 min at 60°C. Then the liposomes were extruded through two stacked polycarbonate filters of 100 nm

pore size (Nucleopore, Whatman) at 60°C on a Thermobarrel Extruder (Lipex Biomembranes, Vancouver, BC, Canada) to produce unilamellar liposomes.

3.2.3 Size, polydispersity and Zeta-potential of cationic liposomes

Physical characterisation of liposomes including vesicle size measurements and polydispersity index (PDI) were determined by dynamic light scattering (DLS) using the photon correlation spectroscopy technique. The liposome size and PDI explore a quick determination of the batch quality and variation in manufacture. The zeta potential (surface charge) of the particles was estimated by laser-Doppler electrophoresis to find the stability of the liposomes. The liposomes with a higher positive and negative charge disfavour aggregation by repelling themselves in the medium whereas uncharged or low charge liposomes tend to agglomerate over time.²⁷⁰ The prepared liposomes were diluted 10-fold in their corresponding buffer solutions to measure vesicle size and PDI as well as diluted 300-fold during zeta potential measurements. All the data were collected with three independent measurements ($n = 3$). The measurements were performed in triplicate at room temperature using a Zetasizer Nano ZS (Malvern Instruments, Worcestershire, UK) equipped with a 633 nm laser and 173° detection optics.

3.2.4 The colloidal stability of prepared liposomes

The colloidal stability of the liposomal suspensions was studied by sealed the undiluted liposomal dispersion in vials (10 mL capacity, $n = 3$) after flushing with nitrogen for various time periods at 4°C and 25°C, respectively. Liposomal stability was determined by particle size distribution at regular intervals.

3.2.5 Drug loading in liposomes

Liposomes are widely used to carry a variety of drug molecules with different physico-chemical properties. Hydrophilic drugs can be loaded in the aqueous core, while hydrophobic drugs are incorporated into the lipid bilayer and amphiphilic drugs can be partitioned at the surface of the bilayer.

Drug DSA loaded dimethyldioctadecylammonium bromide (DDAB) with fatty acyl and fatty amido α -D-benzylmannoside liposomes were prepared by the thin film hydration

method as the lipophilic DSA could be highly embedded in the lipid bilayer during self-assembly step. Briefly, 2 mL of DDAB (5 mg/mL; 8.0 mM) and 0.4 mL of PBM (5 mg/mL, 10 mM), SBM (5 mg/mL, 10 mM), PABM (5 mg/mL, 10 mM), SABM (5 mg/mL, 10 mM) were dissolved in chloroform/methanol (9:1, v/v) respectively in 25 mL bottom flask and mix thoroughly. The desired amount of DSA (0.1 ml from 4 mg/mL) was then added to each formulation to keep the final concentration of DSA 100 µg/mL and the solvent was removed under vacuum resulting in a thin lipid film. The lipid film was dried overnight under low pressure to remove trace amounts of organic solvents. The lipid film was rehydrated in 4.0 mL Tris-buffer (10 mM, pH 7.4), and sonicated for 5 minutes at 60°C, transferred to glass vials. The lipid mixtures were hydrated at 60°C for 30 min with 2 min of vigorous vortex mixing every tenth min. Then, the particle sizes and zeta-potentials were measured before tip-sonication. The dispersion was tip-sonicated for 45 s with 150W Branson tip-sonicator to reduce the size and PDI of the liposomes. The final lipid concentration of DDAB, glycolipids, and DSA were 2.5 mg/mL, 0.5 mg/mL, and 100 µg/mL respectively, corresponding to the DDAB: Sugar molar ratio of 80:20. The liposomes were extruded through a 0.4 µm membrane filter to obtain better PDI. The liposomes were stored at 4°C until further use.

Amikacin was dissolved in sterile Milli Q water prior to hydration of the lipid film. A thin lipid film layer was formed using various lipid formulations as described above prior to addition of aqueous amikacin solution. The resulting lipid film was hydrated for 2h in 1 mL of aqueous amikacin (5 mg/mL). The gel produced was diluted with 4mL of PBS at pH 7.4. Unilamellar liposomes were formed by following tip sonication as well as sequential extrusion procedure described as above. Non-encapsulated amikacin was removed by ultracentrifugation at 100 000 g for 1 h at 4°C. The pellet was washed once with 2 mL of PBS and the final pellet was re-suspended in 4 mL of PBS. The drug-loaded liposomes were ruptured using 10% Triton X-100 to calculate encapsulation efficiency and quantified with a validated spectrophotometric method described below.

3.2.6 Encapsulation efficiency

Encapsulation efficacy (%) was calculated as the amount of amikacin incorporated in the liposomes compared to the initial total amount of amikacin in solution. The loading efficiency is determined from the amount of amikacin fused in liposomes relative to the

amount of total lipid. The concentration of loaded amikacin into liposomes was measured by ultraviolet-visible spectroscopy (UV-vis) at wavelength 349 nm *via* a derivatization method using *o*-phalaldialdehyde (OPA) reported elsewhere.^{260,271,272} Briefly, the derivatization solution was prepared using 10 mg OPA in 200 μ L absolute ethanol, 10 μ L of 2M DTT aqueous solution, and 20 mL sodium carbonate buffer solution at pH 10.5.²⁶⁰ The amount of amikacin was estimated by measuring the absorbance of a mixed solution containing 300 μ L sample containing the drug and 3 mL of OPA derivatization reagent by comparing a known standard curve.

Encapsulation and drug loading efficiencies were calculated as follows:

$$\text{Encapsulation efficiency (\%)} = \frac{\text{Total amount of added amikacin} - \text{Free amikacin}}{\text{Total amount of added amikacin}} \times 100$$

$$\text{Drug loading efficiency (\%)} = \frac{\text{Amount of amikacin in liposomes}}{\text{Amount of recovered lipid}} \times 100$$

3.2.7 *In vitro* drug release studies

The *in vitro* drug release studies were carried out in PBS at pH 7.4 using pellet dispersion method at 37°C to mimic *in vivo* environment. Drug-loaded liposomes were suspended in PBS at a final lipid concentration of 0.5 mg/mL. In order to measure the amikacin delivery, 300 μ L of solution were withdrawn at desired time intervals and analyzed by the UV-vis spectroscopy method described above. The constant volume of total delivery liquid was ensured by replacing with an equal volume of fresh PBS. Each drug release experiment was employed three times to calculate the mean values and standard deviations. Actual drug release % was determined based on the following equation:

$$\text{Drug release (\%)} = \frac{\text{Release of amikacin at a definite time}}{\text{Total amount of amikacin entrapped within liposomes}} \times 100$$

3.2.8 Bacteria Strains and cell lines

S. aureus strain ATCC 25923 was grown in LB medium at 37°C with 160 rpm shaking. Colony forming units (CFU) were determined after serial dilution and plating the *S. aureus* cells on LB agar plates.

The RAW 264.7 macrophage cell line obtained from American Type Culture Collection (ATCC, Manassas, VA, USA) and cultured according to the ATCC procedure. Briefly, cells were cultured in DMEM (Sigma-Aldrich) medium supplemented with 10% heat-inactivated fetal bovine serum (FBS), 100U/mL of penicillin, and 100 µg/mL of Streptomycin (Sigma-Aldrich) in a humidified atmosphere of 5% CO₂ at 37°C and used for experiments between passages 12 and 16.

3.2.9 ELISA (Detection of TNF- α and IL-6)

The RAW264.7 cells (5×10^5 cells/well) were seeded in 12-well tissue culture plates in 1 mL DMEM medium supplemented with 10% FBS and incubate overnight. The macrophage cells were treated with 50 µg/mL of glyco-coated DDAB liposome in fresh culture medium and then collected the cell culture supernatants after 24 h incubation time. 500 µL aliquots were taken from the supernatant and stored at -80°C until measurement of IL-6 and TNF- α . As a positive control for IL-6 and TNF- α release, the cells were treated with 0.1 µg/mL of the lipopolysaccharide (LPS, Sigma-Aldrich, USA) and the resulting TNF- α secretion was also measured.

Both IL-6 and TNF- α cytokines were quantified by enzyme-linked immunosorbent assay (ELISA) obtained from elisakit.com.au, Australia and the ELISA kit was performed according to producer's instructions.²⁷³ Briefly, diluted supernatants (1:5, in DMEM) were incubated in antibody-coated 96-well plates to facilitate binding of released cytokines. The incubation with a biotinylated primary antibody was performed. The next step was an incubation with streptavidin-horseradish peroxidase. All incubation steps were followed by washing, which guarantees the removal of unbound molecules. Horseradish peroxidase can oxidize its substrate tetramethylbenzidine (TMB), which develops a stable staining complex with sulfuric acid detectable at 450 nm by means of a plate reader. Standard curve for the cytokines were made by using the recombinant proteins delivered in the kit. The limit of sensitivity for detection of TNF- α and IL-6 was <5 and <1 pg/mL, respectively, with both intra-assay and inter-assay variability < 10%.

3.2.10 Macrophage infection and intracellular bacterial inhibition assays

Intracellular antibacterial activity was determined in RAW 264.7 cells infected with *S. aureus* (bacteria/cell ratio of 10) using fully validated procedure reported elsewhere.^{206,268,274} Briefly, 5 μL of processed bacteria containing 10^6 bacteria was added into the macrophage cells (10^5 cells per well) distributed in 12-well tissue culture plates. The infected cells were incubated for 2 h 37°C to allow phagocytosis. The cell medium was then washed with fresh media containing 10% FBS to remove extracellular bacteria those are not phagocytized and washed thoroughly with PBS. Macrophages were then treated with fresh media containing different concentration of standard DSA (15 $\mu\text{g}/\text{mL}$), amikacin (15 $\mu\text{g}/\text{mL}$) and DSA/Amikacin (20 $\mu\text{g}/\text{mL}$) solution and amikacin loaded glyco-coated liposomal formulation with concentration 0, 20, 100, 200 and 500 $\mu\text{g}/\text{mL}$. Cells treated with empty liposomes served as control.

Infected macrophages cultures were terminated at 1, 3, 12, and 24 h post infection. Cell free supernatant from infected bacteria were diluted and plated on LB agar plates to determine extracellular bacterial growth. The infected macrophages were lysed with sterile distilled water to evaluate the intracellular bacterial viability and plating the lysates on LB agar followed by visual counting of bacterial colonies.

3.2.11 Statistics

Data from all samples within each group were combined with means \pm standard error of mean (S.E.M). Data were averaged from three independent experiments each containing at least 4 replicates. Statistical significant was determined by one-way analysis of variance (one-way ANOVA) and a Dunnett's multiple comparison was used to compare the effect among groups using GraphPad Prism software (version 6.01, La Jolla, CA). Values with $P < 0.05$ were considered significant.

3.3 Results and Discussions

Liposomes prepared from DDAB have been widely reported for delivering therapeutic to macrophages.^{243,275} All the glycolipid analogues incorporated into the lipid bilayer of DDAB liposomes by thin-film method and homogenized *via* tip-sonication followed by an exhaustive extrusion. Mannose moieties are the hydrophilic branches of glycolipids which promote them to display an outstretched conformation from the surface of the liposome in the aqueous environment (Figure 3.2). The lipid compositions along with the average vesicle size, polydispersity index (PDI) and zeta-potential of the various glyco-coated liposomes used in the experiments are provided in Table 3.1.

Table 3.1: Lipid composition and physical characterization of DDAB/glycolipids liposomes. The vesicles sizes, PDI and zeta-potentials were measured using Tris buffer (10 mM, pH 7.4) with concentration 0.25 mg/mL. Results denotes mean \pm SD ($n=3$).

Liposome	Composition (molar ratio, m/m)	Vesicle Size (nm)	PDI	Zeta-potential (mV)
DDAB	100:0	470 \pm 19	0.459 \pm 0.049	71.7 \pm 6.4
DDAB/PBM	90:10	295 \pm 12	0.292 \pm 0.025	67.3 \pm 4.8
	80:20	163 \pm 9	0.203 \pm 0.005	59.3 \pm 5.4
	70:30	113 \pm 10	0.311 \pm 0.019	52.3 \pm 8.9
DDAB/PABM	90:10	390 \pm 8	0.388 \pm 0.033	69.0 \pm 3.2
	80:20	160 \pm 5	0.175 \pm 0.015	67.9 \pm 2.6
	70:30	107 \pm 9	0.414 \pm 0.061	60.8 \pm 3.6
DDAB/SBM	90:10	273 \pm 6	0.344 \pm 0.027	69.7 \pm 3.3
	80:20	145 \pm 7	0.226 \pm 0.013	61.0 \pm 4.2
	70:30	182 \pm 17	0.359 \pm 0.045	57.2 \pm 3.4
DDAB/SABM	90:10	280 \pm 11	0.333 \pm 0.023	68.4 \pm 2.9
	80:20	195 \pm 7	0.159 \pm 0.005	69.5 \pm 4.8
	70:30	227 \pm 13	0.354 \pm 0.031	66.8 \pm 1.2

The particle sizes and PDI of the prepared mannosylated DDAB liposomes were significantly lower than the bare DDAB liposomes. This decrease is most likely due to the incorporation of neutral amphiphilic glycolipids which results a slight decline of the surface charges (Table 3.1) as well as enhances liposomal hydrophilicity by forming hydrogen bonds between the extended mannose moieties from the liposomal surface and the buffer medium. However, the sizes of the liposomes decrease upon increasing the amount of glycolipids content in the liposomal composition except for DDAB/SABM. Moreover, similar patterns have been observed for the surface charge of the liposomes where all the liposomes exhibit highly cationic charges in between 52 mV and 72 mV and similar positive surface charges have been reported for DDAB formulated liposomes elsewhere.^{243,276,277} Interestingly, vesicle size distributions as measured by PDI of DDAB/glycolipids with molar ratio 80:20 are lower than the other corresponding glyco-coated liposomal molar ratios. This might results from the better interaction of DDAB and glycolipids at this molar ratio in contrast to the lower or higher ratio of glycolipids formulated into liposomes.

The colloidal stabilities of the prepared glyco-coated DDAB liposomes were determined during storage for 8 weeks at 4°C and 25°C, respectively, by means of the changes in average vesicular size of the liposomes as a function of time. The particle sizes of the pure DDAB liposome (without sugar component) increased over time at both 4°C and 25°C, respectively; indicating their instability upon prolonged storage with formation of visible aggregates and precipitates (Figure 3.3 and 3.4). Similar colloidal stability has also been reported for pure DDAB liposomes in other studies.^{270,277} In contrast, after adding small amounts of glycolipids during liposomal preparation, these exhibited little change in particle sizes at both temperatures indicating that the presence of glycolipids in the DDAB bilayers promotes liposomal stability over time up to 8 weeks (Figure 3.3 and 3.4). One possible reason for improving glyco-coated DDAB liposomal stability is from the interaction between the hydrophilic mannose head-group with the surrounding water molecules which enhances the overall hydration of the liposomal surfaces and protects against dehydration of the quaternary ammonium head-group resulting in less charge repulsion. Jesper *et al.* reported trehalose 6,6'-dibehenate (TDB) incorporated DDAB cationic liposomes and revealed high stability of DDAB/TDB liposomes up to 4 months stability at 4°C, however, they described the dispersion of pure DDAB

liposomes aggregated during the first 10 days of storage.²⁷⁰ Camilla and co-worker discovered the colloidal stability of DDAB formulated liposomes upon incorporation of various amount of trehalose 6,6'-diesters by changing the length of fatty acid group from C12 to C22 and found no visible aggregation or significant change in particle size after 16 weeks at both 4°C and 25°C, respectively.²⁴³

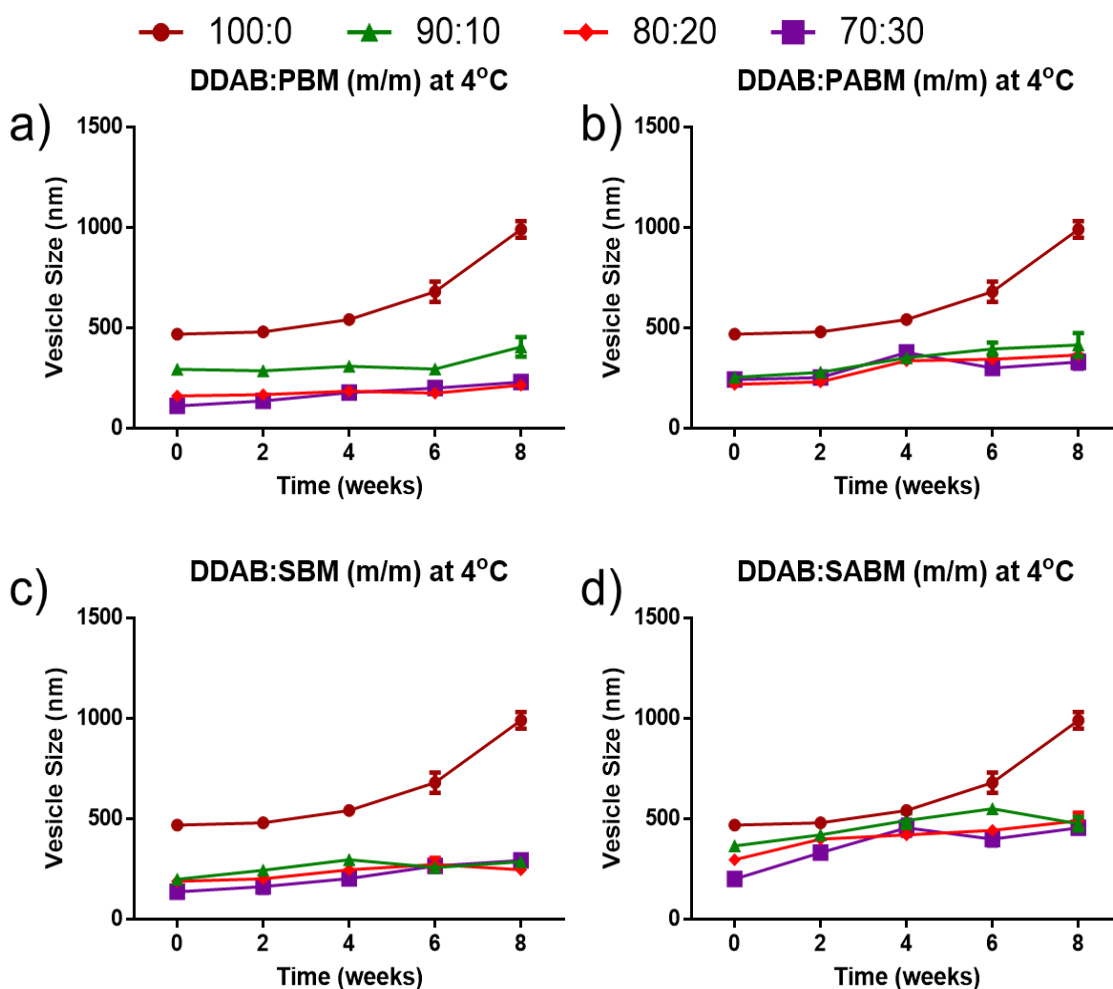


Figure 3.3: Average vesicle size of glyco-coated DDAB liposomes a) DDAB: PBM, b) DDAB: PABM, c) DDAB: SBM, and d) DDAB: SABM containing 0, 10, 20, and 30 mol% of glycolipids at 4°C as an indication of colloidal stability upon storage for 8 weeks. The liposomes were dispersed in 10 mM Tris buffer solution at pH 7.4. Results denote as the means \pm SD of three batches ($n = 3$).

The 20 mol% (80:20) glycolipid containing DDAB liposome show better stability at both temperatures over 8 weeks' time with only very slight change of the particle size (Figure 3.3 and 3.4) which is also confirmed by a reduction in visible precipitates inside the storage vial (photo data not shown). However, vesicle size increases at 25°C after four weeks when we increase the content of glycolipids to 30 mol%. In addition to this, the particle sizes for DDAB:SABM with 10 and 30 mol% of SABM were higher than the other glycolipid formulated liposomes and visible aggregates were observed after 4 weeks' time at both lower and room temperature which could result from the higher PDI of liposomes in those SABM containing molar compositions (PDI data not shown).

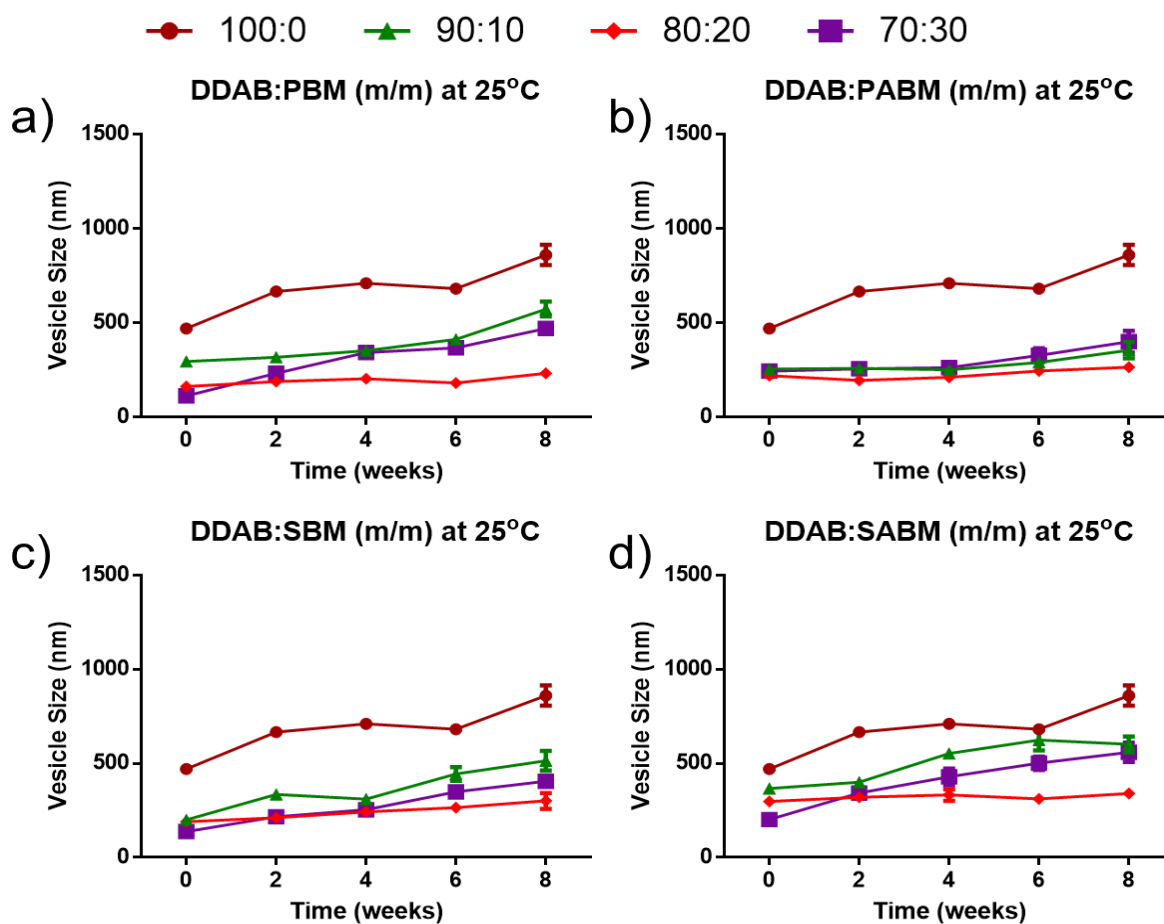


Figure 3.4: Average vesicle size of glyco-coated DDAB liposomes a) DDAB: PBM, b) DDAB: PABM, c) DDAB: SBM, and d) DDAB: SABM containing 0, 10, 20, and 30 mol% of glycolipids at 25°C as an indication of colloidal stability upon storage for 8 weeks. The liposomes were dispersed in 10 mM Tris buffer solution at pH 7.4. Results denote as the means \pm SD of three batches ($n = 3$).

The secretion of IL-6 and TNF- α in the supernatant of RAW 264.7 cells was determined as an indicator in the induction of immune response and the abilities of glyco-coated DDAB liposomes to activate macrophages without further stimulants. To do this, cells were treated with various formulations of pure DDAB or glyco-coated DDAB liposomes dispersions incorporating 10, 20, or 30 mol% of glycolipids, respectively, and measured for cytokines using ELISA. The profiles of pro-inflammatory cytokines including IL-6 and TNF- α are presented in Figure 3.5. Both the cytokines were significantly produced in the LPS-incubated macrophage cells during all experimentation as expected. The amount of secreted IL-6 and TNF- α from RAW 264.7 cells were significantly higher after incubation with all formulations of glyco-coated DDAB liposomes compared to pure DDAB liposomes (Figure 3.5a and 3.5b). Upregulated proinflammatory cytokines are the indicator to generate activated macrophages. It has previously been suggested that mannosylated nanovector enhanced secretion of proinflammatory cytokines and exhibited a higher immune stimulatory activity by shifting to activated macrophages.^{278,279}

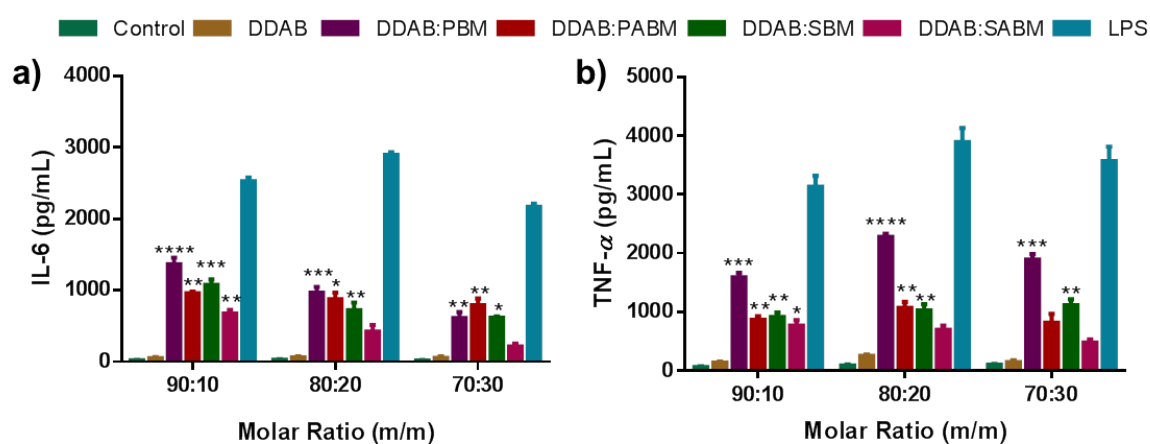


Figure 3.5: Secretion of IL-6 and TNF- α upon treatment with glyco-coated DDAB liposomes in RAW 264.7 cells. Results are presented as mean \pm SEM from three independent experiments. * p <0.05, ** p <0.01, *** p <0.001, and **** p <0.0001 compared to control group. **LPS:** Lipopolysaccharides.

Higher levels of IL-6 secretion were obtained from the macrophages exposed to 10 or 20 mol% DDAB:PBM liposomes compared with those exposed to DDAB:PABM, DDAB:SBM, and DDAB:SABM liposomal formulation. In contrast, the production of

IL-6 was lower for all four glycolipid containing DDAB liposomes when the glycolipids content increases (30 mol %) in the formulation (Figure 3.5a). Additionally, the secretion of TNF- α from macrophage cells stimulated with DDAB:PBM increased in all molar ratios where it secretes the maximum amount (2275.2 ± 57.1 pg/mL) of TNF- α when 20 mol% of PBM was incorporated in the liposomal formulation. In the present study, the dramatically higher amount of proinflammatory cytokines production indicate the strong immunostimulatory capability of the DDAB:glycolipids. This activity is opposite what was observed for treatment with glycolipids alone and indicates these compounds are now presented differently on the liposome surface.²⁶⁷

Table 3.2: Physicochemical characterization of DSA and amikacin encapsulated DDAB/glycolipids (80:20, mol%) liposomes and patterns of the amikacin loading and *in vitro* release. The vesicles sizes, PDI and zeta-potentials were measured using Tris buffer (10 mM, pH 7.4) with concentration 0.25 mg/mL. The *in vitro* drug release studies were carried out in PBS at pH 7.4 using pellet dispersion method at 37°C. Results denotes mean \pm SD ($n=3$).

Liposomes	Particle Size (nm)	PDI	Zeta-potential (mV)	Amikacin content in liposomes (%)	Cumulative release after 24 h (%)
DDAB/Amikacin	459 \pm 20	0.376 \pm 0.027	68.7 \pm 2.7	10.5 \pm 2.48	75.74 \pm 3.97
DDAB:PBM/Amikacin	191 \pm 7	0.233 \pm 0.006	63.5 \pm 7.9	31.2 \pm 4.72	67.69 \pm 2.86
DDAB:PABM/Amikacin	227 \pm 8	0.205 \pm 0.011	68.1 \pm 4.6	22.7 \pm 3.86	79.22 \pm 4.67
DDAB:SBM/Amikacin	167 \pm 4	0.226 \pm 0.013	66.6 \pm 5.8	27.9 \pm 3.31	72.71 \pm 3.29
DDAB:SABM/Amikacin	308 \pm 18	0.281 \pm 0.009	61.9 \pm 3.3	24.4 \pm 2.29	78.32 \pm 1.97
DDAB/DSA	427 \pm 12	0.301 \pm 0.048	65.4 \pm 5.5	-	-
DDAB/DSA/amikacin	383 \pm 25	0.315 \pm 0.014	67.8 \pm 8.1	14.8 \pm 1.63	65.57 \pm 2.33
DDAB:PBM/DSA/Amikacin	220 \pm 11	0.257 \pm 0.003	61.2 \pm 6.3	29.7 \pm 3.75	61.27 \pm 4.14
DDAB:PABM/DSA/amikacin	248 \pm 7	0.294 \pm 0.016	64.3 \pm 5.2	21.9 \pm 2.22	59.42 \pm 3.77
DDAB:SBM/DSA/Amikacin	211 \pm 9	0.273 \pm 0.008	62.2 \pm 3.8	26.2 \pm 4.45	70.74 \pm 3.34
DDAB:SABM/DSA/Amikacin	363 \pm 18	0.316 \pm 0.021	66.1 \pm 4.7	23.6 \pm 4.96	78.99 \pm 3.09

The 20 mol% glycolipid formulated DDAB liposomes were chosen because of their most promising physicochemical (size, PDI and stability) and immunopotentiating (secretion of proinflammatory cytokines) for further evaluation of intracellular bacterial killing efficiency upon encapsulating DSA and amikacin since these antibiotics with many others exhibit poor intracellular penetration into cells. Drug-loaded liposomes were prepared by the thin film hydration method as the lipophilic DSA could be embedded in the lipid bilayer during self-assembled step. The feeding concentration of DSA (100 µg/ml) into all liposomal formulations was kept constant to maintain consistent amount of DSA in each formulation due to a lack of validated quantification methods.

The amount of encapsulated amikacin was determined by UV-vis spectroscopy at wavelength 349 nm *via* a derivatization method using *o*-phthalaldehyde (OPA) reported elsewhere.^{260,271,272} The drug adsorption in liposomal formulation varied based on several factors including particle size, number of lipid bilayers in the liposome, surface charges and composition of lipid molecules and the nature of the drug itself. Based on the liposomal stability over time and immune response as compared to formulations containing pure DDAB, 20 mol% (80:20) of DDAB:glycolipids formulations were considered the ideal composition for loading antibiotic(s) and we used this to evaluate intracellular bactericidal activity. The experimental data showed that the loading capacity of amikacin relies on the structural and textural characteristic of liposomes (Table 3.2). The loading efficiency for pure DDAB liposomes was around 10.5% and slightly increased in amikacin content in the DDAB/DSA liposomes (14.8%). However, the amount of amikacin rises upon incorporation of glycolipids in the DDAB liposomal formulation. For all the DDAB/glycolipids formulations, drug loading efficiency was between 21 and 32%. The estimated amount of amikacin loaded into DDAB:PBM/Amikacin and DDAB:PBM/DSA/Amikacin were 17 µg/100 µg of lipid and 15 µg/100 µg of lipid, respectively.

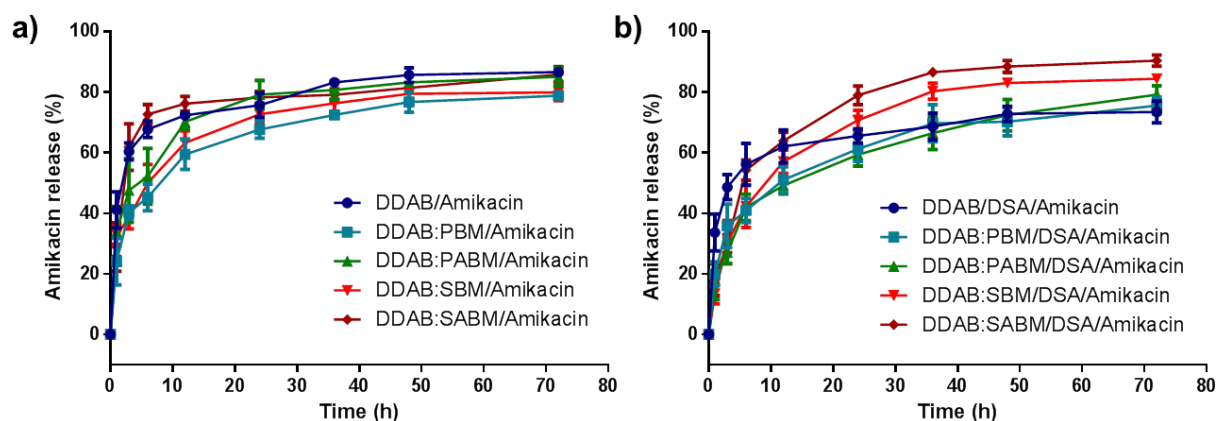


Figure 3.6: The *in vitro* release of amikacin from glyco-coated DDAB liposomes at 37°C in PBS buffer at pH 7.4. Results are expressed as percentage of cumulative amikacin release and represent the mean value \pm S.D of the three replicates.

The *in vitro* release profile of amikacin from glyco-coated DDAB liposomes were calculated as a function of time and the results are shown in Figure 3.6. Drug diffusion, amount of loaded drug in liposomes, liposomal composition and its physical properties can be the factors affecting *in vitro* drug release from liposomes. The drug release pattern showed that around 40% of the adsorbed amikacin was released within 3 h of the experiment followed by sustained release of amikacin after 24 h for both DSA-loaded or unloaded liposomal formulations. The initial burst release of the drug in PBS may be due to the surface bound drugs and the high solubility of amikacin in aqueous solution. This drug release pattern might be favourable in the macrophage targeted antibiotic delivery system where higher drug dose is required in a short period of time.²⁶⁰ More than 55% of the loaded drug was released from glyco-coated DDAB liposomes after 24 h incubation time whereas 70% of drug release from bare DDAB formulated liposomes which could be from the repulsive force between the cationic nature of the drug amikacin and DDAB liposomes (Figure 3.6 a and 3.6b). However, drug release pattern of amikacin did not change significantly upon incorporation of DSA in the DDAB liposomes. The antibiotic delivery was not completed until 72 h incubation period and maximum 86% amikacin was released after 72 h from bare DDAB liposome (Figure 3.6b). Nonetheless, the release of amikacin from DDAB: PBM liposomes were slightly slower and showed sustained release than the other glyco-coated DDAB liposomes. These sustained and slow releasing liposomal formulations

could improve the bioavailability of antibiotics, reduce the toxicity to healthy tissues, and improve the stability in biological environment and loss of drug due to fast clearance and metabolism.

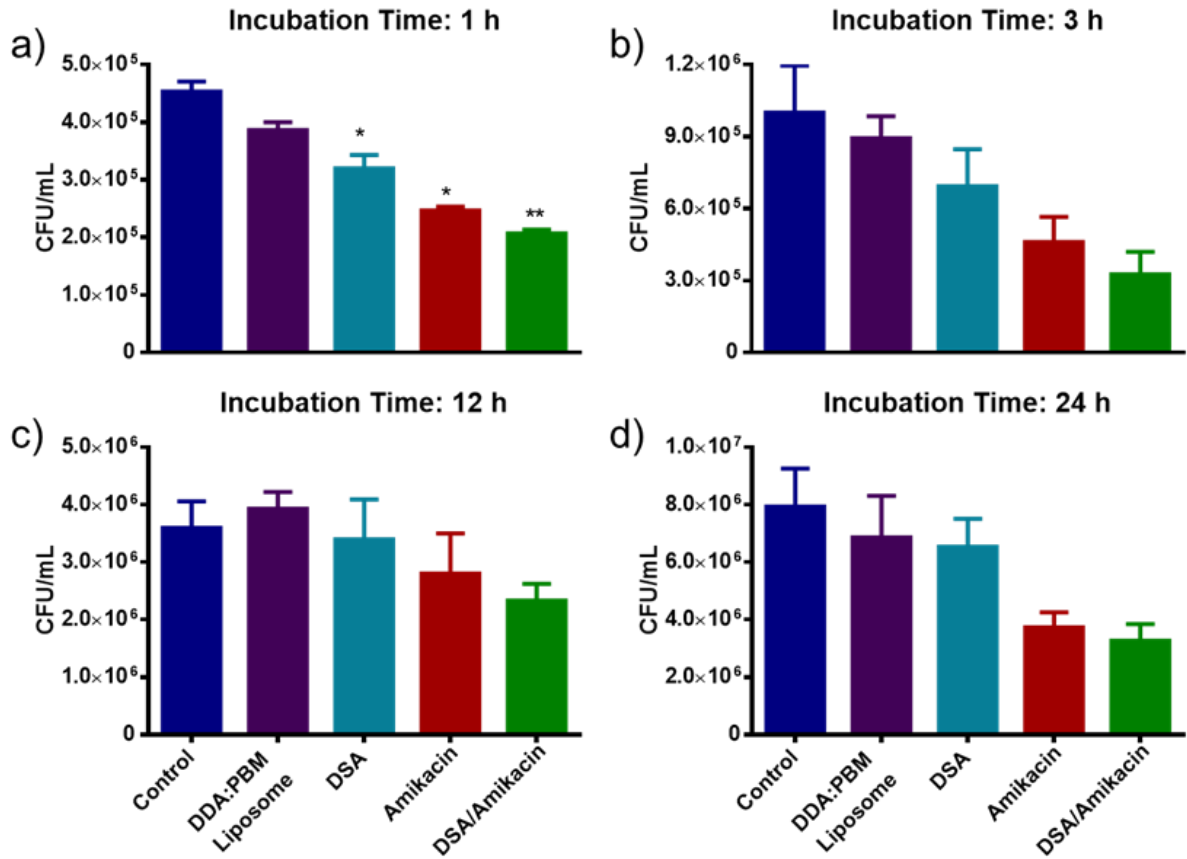


Figure 3.7: Intracellular growth of *S. aureus* inside RAW264.7 macrophages at different time points. Macrophages were infected with bacteria and exposed to DDAB:PBM liposomes (200 $\mu\text{g}/\text{mL}$), antibiotics DSA (15 $\mu\text{g}/\text{mL}$), amikacin (15 $\mu\text{g}/\text{mL}$), and mixture of DSA/Amikacin (1:1 m/m, 20 $\mu\text{g}/\text{mL}$) and incubated for 1, 3, 12 and 24 h, respectively. After incubation for 1 h (a), 3 h (b), 12 h (c) and 24 h (d), macrophages were lysed with sterile distilled water. Finally, the lysates were plated on LB agar plates for counting bacterial colonies. Control was determined from untreated infected macrophages and grew them on LB agar plates prior to lyse the infected cells. Data represent the mean value \pm S.D of the three replicates. * $p < 0.005$, ** $p < 0.01$ and *** $p < 0.001$ compared to control group. CFU, colony-forming units.

After successfully loading the antibiotics into DDAB:glycolipid liposomes, we examined the intracellular bactericidal activity against the prepared formulation to explore its ability to deliver DSA and amikacin into bacteria-infected cells since these exhibit poor intracellular penetration into cells, restricting the antibacterial activity against intracellular infection. The antibiotic DSA, or/and amikacin loaded DDAB:PBM liposomes were selected to perform the intracellular antibacterial test due to its higher loading efficiency and slower drug releasing properties. To perform intracellular antibacterial activity, a mouse macrophage cell line RAW 264.7 expressing the mannose receptor was selected.¹⁷⁶

Initially, RAW264.7 macrophage cells were infected with *S. aureus* bacteria and treated with empty liposomes (without antibiotics) and free antibiotic (DSA, amikacin and DSA/Amikacin) to evaluate their bacterial killing efficiency by counting colony-forming units (CFU) prior to lyse the macrophages and the results are presented in Figure 3.7. There was significant growth of *S. aureus* from the untreated and empty DDAB:PBM treated cells upon incubation between 1 h and 24 h. This result proved that bare DDAB:PBM liposomes without loaded antibiotics were unable to inhibit intracellular bacterial growth. However, significant reduction of intracellular bacteria was observed in macrophages exposed to free DSA (15 µg/mL), amikacin (15 µg/mL) and mixture of DSA/Amikacin (20 µg/mL) just after 1 h incubation (Figure 3.7a). Almost half of the bacterial growth compared to control was inhibited in the first hour of incubation when treated with a DSA and amikacin mixture (1:1, m/m, 20 µg/mL). Macrophages exposed to these compounds treated longer than an hour can also restrict bacterial growth; however, these inhibitions are not statistically significant (Figure 3.7b-3.7d). Among free antibiotics treatment, DSA showed lower intracellular bacterial inhibition compared to aminoglycoside amikacin which could be caused by the poor uptake of the free DSA molecule inside macrophages. The lipidic nature of DSA could cause it to fuse with the cell membrane of macrophages making it unable to reach the cytosol to kill the intracellular bacteria. Moreover, the incubated amount of free DSA (15 µg/mL) was slightly lower than the reported MIC value (16 µg/mL) to kill *S. aureus* and this might be the reason for bacterial growth during longer incubation.²⁸⁰ However, DSA does have two fold lower activities against *S. aureus* compared to amikacin.

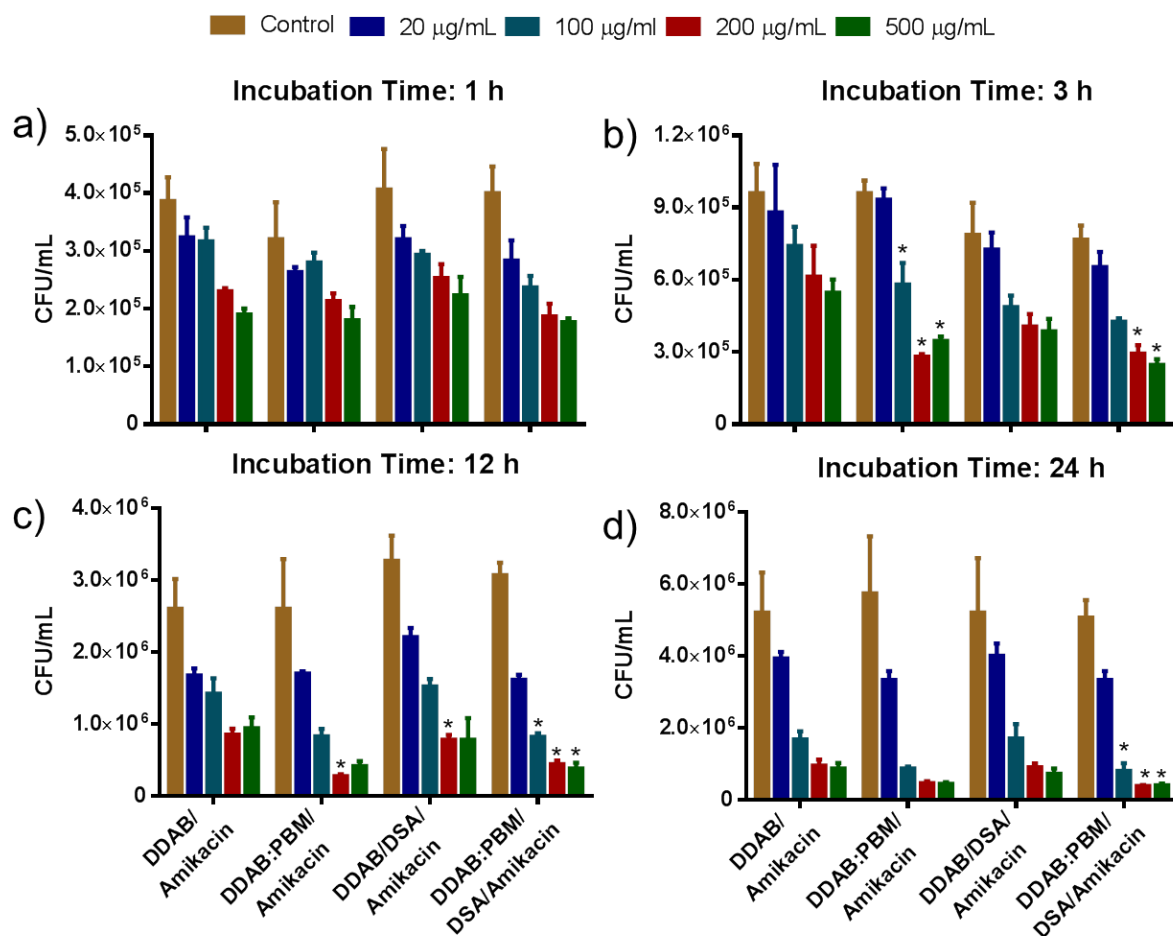


Figure 3.8: Intracellular growth of *S. aureus* inside RAW264.7 macrophages at different time points upon treatment with different antibiotic loaded DDAB liposomal formulation and incubated for 1, 3, 12 and 24 h, respectively. After incubation at 1 h (a), 3 h (b), 12 h (c) and 24 h (d), macrophages were lysed with sterile distilled water and the lysates were plated on LB agar plates for counting bacterial colonies. Control was determined from the treatment with bare liposomes (200 µg/mL) without antibiotic and grew them on LB agar plates prior to lyse the infected cells. Data represent the mean value \pm S.D of the three replicates. * $p < 0.005$, ** $p < 0.01$ and *** $p < 0.001$ compared to control group. CFU, colony-forming units.

In the following experiment, we studied the intracellular antibacterial activity of DSA or/and amikacin loaded DDAB or DDAB/PBM liposomes by counting the CFU of surviving intracellular bacteria over time upon incubation with increasing concentration of liposomal formulations added to RAW 264.7 cells infected by *S. aureus* (results are

shown in Figure 3.8). As shown in Figure 3.8a, there was insignificant intracellular *S. aureus* inhibition at 1 h incubation time upon treatment with DSA or/amikacin loaded DDAB and DDAB:PBM liposomes, but was of similar scale to administration of free drug. The lower bacterial inhibition could be resulted from the less cellular uptake of liposome in RAW 264.7 during an hour of incubation time. It has been reported that macrophage uptake of nanoparticulate vector increases gradually over time and the percentage of uptake does not rises considerably up to 2h (less than 15%).¹⁸⁷ However, the reduction of intracellular *S. aureus* growth after 1 h incubation with antibiotic loaded DDAB or DDAB:PBM liposomes demonstrated the ability to kill intracellular bacteria and suggesting that DSA or/and amikacin can be released from the DDAB or DDAB/PBM liposomes inside macrophages.

The growth of intracellular *S. aureus* exposed to various concentrations of DDAB:PBM/Amikacin and DDAB:PBM/DSA/Amikacin liposomes showed better bactericidal activity after 3, 12 and 24 h incubation, respectively. It has been noted from the Figure 3.8 that DSA and/or amikacin loaded DDAB or DDAB:PBM liposomes revealed concentration-dependent intracellular bacterial growth inhibition. After 3 h of incubation, intracellular growth of *S. aureus* significantly inhibited ($p < 0.005$; CFU/mL reduction by 3 times compared to control) for DDAB:PBM/amikacin and DDAB:PBM/DSA/Amikacin, respectively, when macrophages treated with 200 $\mu\text{g/mL}$ (Figure 3.8b). However, intracellular bacteria treated with lower concentration (20 $\mu\text{g/mL}$) of antibiotic loaded liposomal formulation could not inhibit bacterial growth because of a lower content of antibiotic exposed to macrophages. Surprisingly, the number of intracellular bacteria was higher in treatment with DDAB:PBM/Amikacin with 500 $\mu\text{g/mL}$ compared to macrophages incubated with 200 $\mu\text{g/mL}$ of DDAB:PBM/Amikacin. It is well known that many antibiotics including aminoglycosides are concentration-dependent and the dramatic increase of antibiotics inside cell compartments may enhance the intracellular bactericidal activity.²⁸¹

Additionally, treatment of *S. aureus*-infected macrophages with 200 and 500 $\mu\text{g/mL}$ concentrations of antibiotic loaded liposomal formulation showed a sharp reduction of intracellular bacterial growth at 12 h (Figure 3.8c) and 24 h (Figure 3.8b) incubation, respectively. The glycolipid, PBM, made DDAB liposome loaded with antibiotics

showed improved bactericidal activity compared to drug loaded pure DDAB liposomes. The DDAB:PBM/DSA/Amikacin liposomes significantly inhibit the *S. aureus* growth by 8-fold ($p < 0.005$) after 12 hour of incubation for both 200 and 500 $\mu\text{g/mL}$ concentrations whereas liposome without glycolipid DDAB/DSA/Amikacin inhibited bacteria insignificantly with 500 $\mu\text{g/mL}$ concentrations incubated at the same time (Figure 3.8c). As mannose receptors are present on the surface of monocytes/macrophages, mannosylated DDAB:PBM liposomes could facilitate internalisation of liposomes into macrophages *via* the interaction of mannose moiety with its complementary cell surface receptors consequently increasing the antibiotic content inside the cell and enhancing the bacterial inhibition. The superior inhibition of intracellular bacterial growth by DDAB:PBM/DSA/Amikacin was also observed after 24 h incubation, which can be accounted for by efficient DSA and amikacin delivery and promoted drug release in *S. aureus* infected RAW 264.7 macrophages (Figure 3.8d). It is worth noting that free DSA or/Amikacin, DDAB/Amikacin, DDAB/DSA/Amikacin did not exhibit such significant bacterial inhibition upon incubation between 1 h and 24 h (Figure 3.7).

3.4 Conclusions

Intracellular bacterial infections are difficult to eradicate because bacteria capable of surviving in host-infected cells and protect them from the killing actions of antibiotics. Inadequate antibiotic penetration to infected cells is one of the key causes for therapy failure as it requires a necessary concentration of active therapeutic to kill or suppress the bacterial growth. Therefore, targeted antibiotic delivery could be an efficient system to deliver the drug to infected cells *via* specific interaction with cell-surface receptors. Here, we describe the incorporation of glycolipids based on benzyl mannoside with varying chain length of fatty acid group at the C-6 (Carbon-6) position and incorporation into cationic dimethyldioctadecylammonium bromide (DDAB) liposomes using the thin film hydration method. The physicochemical and immunopotentiating properties of the prepared glyco-coated DDAB liposomes were investigated. The vesicle sizes and polydispersity index of the glyco-coated DDAB liposomes significantly decreased upon incorporation of 20 mol% glycolipid into the liposomal formulation without dramatically affecting its cationic surface charges. The improved

long term colloidal stabilities (8 weeks) have been noted for glyco-coated DDAB liposomes in comparison to pure DDAB liposomes by measuring their vesicle sizes at various time points. The adjuvant properties of glyco-coated DDAB liposomes were evaluated *in vitro* against RAW264.7 macrophages by measuring their ability to induce the proinflammatory cytokines including tumor necrosis factor (TNF- α) and interleukin (IL-6) and the results showed a higher level of cytokine (both TNF- α and IL-6) production upon incubation with glyco-coated DDAB liposomes compared to pure DDAB liposomes. As antibiotics, *n*-decanesulphonylacetamide (DSA) and amikacin were used to encapsulate into the glyco-coated liposomal formulation and we successfully loaded these antibiotics with an efficient loading capacity of 25% to 32% compared to pure DDAB liposomes. The *in vitro* antibiotic release profile also measured over time and results showed slow and steady release of drug from the glyco-coated DDAB liposomes in comparison to antibiotic encapsulated DDAB formulated liposomes. Finally, the intracellular viability of *S. aureus* infected RAW 264.7 macrophages was evaluated against prepared antibiotic encapsulated glyco-coated DDAB liposomes and the results showed efficient intracellular bacterial growth inhibition.

Chapter 4

Synthesis and characterization of glycosylated chitosan nanoparticles for drug delivery

4.1. Introduction

Carbohydrates represent an important structural component of all living cells and are the most abundant natural organic matter.²⁶ There are only a limited number of monosaccharides, however, these simple monosaccharides can generate a large number of di-, oligo-, and polysaccharides *via* various regio- and stereo-chemical linkages.^{2,27} Moreover, carbohydrates play important roles in various biological processes including energy production, reproduction, cellular development, signal transmission, inflammation, and infection.^{54,244} Their high biocompatibility, excellent biodegradability, solubility in water, low toxicity and ability to be recognized by cell-surface receptors gives carbohydrates great potential for therapeutic applications.²⁸ However, the complex chemical composition of carbohydrates makes it difficult to synthesise and process these structures which are a major drawback in practical uses.^{282,283} The recent discoveries in glycoscience make favourable the design and synthesis of carbohydrate-based materials, particularly, natural polysaccharides, synthetic glycopolymer and glyconanoparticles (GNPs), and these areas have seen intense research attention in the last few decades.^{173,245,284}

In recent times, naturally occurring polysaccharides have established prominence in the field of drug delivery systems (DDS) because of their outstanding merits including anticoagulant, anti-inflammatory, anti-microbial and anti-tumor properties.^{3,39} Polysaccharides contain a large number of reactive groups, variety of chemical composition and a wide range of molecular weights which is due to their differences in structure and in various physicochemical and biological properties.^{244,285} For instance, some polysaccharides are negatively charged (heparin, alginate, hyaluronic acid and pectin), some are positively charged (chitosan) and others have a neutral charge (dextran and cyclodextrins) at pH 7.^{27,244} Moreover, the formation of self-assembled GNPs after chemically modification of polysaccharide with hydrophobic molecules and sugar residues on the surface has been widely utilized to explore carbohydrate-carbohydrate and carbohydrate-protein interaction.^{176,187,286} The structure and chemical composition of polysaccharides can be determined from the physicochemical

characteristics of the drug (i.e., anionic, cationic, neutral) to be loaded and the possible route of administration of the drug composites. Furthermore, the formation of micelles or GNPs can be controlled by balancing the interaction between the hydrophilic chains of polysaccharides and grafted hydrophobic groups like small surfactants or lipids onto the polysaccharide's backbone.^{221,287,288}

Among natural polysaccharides, chitosan has been one of the most popular biopolymers investigated by biomedical and pharmaceutical researchers due to its excellent biocompatibility, high biodegradability, low toxicity, pH sensitivity, abundant availability, low cost, ease of chemical modification, bioadhesive and unique cationic properties, and permeation enhancing properties.^{28,55,289} The chemical composition of chitosan consists of a linear heteropolymer of D-glucosamine and *N*-acetyl-D-glucosamine linked by β -(1-4)glycosidic bonds which are randomly distributed. Chitosan is obtained commercially by the partial deacetylation of chitin which is the most abundant and second largest polysaccharide in nature after cellulose.²⁹⁰ Chitin is mainly derived from the exoskeleton of crustaceans including shrimp, crab, or lobster and can also be found in the cell walls of fungi and insects. The degree of deacetylation (DDA) is an important characteristic of chitosan which represents the fraction of deacetylation of *N*-acetyl-D-glucosamine units transformed to the D-glucosamine relative to the total number of monosaccharide units. After deacetylation of chitin, the solubility of chitosan improves immensely by protonation of the amine functional groups in acidic solutions (pKa ~ 6.0-6.5) which are present in the D-glucosamine on the macromolecule.²⁹¹ Moreover, the cationic characteristic of chitosan exhibits mucoadhesive properties through the interaction with the negatively charged proteins and lipids presented on the cell membranes. Chitosan and its derivatives also have antibacterial and antiparasitic activities and have been broadly used in orthopaedic applications. It should be noted that chitosan can be degraded by various enzymes including protease, lysozymes, and by some lipases which demonstrates its biodegradability.⁵⁴

The chemical modification of chitosan can be performed by grafting molecules on its backbone that can react with the hydroxyl and/or the amino group of chitosan. As the amine groups of chitosan are more reactive than the hydroxyl groups, *N*-acylation

reactions are widely utilized to functionalize chitosan using fatty acid, fatty acid chloride, and acid anhydride.^{26,233} For instance, lauroic, palmitic, stearic, linoleic, oleic, deoxycholic acids were reported to graft on chitosan backbone *via* *N*-acylation reactions.^{99,292} Moreover, reductive *N*-alkylation, caboxymethylation and quaternarization reactions were also performed to obtain amphiphilic chitosan.²⁰⁰ Ivan and his group reported the *N*-alkylation reaction of chitosan *via* reductive amination of lactose moieties on the polysaccharide chain and explored its biological significance.^{293,294} Wenjun *et al.* described the synthesis of mannose modified chitosan *via* reductive amination using modified mannose moieties.^{233,295}

Protein-carbohydrate interactions are wide spread in living systems and critical in many biological processes including immune response, cellular recognition, and infection. Glyco-ligands targeting proteins have a potential role for disease diagnosis, treatment, and prevention, however the major disadvantage is the low-affinity of interactions between the biomolecules and carbohydrates. The binding strength may be improved by exploiting multivalency such as multivalent glycoligands bind simultaneously to the proteins of interest. Coupling many monomeric ligands or drugs onto appropriate scaffolds such as polymers can create multivalent systems to enhance the activity and stability and lower toxicity. Therefore, the natural polysaccharide chitosan was selected to conjugate specific carbohydrate sequences on its backbone to target macrophages.

It is well known that mannose receptors used for phagocytosis and endocytosis of antigens are predominantly expressed on antigen presenting cells (APCs) such as macrophages and dendritic cells.²³³ Macrophages are a promising target for carbohydrate-based therapeutics as they express carbohydrate binding receptors which internalize bound material *via* receptor-mediated endocytosis.¹⁷⁸ Mannose can also recognize the cell-surface mannose receptors by specific ligand-receptor interactions such as macrophage mannose receptor (MMR; CD206) bind oligosaccharides containing terminal mannose residues on infectious agents and transport them into endocytic pathways. For selective drug delivery to infected cells, here, we target mannose receptors of macrophages that have a higher affinity for simple mannoside than the corresponding glucosides. For this, we designed to modify mannoside at the anomeric and C-6 positions with various moieties to furnish a diverse suite of

compounds that will be tested against macrophages. On the other hand, macrophage galactose-type lectin (MGL) is expressed at high levels by activated macrophages under inflammatory conditions.^{2,296} Almost all known glycosylated chitosan derivatives have a single sugar modification to utilize them as a targeting ligand to various immune cells.^{18,293,297} Therefore, to develop novel GNPs, different target ligands such as mannose and galactose were grafted onto the chitosan main chain to enhance the internalization of the therapeutics. We believe this will provide greater diversity in the carbohydrates presented to the macrophages and will more closely resemble glyco-diversity found on a pathogen. Moreover, multivalent sugar molecules on the surfaces of the prepared GNPs will improve the synergistic interaction with macrophages as well as promote internalization of the GNPs into the macrophages. Finally, an aminoglycoside (amikacin) and *n*-decanesulphonylacetamide (DSA) were loaded into the synthesized GNPs to find the *in vitro* bactericidal efficacy of the nanocarriers as was explored with liposomes in the previous chapter.

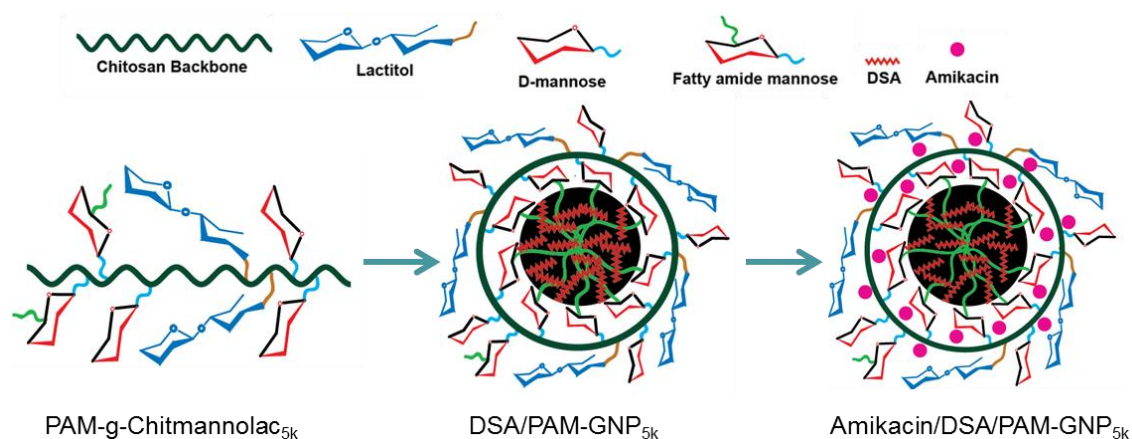


Figure 4.1: Schematic representation of self-assembled antibiotic loaded chitosan based GNPs.

In this study, we describe the facile synthesis procedure of chitosan-based GNPs by grafting hydrophilic sugar molecules and hydrophobic sugar conjugated lipid moieties onto the chitosan backbone. Initially, a reductive amination reaction (*N*-alkylation) was performed to exploit the masked aldehyde group of lactose and the amino group of the glucosamine residues of chitosan to obtain a highly soluble engineered lactose modified chitosan (Chitlac) molecule. Then, the modified mannose precursors were grafted to the chitosan backbone *via* carbodiimide chemistry. Next, the GNPs were developed by self-

assembling of the modified chitosan where the long lipid chain modified mannose moiety and the hydrophobic bactericidal agents DSA molecules assembled into the core of the micelles in aqueous environment (Figure 4.1). Furthermore, a fluorescence molecule, fluorescein, was attached to the GNPs to trace the cellular uptake of prepared GNPs. Finally, amikacin was encapsulated to the DSA loaded GNPs to amplify the antibacterial activity of the prepared nano-vehicle.

4.2. Experimental Section

4.2.1. General

^1H and ^{13}C NMR spectra were recorded in the designated solvents and temperatures on a Bruker Ascend 400 MHz and 100 MHz respectively. Chemical shifts (δ) are expressed to two decimal place in parts per millions (ppm) relative to tetramethylsilane (0 ppm) and coupling constants (J) are in hertz (Hz). Abbreviations of multiplicities are indicated using standard notation; singlet (s), doublet (d), doublet of doublets (dd), doublet of doublet of doublets (ddd), triplet (t), quartet (q), and multiplet (m). Standard prefixes are used including broad (br.) and apparent (app.).

Electrospray ionisation (ESI) low resolution mass spectrometry (LRMS m/z) was recorded on a Bruker Daltronics Esquire 3000 Ion-Trap LC MS, using Bruker Daltronics esquire control 5.0 software. All spectra were recorded in positive-ion mode at a concentration of 0.1-0.3 mg/mL with sample introduction at 300 $\mu\text{L}/\text{h}$.

All reactions were monitored by thin layer chromatography (TLC) on Merck silica gel plates (GF₂₅₄, cat No. 1.055545 on aluminium) and spots were visualized by UV light at 254 nm and then developed by dipping plates into a solution of 5% H₂SO₄ in ethanol and heating the plates at ~200°C. Flash column chromatography was performed using Merck 230-400 mesh silica gel for purification. Reaction products were purified by flash chromatography with silica gel 60 (0.040-0.063 micron, cat No 1.09385).

All solvents used in reactions were of analytical grade, distilled, or dried before use. All solvents used for chromatography were distilled prior to use. The reactions were conducted under dry N₂ wherever anhydrous conditions were required.

4.2.2. Materials

D-mannose, allyl alcohol, 3-mercaptopropionic acid, 1-ethyl-3-[3-dimethylaminopropyl] carbodiimide hydrochlorides (EDC), N-hydroxysuccinimide (NHS), sodium azide, p-toluene sulfonyl chloride, lauroyl chloride, palmitoyl chloride, stearoyl chloride were purchased from Sigma-Aldrich. 6-(3-Carboxypropylaminocarbonyl)fluorescein was synthesized by following the procedure elsewhere by our group.²⁹⁸

Low molecular weight chitosan (LMWC) having M_n of 164 kDa, 75-85% degree of deacetylation and a viscosity of 0.026 Pa.s for a 1 wt% solution in 1% acetic acid was purchased from Sigma-Aldrich (Castle Hill, NSW, Australia). The commercial chitosan sample was purified by precipitation with isopropanol from an acidified aqueous solution (pH 4.0). Solution of the recovered polymer was then exhaustively dialyzed against deionized water (DI water), filtered through 0.45 μ m Millipore filters and then freeze-dried.

4.2.3. Synthesis of Allyl 2,3,4,6-tetra-acetyl- α -D-mannoside (2)

Allyl α -D mannose was synthesized according to the literature reported by Zong *et al.*²³³ Briefly, D-mannose (12 g, 66.8 mmol) and p-toluene sulfonyl chloride (0.072 g, 0.4 mmol) was dissolved in allyl alcohol (80 mL, 1176 mmol) and stirred under N_2 at 100°C for 36 hours. After reaction time, the reaction solution was concentrated by vacuum distillation. The reaction mixture was then poured into water (150 mL), washed with EtOAc (3 x 50 mL). The combined organic fractions were washed with water (2 x 50 mL) and the combined aqueous phase was concentrated under reduced pressure to a clear oily residue to yield allyl α -D mannose (13.5 g, 92%).

¹H-NMR (400 MHz, D₂O) δ : 3.53-3.61 (m, 2H, H-6a, CH₂=CH-CH₂O-), 3.65-3.76 (m, 2H, H-3,4), 3.81 (d, J = 12.1 Hz, 1H, H-2), 3.87 (dd, J = 3.4, 1.7 Hz, 1H, H-5), 4.00 (dd, J = 12.8, 6.3 Hz, 1H, CH₂=CH-CH₂O-), 4.16 (dd, J = 12.8, 5.5 Hz, 1H, H-6b), 4.83 (d, J = 1.5 Hz, 1 H, H-1), 5.17-5.32 (m, 2H, CH₂=CH-), 5.90 (ddd, J = 22.7, 11.0, 5.9 Hz, 1H, CH₂=CH-); ¹³C NMR (100 MHz, D₂O) δ : 60.88 (C-6), 66.74 (OCH₂CH=CH₂), 68.09 (C-4), 70.0 (C-2), 70.54 (C-5), 72.77 (C-3), 98.99 (C-1), 118.43(CH=CH₂), 133.23 (CH₂CH=CH₂); ES-MS: m/z = 242.9 [M + Na]⁺.

Allyl α -D mannose (3.4 g, 16.7 mmol) was reacted with acetic anhydride (12 mL, 130 mmol) in pyridine (30 mL) solution for 24 h.²⁹⁹ The reaction mixture was then concentrated and ice cold deionized water (100 mL) was added, extracted by ethyl acetate (3 x 30 mL). The following combined organic phase was washed by deionized water (50 mL) and 5% NaHCO₃ (3 x 40 mL) dried over Na₂SO₄, concentrated to give a precipitate. After further purification by silica column chromatography using ethyl acetate: hexane (EtOAc: Hex) = 1:3 as eluent gave allyl 2,3,4,6-tetra-acetyl- α -D-mannoside **2** (4.86 g, 75%) as a colourless syrup. The ¹H-NMR data matches with the published literature.²⁹⁹

TLC (EtOAc/Hex, 1:3) **R_f** = 0.29, **¹H-NMR** (400 MHz, CDCl₃) δ : 2.00, 2.05, 2.11, 2.16 (4s, 12H, CH₃CO), 4.04 (dddd, J = 9.7, 7.3, 4.0, 1.8 Hz, 2H, H-5, CH₂=CH-CH₂O-), 4.12 (m, 1H, H-6b), 4.20 (dd, J = 12.8, 5.3 Hz, 1H, CH₂=CH-CH₂O-), 4.30 (dd, J = 12.2, 5.3 Hz, 1H, H-6a), 4.88 (d, J = 1.6 Hz, 1 H, H-1), 5.23-5.40 (m, 5H, H-2,3,4 CH₂=CH-), 5.91 (dddd, J = 16.8, 10.4, 6.2, 5.4 Hz, 1H, CH₂=CH-).

4.2.4. Synthesis of 3-Thia-heptanoic acid-2,3,4,6-tetra-O-acetyl- α -D-mannoside (**3**)

Compound **2** (1.2 g, 3.09 mmol) was dissolved in deoxygenated CH₃CN (30 mL) (obtained by bubbling N₂) containing 3-mercaptopropionic acid (0.9 mL, 10.8 mmol). The reaction mixture was irradiated with UV light at 254 nm (UVG-11 Mineralight) for 2h at 30°C.²⁹⁹ The solvent was evaporated under reduced pressure and the residual oil was dissolved in EtOAc and successively washed with equal volumes of water and saturated NaCl solution. The organic phase was dried over anhydrous Na₂SO₄ and evaporated under reduced pressure. The product was purified by silica gel column chromatography using CH₂Cl₂: MeOH = 8:1 (by vol) as eluent giving pure **3** (1.436 g, 94%) as colourless oil.

TLC (CH₂Cl₂/MeOH, 8:1) **R_f** = 0.42, **¹H-NMR** (400 MHz, CDCl₃) δ : 1.85-1.97 (m, 2H, OCH₂CH₂), 2.02, 2.08, 2.12, 2.16 (4s, 12H, CH₃CO), 2.62-2.84 (m, 6H, OCH₂CH₂CH₂-S-CH₂CH₂COOH), 3.49-3.59 (m, 1H, OCH₂CH₂), 3.83 (ddd, J = 9.8, 6.8, 5.6 Hz, 1H, OCH₂CH₂), 4.01 (ddd, J = 9.6, 5.2, 2.4 Hz, 1H, H-5), 4.14 (dd, J = 12.2, 2.4 Hz, 1H, H-6b), 4.28 (dt, J = 15.1, 7.5 Hz, 1H, H-6a), 4.84 (d, J = 1.6 Hz, 1 H, H-1), 5.17-5.41 (m, 3H, H-2,3,4). **¹³C NMR** (101 MHz, CDCl₃) δ : 20.72 (CH₃CO),

20.78 (CH₃CO), 20.86 (CH₃CO), 20.91 (CH₃CO), 28.63 (S-CH₂CH₂COOH), 33.79 (OCH₂CH₂CH₂-S-), 34.59 (OCH₂CH₂CH₂-S-), 62.54 (C-6), 65.88 (C-5), 66.17 (C-4), 68.56 (C-2), 69.61 (C-3), 97.56 C-1), 170.16 (CH₃CO), 170.23 (CH₃CO), 170.87 (CH₃CO), 177.10 (S-CH₂CH₂COOH).

4.2.5. Synthesis of 3-thia-heptanoic acid- α -D-mannoside (4)

Compound **3** (0.5 g, 1.01 mmol) was dissolved in methanol: water (1:1, 20 mL). 5 mL 1M NaOH (0.2 g, 5 mmol, pH \geq 8.5) was added to the reaction mixture at 0°C and stirred for 0.5 h. Then the reaction mixture was stirred at room temperature overnight and monitored by TLC. The solution was neutralized with Amberlite IR-120 (H⁺) ion exchange resin to reach pH \sim 3.0, filtered and concentrated under reduced pressure to give **4** (0.31 g, 94%) as an amorphous white solid.

¹H-NMR (400 MHz, CDCl₃) δ : 1.79-1.89 (m, 2H, OCH₂CH₂), 2.58-2.71 (m, 6H, OCH₂CH₂CH₂-S-CH₂CH₂COOH), 3.52 (dd, J = 10.1, 5.8 Hz, 1H, H-6a), 3.56 (dd, J = 6.3, 4.3 Hz, 2H, OCH₂CH₂), 3.67 (d, 2H, J = 5.5 Hz, OCH₂CH₂), 3.64-3.76 (m, 3H, H-2,3,4), 3.78-3.83 (m, 1H, H-6b), 3.86 (dd, J = 3.4, 1.7 Hz, 1H, H-5), 4.78 (d, J = 1.6 Hz, 1 H, H-1). ¹³C NMR (101 MHz, CD₃OD) δ : 28.13 (OCH₂CH₂CH₂-S-), 29.19 (OCH₂CH₂CH₂-S-), 32.91 (OCH₂CH₂CH₂-S-), 33.37, 34.31 (OCH₂CH₂CH₂-S-), 34.51, 37.97 (OCH₂CH₂CH₂-S-), 61.49 (C-6), 65.53 (OCH₂CH₂CH₂-S-), 70.64 (C-4), 71.16 (C-2), 71.25 (C-3), 73.23 (C-5), 100.21 (C-1), 174.41 (S-CH₂CH₂COOH). ES-MS (LR): m/z = 349.1 [M + Na]⁺.

4.2.6. Synthesis of allyl 6-azido α -D-mannoside (5)

A mixture of allyl α -D mannose (5 g, 22.7 mmol) in pyridine (50 mL) was treated with p-TsCl at 0°C and the resulting mixture was stirred for 12 h.³⁰⁰ After reaction, water was added to it and stirred for additional 2 h. The mixture was then partitioned with EtOAc (100 mL), water (3 x 50 mL). The organic layer was purified with brine (50 mL) and dried over Na₂SO₄, filtered and concentrated to give allyl 6-tosyl- α -D mannose. A mixture of allyl 6-tosyl- α -D mannose and sodium azide (5.25 g, 80.1 mmol) in DMF (50 mL) was stirred for 24 h at 70°C.³⁰¹ After reaction, the solvent was removed under vacuum and the residue was purified by silica gel column chromatography

(dichloromethane/MeOH = 8/1) to yield allyl 6-azido- α -D mannose (3.1 g, 92%) as a white solid.

^1H NMR (400 MHz, CD_3OD) δ : 3.43 – 3.47 (m, 1H, $\text{CH}_2=\text{CH}-\text{CH}_2\text{O}-$), 3.50 (dd, $J = 13.0, 2.5$ Hz, 1H, H-6a), 3.56 – 3.63 (m, 1H, H-5), 3.66 – 3.73 (m, 2H, H-3,4), 3.84 (dd, $J = 3.3, 1.7$ Hz, 1H, H-2), 4.06 (ddt, $J = 13.0, 6.0, 1.4$ Hz, 1H, $\text{CH}_2=\text{CH}-\text{CH}_2\text{O}-$), 4.25 (ddt, $J = 13.0, 5.1, 1.5$ Hz, 1H, 6b), 4.82 (d, $J = 1.6$ Hz, 1H, H-1), 5.21 (dq, $J = 10.4, 1.3$ Hz, 1H, $\text{CH}_2=\text{CH}-$), 5.33 (dq, $J = 17.2, 1.7$ Hz, 1H, $\text{CH}_2=\text{CH}-$), 5.97 (dddd, $J = 17.1, 10.5, 6.0, 5.2$ Hz, 1H, $\text{CH}_2=\text{CH}-$). ^{13}C NMR (100 MHz, CD_3OD) δ : 51.54 (C-6), 67.65 ($\text{OCH}_2\text{CH}=\text{CH}_2$), 68.12 (C-4), 70.66 (C-2), 71.01 (C-5), 72.58 (C-3), 99.32 (C-1), 116.19 ($\text{CH}=\text{CH}_2$), 133.88 ($\text{CH}_2\text{CH}=\text{CH}_2$). **FT-IR**: 2099.97 cm^{-1} (N_3); **ES-MS** (LR): $m/z = 268.7$ [$\text{M} + \text{Na}$] $^+$.

4.2.7. Synthesis of allyl 6-amino α -D-mannoside (6)

Allyl 6-azido- α -D mannose (3 g, 8.1 mmol) was dissolved in a mixture of MeOH/ H_2O (9:1, 20mL). The reaction was cooled to 0°C and under vigorous stirring, NH_4Cl (2.4 g, 42 mmol) and Zn dust (5.4 g, 81 mmol) were added.^{302,303} After 30 min, the solution were filtered through Celite and the solvent was removed under vacuum to give allyl 6-amino- α -D mannose (2.1 g, 65%) as a white powder and used for the next step without further purification.

4.2.8. Synthesis of allyl 6-fatty amido- α -D-mannoside: General Procedures (7/8/9)

Allyl 6-amino- α -D-mannoside (1.0 g, 4.6 mmol) was dissolved in dry pyridine (20 mL) and corresponded fatty acid chloride was added to it dropwise at 0°C and stirred for 4 h. After reaction time, the solvent was evaporated under vacuum. The crude compound was then dissolved in CH_2Cl_2 (50 mL) and washed with 1 M HCl (3x 50 mL), NaHCO_3 (50 mL), and brine (50 mL), dried over Na_2SO_4 , filtered and concentrated to yield yellowish solid compound. The residue was purified by flash chromatography using DCM/MeOH 10:1 to as eluent to yield allyl 6-fattyamido- α -D-mannoside as white solid.

4.2.8.1 Synthesis of allyl 6-lauroylamido- α -D-mannoside (7)

Allyl 6-lauroylamido- α -D-mannoside (7) was obtained from allyl 6-amino- α -D mannose in 42% yield.

^1H NMR (400 MHz, CDCl_3) δ : 0.90 (t, $J = 6.8$ Hz, 3H, RCH_3), 1.29 (d, $J = 13.9$ Hz, 18H, RCH_2R), 1.65 (q, $J = 7.2$ Hz, 2H, RCH_2R), 2.28 (td, $J = 7.3, 1.7$ Hz, 2H, OCH_2CH_2), 3.09 (ddd, $J = 14.9, 4.5, 2.6$ Hz, 1H, H-6a), 3.45 – 3.54 (m, 1H, H-4), 3.62 (dt, $J = 9.8, 2.5$ Hz, 1H, H-3), 3.89 – 4.02 (m, 1H, H-2), 4.06 (ddd, $J = 14.9, 8.6, 2.7$ Hz, 1H, H-5), 4.16 (ddt, $J = 12.9, 5.1, 1.4$ Hz, 1H, H-6b), 4.86 (s, 1H, H-1), 5.22 (dd, $J = 10.4, 1.4$ Hz, 1H, $\text{CH}=\text{CH}_2$), 5.30 (dq, $J = 17.3, 1.5$ Hz, 1H, $\text{CH}=\text{CH}_2$), 5.83 – 5.97 (m, 1H, $\text{CH}=\text{CH}_2$), 6.19 (dd, $J = 8.3, 4.6$ Hz, 1H, $-\text{CO}-\text{NH}-\text{R}$). ^{13}C NMR (100 MHz, CDCl_3) δ : 14.12 (RCH_3), 22.69 (RCH_2R), 25.75 (RCH_2R), 29.29 (RCH_2R), 29.34 (RCH_2R), 29.50 (RCH_2R), 29.62 (RCH_2R), 31.91 (RCH_2R), 36.51 ($-\text{COCH}_2\text{R}$), 39.89 (C-6), 68.13 ($\text{OCH}_2\text{CH}=\text{CH}_2$), 70.27 (C-4), 70.52 (C-3), 71.28 (C-2), 76.71 (C-5), 99.06 (C-1), 117.56 ($\text{CH}=\text{CH}_2$), 133.57 ($\text{CH}_2\text{CH}=\text{CH}_2$), 176.08 ($-\text{COCH}_2\text{R}$). ES-MS (LR): $m/z = 424.5$ $[\text{M} + \text{Na}]^+$

4.2.8.2 Synthesis of allyl 6-palmitoylamido- α -D-mannoside (8)

Allyl 6-palmitoylamido- α -D-mannoside (8) was obtained from allyl 6-amino- α -D mannose in 35% yield.

^1H NMR (400 MHz, CDCl_3) δ : 0.90 (t, $J = 6.8$ Hz, 3H, RCH_3), 1.28 (s, 26H, RCH_2R), 1.65 (d, $J = 7.3$ Hz, 5H, RCH_2R), 2.23 – 2.32 (m, 2H, OCH_2CH_2), 3.07 (ddd, $J = 15.0, 4.6, 2.6$ Hz, 1H, H-6a), 3.49 (t, $J = 9.6$ Hz, 1H, H-4), 3.63 (dt, $J = 9.8, 2.4$ Hz, 1H, H-3), 3.89 – 4.02 (m, 1H, H-2), 4.05 – 4.20 (m, 2H, H-5 & H-6b), 4.87 (s, 1H, H-1), 5.19 – 5.34 (m, 2H, $\text{CH}=\text{CH}_2$), 5.90 (ddd, $J = 22.3, 10.6, 5.6$ Hz, 1H, $\text{CH}=\text{CH}_2$), 6.10 (dd, $J = 8.5, 4.5$ Hz, 1H, $-\text{CO}-\text{NH}-\text{R}$). ^{13}C NMR (100 MHz, CDCl_3) δ : 14.12 (RCH_3), 22.69 (RCH_2R), 24.77 (RCH_2R), 24.97 (RCH_2R), 25.52 (RCH_2R), 25.77 (RCH_2R), 29.12 (RCH_2R), 29.16 (RCH_2R), 29.30 (RCH_2R), 29.36 (RCH_2R), 29.46 (RCH_2R), 29.60 (RCH_2R), 29.66 (RCH_2R), 29.70 (RCH_2R), 36.47 ($-\text{COCH}_2\text{R}$), 39.95 (C-6), 67.29 (C-4), 68.13 ($\text{OCH}_2\text{CH}=\text{CH}_2$), 70.33 (C-3), 70.53 (C-2), 76.71 (C-5), 99.11 (C-1), 117.53

(CH=CH₂), 133.58 (CH₂CH=CH₂), 177.94 (-COCH₂R). ES-MS (LR): m/z = 480.8 [M + Na]⁺

4.2.8.3 Synthesis of allyl 6-stearoylamido- α -D-mannoside (9)

Allyl 6-stearoylamido- α -D-mannoside (9) was obtained from allyl 6-amino- α -D-mannose in 26% yield.

¹H NMR (400 MHz, CDCl₃) δ : 0.90 (t, J = 6.7 Hz, 3H, RCH₃), 1.27 (s, 29H, RCH₂R), 1.66 (s, 6H, RCH₂R), 2.27 (d, J = 8.2 Hz, 2H, OCH₂CH₂), 3.00 – 3.15 (m, 1H, H-6a), 3.49 (t, J = 9.6 Hz, 1H, H-4), 3.63 (d, J = 9.7 Hz, 1H, H-3), 3.93 – 4.03 (m, 1H, H-2), 4.06 – 4.23 (m, 2H, H-5 & H-6b), 4.87 (s, 1H, H-1), 5.19 – 5.35 (m, 2H, CH=CH₂), 5.90 (ddt, J = 16.5, 10.9, 5.6 Hz, 1H, CH=CH₂), 6.10 (dd, J = 8.0, 4.3 Hz, 1H, -CO-NH-R). ¹³C NMR (100 MHz, CDCl₃) δ : 14.13 (RCH₃), 22.70 (RCH₂R), 25.75 (RCH₂R), 29.27 (RCH₂R), 29.34 (RCH₂R), 29.37 (RCH₂R), 29.50 (RCH₂R), 29.62 (RCH₂R), 29.67 (RCH₂R), 29.71 (RCH₂R), 31.94 (RCH₂R), 36.53 (-COCH₂R), 39.89 (C-6), 67.04 (C-4), 68.13 (OCH₂CH=CH₂), 70.20 (C-4), 70.51 (C-3), 71.26 (C-2), 76.71 (C-5), 99.03 (C-1), 117.56 (CH=CH₂), 133.56 (CH₂CH=CH₂), 176.14 (-COCH₂R). ES-MS (LR): m/z = 634.9 [M + Na]⁺

4.2.9. Synthesis of 3-thio-heptanoic acid-2,3,4-tri-*O*-acetyl -6-fatty amido- α -D-mannoside: General Procedures (13/14/15)

Allyl 6-fattyamido- α -D-mannoside (0.5 g, 1 mmol) was reacted with acetic anhydride (2 mL, 21.6 mmol) in pyridine (15 mL) solution overnight to produce allyl 2,3,4-tri-*O*-acetyl -6-fatty amido- α -D-mannoside as brownish solid residue (10/11/12) and the crude compounds were used without further purification.

Allyl 2,3,4,6-tetra acetyl-6-fatty amido- α -D-mannoside was dissolved in anhydrous DMF in a 100 mL flask and transferred it to an immersion-well batch UV reactor with 125 W medium pressure Hg lamp vessel under argon atmosphere. 3-Mercaptopropionic acid was added to it dropwise and stirred the reaction for 2 h. The overall reaction was monitored *via* TLC. After completing the reaction, the solvent was removed in vacuum, dissolved in water (100 mL), washed with CH₂Cl₂ (3x 100 mL). The combined organic layer was washed with water (3x100 mL) and brine (50 mL), dried over Na₂SO₄, filtered and condensed to colourless oil. The residue

chromatographed in silica using EtOAc/Hexane/AcOH, 3:2:0.05 were used to obtain the desired 3-thia-heptanoic acid-2,3,4-triacetyl-6-fatty amido- α -D-mannopyranoside (**13/14/15**).

4.2.9.1 Synthesis of 3-thio-heptanoic acid-2,3,4-tri-*O*-acetyl -6-lauroyl amido- α -D-mannoside (**13**)

3-Thia-heptanoic acid-2,3,4-triacetyl-6-lauroyl amido- α -D-mannopyranoside (**13**) was synthesized from allyl 2,3,4-tri-*O*-acetyl -6-lauroyl amido- α -D-mannoside with 84% yield.

^1H NMR (400 MHz, CDCl_3) δ : 0.87 (t, $J = 6.8$ Hz, 3H, RCH_3), 1.27 (d, $J = 16.1$ Hz, 19H, RCH_2R), 1.62 (p, $J = 7.3$ Hz, 2H, RCH_2R), 1.79 – 1.96 (m, 2H, $\text{OCH}_2\text{CH}_2\text{CH}_2\text{S-}$), 1.99 (s, 3H, CH_3CO), 2.08 (s, 3H, CH_3CO), 2.14 (s, 3H, CH_3CO), 2.18 – 2.27 (m, 2H, OCH_2CH_2), 2.56 – 2.71 (m, 5H, $\text{OCH}_2\text{CH}_2\text{CH}_2\text{-S-CH}_2\text{CH}_2\text{COOH}$), 2.79 (d, $J = 6.8$ Hz, 2H, $\text{OCH}_2\text{CH}_2\text{CH}_2\text{-S-CH}_2\text{CH}_2\text{COOH}$), 3.22 (dt, $J = 14.1, 5.8$ Hz, 1H, H-6a), 3.50 (dt, $J = 9.7, 5.7$ Hz, 1H, H-6b), 3.74 (dddt, $J = 21.2, 9.3, 6.8, 4.1$ Hz, 2H, $\text{OCH}_2\text{CH}_2\text{CH}_2\text{S-}$), 3.88 (ddd, $J = 9.6, 6.5, 2.6$ Hz, 1H, H-5), 4.74 – 4.78 (m, 1H, H-4), 5.10 (t, $J = 10.0$ Hz, 1H, H-2), 5.23 (dd, $J = 3.2, 1.5$ Hz, 1H, H-3), 5.31 (dd, $J = 10.0, 3.4$ Hz, 1H, H-1), 6.02 (t, $J = 5.8$ Hz, 1H, $-\text{CO-NH-R}$). ^{13}C NMR (100 MHz, CDCl_3) δ : 14.10 (RCH_3), 20.69 (CH_3CO), 20.76 (CH_3CO), 20.86 (CH_3CO), 22.66 (RCH_2R), 24.58 (RCH_2R), 25.71 (RCH_2R), 26.81 (RCH_2R), 27.70 (RCH_2R), 27.90 (RCH_2R), 28.64 (RCH_2R), 28.75 (RCH_2R), 29.28 (RCH_2R), 29.31 (RCH_2R), 29.35 (RCH_2R), 29.48 (RCH_2R), 29.59 (RCH_2R), 29.61 (RCH_2R), 31.89 ($\text{S-CH}_2\text{CH}_2\text{COOH}$), 32.16 ($\text{OCH}_2\text{CH}_2\text{CH}_2\text{-S-}$), 34.74 ($\text{OCH}_2\text{CH}_2\text{CH}_2\text{-S-}$), 35.30 ($\text{S-CH}_2\text{CH}_2\text{COOH}$), 36.78 ($-\text{COCH}_2\text{R}$), 39.47 (C-6), 44.17, 66.17 (C-5), 67.11 ($\text{OCH}_2\text{CH}_2\text{CH}_2\text{-S}$), 67.99 (C-4), 68.83, 68.99 (C-2), 69.60 (C-3), 97.38 (C-1), 170.00 (CH_3CO), 170.01 (CH_3CO), 170.36 (CH_3CO), 173.88 ($\text{S-CH}_2\text{CH}_2\text{COOH}$), 175.37 ($-\text{COCH}_2\text{R}$). ES-MS (LR): $m/z = 656.5$ [$\text{M} + \text{Na}$] $^+$

4.2.9.2 Synthesis of 3-thio-heptanoic acid-2,3,4-tri-*O*-acetyl -6-palmitoyl amido- α -D-mannoside (**14**)

3-Thia-heptanoic acid-2,3,4-triacetyl-6-palmitoyl amido- α -D-mannopyranoside (**14**) was synthesized from allyl 2,3,4-tri-*O*-acetyl -6-palmitoyl amido- α -D-mannoside with 78% yield.

^1H NMR (400 MHz, CDCl_3) δ : 0.89 (t, $J = 6.8$ Hz, 3H, RCH_3), 1.26 (s, 27H, RCH_2R), 1.63 (q, $J = 7.2$ Hz, 2H, RCH_2R), 1.91 (dt, $J = 13.0, 6.2$ Hz, 2H, $\text{OCH}_2\text{CH}_2\text{CH}_2\text{S-}$), 2.00 (s, 3H, CH_3CO), 2.10 (d, $J = 4.0$ Hz, 3H, CH_3CO), 2.15 (s, 3H, CH_3CO), 2.19 – 2.28 (m, 2H, OCH_2CH_2), 2.58 – 2.74 (m, 4H, $\text{OCH}_2\text{CH}_2\text{CH}_2\text{-S-CH}_2\text{CH}_2\text{COOH}$), 2.77 – 2.85 (m, 2H, $\text{OCH}_2\text{CH}_2\text{CH}_2\text{-S-CH}_2\text{CH}_2\text{COOH}$), 3.23 (dt, $J = 14.3, 5.4$ Hz, 1H, H-6a), 3.52 (dt, $J = 9.6, 5.7$ Hz, 1H, H-6b), 3.69 – 3.82 (m, 2H, $\text{OCH}_2\text{CH}_2\text{CH}_2\text{S-}$), 3.89 (ddd, $J = 9.7, 6.6, 2.8$ Hz, 1H, H-5), 4.77 (d, $J = 1.5$ Hz, 1H, H-4), 5.11 (t, $J = 10.1$ Hz, 1H, H-2), 5.25 (dd, $J = 3.4, 1.7$ Hz, 1H, H-3), 5.33 (dd, $J = 10.1, 3.5$ Hz, 1H, H-1), 6.01 (t, $J = 5.9$ Hz, 1H, $-\text{CO-NH-R}$). ^{13}C NMR (101 MHz, CDCl_3) δ : 14.12 (RCH_3), 20.71 (CH_3CO), 20.73 (CH_3CO), 20.77 (CH_3CO), 22.68 (RCH_2R), 25.72 (RCH_2R), 26.79 (RCH_2R), 28.66 (RCH_2R), 28.76 (RCH_2R), 29.30 (RCH_2R), 29.35 (RCH_2R), 29.51 (RCH_2R), 29.65 (RCH_2R), 29.66 (RCH_2R), 29.69 (RCH_2R), 31.92 ($\text{S-CH}_2\text{CH}_2\text{COOH}$), 34.77 ($\text{OCH}_2\text{CH}_2\text{CH}_2\text{-S-}$), 36.81 ($-\text{COCH}_2\text{R}$), 39.49 (C-6), 66.18 (C-5), 67.14 ($\text{OCH}_2\text{CH}_2\text{CH}_2\text{-S}$), 69.00 (C-4), 69.06 (C-2), 69.68 (C-3), 97.39 (C-1), 170.03 (CH_3CO), 170.09 (CH_3CO), 170.39 (CH_3CO), 173.89 (CH_3CO), 175.85 ($\text{S-CH}_2\text{CH}_2\text{COOH}$), 176.50 ($-\text{COCH}_2\text{R}$). ES-MS (LR): $m/z = 712.5$ [$\text{M} + \text{Na}$] $^+$

4.2.9.3 Synthesis of 3-thio-heptanoic acid-2,3,4-tri-*O*-acetyl -6-stearoyl amido- α -D-mannoside (15)

3-Thia-heptanoic acid-2,3,4-triacetyl-6-stearoyl amido- α -D-mannopyranoside (**15**) was synthesized from allyl 2,3,4-tri-*O*-acetyl -6-stearoyl amido- α -D-mannoside with 90% yield.

^1H NMR (400 MHz, CDCl_3) δ : 0.81 (t, $J = 6.8$ Hz, 3H, RCH_3), 1.18 (s, 27H, RCH_2R), 1.55 (q, $J = 7.2$ Hz, 2H, RCH_2R), 1.92 (s, 3H, CH_3CO), 2.02 (s, 3H, CH_3CO), 2.08 (d, $J = 3.1$ Hz, 3H, CH_3CO), 2.13 – 2.20 (m, 2H, OCH_2CH_2), 2.56 – 2.62 (m, 4H, $\text{OCH}_2\text{CH}_2\text{CH}_2\text{-S-CH}_2\text{CH}_2\text{COOH}$), 2.74 (t, $J = 6.3$ Hz, 2H, $\text{OCH}_2\text{CH}_2\text{CH}_2\text{-S-CH}_2\text{CH}_2\text{COOH}$), 3.11 (dt, $J = 14.2, 5.8$ Hz, 1H, H-6a), 3.39 – 3.48 (m, 1H, H-6b), 3.70 (ddt, $J = 9.8, 7.1, 4.8$ Hz, 2H, $\text{OCH}_2\text{CH}_2\text{CH}_2\text{S-}$), 3.82 (ddd, $J = 9.7, 6.6, 2.8$ Hz, 1H, H-5), 4.69 (d, $J = 1.4$ Hz, 1H, H-4), 5.03 (t, $J = 10.1$ Hz, 1H, H-2), 5.17 (dd, $J = 3.4, 1.7$ Hz, 1H, H-3), 5.25 (dt, $J = 9.9, 3.5$ Hz, 1H, H-1), 5.88 – 6.01 (m, 1H, $-\text{CO-NH-R}$). ^{13}C NMR (100 MHz, CDCl_3) δ : 14.13 (RCH_3), 20.73 (CH_3CO), 20.80 (CH_3CO), 20.89 (CH_3CO), 22.69 (RCH_2R), 24.58 (RCH_2R), 25.56 (RCH_2R), 25.72 (RCH_2R), 26.87

(RCH₂R), 27.60 (RCH₂R), 28.67 (RCH₂R), 28.77 (RCH₂R), 29.31 (RCH₂R), 29.37 (RCH₂R), 29.52 (RCH₂R), 29.66 (RCH₂R), 29.68 (RCH₂R), 29.71 (RCH₂R), 31.93 (S-CH₂CH₂COOH), 32.20 (S-CH₂CH₂COOH), 34.88 (OCH₂CH₂CH₂-S-), 36.84 (-COCH₂R), 39.55 (C-6), 66.20 (C-5), 66.80 (OCH₂CH₂CH₂-S), 67.24 (OCH₂CH₂CH₂-S), 69.01 (C-4), 69.54 (C-3), 69.69 (C-2), 97.35 (C-1), 170.04 (CH₃CO), 170.45 (CH₃CO), 170.84 (CH₃CO), 173.95 85 (S-CH₂CH₂COOH), 174.85 (-COCH₂R). ES-MS (LR): $m/z = 740.95 [M + Na]^+$

4.2.10. Synthesis of 3-thio-heptanoic acid-6-fatty amido- α -D-mannoside: General Procedures (16/17/18)

3-Thia-heptanoic acid-2,3,4-triacetyl-6-fatty amido- α -D-mannopyranoside (0.5 g, 0.7 mmol) was dissolved in 30 ml dry methanol and Na metal (0.2 g, 3.2 mmol) was added to it at freezing temperature and stirred vigorously at that temperature until dissolve the sodium. The ice bath was removed and stirred the solution for an hour at room temperature and monitored via TLC. After completing the reaction, the solution was neutralized with ion exchange resin (Dowex 50W X8-400 ion exchange resin, Sigma-Aldrich) to reach pH ~ 3, filtered and concentrated under reduced pressure to give 3-thio-heptanoic acid-6-fatty amido- α -D-mannopyranoside as white powder (16/17/18).

4.2.10.1 Synthesis of 3-thio-heptanoic acid-6-lauroylamido- α -D-mannoside (16)

3-Thia-heptanoic acid-6-lauroyl amido- α -D-mannopyranoside (16) was synthesized from 3-thia-heptanoic acid- 2,3,4-tri-*O*-acetyl -6-lauroyl amido- α -D-mannoside with 73% yield.

¹H NMR (400 MHz, CDCl₃) δ : 0.81 (t, $J = 6.8$ Hz, 3H, RCH₃), 1.08 – 1.31 (m, 19H, RCH₂R), 1.56 (s, 2H, RCH₂R), 1.65 – 1.94 (m, 2H, OCH₂CH₂CH₂S-), 2.19 (s, 2H, OCH₂CH₂CH₂S-), 2.54 (t, $J = 7.2$ Hz, 4H, OCH₂CH₂CH₂-S-CH₂CH₂COOH), 2.71 (t, $J = 7.2$ Hz, 2H, OCH₂CH₂CH₂-S-CH₂CH₂COOH), 3.10 (d, $J = 13.6$ Hz, 1H, H-6a), 3.34 – 3.57 (m, 4H, OCH₂CH₂CH₂S), 3.72 – 4.04 (m, 6H, H-5, H-4, H-3 and H-2), 4.72 (s, 1H, H-1), 6.31 (s, 1H, -CO-NH-R). ¹³C NMR (100 MHz, CDCl₃) δ : 14.12 (RCH₃), 22.69 (RCH₂R), 25.80 (RCH₂R), 25.85 (RCH₂R), 26.96 (RCH₂R), 27.29 (RCH₂R), 28.75 (RCH₂R), 29.09 (RCH₂R), 29.32 (RCH₂R), 29.35 (RCH₂R), 29.39 (RCH₂R),

29.44 (RCH₂R), 31.91 (S-CH₂CH₂COOH), 34.63 (OCH₂CH₂CH₂-S-) , 34.91 (OCH₂CH₂CH₂-S), 36.50 (-COCH₂R), 40.07 (C-6), 67.43 (OCH₂CH₂CH₂-S), 70.39 (C-5), 70.71 (C-4), 71.00 (C-2), 71.26 (C-3), 99.99 (C-1), 172.44 (S-CH₂CH₂COOH), 175.97 (-COCH₂R). ES-MS (LR): $m/z = 506.2$ [M - H]⁻

4.2.10.2 Synthesis of 3-thio-heptanoic acid-6-palmitoylamido- α -D-mannoside (17)

3-Thia-heptanoic acid-6-palmitoyl amido- α -D-mannopyranoside (**17**) was synthesized from 3-thia-heptanoic acid- 2,3,4-tri-*O*-acetyl -6-palmitoyl amido- α -D-mannoside with 78% yield.

¹H NMR (400 MHz, CD₃OD) δ : 0.92 (t, $J = 6.8$ Hz, 3H, RCH₃), 1.32 (d, $J = 10.2$ Hz, 26H, RCH₂R), 1.58 – 1.69 (m, 2H, RCH₂R), 1.88 (dq, $J = 13.0, 6.9$ Hz, 2H, OCH₂CH₂CH₂S-), 2.21 – 2.28 (m, 2H, OCH₂CH₂CH₂S-), 2.60 (t, $J = 7.1$ Hz, 2H, (S-CH₂CH₂COOH), 2.65 (t, $J = 7.1$ Hz, 2H, OCH₂CH₂CH₂-S-), 2.77 (t, $J = 7.2$ Hz, 2H, (CH₂CH₂COOH), 3.42 – 3.51 (m, 2H, H-6a, H-5), 3.52 (s, 1H, H-6b), 3.69 (dd, $J = 9.2, 3.5$ Hz, 1H, H-4), 3.82 (dd, $J = 3.3, 1.6$ Hz, 2H, H-3 & H-2), 4.74 (d, $J = 1.4$ Hz, 1H, H-1). ¹³C NMR (100 MHz, CD₃OD) δ : 13.08 (RCH₃), 22.35 (RCH₂R), 25.77 (RCH₂R), 26.51 (RCH₂R), 28.15 (RCH₂R), 29.05 (RCH₂R), 29.09 (RCH₂R), 29.14 (RCH₂R), 29.26 (RCH₂R), 29.39 (RCH₂R), 29.41 (RCH₂R), 31.69 (S-CH₂CH₂COOH), 34.32 (OCH₂CH₂CH₂-S-), 35.72 (-COCH₂R), 40.01 (C-6), 65.42 (OCH₂CH₂CH₂-S), 68.27 (C-5), 70.75 (C-4), 70.88 (C-2), 71.28 (C-3), 100.25 (C-1), 174.29 (S-CH₂CH₂COOH), 175.40 (-COCH₂R). ES-MS (LR): $m/z = 586.4$ [M + Na]⁺

4.2.10.3 Synthesis of 3-thio-heptanoic acid-6-stearoylamido- α -D-mannoside (18)

3-Thia-heptanoic acid-6-stearoyl amido- α -D-mannopyranoside (**18**) was synthesized from 3-thia-heptanoic acid- 2,3,4-tri-*O*-acetyl -6-stearoyl amido- α -D-mannoside with 72% yield.

¹H NMR (400 MHz, CD₃OD) δ : 0.87 – 0.97 (m, 3H, RCH₃), 1.31 (s, 31H, RCH₂R), 1.63 (s, 2H, RCH₂R), 1.88 (d, $J = 5.9$ Hz, 2H, OCH₂CH₂CH₂S-), 2.21 – 2.29 (m, 2H, OCH₂CH₂CH₂S-), 2.63 (dt, $J = 23.0, 7.3$ Hz, 4H, S-CH₂CH₂COOH), 2.77 (t, $J = 7.1$ Hz, 2H, OCH₂CH₂CH₂S-), 3.41 – 3.63 (m, 3H, H-5, H-6a & H-6b), 3.69 (dd, $J = 9.3, 3.4$

Hz, 1H, H-4), 3.77 – 3.87 (m, 2H, H-2 & H-3), 4.74 (d, $J = 1.6$ Hz, 1H, H-1). ^{13}C NMR (100 MHz, CD_3OD) δ : 13.06 (RCH₃), 22.35 (RCH₂R), 25.77 (RCH₂R), 26.52 (RCH₂R), 28.15 (RCH₂R), 29.05 (RCH₂R), 29.08 (RCH₂R), 29.14 (RCH₂R), 29.26 (RCH₂R), 29.40 (RCH₂R), 31.69 (S-CH₂CH₂COOH), 34.34 (OCH₂CH₂CH₂-S-), 35.72 (-COCH₂R), 40.01 (C-6), 65.42 (OCH₂CH₂CH₂-S), 68.28 (C-5), 70.75 (C-4), 70.88 (C-2), 71.28 (C-3), 100.25 (C-1), 174.33 (S-CH₂CH₂COOH), 175.40 (-COCH₂R).). ES-MS (LR): $m/z = 614.5$ [M + Na]⁺

4.2.11. Digestion and purification of commercially available chitosan

The commercial chitosan was digested with hydrogen peroxide (H_2O_2 , 33%) with varying incubation time to produce low molecular weight chitosan by cleaving the ether bonds between glucosamine units of chitosans according to the procedure describes elsewhere.^{304,305} Briefly, chitosan (10 g) was dissolved in 400 mL of acidified water (400 mL, pH 3) in two large round bottom flask and stirred vigorously. H_2O_2 (30 mL) was slowly added to the solution and stirred continuously. The reaction mixture was quenched by adding 50 mL of methanol after 3.5 h and 9.0 h and the pH was adjusted to 7. The digested low molecular weight chitosans (LMWCs) with reaction time 3.5 h and 9.0 h were exhaustively dialyzed against deionized water (DI) for 72 h with a molecular weight cutoff (MWCO) of 3.5 kDa and 1 kDa, respectively and lyophilized to obtain white powder with yield 90% and 70 % respectively. The reported molecular weights (MWs) of digested chitosan were broadly distributed ranging from 4-6.5 kDa (weight average MW 4.3 kDa; LMWC_{5k}) and 2-4 kDa (weight average MW 2.1 kDa; LMWC_{2k}) after 3.5 h and 9.0 h digestion, respectively.³⁰⁵

4.2.12. Synthesis of c: General procedure

Lactose grafted chitosan (Chitlac) samples with various degree of lactosylation were synthesized from purified and digested chitosan according the procedure reported elsewhere.²⁹³ Briefly, chitosan (M_n 50-190 kDa), LMWC_{5k} (M_n 4-6.5 kDa) and LMWC_{2k} (M_n 2-4 kDa) were dissolved in a 1: 1 mixture of methanol and 1% acetic acid (30 mL) in three separate reaction flask and stir the solution for 30 min. Lactose and sodium cyanoborohydride were dissolved in the same MeOH and 1% AcOH (20 mL) mixture and transferred to the polymer solution. The reaction mixture was stirred for 48 h at room temperature and after dilution with water (30 mL), exhaustively dialysed (~ 5

d) against DI water. The polymer solution was then filtered through 0.45 μm Millipore filters and lyophilized to obtain Chitlac, Chitlac_{5k}, and Chitlac_{2k} with different degree of lactosylation. The reaction condition details are described in Table 4.1.

Table 4.1: Reaction conditions by altering the amount of lactose molecule to synthesize Chitlac A, Chitlac B, Chitlac C, Chitlac D, Chitlac_{5k}, and Chitlac_{2k}.

Sample	Lactose			NaBH ₃ CN		
	a	Amount	mmol	a	Amount	mmol
Chitlac A	2.5	1.25 g	3.66	6.0	0.55 g	8.78
Chitlac B	1.0	0.47 g	1.36	2.5	0.22 g	3.5
Chitlac C	0.8	0.38 g	1.10	2.0	0.17 g	2.75
Chitlac D	0.5	0.23 g	0.68	1.3	0.11 g	1.71
Chitlac _{5k}	0.2	1.0 g	0.2	0.5	0.15	2.5
Chitlac _{2k}	0.2	0.2 g	0.095	0.5	0.03	0.5

a is the equivalents used per repeating unit of chitosan

4.2.13. Synthesis of lactose and mannose conjugated chitosan (Chitmannolac):

General procedure

Coupling of 3-thio-heptanoic acid- α -D-mannoside (compound **4**) with the Chitlac was performed using EDC and NHS *via* amide bond formation. Briefly, desired amount of 3-thio-heptanoic acid- α -D-mannoside (20 mol% of the repeating unit of GlcNH₂ in chitosan) was dissolved in 5 ml of distilled water and activated with a mixture of NHS and EDC for 3 hours. Subsequently, desired amount of Chitlac was dissolved in 5 mL of 0.1 M HCl (pH~4) solution and then added into the activated 3-thio-heptanoic acid- α -D-mannoside solution. The reaction was performed for 72 h at RT. The resulting product was purified using a dialysis tube (ranges from 1000 to 12000-14000 MWCO based on chitosan molecular weight) against DI water for ~3 days and lyophilized to obtain mannose modified chitosan (Chitman) as a white powder. The reaction conditions are described in Table 4.2.

Table 4.2: Reaction conditions to synthesize Chitmannolac, Chitmannolac_{5k} and Chitmannolac_{2k}.

Sample	Compound 4		EDC		NHS		Chitmannolac (yield)
	Amount	mmol	Amount	mmol	Amount	mmol	
Chitlac (0.05 g, 0.25 μ mol)	0.047 g	0.15	0.04 g	0.22	0.017	0.15	0.068 g (53 %)
Chitlac _{5k} (0.2 g, 0.03 mmol)	0.064 g	0.2	0.06 g	0.3	0.035	0.3	0.19 g (77 %)
Chitlac _{2k} (0.1 g, 0.03 mmol)	0.033 g	0.1	0.04 g	0.2	0.023	0.2	0.11 g (90 %)

a is the equivalents used per repeating unit of chitosan

4.2.14. Synthesis of palmitoyl amido mannoside-g- Chitmannolac (PAM-g-Chitmannolac)

Coupling of 3-thia-heptanoic acid-6-palmitoyl amido- α -D-mannopyranoside (**17**, 30 mol% of the repeating unit of GlcNH₂ in chitosan) with the Chitmannolac was performed according the similar procedure describe above to synthesis Chitmannolac *via* carbodiimide chemistry. The reaction conditions are described in Table 4.3.

Table 4.3: Reaction conditions to synthesize palmitoyl amido mannoside-g-Chitmannolac (PAM-g-Chitmannolac).

Sample	Compound 17		EDC		NHS		PAM-g-Chitmannolac (yield)
	Amount	mmol	Amount	mmol	Amount	mmol	
Chitmannolac _{5k} (0.02 g, 0.0024 mmol)	0.022 g	0.04	0.016 g	0.08	0.009	0.08	0.035 g (82 %)
Chitmannolac _{2k} (0.02 g, 0.0015 mmol)	0.012 g	0.02	0.01 g	0.05	0.006	0.06	0.027 g (70 %)

a is the equivalents used per repeating unit of chitosan

4.2.15. Synthesis of stearoyl amido mannoside-g- Chitmannolac (SAM-g-Chitmannolac)

Coupling of 3-thia-heptanoic acid-6-stearoyl amido- α -D-mannopyranoside (**18**, 30 mol% of the repeating unit of GlcNH₂ in chitosan) with the Chitmannolac was performed according the similar procedure describe above to synthesis Chitmannolac *via* carbodiimide chemistry. The reaction conditions are described in Table 4.4.

Table 4.4: Reaction conditions to synthesize stearyl amido mannoside-g-Chitmannolac (SAM-g-Chitmannolac).

Sample	Compound 18		EDC		NHS		SAM-g-Chitmannolac (yield)
	Amount	mmol	Amount	mmol	Amount	mmol	
Chitmannolac _{5k} (0.02 g, 0.0024 mmol)	0.022 g	0.04	0.016 g	0.08	0.009	0.08	0.045 g (88 %)
Chitmannolac _{2k} (0.02 g, 0.0015 mmol)	0.012 g	0.02	0.01 g	0.05	0.006	0.06	0.032 g (75 %)

a is the equivalents used per repeating unit of chitosan

4.2.16. Synthesis of fluorescein and glycolipid grafted chitosan

6-(3-Carboxypropylaminocarbonyl)fluorescein (5 mol% of the repeating unit of GlcNH₂ in chitosan) was conjugated to the chitosan backbone using EDC and NHS *via* amide bond formation as described above. The reaction conditions are described in Table 4.5.

Table 4.5: Reaction conditions to synthesize fluorescein-c-palmitoyl amido mannoside-g-Chitmannolac (Fluorescein-c-PAM-g-Chitmannolac) and fluorescein-c-stearyl amido mannoside-g-Chitmannolac (Fluorescein-c-SAM-g-Chitmannolac).

Sample	Fluorescein		EDC		NHS		Chitmannolac (yield)
	Amount	mmol	Amount	mmol	Amount	mmol	
PAM-g-Chitmannolac _{5k} (0.02 g, 17.5 μmol)	0.008 g	0.015	0.005 g	0.015	0.003	0.015	0.015 g (58 %)
SAM-g-Chitmannolac _{5k} (0.02 g, 17.5 μmol)	0.008 g	0.015	0.005 g	0.015	0.003	0.015	0.01 g (42 %)

Fluorescein-c-chitosan_{5k} (Flu-c-Chitosan_{5k}) was also synthesized as control compound following the similar procedure describe above.

4.2.17. Preparation of DSA encapsulated chitosan based glyconanoparticles

The chitosan based glyconanoparticles were prepared using nanoprecipitation method through self-assembly of the glycolipid-g-Chitmannolac followed by probe sonication as described elsewhere.²⁰⁸ Briefly, 20 mg of PAM-g-Chitmannolac_{5k} or SAM-g-Chitmannolac_{5k} in 10 ml of 0.1 M acetic acid was mixed with 5 mg of DSA in 2.5 ml ethanol in 25 mL round bottom flask and constant stirring for 1 h. The resultant dispersion was processed for size reduction using a tip-type sonicator (Branson,

Danbury, CT, USA) for 5 min at 20% amplitude (20 s pulse on and 5 s pulse off). The solution was then stirred overnight at room temperature to remove the organic solvent and the pH was adjusted to 7.0 with 0.1 M NaOH solution. The untrapped DSA was removed *via* dialysis using dialysis membrane tubing (MWCO 3500) against 1000 mL water for 24 h. Finally, the prepared DSA loaded GNPs were passes through 0.45 μm Millipore filters and lyophilized. The DSA loaded GNPs prepared from PAM-g-Chitmannola_{5k} and from SAM-g-Chitmannola_{5k} were denoted as DSA/PAM-GNP_{5k} and DSA/SAM-GNP_{5k}, respectively.

Fluorescein conjugated GNPs were prepared by following the similar procedure describe above using hydrophobic DSA molecules along with fluorescein-c-PAM-g-Chitmannolac_{5k} or fluorescein-c-SAM-g-Chitmannolac and the prepared GNPs are denoted as DSA/Flu-c-PAM-GNP_{5k} and DSA/Flu-c-SAM-GNP_{5k}, respectively.

4.2.18. Immobilization of amikacin into the DSA/PAM-GNP_{5k} and DSA/SAM-GNP_{5k}

The DSA/PAM-GNP_{5k} and DSA/SAM-GNP_{5k} (10 mg each) were dissolved in 6 ml ultrapure water in a 10 mL vial and 2 mg of amikacin sulphate was added to it. The solution mixture was then stirred for 2 h. Non-encapsulated amikacin was removed by centrifugation at 14 000 *g* for 15 h at 4°C. The amount of encapsulated amikacin was determined from the unbound amikacin in the supernatants *via* ultraviolet-visible spectroscopy (UV-vis) at wavelength 349 nm through a derivatization method using *o*-phalaldialdehyde (OPA) which is described in the previous chapter. The amikacin encapsulated DSA/PAM-GNP_{5k} and DSA/SAM-GNP_{5k} were denoted as amikacin/DSA/PAM-GNP_{5k} and Amikacin/DSA/SAM-GNP_{5k} respectively.

4.2.19. *In vitro* amikacin release studies

The *in vitro* drug release studies were carried out in PBS at pH 5.5 and pH 7.4 using dialysis chambers at 37°C to mimic *in vivo* environment. The chambers were immersed in 30 mL of release medium at pH 5.5 and pH 7.4. Finally, the sample was place in a shake incubator at 37°C. In order to measure the amikacin delivery, 3 mL of solution were withdrawn at desired time intervals from the outside released medium and analyzed by the UV-vis spectroscopy method described above. The constant volume of

total delivery liquid was ensured by replacing with an equal volume of fresh released medium. Each drug release experiment was employed three times to calculate the mean values and standard deviations. Actual drug release % was determined based on the following equation:

$$\text{Drug release (\%)} = \frac{\text{Release of amikacin at a definite time}}{\text{Total amount of amikacin entrapped within the GNPs}} \times 100$$

4.2.20. Characterization of the prepared GNPs

High temperature nuclear magnetic resonance (NMR) spectra were recorded on Bruker Avance 400 spectrometer operating at 400 MHz using deuterium oxide as the solvent. Physical characterisation of GNPs including particle size measurements was determined by dynamic light scattering (DLS) using the photon correlation spectroscopy technique. The zeta potential (surface charge) of the particles was estimated by laser-Doppler electrophoresis to find the stability of the GNPs. The prepared GNPs were diluted 10-fold in water to measure the particle size as well as diluted 300-fold during zeta potential measurements respectively. All the data were collected with three independent measurements ($n = 3$). The measurements were performed in triplicate at room temperature using a Zetasizer Nano ZS (Malvern Instruments, Worcestershire, UK) equipped with a 633 nm laser and 173° detection optics.

The critical micelle concentrations (CMC) were measured using DLS following a procedure published elsewhere.³⁰⁶ Initially, DSA/PAM-GNP_{5k} and DSA/SAM-GNP_{5k} were dissolved in 1% acetic acid at concentration 2 mg/mL and adjusted to pH 5.5 using 1N NaOH. Then, concentration ranges of 1.0 µg/ml to 1.0 mg/mL were prepared using water and stirred for 1 h. The intensity of the scattered light was measured by DLS (expressed in kilo counts per second) and run for five times for each dilution. Finally, intensities were plotted as a function of the DSA/PAM-GNP_{5k} and DSA/SAM-GNP_{5k} concentrations (µg/ml) and the CMC was determined as the intersection between the two straight lines.

UV-vis spectroscopy measurements were performed in a Cintra 300 UV-vis spectrophotometer and the spectra were collected between 200 to 600 nm. The transmittance of the modified chitosan was also studied using UV-vis spectroscopy at

different pH solution. The polymer samples were dissolved in 1% acetic acid (0.2 mg/mL) and measured the transmittance after 24 h at 600 nm. The pH of the solution ranges between 5.5 and 8.5 was adjusted using 2N NaOH solution. Fluorescence measurements were recorded in 3 mL quartz cuvettes using FluoroMate FS-2 fluorescence spectrometer equipped with a xenon lamp excitation source. All fluorescence spectra were measured at an excitation wavelength of 440 nm.

4.2.21. Macrophage cell culture

The RAW 264.7 macrophage cell line obtained from American Type Culture Collection (ATCC, Manassas, VA, USA) and cultured according to the ATCC procedure. Briefly, cells were cultured in DMEM (Sigma-Aldrich) medium supplemented with 10% heat-inactivated foetal bovine serum (FBS), 100U/mL of penicillin, and 100 µg/mL of Streptomycin (Sigma-Aldrich) in a humidified atmosphere of 5% CO₂ at 37°C and used for experiments between passages 12 and 16.

4.2.22. Determination of cellular toxicity using MTT Assays

Cell proliferation was evaluated using the 3-(4,5-dimethylthiazol-2-yl)2,5-diphenyltetrazolium bromide (MTT) assay. Briefly, RAW264.7 cells were seeded into 96-well plate (5×10^3 cells/well) for 12 h, washed, and treated with 0, 0.25, 0.5, 1.0 and 2.0 mg/mL of DSA/PAM-GNP_{5k}, DSA/SAM-GNP_{5k}, amikacin/DSA/PAM-GNP_{5k} and Amikacin/DSA/SAM-GNP_{5k} for 24 h at 37°C. After treatment, cells were washed with PBS and MTT stock solution (5mg/mL) was then added to each well and incubated for an additional 4 h. At the end of the experiment, the medium was replaced with 100 µL of DMSO to dissolve the formazan crystals, and the absorbance was measured at 540 nm using Polarstar Omega 96-well microplate reader (BMG Labtech GmbH, Germany). The cell viability was calculated using the following formula: Cell viability (%) = $(OD_{\text{exp}} - OD_{\text{blank}})/(OD_{\text{control}} - OD_{\text{blank}}) \times 100\%$.

4.2.23. Enzyme-linked immunosorbent assay (ELISA): Determination of the TNF- α and IL-6 Release

The secreted cytokines were measured from RAW 264.7 macrophage cell after treating with various concentrations of DSA/PAM-GNP_{5k} and DSA/SAM-GNP_{5k} in fresh culture medium for 12, 24 and 48 h. Then, 500 µL aliquots were taken from the

supernatant and stored at -80°C until they were used for measurements by sandwich ELISA assays. Supernatant taken from the untreated cells were used as control and supernatant from lipopolysaccharide treated cells were used as positive control (LPS, 50 ng/mL, Sigma-Aldrich, USA).

The proinflammatory cytokines, TNF- α and IL-6, were quantified by enzyme-linked immunosorbent assay (ELISA) obtained from elisakit.com.au, Australia and the ELISA kit was performed according to producer's instructions. Briefly, diluted supernatants (1:5, in DMEM) were incubated in antibody-coated 96-well plates to facilitate binding of released cytokines. The incubation with a biotinylated primary antibody was performed. The next step was incubation with streptavidin-horseradish peroxidase. All incubation steps were followed by washing, which guarantees the removal of unbound molecules. Horseradish peroxidase is capable of oxidizing its substrate tetramethylbenzidine (TMB), which develops a stable staining complex with sulfuric acid detectable at 450 nm by means of a plate reader. The limit of sensitivity for detection of TNF- α and IL-6 was <5 and <1 pg/mL, respectively, with both intra-assay and inter-assay variability $< 10\%$.

4.2.24. Confocal images

RAW264.7 cells were plated on a sterile cover slide in a 12 well plate at a density of 5×10^4 cells/well and incubated overnight at 37°C . Cells were washed twice with PBS and treated with Flu-c-Chitosan_{5k} and DSA/Flu-c-PMA-GNP_{5k} for 4 hours. After treatment, cells are washed thoroughly with ice-cold PBS (3 times) and fixed with 0.5 mL of 4% (w/v) paraformaldehyde for 10 min at room temperature. Cells were then permeabilized with 0.1% Triton X-100 in PBS for 5 min at room temperature and washed twice with PBS. The nucleus of the cells were stained with Hoechst 33342 for 5 min at room temperature in the dark and washed thrice after staining. The cover slide were carefully fixed onto a clean and clear tissue culture glass slide using mounting media and dried overnight. Finally, the cells were examined by using a Nikon A1R+

confocal microscope and images were acquired with a Nikon digital camera and NIS-Elements acquisition software (version 4.13).

4.2.25. Macrophage infection and intracellular bacterial inhibition assays

S. aureus strain ATCC 25923 was grown in LB medium at 37°C with 160 rpm shaking. Colony forming units (CFU) were determined after serial dilution and plating the *S. aureus* cells on LB agar plates

Intracellular antibacterial activity was determined in RAW 264.7 cells infected with *S. aureus* (bacteria/cell ratio of 10) using fully validated procedure reported elsewhere.^{44,45,50} Briefly, 5 µL of processed bacteria containing 10⁶ bacteria was added into the macrophage cells (10⁵ cells per well) distributed in 12-well tissue culture plates. The infected cells were incubated for 2 h 37°C to allow phagocytosis. The cell medium was then washed with fresh media containing 10% FBS to remove extracellular bacteria those are not phagocytized and washed thoroughly with PBS. Macrophages were then treated with fresh media containing different concentration of DSA/PAM-GNP_{5k} and Amikacin/DSA/SAM-GNP_{5k} with concentration 0, 50, 100, 200 and 400 µg/mL. Untreated cells were served as control.

Infected macrophages cultures were terminated at 1, 3, 6, 12, and 24 h post infection. Cell free supernatant from infected bacteria were diluted and plated on LB agar plates to determine extracellular bacterial growth. The infected macrophages were lysed with sterile distilled water to evaluate the intracellular bacterial viability and plating the lysates on LB agar followed by visual counting of bacterial colonies.

4.2.26. Statistical Analysis

Data from all samples within each group were combined with means ± standard error of mean (S.E.M). Data were averaged from three independent experiments each containing at least 4 replicates. Statistical significant was determined by one-way analysis of variance (one-way ANOVA) and a Dunnett's multiple comparison was used to compare the effect among groups using GraphPad Prism software (version 6.01, La Jolla, CA). Values with P<0.05 were considered significant.

4.3. Results and Discussion

Generally, mannopyranosyl phenylisothiocyanate and formylmethyl mannopyranoside were designed as mannosylated reagents to modify polysaccharides.²³³ Holl *et al.* prepared some monosaccharide modified chitosan derivatives using formylmethyl glycosides which were produced via oxidation of the allyl group at -78°C using an ozone generator.³⁰⁷ Zong's group oxidized allyl mannose using the very toxic compound OsO_4 and NaIO_4 for mannose modification to chitosan.²⁴⁷ On the other hand, researchers selected mannose phenylisothiocyanate as a mannose-modifying reagent that unfortunately is unstable, expensive, and may have toxicity because of the phenylisothiocyanate bridge for linking the mannose residues to chitosan, and should be handled carefully due to the fact that the toxicity of therapeutic carriers affects the therapeutic efficiency *in vitro* and *in vivo*.^{38,98} Here, a new and practical approach to modify chitosan has been developed using mannose as a precursor.

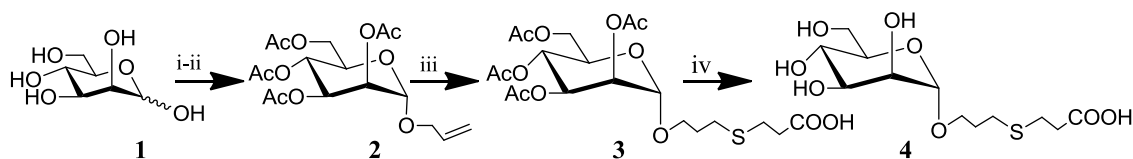


Figure 4.2. Synthesis route of 3-thio-heptanoic acid- α -D-mannoside. Reagents and conditions: (i) p-TsCl, allyl alcohol, 100°C , 36 h, 92 %; (ii) Ac_2O , pyridine, RT, 24 h, 75.7 %; (iii) $\text{HSCH}_2\text{CH}_2\text{COOH}$, CH_3CN , hv, 4 h, 94%; (iv) 1M NaOH, MeOH/ H_2O (5:1), $0^{\circ}\text{C} \rightarrow \text{RT}$, 12 h, 98%.

As shown in **Figure 4.3**, the process to synthesise the mannose precursor to conjugate with chitosan consists of four steps. Allyl mannopyranoside was obtained by glycosylation of mannose and allyl alcohol under refluxing and catalysing with p-TsCl to generate HCl.²³³ The concentrated syrup was acetylated by Ac_2O /pyridine and only α -isomer of tetra acetate **2** was obtained in 75% yield. This was followed by anti-Markovnikov addition of 3-mercaptopropionic acid by photolysis ($h\nu = 254 \text{ nm}$) to give thiopropanoic derivative **3** in 94% yield.²⁹⁹ Standard de-*O*-acetylation was then undertaken using NaOMe, MeOH, $\text{pH} \geq 8$) to afford the unprotected mannose derivatives **4** in quantitative yield.

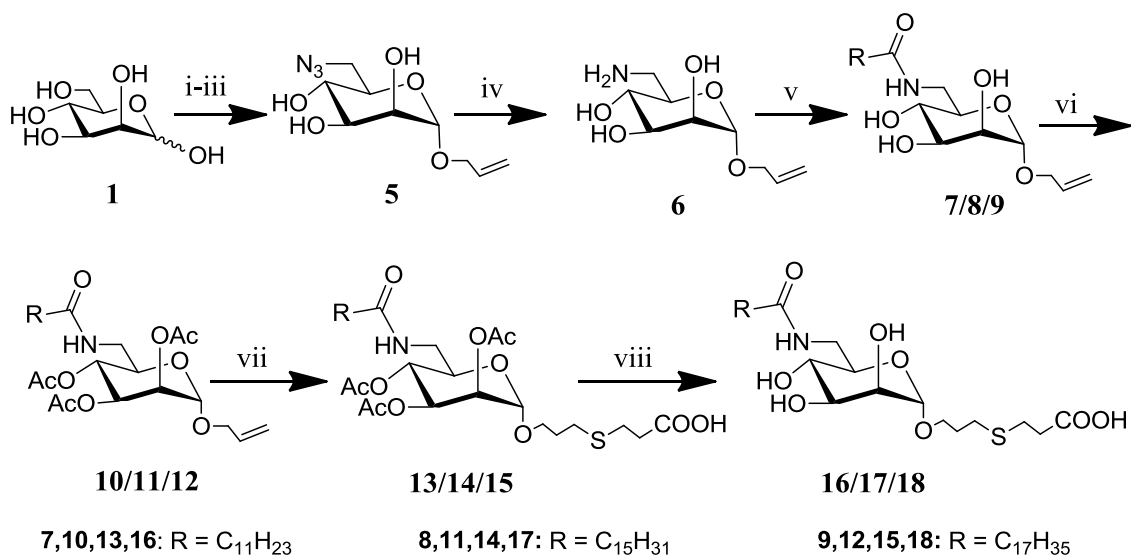


Figure 4.3. Synthesis route of 3-thio-heptanoic acid- α -D-mannoside. Reagents and conditions: (i) p-TsCl, allyl alcohol, 100°C, 36 h, 92 %; (ii) p-TsCl, pyridine, 0°C, 12 h; (iii) NaN₃, DMF, 100°C, 24 h, 44%; (iv) Zn/NH₄Cl, methanol/water (9:1), rt, 1 h; (v) Fatty acid chloride, pyridine, 0°C, 12 h; (vi) Ac₂O, pyridine, RT, 24 h, 76%; (vii) HSCH₂CH₂COOH, DMF, hv, 2 h; (viii) Na, methanol, rt, 24 h.

The synthesis of 6-fatty amide mannoside started from allyl mannoside. The moderately reactive toluenesulfonyl leaving group was added to the primary hydroxyl group (C-6 position) and converted to the tosylated mannoside in 34% yield (Figure 4.2).¹⁶⁹ The next step was the treatment of tosylated allyl mannoside with sodium azide in DMF at 100°C (12 h) to afford the azido allyl mannoside **5** in 44% yield.³⁰⁸ A reduction of **5** with Zn/NH₄Cl afford the amino allyl mannoside **6** and this was used as a precursor to conjugate various fatty acid chlorides.³⁰² Fatty acid chloride with chain length C12 (lauroyl chloride **7**), C16 (palmitoyl chloride **8**) and C18 (stearoyl chloride **9**) were conjugated at C-6 position of mannoside *via* amide bond formation using nucleophilic addition reaction. 3-mercaptopropionic acid was added the anomeric position following the similar procedure described above to obtain **13-15** prior to acetylation of the C-2, C-3 and C-4 positions of mannoside (**10-12**). Finally, the 3-thiaheptanoic acid-6-fatty amido mannosides (**16-18**) with varying chain length, as a precursor to conjugate onto the chitosan backbone, were produced after deacetylation step of (**13-15**) using sodium metal in methanol with yields between 70 and 80%.

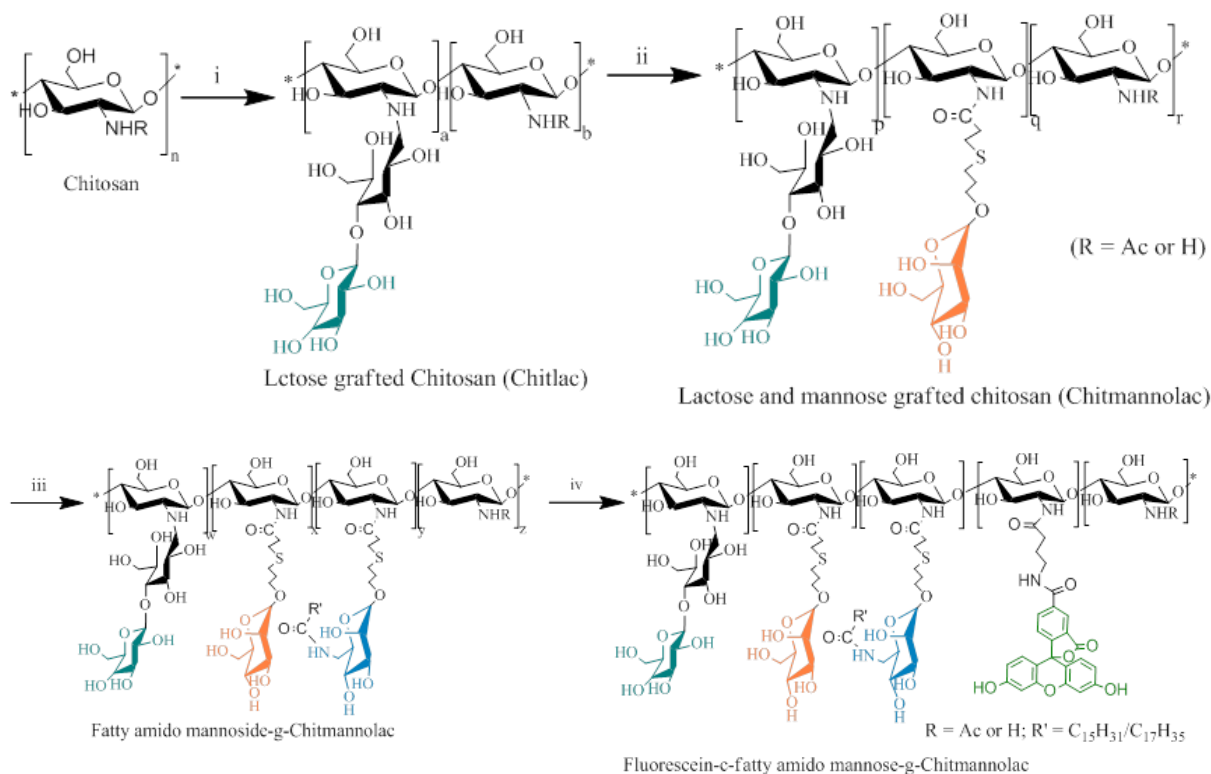


Figure 4.4. Synthesis of lactose grafted chitosan (Chitlac) via *N*-alkylation of chitosan with lactose and the synthesis pathway of mannose and lactose grafted chitosan (Chitmannolac) using EDC-NHS coupling (top). Synthesis route of fatty amido mannoside grafted Chitmannolac and fluorescein conjugated fatty amido mannoside-grafted Chitmannolac (bottom). Reagents and conditions: i) Lactose, NaBH_3CN , 1% AcOH/MeOH , rt, 24 h ii) 3-Thia-heptanoic acid- α -D-mannose, EDC, NHC, 0.05 M HCl , rt, 72 h. iii) 3-Thia-heptanoic acid-6-fatty amido- α -D-mannose, EDC, NHC, 0.05 M HCl , rt, 48 h. iv) 6-(3-Carboxypropylaminocarbonyl)fluorescein, EDC, NHC, 0.05 M HCl , rt, 48 h.

The degree of deacetylation (DDA) of purified commercial chitosan with M_n 164 kDa was determined by ^1H NMR spectroscopy using the area of the peaks assigned to H2-H6 of both monomers between 3.4 and 4.0 ppm and the peak of acetyl group H-Ac at ~ 2.0 ppm.³⁰⁹ The estimated DDA was found to be 81.5 mol%. The purified commercial chitosan was digested using peroxide after cleaving the ether bond between glucosamine units of chitosan to obtain low molecular weight (MW) chitosan. Based on the digestion time 3.5 h and 9.0 h, the MWs of chitosan gradually decreased and produce chitosan with broad MW ranges from 4 to 6.5 kDa (Chitosan_{5k}) and 2 to 4 kDa

(Chitosan_{2k}), respectively.³⁰⁵ The prepared Chitosan_{5k} and Chitosan_{2k} showed improved solubility against a broad range of pH compared to high molecular commercial chitosan (data not shown).

Table 4.6: Preparation and structural parameters of lactose modified chitosan (Chitlac).

Sample	Lactose ^a	NaBH ₃ CN ^a	Compositions (%) ^b			Yield (%)	M _w ^b (kDa)
			GlcNH ₂	GlcNAc	GlcNH-Lac		
Chitosan	0	0	81.5	18.5	0	-	164.0
Chitlac A	2.5	6.0	24.8	18.5	56.7	70.7	289.5
Chitlac B	1.0	2.5	45.3	18.5	36.2	55.5	234.4
Chitlac C	0.8	2.0	58.8	18.5	22.7	54.8	225.04
Chitlac D	0.5	1.3	65.6	18.5	15.9	64.0	206.9
Chitlac _{5k}	0.2	0.5	-	-	-	76.4	6.7
Chitlac _{2k}	0.2	0.5	-	-	-	85.7	2.8

^aEquivalents used per repeating unit of chitosan. ^bComposition as determined by ¹H-NMR spectroscopy.

The synthesis procedure of fatty amido mannose grafted Chitmannolac are described in Figure 4.4. Initially, the *N*-alkyl derivatives of purified chitosan (Figure 4.4) were prepared with various degree of lactosylation (namely Chitlac A, Chitlac B, Chitlac C, Chitlac D, Chitlac_{5k} and Chitlac_{2k}) as shown in Table 4.6 using reductive amination and the products were confirmed by ¹H-NMR spectra analysis (Figure 4.5). The signals pertaining to the backbone of chitosan are sharper in the absence of substitution and this effect depends on the degree of lactosylation of the chitosan molecules. The Chitlac samples with highest amount of lactitol side chains (56.7%) showing the broader NMR signals from the backbone (Figure 4.6). This can be due to the increase in molecular weight as a consequence of the derivatization that leads to a reduced overall tumbling of the molecules shortening transversal relaxation time of the polysaccharide backbone.³¹⁰ Moreover, the anomeric region of the ¹H-NMR spectrum of Chitlac displays two additional peaks at 4.1 and 4.45 ppm belonging to the anomeric proton of the β -galactose side chain unit and the H1 resonance of *N*-alkylated Glc-NH₂ moieties, respectively. The molecular weight of the lactose modified chitosan was estimated from the composition of the polymer by multiplying the number of units including GlcNH₂, GlcNAc, and GlcNH-Lac. Further characterization by ¹³C NMR spectroscopy failed

because of the rigid chitosan backbone and increased macromolecular size of the conjugates reduced sensitivity.³¹¹

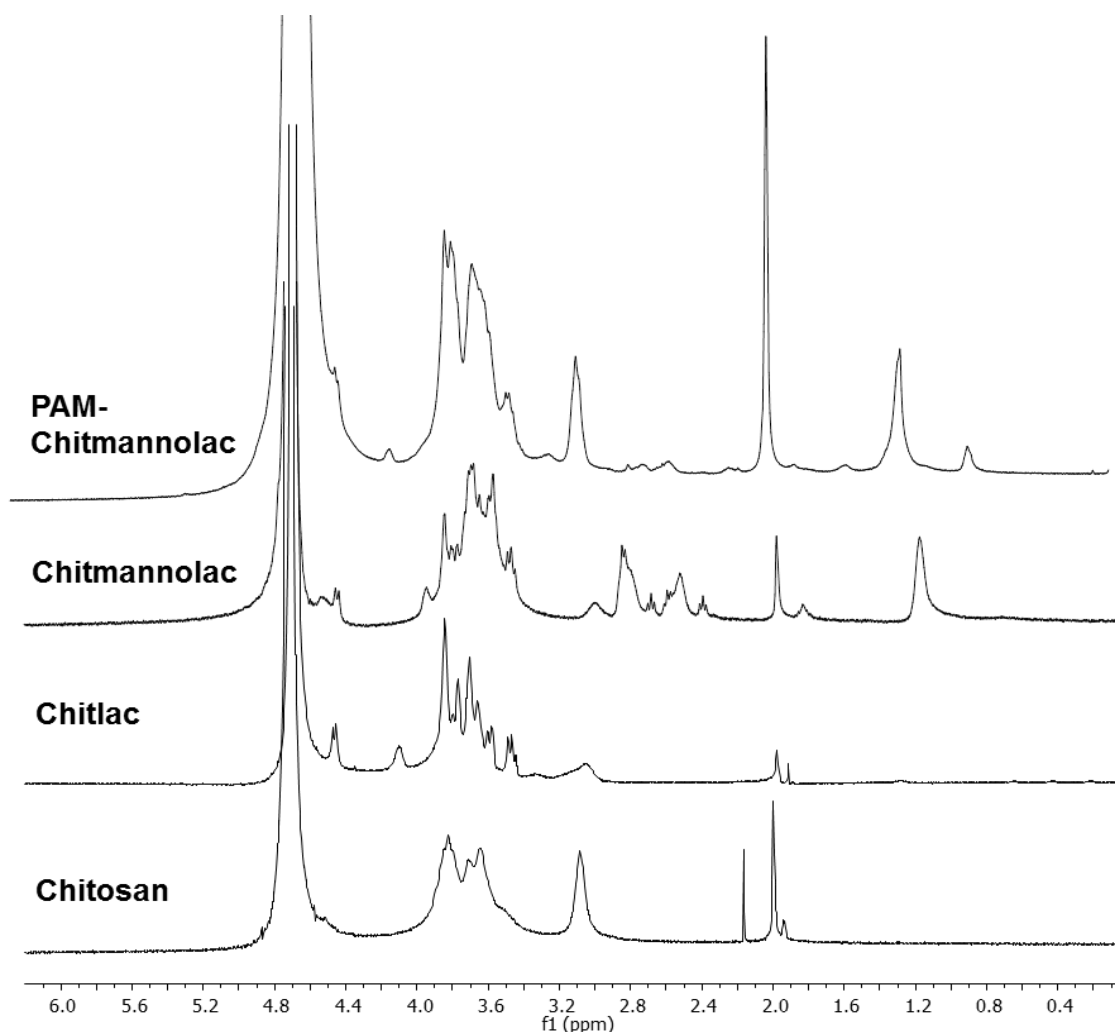


Figure 4.5: ^1H NMR spectra of chitosan, Chitlac, Chitmannolac and PAM-g-Chitmannolac_{5k} at 298K in D₂O

The degree of lactosylation and acetylation can be estimated from the analysis of ^1H NMR spectrum recorded at 343 K, to avoid the overlapping of the anomeric protons of the ring and the residual water signal, by using the H2 proton of the sugar rings as shown in Figure 15. From the integral values of the signal, the estimated degrees of lactosylation for Chitlac A, Chitlac B, Chitlac C, and Chitlac D were found to be 56.7, 36.2, 22.7, 15.9 mol% respectively. The degrees of lactosylation depend on the feeding ratio of lactose and reducing agents into the available amino groups of chitosan

backbone.¹⁷⁵ The percentage is drastically reduced to 15.9% when a lower amount of disaccharide and reducing agent is used (Chitlac D).

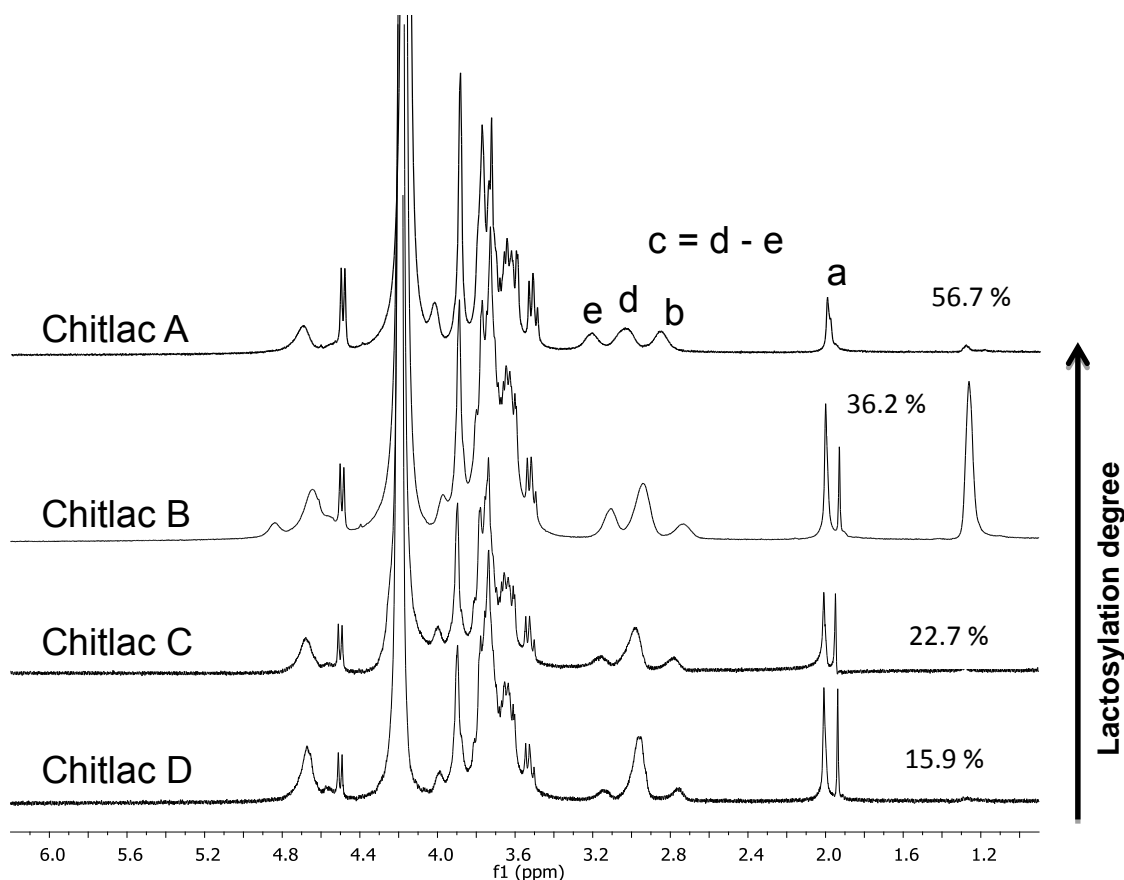


Figure 4.6: ¹H NMR spectra of Chitlac with increasing degree of lactosylation at 343 K, in D₂O/CD₃COOD (pH 4). The estimated acetylation $\alpha = ((100a/3)/(a/3 + b + c))$ and lactosylation $\beta = (b(100-\alpha)/(a/3 + b + c))$ can be determined by substituting the integral of corresponding label in the formulas.³¹⁰ “a” indicate the methyl group of *N*-acetylglusamine residues, “b” is the H2 proton of the ring bearing secondary amine, “c” is the H2 of the ring bearing primary amine which is determined by subtracting the overlapped H1 and H2 from integral “d”, and “e” is the integral of equally intense germinal H1 and H2 proton.

The synthesis of mannose and lactose grafted chitosan (Chitmannolac) was commenced with assembly of mannoside bearing a 3-thia-heptanoic acid spacer (**compound 4**) that can be coupled with Chitlac amino groups *via* carbodiimide chemistry (Figure 4.4). The reaction condition for the synthesis of Chitmannolac from Chitlac was mild and controllable. Briefly, Chitlac B, Chitlac_{5k} and Chitlac_{2k} were stirred with sugar **4**

separately in water prior to activation using EDC and NHS for 24 h to obtain the correspondent Chitmannolac after 5 days dialysis and lyophilisation. To the best of our knowledge, there is no report for the mannosylation of chitosan backbone through amide linkages. Moreover, using an alkyl chain as the bridge for linking mannose to chitosan backbone exhibited lower cytotoxicity compared to phenyl isothiocyanate.²⁹⁵

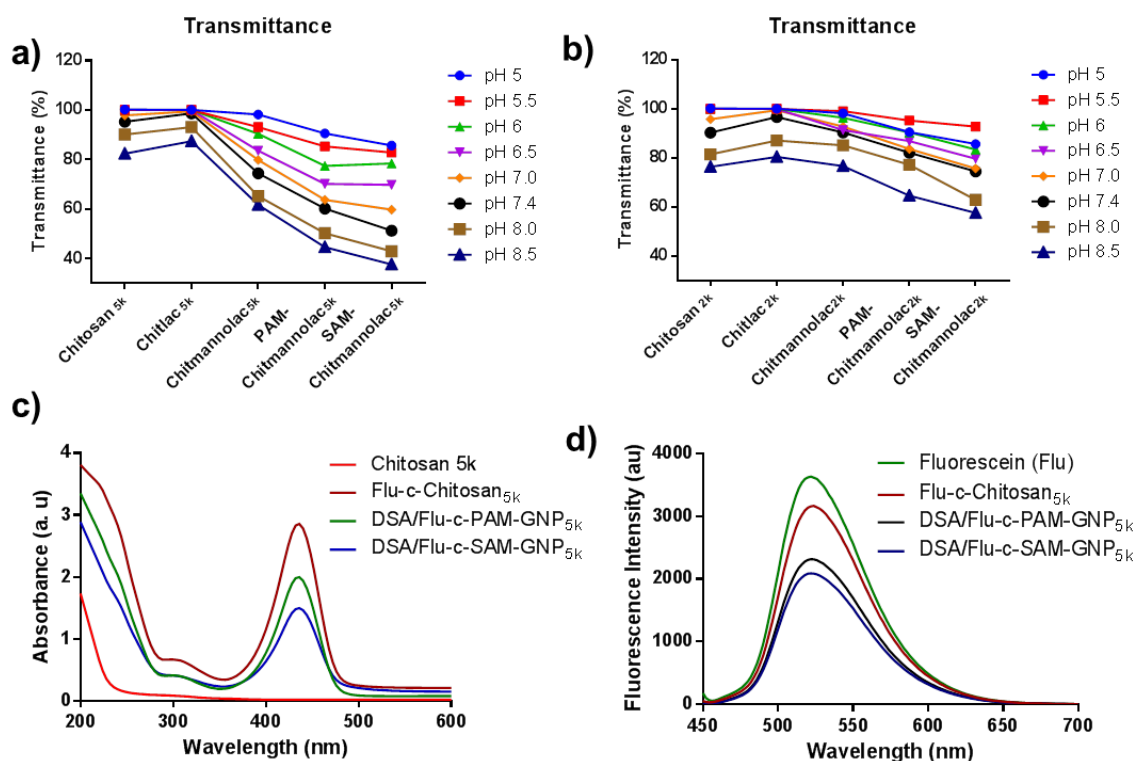


Figure 4.7: Comparison of solubility of chitosan and its derivatives (a) Chitosan_{5k} derivatives and (b) Chitosan_{2k} derivatives at different pH values as determined by light transmittance at a fixed wavelength of 600 nm. UV-vis (c) and fluorescence spectra (Ex: 440 nm) of the prepared fluorescein conjugated GNP_{5k} (d).

The conjugation of mannose precursor to Chitlac was confirmed *via* ¹H-NMR spectroscopy (Figure 4.5). The signals between 2.35 and 2.7 ppm could be contributed to the protons of the $-\text{CH}_2-\text{CH}_2-\text{S}-\text{CH}_2-\text{CH}_2-\text{CH}_2-$ groups which was the bridge for linking mannose to chitosan. The signals of the multiplet peaks within 3.3-4.0 ppm correspond to the protons of mannose and lactose overlapping with the protons of chitosan. The degree of substitution of mannose residues in Chitmannolac was estimated by comparing the characteristic peak areas of mannose residues to chitosan acetamide peaks at 2.0 ppm and the degree of mannosylation was found to be between

15-25 mol% (^1H NMR spectra data shown in the appendix). The solubility of the Chitmannolac prepared from Chitlac B dropped enormously and precipitated within an hour time (photo data not shown) which resulted in elimination of this co-polymer for further modification with synthesized glycolipids.

Among the synthesized glycolipids, palmitoyl (C16) and stearoyl (C18) amido mannoside were utilized to graft onto the Chitmannolac backbone prior to formation of GNPs. The modified glycolipid 3-thioheptanoicacid-6-fatty amido- α -D-mannose was conjugated following the similar process to graft 3-thioheptanoicacid-- α -D-mannose to Chitlac describe above. The glycolipids conjugated Chitmannolac were denoted as PAM-Chitmannolac_{5k} (palmitoyl fatty amido mannose with Chitmannolac_{5k}), SAM-Chitmannolac_{5k} (stearoyl fatty amido mannose with Chitmannolac_{5k}), PAM-Chitmannolac_{2k} (palmitoyl fatty amido mannose with Chitmannolac_{2k}), and SAM-Chitmannolac_{2k} (stearoyl fatty amido mannose with Chitmannolac_{2k}). The conjugations of the glycolipids to the Chitmannolac backbone were confirmed *via* ^1H NMR spectroscopy (Figure 4.5) where the long lipid chain peak around 1.25 ppm from the glycolipids confirm the conjugation onto the Chitmannolac backbone (all ^1H NMR spectra data are shown in appendix). 6-(3-Carboxypropylaminocarbonyl) fluorescein was conjugated the PAM-Chitmannolac_{5k} and SAM-Chitmannolac_{5k} *via* carbodiimide chemistry and the conjugation was confirmed by UV-vis and fluorescence spectra (data not shown). All the chemical modifications occurred with the amino group which are located at the glucosamine units (2-*N*) of chitosan. There is no further change in chitosan backbone structure which supports the digestion of the β -1,4 glycosidic linkage of the chitosan backbone by the lysozyme and *N*-acetyl- β -D-glucosaminidase in human body.⁵⁷

The solubility of the chitosan derivatives in aqueous media was examined by light transmittance and shown in Figure 4.7 (a and b). Both Chitosan_{5k} and Chitosan_{2k} are soluble in a wider pH ranges from 5.0 to 8.5 and form clear solutions which were stable at room temperature for several weeks. However, depending on the degree of substitution, the transmittance of the chitosan derivatives upon conjugation of sugar molecules onto the chitosan backbone decreases and form macromolecular structure at pH 7.0 and over. For instance, the transmittance percentage of PAM-Chitmannolac_{5k}

declined to 40% at pH 8.5. Nonetheless, the transmittances of the Chitosan_{5k} and Chitosan_{2k} derivatives are similar in acidic solution and highly soluble at pH below 6.0. It is well known that the protonation in the acidic solution of the free amino groups glucosamine unit of chitosan enhance the solubility of chitosan and its derivatives *via* an expanded and swollen state.⁹³ Moreover, the molecular weight also influences the solubility of the chitosan where it increases upon decreases the average MW of the polymer. It has been noted that Chitosan_{2k} derivatives have improved solubility compared to Chitosan_{5k} derivatives while pH ranges from 7.0 to 8.5. However, all of these copolymers are highly soluble at pH below 6.5. The wide ranges of water solubility to various biological and physiological conditions of both chitosan derivatives could expand the application of these co-polymers dramatically.

The decanesulfonylacetamide (DSA) loaded chitosan based glyconanoparticles (GNPs) were prepared using nanoprecipitation method through self-assembly of the amphiphilic glycolipid-g-Chitmannolac copolymer followed by probe-type ultrasonication and dialysis method.^{208,312} The amphiphilic sugar modified chitosan backbone served as a hydrophilic shell, and the lipid moiety from the fatty amido mannoside group along with lipidic antibiotic DSA used as the hydrophobic core (Figure 1). In this study, the encapsulation of DSA into all prepared GNPs was kept constant (DSA/GNPs: 1:4 w/w) to maintain consistent amount of DSA in each GNPs due to a lack of validated quantification methods. We hypothesized that the surface functionalization of prepared GNPs with multivalent lectin binding sugar molecules including mannose, galactose and glycolipids combined the advantageous properties of GNPs would improve the potential interaction to specific receptors of macrophages to control and targeted release of drug at the site of infection as well as promote the stability, rigidity, solubility and pharmacokinetic profile of the GNPs.³¹³ We also anticipated that the hydrophobic domain of the synthesized copolymer has the ability to encapsulate lipophilic or poorly water soluble drug molecules and promote the drug payload and the sustained release of drug over time. Furthermore, the hydrophilic shell of the GNPs might prevent the free diffusion of drug by forming a monolayer with a hydrophobic core.²⁰⁸

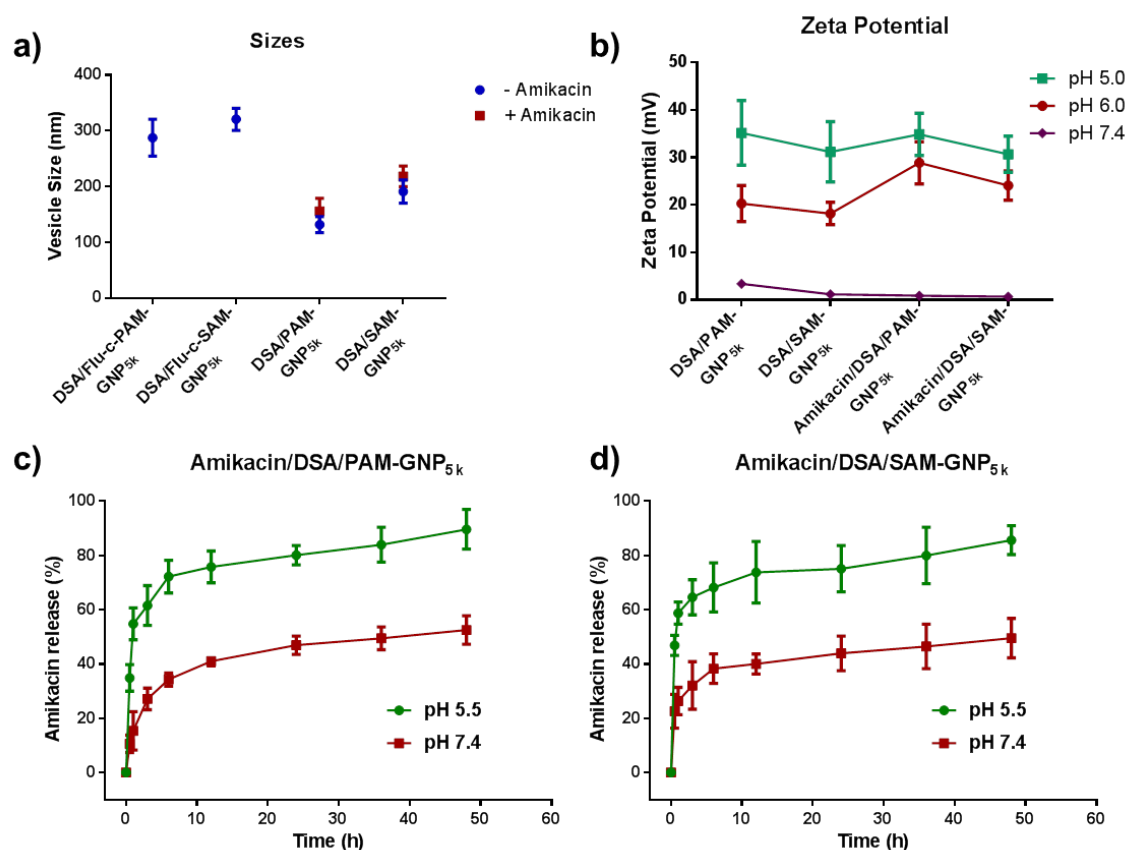


Figure 4.8: Average particle size of the prepared DSA loaded GNPs before and after amikacin encapsulation (a) in PBS solution at pH 7.4. Results denote as the means \pm SD of three batches ($n = 3$). The zeta potential of the prepared amikacin and DSA loaded GNPs at different pH (b). Samples were dissolved in 1% acetic acid and adjust the pH using 2N NaOH to measure the surface charge. Results denote as the means \pm SD of three batches ($n = 3$). The *in vitro* amikacin release profile at various pH for amikacin/DSA/PAM-GNP_{5k} (c) and amikacin/DSA/SAM-GNP_{5k} (d). Results are expressed as percentage of cumulative amikacin release and represent the mean value \pm S.D of the three replicates.

Fluorescein conjugated GNPs were also prepared using the same nanoprecipitation method described above and characterized *via* UV-vis (Figure 4.7c) and fluorescence spectroscopy (Figure 4.7d). The UV light absorption at around 440 nm wavelength confirm the fluorescein binding in the prepared DSA/Flu-c-PAM-GNPs and DSA/Flu-c-SAM-GNPs. However, the absorbance intensity of the DSA/Flu-c-PAM-GNPs was lower than the control compound Flu-c-Chitosan_{5k} which was as expected due to the

linear properties of fluorescein conjugated chitosan and lower molecular weight compared to Flu-c-PAM-Chitosan_{5k}. (Figure 4.7c). The fluorescence spectroscopy data in Figure 4.7d also confirm the fluorescein binding with prepared GNPs by providing green light emission at round 540 nm upon excitation at 440 nm.

Encapsulation of drug into the GNPs can be influenced by several factors including method of preparation, sizes of the GNPs, drug and GNPs concentration and their interaction, and the physiochemical properties of the drug.³¹⁴ Aminoglycoside amikacin was loaded to the prepare DSA/PAM-GNP_{5k} and DSA/SAM-GNP_{5k} nanoparticles with amikacin/GNPs ratio of 1:6 and the amikacin may also be present at the interface of the Chitosan shell. The encapsulation efficiency was observed from the unbound amikacin in the supernatants *via* UV-vis spectroscopy at wavelength 349 nm through a derivatization method using *o*-phalaldialdehyde (OPA)²⁷¹ indicating that 37.5% (0.75 mg out of 3.0 mg) and 18.7% (0.37 mg out of 2.0 mg) of the amikacin had encapsulated into the DSA/PAM-GNP_{5k} and DSA/SAM-GNP_{5k} nanoparticles, respectively.

The formation of GNPs in aqueous medium was determined from the critical micelle concentration (CMC) of DSA/PAM-GNP_{5k} and DSA/SAM-GNP_{5k} using DLS. The intensity of the scattered light was measured by DLS (expressed in kilo counts per second) and run for five times for each dilution. Finally, intensities were plotted as a function of the DSA/PAM-GNP_{5k} and DSA/SAM-GNP_{5k} concentrations ($\mu\text{g/ml}$) and the CMC was determined as the intersection between the two straight lines. The CMC values of DSA/PAM-GNP_{5k} and DSA/SAM-GNP_{5k} were found to be 47 $\mu\text{g/ml}$ and 32 $\mu\text{g/ml}$, respectively.

The size and distribution of the particle might play an important role in the route of drug delivery and determine the fate of the drug carrier after administration into the body. Generally, particle sizes less than 100 nm can be translocated by endocytosis whereas larger particle sizes over 200 nm are more likely uptaken and translocated by epithelial cells.³¹⁵ The mean particle size distribution of the prepared DSA/PAM-GNP_{5k} and DSA/SAM-GNP_{5k} nanoparticles before and after amikacin encapsulation were determined by DLS and shown in Figure 4.8a. The DLS results exhibit that the average diameter of the DSA/PAM-GNP_{5k} and DSA/SAM-GNP_{5k} nanoparticles were 131.9 ± 14.3 nm and 191.2 ± 20.8 nm, respectively with low PDI (<0.3). There was no

significant increase of particle size after encapsulation of the amikacin. Moreover, the average particle sizes of the GNPs prepared using fluorescein conjugated Chitmannolac show a slightly bigger diameter between 280 and 300 nm. All these mean particle sizes of the prepared GNPs are favourable to be uptaken by macrophages by multiple pathways including endocytosis. Figure 4.8b illustrated the effect of pH changes of the prepared antibiotic loaded GNPs on the zeta-potential. Generally, zeta-potential strongly influences the stability, either short-term or long-term, of the nanoparticle dispersion.³¹⁶ As can be seen, the net positive charge of all the antibiotic loaded GNPs gradually increased while decreasing the pH of the solution. For instance, zeta-potential of DSA/PAM-GNP_{5k} was found to be (+) 3.4 ± 0.4 , (+) 20.3 ± 3.8 and (+) 35.2 ± 6.8 mV at pH 7.4, 6.0 and 5.0, respectively and the positive charges demonstrates the protonation of amino groups on chitosan. Furthermore, encapsulation of amikacin on DSA/PAM-GNP_{5k} and DSA/SAM-GNP_{5k} nanoparticles increases its positive zeta-potential at lower pH due to the positive amino groups of amikacin as shown in Figure 4.8b. Therefore, increase in sizes and zeta-potential after encapsulation of amikacin to the DSA/PAM-GNP_{5k} and DSA/SAM-GNP_{5k} suggests the loading of amikacin in DSA/PAM-GNP_{5k} and DSA/SAM-GNP_{5k} nanoparticles.

The cumulative amikacin release studies were carried out *in vitro* to understand the rate of drug release in a pH gradient simulating the pH of the lysosome (pH 5.5) and the pH of the blood circulation (pH 7.4) in order to simulate *in vivo* biological conditions. To simulate the body temperature, the experiments were performed at 37°C. As shown in Figure 4.8c and 4.8d, there was a burst release of amikacin from both the amikacin/DSA/PAM-GNP_{5k} and amikacin/DSA/SAM-GNP_{5k} in the first hour of incubation in PBS buffer at pH 5.5. More than half proportion of the encapsulated amikacin were released out from the GNPs within an hour which is due to the protonation characteristic of amikacin and chitosan favoured to swell in water and rapid diffusion of amikacin at this physiological condition. However, less than 25% of amikacin released at blood pH 7.4 at the same time interval. The amikacin release rate was then slowed down, and was similar for all GNPs during the first 3 h. It was observed that the release of amikacin at pH 7.4 for both GNPs almost plateaued, whereas it kept increasing at pH 5.5. By the end of 6 h, $76.4 \pm 6.2\%$ and $68.2 \pm 9.2\%$ of total amikacin were released from amikacin/DSA/PAM-GNP_{5k} and

amikacin/DSA/SAM-GNP_{5k}, respectively at pH 5.5 followed by a sustained release of drug over a period of 48 h. However, only $34.5 \pm 2.4\%$ and $38.8 \pm 5.4\%$ of amikacin released at pH 7.4 for amikacin/DSA/PAM-GNP_{5k} and amikacin/DSA/SAM-GNP_{5k}, respectively which may indicate that the encapsulated amikacin agglomerate with the GNPs at basic condition and disfavour the release of drug from the macrostructure. At the end of 48 h, about 90% of the amikacin had been released from amikacin/DSA/PAM-GNP_{5k} at lower pH, which was subsequently used for the intracellular antibacterial studies.

Stability, biocompatibility, and reduced interference with the biological functions of cells and animal functions of these prepared GNPs are critical to use as antimicrobial agents. The most important features of chitosan are low toxicity and good biodegradability which are very essential for the biomedical application. As toxicity is a major issue with many chitosan derivatives, the cytotoxicity of DSA/PAM-GNPs_{5k}, DSA/SAM-GNP_{5k}, amikacin/DSA/PAM-GNP_{5k} and amikacin/DSA/SAM-GNP_{5k} against RAW 264.7 cells were determined by MTT assays after 24 h incubation (Figure 4.9). The results showed that all samples were practically nontoxic to RAW264.7 cells (cell viabilities: 85.5 - 99.9%) at concentration of 0.125 to 0.5 mg/ml, indicating that all GNPs possess excellent biocompatibility with no significant toxicity to the cells at these concentrations, however, significant toxicity of the prepared GNPs showed at higher concentrations (2 mg/ml) and this concentration was not used for any subsequent studies. A similar observation was also reported by Yikun Gao *et al.*³¹⁷ and Xin Want *et al.*³¹⁸ These results are attributed the biocompatibility of chitosan used as the formation of GNPs. The lower cellular toxicities from the prepared GNPs were also observed due to the chitosan modification and purification was performed in water which eliminated potential cytotoxicity originating from organic solvent. Moreover, the chitosan was modified with simple sugar molecules including mannose and lactose which are nontoxic to eukaryotes. Although aminoglycosides can be toxic (including nephron-and ototoxicity), the targeted drug delivery system to macrophages can reduce these toxic side effects.³¹⁹ The toxic effects of these manufactured antibiotic encapsulated GNPs against bacteria along with their compatibility against macrophages can establish them as an effective antibacterial agent.

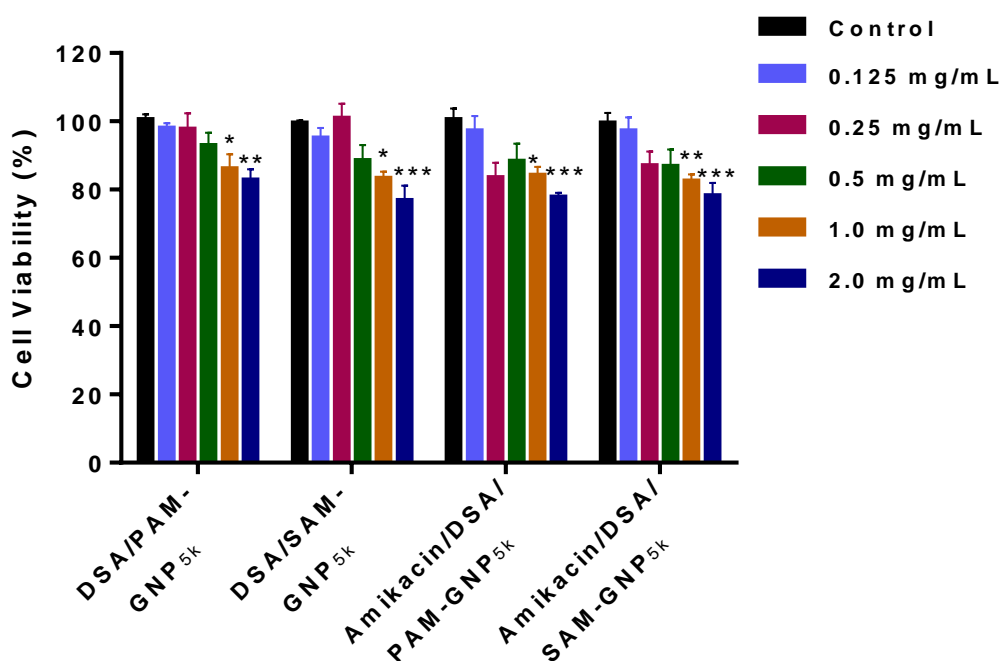


Figure 4.9. Effects of antibiotic loaded GNPs on RAW264.7 macrophage cell viability. A MTT assay was performed to detect *in vitro* cytotoxic effects of DSA/PAM-GNPs_{5k}, DSA/SAM-GNP_{5k}, amikacin/DNA/PAM-GNP_{5k} and amikacin/DNA/SAM-GNP_{5k} against RAW264.7 cells after 24 h incubation. Cells were treated with 0.125-2.0 mg/mL of corresponding antibiotic loaded GNPs. Results were expressed as mean \pm S.D (n = 6) of three independent experiments. * $p < 0.05$, ** $p < 0.01$, *** $p < 0.001$ vs. blank control group (untreated cells).

Macrophages play an important role in the initiation, resolution and maintenance of inflammation after stimulation by various bacterial endotoxins including lipopolysaccharides (LPS). A large amount of inflammatory cytokines such as TNF- α and IL-6 are secreted by macrophages when incubated with LPS. The secreted cytokines further activate macrophages and enhance the inflammatory responses.³²⁰ Therefore, it is important to determine the pro-inflammatory cytokines profile for therapeutic intervention targeting macrophages. In this study, the secretion of pro-inflammatory cytokines TNF- α and IL-6 in the supernatant of RAW264.7 cells were determined as an indicator in the induction of immune response and the secreted amounts of cytokines of the prepared GNPs are shown in Figure 4.10. The macrophage cells were treated with different concentrations of DSA/PAM-GNP_{5k}, DSA/SAM-

GNP_{5k} nanoparticles at different incubation time and measured for cytokines using ELISA.

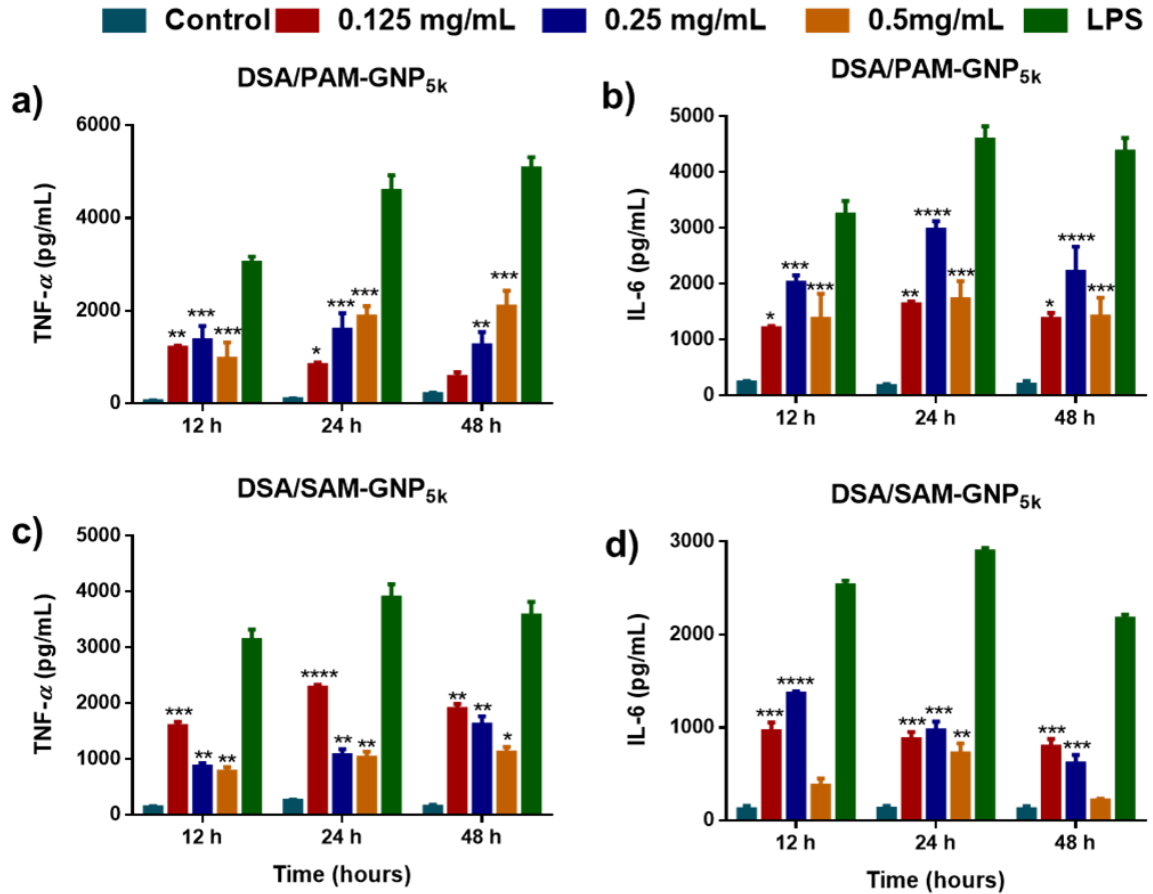


Figure 4.10. Production of proinflammatory (TNF- α and IL-6) cytokines upon 12, 24 and 48 h treatment with DSA/PAM-GNP_{5k} (a and b) and DSA/SAM-GNP_{5k} (c and d) against RAW264.7 macrophage cells. The supernatants were analysed for TNF- α and IL-6 production using ELISA. For all graphs, results were expressed as mean \pm S.D (n = 3) of three independent experiments. * $p < 0.05$, ** $p < 0.01$, *** $p < 0.001$ vs. blank control group (untreated cells). **LPS:** Lipopolysaccharides used as positive control.

The production of TNF- α and IL-6 from RAW264.7 cells were significantly increased when the cells were treated with the prepared GNPs in comparison to untreated macrophages (control). For instance, the amount of TNF- α released from macrophages exposed to the DSA/PAM-GNP_{5k} nanoparticles was significantly higher for all concentration ($p < 0.01$) compared to control when incubated for 12 and 24 h (Figure 4.10a). Similar results have been observed in terms of TNF- α production when cells

were incubated with DSA/SAM-GNP_{5k} nanoparticles. Interestingly, the released amount of TNF- α was greater when DSA/SAM-GNP_{5k} at lower concentration (0.125 mg/mL) in comparison to higher concentration (Figure 4.10c). It is well known that upregulated proinflammatory cytokines are the indicator to generate activated macrophages. It has previously been suggested that mannosylated chitosan enhanced secretion of proinflammatory cytokines and exhibited a higher immune stimulatory activity by shifting to activated macrophages.^{278,279} Moreover, Ning Wu *et al.* reported that the low molecular weight chitosan served as an immunostimulant by enhancing the secretion of TNF- α and IL-6 in a molecular-weight dependent manner.^{321,322} Furthermore, higher levels of IL-6 secretion were also released from the macrophages exposed to DSA/PAM-GNP_{5k}, DSA/SAM-GNP_{5k} nanoparticles (Figure 4.10 b and d). However, it has been observed that DSA/PAM-GNP_{5k} released a higher amount of IL-6 compared to DSA/PSM-GNP_{5k} nanoparticles for all incubation time which could be resulted from the better inaction of DSA/PAM-GNP_{5k} nanoparticles with macrophages compared to DSA/SAM-GNP_{5k} nanoparticles. In the present study, the dramatically higher amount of proinflammatory cytokines production indicates the strong immunostimulatory capability of the prepared GNPs, and this may stimulate uptake.

The sugar-modified nanoparticles are of great interest for active targeting of macrophages as the presence of lectin receptors on the cell surface can recognize sugar moieties including mannose, fucose, and galactose.¹⁷² In the present study, fluorescein conjugated chitosan and GNPs were prepared in order to determine the macrophage cells uptake characteristic. The RAW267.4 cells were incubated with Flu-c-chitosan_{5k} co-polymer and DSA/Flu-c-PAM-GNP_{5k} nanoparticles for 4 hour at 37°C. The fluorescence uptake properties were studied by CLSM and the results are shown in Figure 4.11. The confocal images clearly shows an increased fluorescence in the cell while incubating with DSA/Flu-c-PAM-GNP_{5k} nanoparticles compared to the Flu-c-chitosan_{5k} alone indicating higher cellular uptake by the DSA/Flu-c-PAM-GNP_{5k} nanoparticles. This higher uptake of DSA/Flu-c-PAM-GNP_{5k} nanoparticles may be attributed to multiple lectin conjugation to the GNPs which facilitates binding to lectin receptors widely overexpressed on the macrophage cell membrane. It has been reported

that surface modification of nanoparticles with multivalent lectin promote the interaction with four sugar binding site of lectin receptors present on the macrophages which leads to vacuolation and subsequent internalization.²⁰⁸

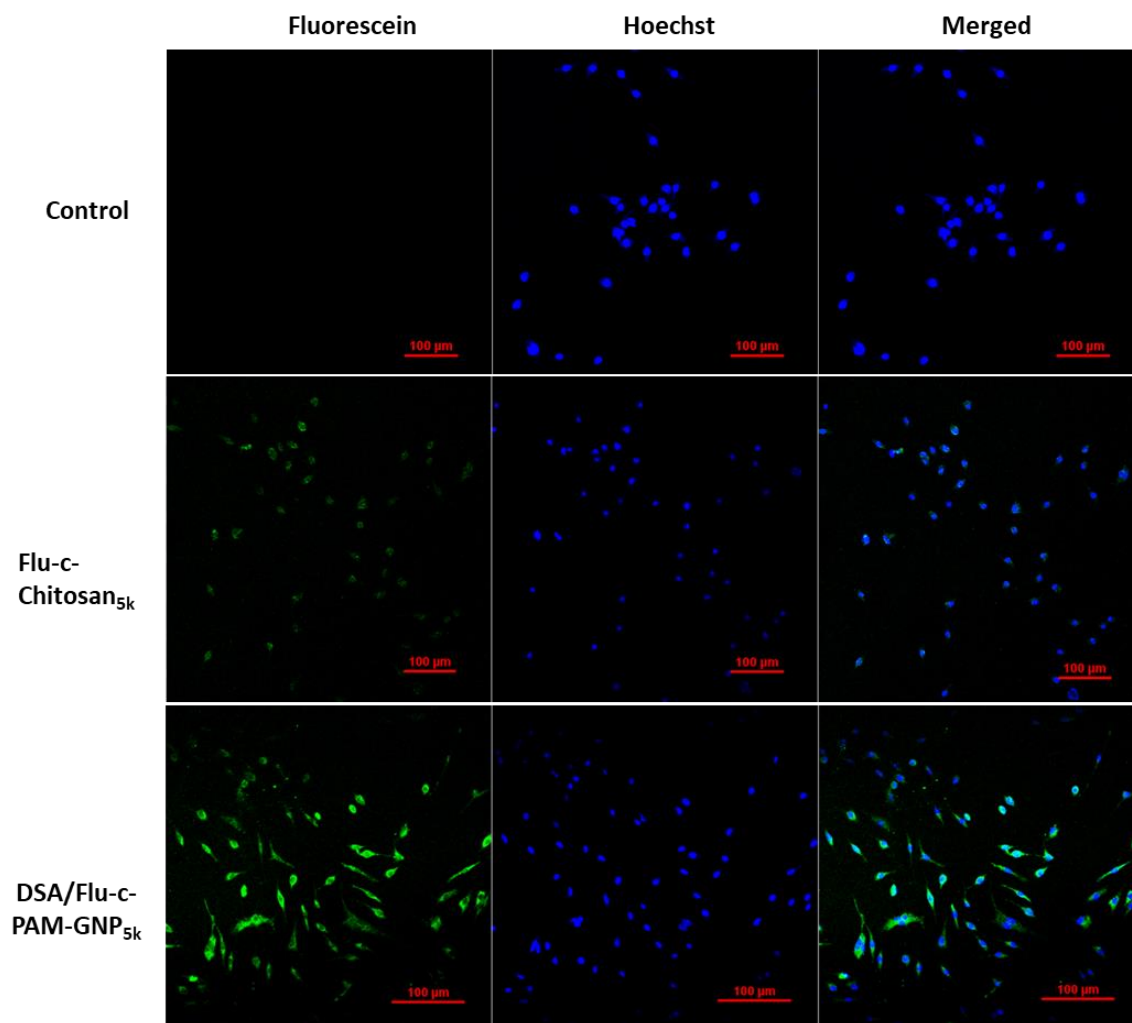


Figure 4.11. Confocal laser scanning microscope (CLSM) of Flu-c-Chitosan and DSA/Flu-c-PAM-GNP_{5k} using RAW 264.7 macrophage cell after 4 h incubation to describe the intracellular uptake characteristic.

In the following experiment, we studied the intracellular antibacterial activity DSA/PAM-GNP_{5k} and amikacin/DSA/PAM-GNP_{5k} nanoparticles by counting the CFU of surviving intracellular bacteria over time upon incubation with increasing

concentration of GNPs added to RAW264.6 cells infected by *S. aureus* (results are shown in Figure 4.12). As shown in Figure 4.12a, there were insignificant intracellular *S. aureus* inhibitions after 24 h incubation time upon treatment with lower concentration between 50 and 200 $\mu\text{g/mL}$ of DSA/PAM-GNP_{5k}. As shown in previous chapter, DSA exhibits bactericidal activity against *S. aureus* at higher concentration, DSA/PAM-GNP_{5k} nanoparticles reduce the bacterial growth significantly at higher concentration of 400 $\mu\text{g/mL}$ ($p < 0.01$). This result could be attributed from the high loading content of DSA into the GNPs and/or from the bactericidal activity of low molecular weight chitosan reported elsewhere.^{323,324}

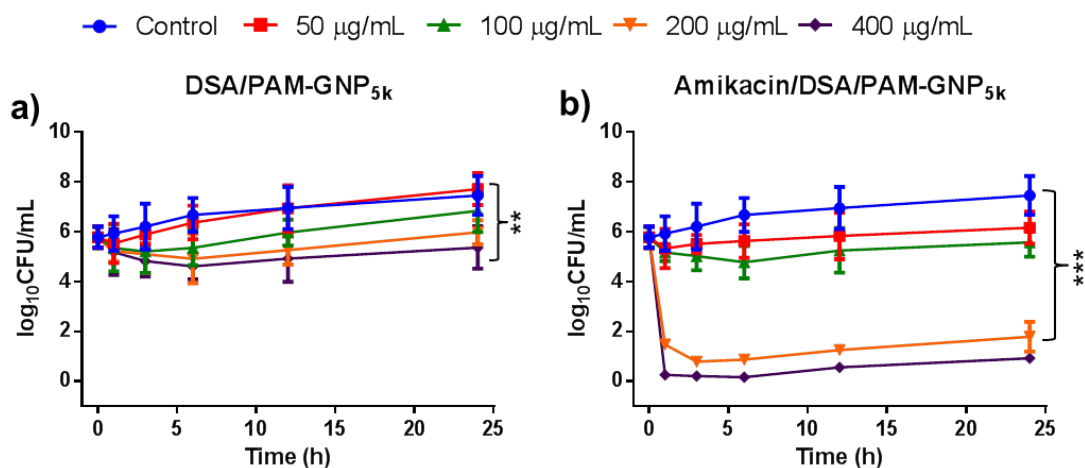


Figure 4.12: Intracellular growth of *S. aureus* inside RAW264.7 macrophages against various concentrations of DSA/PAM-GNP_{5k} (a) and amikacin/DNA/PAM-GNP_{5k} (b) nanoparticles and incubated for 1, 3, 6, 12 and 24 h, respectively. After incubation at 1 h, 3 h, 6 h, 12 h and 24 h, macrophages were lysed with sterile distilled water and the lysates were plated on LB agar plates for counting bacterial colonies. Control was determined from the untreated macrophages and grew them on LB agar plates prior to lyse the infected cells. Data represent the mean value \pm S.D of the three replicates. * $p < 0.005$, ** $p < 0.01$ and *** $p < 0.001$ compared to control group. CFU, colony-forming units.

The growth of intracellular *S. aureus* exposed to various concentrations of amikacin/DNA/PAM-GNP_{5k} nanoparticles showed concentration-dependent intracellular bacterial growth inhibition (Figure 4.12b). There was no significant bacterial growth inhibition by amikacin/DNA/PAM-GNP_{5k} nanoparticles upon

incubation for 24 h with 100 $\mu\text{g/mL}$ (7.5 μg of amikacin in 100 μg of amikacin/DSA/PAM-GNP_{5k}). However, significant bacterial inhibition occurred within an hour incubation of amikacin/DSA/PAM-GNP_{5k} nanoparticles at concentration 200 and 400 $\mu\text{g/mL}$, respectively ($p < 0.001$). Almost 100% bacterial growth was inhibited by amikacin/DSA/PAM-GNP_{5k} nanoparticles with 30 min incubation when the infected macrophages treated with 400 $\mu\text{g/mL}$ ($p < 0.001$). It is well known that many antibiotics including aminoglycosides are concentration-dependent and the dramatic increase of antibiotics inside cell compartments may enhance the intracellular bactericidal activity.²⁸¹ These results indicate the potential application of antibiotic loaded amikacin/DSA/PAM-GNP_{5k} nanoparticles as an antimicrobial agent.

4.4. Conclusions

In this chapter, we describe the facile synthesis procedure of chitosan-based GNPs by grafting hydrophilic sugar molecules and hydrophobic sugar conjugated lipid moieties onto the chitosan backbone. Primarily, we describe the modification of mannose as a precursor of chitosan and subsequently conjugated the sugar molecules using biological friendly carbodiimide chemistry. Then, the chitosan based glyconanoparticles (GNPs) were prepared using nanoprecipitation method and successfully encapsulated a hydrophobic antibiotic DSA and hydrophilic aminoglycoside amikacin into the prepared GNPs. The prepared GNPs were well characterized using NMR spectroscopy, UV-vis spectroscopy, fluorescence spectroscopy and DLS. We also confirmed that the prepared GNPs are safe to use in the biological system by exploring its toxic characteristics through MTT assays although detailed toxicity studies are required (including *in vivo* toxicity) to determine the safer doses. Moreover, the proinflammatory cytokines of the GNPs were determined to demonstrate an immunostimulative profile against macrophages. The cellular uptake behaviour of the GNPs confirmed the greater internalization ability of GNPs compared to unmodified chitosan. Finally, the intracellular antibacterial activity indicated the bacterial growth inhibition capability of the DSA and amikacin loaded GNPs demonstrating this artificial nano-drug carrier has great potential for targeted delivery of antimicrobial agents. Future work will involve application of these GNPs to the treatment of tuberculosis, as both amikacin and DSA are potent antitubercular compounds.

Chapter 5

5.0. Conclusions and Future Directions

Delivery of therapeutic agents to the target site is still a major concern in the treatment of many diseases. Conventional application of many potential drugs is often characterized by limited effectiveness, poor biodistribution, and lack of selectivity. Recent developments in nanoengineered non-viral drug delivery systems (DDS) can deliver their encapsulated therapeutics at a well-defined time, place, or in response to a specific stimulus with minimum cytotoxicity. The preparation of nano-drug carriers for DDS depends on the selective combination of the carrier materials to attain suitable release properties and the surface modification of the nanoparticles to enhance their targeting capability. In this thesis, we successfully design and develop antibiotic encapsulated glyconanoparticles and glyco-coated liposomes for active targeting of macrophages to treat a range of infectious diseases. We performed the background study of the reported antibiotic delivery system and describe them all in the introduction chapter.

In Chapter 2, we have noted the close structural similarity between TDM and both phosphatidylinositol mannosides (PIMs) from mycobacteria and phospholipomannan (PLM) from *Candida albicans* and believe that this motif (2-mannosylinositol) is likely to be recognized by Mincle. The structures of trehalose and 2-mannosylated inositol are quite similar and the difference between PIM and PLM occurs at C-6 of mannose where some PIM derivatives contain fatty esters and PLM extends a large oligosaccharide (mannan) at this site. Therefore, we reported the direct synthesis of 6-fatty acyl and amido mannosides with varying lipid lengths and benzyl mannoside derivatives as the aromatic ring is expected to mimic the hydrophobic face of inositol. The C-6 primary alcohol of benzyl α -D-mannoside was selectively esterified using 2,4,6-trimethylpyridine activation of fatty acid chlorides at -40°C . Four novel compounds were reported by this protocol in reasonable yields (65-75%).²⁸⁰ The cytotoxicity of these compounds was investigated against activated monocyte using MTT assays after treating with 10-80 μM of glycolipids over 24 h incubation time and results showed no significant toxicity from glycolipids even at the high concentration. The proinflammatory cytokines measurements against these glycolipids discovered the anti-inflammatory activity against LPS-activated human macrophages. However, further

work is necessary to confirm the immune cell targets (including MMR, Mincl, and TLR4) of these reported glycolipids.

Liposomes are the most extensively studied class of nanocarriers and can be prepared with different lipid compositions in various particle sizes and charges. The ease of design and preparation of liposomes allows formulation of optimal therapeutic loading and drug delivery to target specific cells or tissues. In Chapter 3, novel glyco-coated liposomal antibiotic delivery system was studied to eradicate intracellular bacteria. Dimethyldioctadecylammonium bromides (DDAB) with varying concentrations of prepared glycolipids were formulated to prepare glyco-coated cationic liposomes. The physicochemical and immunopotentiating properties of the prepared glyco-coated DDAB liposomes were investigated. The vesicle sizes and polydispersity index of the glyco-coated DDAB liposomes significantly decreased upon incorporation of 20 mol% glycolipid into the liposomal formulation without dramatically affecting its cationic surface charges. The adjuvant properties of glyco-coated DDAB liposomes were evaluated and the results showed a higher level of cytokine (both TNF- α and IL-6) production upon incubation with glyco-coated DDAB liposomes compared to pure DDAB liposomes. As antibiotics, *n*-decanesulphonylacetamide (DSA) and amikacin were used to encapsulate into the glyco-coated liposomal formulation and we successfully loaded these antibiotics with an efficient loading capacity of 25% to 32% compared to pure DDAB liposomes. Finally, the intracellular viability of *S. aureus* infected RAW 264.7 macrophages was evaluated against prepared antibiotic encapsulated glyco-coated DDAB liposomes and the results showed efficient intracellular bacterial growth inhibition.

In Chapter 4, we described the successful synthesis and characterization of chitosan derivatives and preparation and characterization of antibiotic loaded glyconanoparticles (GNPs). To modify chitosan backbone with sugar molecules, the anomeric and C-6 position of the ally mannoside was modified by a carboxylic acid group and a fatty acid moiety, respectively. The commercially available chitosan was digested to low molecular weight chitosan and successfully modify the low molecular weight chitosan with different sugar molecules. The nanoprecipitation method was employed to generate nanoparticles with hydrophobic drug DSA. Amikacin loaded DSA/GNPs were also

prepared to evaluate the intracellular bacterial growth inhibition and the results showed excellent antibacterial activity of the artificial antibiotic encapsulated GNPs.

This thesis has focused on the design, synthesis and characterization of the novel therapeutic application of antibiotic loaded glyco-nanocarrier to target macrophages. The primary purposes of this research project has been achieved, however, there are a number of issues and follow-up studies that require further investigation and in-depth understanding in future.

(i) Initially, the reported glycolipids tested against LPS activated macrophages showed anti-inflammatory activity, however, the possibility exists that the glycolipids are antagonists of LPS-activation of TLR4 which is expressed in U937 macrophages. Therefore, it is required to explore the possible immune cell targets (including MMR, Mincle, and TLR4) of these glycolipids.

(ii) DSA and amikacin were tested against *S. aureus* infected macrophages at the same concentration to explore their antibacterial activity, however, amikacin showed more potency against intracellular *S. aureus* than DSA. Therefore, future work might test these therapeutic at various concentrations to determine their potency such as EC 50 or EC80 concentrations.

(iii) The qualitative measurements of the prepared GNPs can be further explored using spectroscopy techniques to find the variation in nanoparticles sizes and shapes.

(iv) The quantification of DSA was not performed as lack for validated quantification method. In future is require to synthesise isotope labelled (¹⁵N) DSA and determine the exact loaded amount of DSA in the liposomes and GNPs.

(v) As amikacin and DSA are both potent against mycobacterium, future work will involve testing of these drug-loaded nano-carriers to the treatment of tuberculosis.

(vi) The cellular uptake characteristic was determined by confocal microscope to confirm the internalization of the GNPs using fluorophores. Nonetheless, a common way of proving this is to also stain the cell membrane and take images of the samples at multiple focal depths (z-sections); when sections that passes through the cells show GNPs within the boundary of the cell membrane to confidently state that the

internalised particle. A future work is required to perform experiment following the above process to confirm the cellular internalization.

(vi) The toxic characteristic of the prepared GNPs were measured using MTT assays although further studies are required (including using a control against amikacin and *in vivo*) toxicity to determine the safer doses.

(vii) *In vivo* antibacterial activity of the infected animal against these artificial glyco nano-carriers need to be explored.

In summary, this PhD thesis has advanced knowledge in drug delivery by developing a new strategy to deliver both hydrophobic and hydrophilic therapeutics to macrophages. Glyco-coated liposomes and micelles were developed to elucidate their stability, antibiotic loading efficiency, and drug release profile. In addition, this thesis explored the intracellular antibacterial activity after encapsulation of two different types of antibiotic and proved that the artificial glyco-nanocarrier improved the cellular interaction making these glyco-nanocarriers potential therapeutic carriers to macrophages. Finally, this research has demonstrated improved intracellular bactericidal activity against *S. aureus* infected macrophages.

References

- (1) De Cock, L. J.; De Koker, S.; De Geest, B. G.; Grooten, J.; Vervaet, C.; Remon, J. P.; Sukhorukov, G. B.; Antipina, M. N. Polymeric Multilayer Capsules in Drug Delivery. *Angewandte Chemie International Edition* **2010**, *49* (39), 6954.
- (2) Raemdonck, K.; Martens, T. F.; Braeckmans, K.; Demeester, J.; De Smedt, S. C. Polysaccharide-based nucleic acid nanoformulations. *Advanced Drug Delivery Reviews* **2013**, *65* (9), 1123.
- (3) Xie, S.; Tao, Y.; Pan, Y.; Qu, W.; Cheng, G.; Huang, L.; Chen, D.; Wang, X.; Liu, Z.; Yuan, Z. Biodegradable nanoparticles for intracellular delivery of antimicrobial agents. *Journal of Controlled Release* **2014**, *187* (0), 101.
- (4) Forier, K.; Raemdonck, K.; De Smedt, S. C.; Demeester, J.; Coenye, T.; Braeckmans, K. Lipid and polymer nanoparticles for drug delivery to bacterial biofilms. *Journal of Controlled Release* **2014**, *190* (0), 607.
- (5) Wilczewska, A. Z.; Niemirowicz, K.; Markiewicz, K. H.; Car, H. Nanoparticles as drug delivery systems. *Pharmacological Reports* **2012**, *64* (5), 1020.
- (6) Toti, U. S.; Guru, B. R.; Hali, M.; McPharlin, C. M.; Wykes, S. M.; Panyam, J.; Whittum-Hudson, J. A. Targeted delivery of antibiotics to intracellular chlamydial infections using PLGA nanoparticles. *Biomaterials* **2011**, *32* (27), 6606.
- (7) Fontana, G.; Licciardi, M.; Mansueto, S.; Schillaci, D.; Giammona, G. Amoxicillin-loaded polyethylcyanoacrylate nanoparticles: influence of PEG coating on the particle size, drug release rate and phagocytic uptake. *Biomaterials* **2001**, *22* (21), 2857.
- (8) Zhang, H.; Ma, Y.; Sun, X.-L. Recent developments in carbohydrate-decorated targeted drug/gene delivery. *Medicinal Research Reviews* **2010**, *30* (2), 270.
- (9) Ahmed, M.; Narain, R. Glyconanoparticles for Gene Delivery. **2012**, *1119*, 81.
- (10) Chellat, F.; Merhi, Y.; Moreau, A.; Yahia, L. H. Therapeutic potential of nanoparticulate systems for macrophage targeting. *Biomaterials* **2005**, *26* (35), 7260.
- (11) Sahoo, S. K.; Parveen, S.; Panda, J. J. The present and future of nanotechnology in human health care. *Nanomedicine: Nanotechnology, Biology and Medicine* **2007**, *3* (1), 20.

- (12) Mehanna, M. M.; Mohyeldin, S. M.; Elgindy, N. A. Respirable nanocarriers as a promising strategy for antitubercular drug delivery. *Journal of Controlled Release* **2014**, *187* (0), 183.
- (13) Abed, N.; Couvreur, P. Nanocarriers for antibiotics: A promising solution to treat intracellular bacterial infections. *International journal of antimicrobial agents* **2014**, *43* (6), 485.
- (14) Nitta, S. K.; Numata, K. Biopolymer-based nanoparticles for drug/gene delivery and tissue engineering. *International journal of molecular sciences* **2013**, *14* (1), 1629.
- (15) Xiong, M.-H.; Bao, Y.; Yang, X.-Z.; Zhu, Y.-H.; Wang, J. Delivery of antibiotics with polymeric particles. *Advanced Drug Delivery Reviews* **2014**, *78* (0), 63.
- (16) Chen, G.; Roy, I.; Yang, C.; Prasad, P. N. Nanochemistry and Nanomedicine for Nanoparticle-based Diagnostics and Therapy. *Chemical Reviews* **2016**, *116* (5), 2826.
- (17) Lawlor, C.; Kelly, C.; O'Leary, S.; O'Sullivan, M. P.; Gallagher, P. J.; Keane, J.; Cryan, S. A. Cellular targeting and trafficking of drug delivery systems for the prevention and treatment of MTb. *Tuberculosis (Edinb)* **2011**, *91* (1), 93.
- (18) Irache, J. M.; Salman, H. H.; Gamazo, C.; Espuelas, S. Mannose-targeted systems for the delivery of therapeutics. *Expert Opinion on Drug Delivery* **2008**, *5* (6), 703.
- (19) Loira-Pastoriza, C.; Todoroff, J.; Vanbever, R. Delivery strategies for sustained drug release in the lungs. *Advanced Drug Delivery Reviews* **2014**, *75* (0), 81.
- (20) Kreuter, J. Drug delivery to the central nervous system by polymeric nanoparticles: What do we know? *Advanced Drug Delivery Reviews* **2014**, *71* (0), 2.
- (21) Briones, E.; Isabel Colino, C.; Lanao, J. M. Delivery systems to increase the selectivity of antibiotics in phagocytic cells. *Journal of Controlled Release* **2008**, *125* (3), 210.
- (22) Paques, J. P.; van der Linden, E.; van Rijn, C. J. M.; Sagis, L. M. C. Preparation methods of alginate nanoparticles. *Advances in Colloid and Interface Science* **2014**, *209* (0), 163.

- (23) Elsabahy, M.; Wooley, K. L. Design of polymeric nanoparticles for biomedical delivery applications. *Chemical Society Reviews* **2012**, *41* (7), 2545.
- (24) Chacko, R. T.; Ventura, J.; Zhuang, J.; Thayumanavan, S. Polymer nanogels: A versatile nanoscopic drug delivery platform. *Advanced Drug Delivery Reviews* **2012**, *64* (9), 836.
- (25) De Souza, R.; Zahedi, P.; Allen, C. J.; Piquette-Miller, M. Polymeric drug delivery systems for localized cancer chemotherapy. *Drug Delivery* **2010**, *17* (6), 365.
- (26) Zhang, N.; Wardwell, P.; Bader, R. Polysaccharide-Based Micelles for Drug Delivery. *Pharmaceutics* **2013**, *5* (2), 329.
- (27) Liu, Z.; Jiao, Y.; Wang, Y.; Zhou, C.; Zhang, Z. Polysaccharides-based nanoparticles as drug delivery systems. *Advanced Drug Delivery Reviews* **2008**, *60* (15), 1650.
- (28) Lemarchand, C.; Gref, R.; Couvreur, P. Polysaccharide-decorated nanoparticles. *European Journal of Pharmaceutics and Biopharmaceutics* **2004**, *58* (2), 327.
- (29) Shu, S.; Sun, L.; Zhang, X.; Wu, Z.; Wang, Z.; Li, C. Polysaccharides-based polyelectrolyte nanoparticles as protein drugs delivery system. *Journal of Nanoparticle Research* **2011**, *13* (9), 3657.
- (30) Saravanakumar, G.; Jo, D. G.; Park, J. H. Polysaccharide-Based Nanoparticles: A Versatile Platform for Drug Delivery and Biomedical Imaging. *Current Medicinal Chemistry* **2012**, *19* (19), 3212.
- (31) Lin, Y.-H.; Tsai, S.-C.; Lai, C.-H.; Lee, C.-H.; He, Z. S.; Tseng, G.-C. Genipin-cross-linked fucose–chitosan/heparin nanoparticles for the eradication of *Helicobacter pylori*. *Biomaterials* **2013**, *34* (18), 4466.
- (32) Wibowo, A.; Peters, E. C.; Hsieh-Wilson, L. C. Photoactivatable Glycopolymers for the Proteome-Wide Identification of Fucose- α (1-2)-Galactose Binding Proteins. *Journal of the American Chemical Society* **2014**, *136* (27), 9528.
- (33) Gu, Z.; Aimetti, A. A.; Wang, Q.; Dang, T. T.; Zhang, Y.; Veiseh, O.; Cheng, H.; Langer, R. S.; Anderson, D. G. Injectable Nano-Network for Glucose-Mediated Insulin Delivery. *ACS Nano* **2013**, *7* (5), 4194.

- (34) Zhao, L.; Xiao, C.; Ding, J.; He, P.; Tang, Z.; Pang, X.; Zhuang, X.; Chen, X. Facile one-pot synthesis of glucose-sensitive nanogel via thiol-ene click chemistry for self-regulated drug delivery. *Acta Biomaterialia* **2013**, *9* (5), 6535.
- (35) Lai, C.-H.; Chang, T.-C.; Chuang, Y.-J.; Tzou, D.-L.; Lin, C.-C. Stepwise Orthogonal Click Chemistry toward Fabrication of Paclitaxel/Galactose Functionalized Fluorescent Nanoparticles for HepG2 Cell Targeting and Delivery. *Bioconjugate Chemistry* **2013**, *24* (10), 1698.
- (36) Ladmiral, V.; Semsarilar, M.; Canton, I.; Armes, S. P. Polymerization-Induced Self-Assembly of Galactose-Functionalized Biocompatible Diblock Copolymers for Intracellular Delivery. *Journal of the American Chemical Society* **2013**, *135* (36), 13574.
- (37) Yang, R.; Xu, J.; Xu, L.; Sun, X.; Chen, Q.; Zhao, Y.; Peng, R.; Liu, Z. Cancer Cell Membrane-Coated Adjuvant Nanoparticles with Mannose Modification for Effective Anticancer Vaccination. *ACS Nano* **2018**, *12* (6), 5121.
- (38) Jiang, H. L.; Kang, M. L.; Quan, J. S.; Kang, S. G.; Akaike, T.; Yoo, H. S.; Cho, C. S. The potential of mannosylated chitosan microspheres to target macrophage mannose receptors in an adjuvant-delivery system for intranasal immunization. *Biomaterials* **2008**, *29* (12), 1931.
- (39) Tripathi, P.; Dwivedi, P.; Khatik, R.; Jaiswal, A. K.; Dube, A.; Shukla, P.; Mishra, P. R. Development of 4-sulfated N-acetyl galactosamine anchored chitosan nanoparticles: A dual strategy for effective management of Leishmaniasis. *Colloids and Surfaces B: Biointerfaces* **2015**, *136*, 150.
- (40) Singodia, D.; Verma, A.; Verma, R. K.; Mishra, P. R. Investigations into an alternate approach to target mannose receptors on macrophages using 4-sulfated N-acetyl galactosamine more efficiently in comparison with mannose-decorated liposomes: an application in drug delivery. *Nanomedicine: Nanotechnology, Biology and Medicine* **2012**, *8* (4), 468.
- (41) Papp, I.; Sieben, C.; Ludwig, K.; Roskamp, M.; Böttcher, C.; Schlecht, S.; Herrmann, A.; Haag, R. Inhibition of Influenza Virus Infection by Multivalent Sialic-Acid-Functionalized Gold Nanoparticles. *Small* **2010**, *6* (24), 2900.
- (42) Tosi, G.; Vergoni, A. V.; Ruozi, B.; Bondioli, L.; Badiali, L.; Rivasi, F.; Costantino, L.; Forni, F.; Vandelli, M. A. Sialic acid and glycopeptides

- conjugated PLGA nanoparticles for central nervous system targeting: In vivo pharmacological evidence and biodistribution. *Journal of Controlled Release* **2010**, *145* (1), 49.
- (43) Marsich, E.; Borgogna, M.; Donati, I.; Mozetic, P.; Strand, B. L.; Salvador, S. G.; Vittur, F.; Paoletti, S. Alginate/lactose-modified chitosan hydrogels: a bioactive biomaterial for chondrocyte encapsulation. *Journal of Biomedical Materials Research. Part A* **2008**, *84* (2), 364.
- (44) Fernández-Ferreiro, A.; Fernández Bargiela, N.; Varela, M. S.; Martínez, M. G.; Pardo, M.; Piñeiro Ces, A.; Méndez, J. B.; Barcia, M. G.; Lamas, M. J.; Otero-Espinar, F. J. Cyclodextrin–polysaccharide-based, in situ-gelled system for ocular antifungal delivery. *Beilstein Journal of Organic Chemistry* **2014**, *10*, 2903.
- (45) van de Manakker, F.; Vermonden, T.; van Nostrum, C. F.; Hennink, W. E. Cyclodextrin-Based Polymeric Materials: Synthesis, Properties, and Pharmaceutical/Biomedical Applications. *Biomacromolecules* **2009**, *10* (12), 3157.
- (46) Song, W.; Yu, X.; Wang, S.; Blasier, R.; Markel, D. C.; Mao, G.; Shi, T.; Ren, W. Cyclodextrin-erythromycin complexes as a drug delivery device for orthopedic application. *International Journal of Nanomedicine* **2011**, *6*, 3173.
- (47) Abdelghany, S. M.; Schmid, D.; Deacon, J.; Jaworski, J.; Fay, F.; McLaughlin, K. M.; Gormley, J. A.; Burrows, J. F.; Longley, D. B.; Donnelly, R. F. et al. Enhanced Antitumor Activity of the Photosensitizer meso-Tetra(N-methyl-4-pyridyl) Porphine Tetra Tosylate through Encapsulation in Antibody-Targeted Chitosan/Alginate Nanoparticles. *Biomacromolecules* **2013**, *14* (2), 302.
- (48) Tiwari, S.; Chaturvedi, A. P.; Tripathi, Y. B.; Mishra, B. Microspheres based on mannosylated lysine-co-sodium alginate for macrophage-specific delivery of isoniazid. *Carbohydrate Polymer* **2012**, *87* (2), 1575.
- (49) Pelaz, B.; Alexiou, C.; Alvarez-Puebla, R. A.; Alves, F.; Andrews, A. M.; Ashraf, S.; Balogh, L. P.; Ballerini, L.; Bestetti, A.; Brendel, C. et al. Diverse Applications of Nanomedicine. *ACS Nano* **2017**, *11* (3), 2313.
- (50) Date, A. A.; Shibata, A.; McMullen, E.; La Bruzzo, K.; Bruck, P.; Belshan, M.; Zhou, Y.; Destache, C. J. Thermosensitive Gel Containing Cellulose Acetate

Phthalate-Efavirenz Combination Nanoparticles for Prevention of HIV-1 Infection.

- (51) Zhang, Q.; Lin, D.; Yao, S. Review on biomedical and bioengineering applications of cellulose sulfate. *Carbohydrate Polymer* **2015**, *132*, 311.
- (52) Ernsting, M. J.; Tang, W.-L.; MacCallum, N.; Li, S.-D. Synthetic Modification of Carboxymethylcellulose and Use Thereof to Prepare a Nanoparticle Forming Conjugate of Docetaxel for Enhanced Cytotoxicity against Cancer Cells. *Bioconjugate Chemistry* **2011**, *22* (12), 2474.
- (53) Kaihara, S.; Suzuki, Y.; Fujimoto, K. In situ synthesis of polysaccharide nanoparticles via polyion complex of carboxymethyl cellulose and chitosan. *Colloids and Surfaces B: Biointerfaces* **2011**, *85* (2), 343.
- (54) Luo, Y.; Wang, Q. Recent development of chitosan-based polyelectrolyte complexes with natural polysaccharides for drug delivery. *International Journal of Biological Macromolecules* **2014**, *64* (0), 353.
- (55) Casettari, L.; Illum, L. Chitosan in nasal delivery systems for therapeutic drugs. *Journal of Controlled Release* **2014**, *190* (0), 189.
- (56) Joshi, N.; Saha, R.; Shanmugam, T.; Balakrishnan, B.; More, P.; Banerjee, R. Carboxymethyl-Chitosan-Tethered Lipid Vesicles: Hybrid Nanoblanket for Oral Delivery of Paclitaxel. *Biomacromolecules* **2013**, *14* (7), 2272.
- (57) Shi, B.; Shen, Z.; Zhang, H.; Bi, J.; Dai, S. Exploring N-Imidazolyl-O-Carboxymethyl Chitosan for High Performance Gene Delivery. *Biomacromolecules* **2011**, *13* (1), 146.
- (58) Yoon, H. Y.; Son, S.; Lee, S. J.; You, D. G.; Yhee, J. Y.; Park, J. H.; Swierczewska, M.; Lee, S.; Kwon, I. C.; Kim, S. H. et al. Glycol chitosan nanoparticles as specialized cancer therapeutic vehicles: Sequential delivery of doxorubicin and Bcl-2 siRNA. *Scientific Reports* **2014**, *4*, 6878.
- (59) Trapani, A.; Di Gioia, S.; Ditaranto, N.; Cioffi, N.; Goycoolea, F. M.; Carbone, A.; Garcia-Fuentes, M.; Conese, M.; Alonso, M. J. Systemic heparin delivery by the pulmonary route using chitosan and glycol chitosan nanoparticles. *International Journal of Pharmaceutics* **2013**, *447* (1–2), 115.
- (60) Amidi, M.; Romeijn, S. G.; Borchard, G.; Junginger, H. E.; Hennink, W. E.; Jiskoot, W. Preparation and characterization of protein-loaded N-trimethyl

- chitosan nanoparticles as nasal delivery system. *Journal of Controlled Release* **2006**, *111* (1–2), 107.
- (61) Cafaggi, S.; Russo, E.; Stefani, R.; Leardi, R.; Caviglioli, G.; Parodi, B.; Bignardi, G.; De Toterò, D.; Aiello, C.; Viale, M. Preparation and evaluation of nanoparticles made of chitosan or N-trimethyl chitosan and a cisplatin–alginate complex. *Journal of Controlled Release* **2007**, *121* (1–2), 110.
- (62) Hettiaratchi, M. H.; Miller, T.; Temenoff, J. S.; Guldberg, R. E.; McDevitt, T. C. Heparin microparticle effects on presentation and bioactivity of bone morphogenetic protein-2. *Biomaterials* **2014**, *35* (25), 7228.
- (63) Soppimath, K. S.; Kulkarni, A. R.; Aminabhavi, T. M. Chemically modified polyacrylamide-g-guar gum-based crosslinked anionic microgels as pH-sensitive drug delivery systems: preparation and characterization. *Journal of Controlled Release* **2001**, *75* (3), 331.
- (64) Toti, U. S.; Aminabhavi, T. M. Modified guar gum matrix tablet for controlled release of diltiazem hydrochloride. *Journal of Controlled Release* **2004**, *95* (3), 567.
- (65) Cui, L.; Cohen, J. A.; Broaders, K. E.; Beaudette, T. T.; Fréchet, J. M. J. Mannosylated Dextran Nanoparticles: A pH-Sensitive System Engineered for Immunomodulation through Mannose Targeting. *Bioconjugate Chemistry* **2011**, *22* (5), 949.
- (66) Lu, E.; Franzblau, S.; Onyuksel, H.; Popescu, C. Preparation of aminoglycoside-loaded chitosan nanoparticles using dextran sulphate as a counterion. *Journal of Microencapsulation* **2009**, *26* (4), 346.
- (67) Lu, E.; Franzblau, S.; Onyuksel, H.; Popescu, C. Preparation of aminoglycoside-loaded chitosan nanoparticles using dextran sulphate as a counterion. *Journal of Microencapsulation* **2009**, *26* (4), 346.
- (68) Heo, R.; You, D. G.; Um, W.; Choi, K. Y.; Jeon, S.; Park, J.-S.; Choi, Y.; Kwon, S.; Kim, K.; Kwon, I. C. et al. Dextran sulfate nanoparticles as a theranostic nanomedicine for rheumatoid arthritis. *Biomaterials* **2017**, *131*, 15.
- (69) Ha, W.; Wu, H.; Wang, X.-L.; Peng, S.-L.; Ding, L.-S.; Zhang, S.; Li, B.-J. Self-aggregates of cholesterol-modified carboxymethyl konjac glucomannan

- conjugate: Preparation, characterization, and preliminary assessment as a carrier of etoposide. *Carbohydrate Polymer* **2011**, *86* (2), 513.
- (70) Zhang, Y.-q.; Xie, B.-j.; Gan, X. Advance in the applications of konjac glucomannan and its derivatives. *Carbohydrate Polymer* **2005**, *60* (1), 27.
- (71) Xiao, J.-X.; Wang, L.-H.; Xu, T.-C.; Huang, G.-Q. Complex coacervation of carboxymethyl konjac glucomannan and chitosan and coacervate characterization. *International Journal of Biological Macromolecules* **2019**, *123*, 436.
- (72) Tang, D.-W.; Yu, S.-H.; Ho, Y.-C.; Mi, F.-L.; Kuo, P.-L.; Sung, H.-W. Heparinized chitosan/poly(γ -glutamic acid) nanoparticles for multi-functional delivery of fibroblast growth factor and heparin. *Biomaterials* **2010**, *31* (35), 9320.
- (73) Choi, K. Y.; Yoon, H. Y.; Kim, J.-H.; Bae, S. M.; Park, R.-W.; Kang, Y. M.; Kim, I.-S.; Kwon, I. C.; Choi, K.; Jeong, S. Y. et al. Smart Nanocarrier Based on PEGylated Hyaluronic Acid for Cancer Therapy. *ACS Nano* **2011**, *5* (11), 8591.
- (74) Minaberry, Y.; Chiappetta, D. A.; Sosnik, A.; Jobbágy, M. Micro/Nanostructured Hyaluronic Acid Matrices with Tuned Swelling and Drug Release Properties. *Biomacromolecules* **2012**, *14* (1), 1.
- (75) Yoon, H. Y.; Koo, H.; Choi, K. Y.; Chan Kwon, I.; Choi, K.; Park, J. H.; Kim, K. Photo-crosslinked hyaluronic acid nanoparticles with improved stability for in vivo tumor-targeted drug delivery. *Biomaterials* **2013**, *34* (21), 5273.
- (76) Birch, N. P.; Schiffman, J. D. Characterization of Self-Assembled Polyelectrolyte Complex Nanoparticles Formed from Chitosan and Pectin. *Langmuir* **2014**, *30* (12), 3441.
- (77) Chang, Y.; McLandsborough, L.; McClements, D. J. Interactions of a Cationic Antimicrobial (ϵ -Polylysine) with an Anionic Biopolymer (Pectin): An Isothermal Titration Calorimetry, Microelectrophoresis, and Turbidity Study. *Journal of Agricultural and Food Chemistry* **2011**, *59* (10), 5579.
- (78) Gregoriadis, G.; McCormack, B.; Wang, Z.; Lively, R. Polysialic acids: potential in drug delivery. *FEBS Letters* **1993**, *315* (3), 271.

- (79) Zhang, W.; Dong, D.; Li, P.; Wang, D.; Mu, H.; Niu, H.; Duan, J. Novel pH-sensitive polysialic acid based polymeric micelles for triggered intracellular release of hydrophobic drug. *Carbohydrate Polymer* **2016**, *139*, 75.
- (80) Zhang, C.; An, T.; Wang, D.; Wan, G.; Zhang, M.; Wang, H.; Zhang, S.; Li, R.; Yang, X.; Wang, Y. Stepwise pH-responsive nanoparticles containing charge-reversible pullulan-based shells and poly(β -amino ester)/poly(lactic-co-glycolic acid) cores as carriers of anticancer drugs for combination therapy on hepatocellular carcinoma. *Journal of Controlled Release* **2016**, *226*, 193.
- (81) Liang, Y.; Zhao, X.; Ma, P. X.; Guo, B.; Du, Y.; Han, X. pH-responsive injectable hydrogels with mucosal adhesiveness based on chitosan-grafted-dihydrocaffeic acid and oxidized pullulan for localized drug delivery. *Journal of Colloid and Interface Science* **2019**, *536*, 224.
- (82) Singh, B.; Sharma, V. Designing galacturonic acid /arabinogalactan crosslinked poly(vinyl pyrrolidone)- co-poly(2-acrylamido-2-methylpropane sulfonic acid) polymers: Synthesis, characterization and drug delivery application. *Polymer* **2016**, *91*, 50.
- (83) Zhang, Z.; Yang, L.; Hou, J.; Xia, X.; Wang, J.; Ning, Q.; Jiang, S. Promising positive liver targeting delivery system based on arabinogalactan-anchored polymeric micelles of norcantharidin. *Artificial Cells, Nanomedicine, and Biotechnology* **2018**, *46* (sup3), S630.
- (84) Zhang, Y.; Kong, H.; Fang, Y.; Nishinari, K.; Phillips, G. O. Schizophyllan: A review on its structure, properties, bioactivities and recent developments. *Bioactive Carbohydrates and Dietary Fibre* **2013**, *1* (1), 53.
- (85) Kim, Y.-R.; Hwang, J.; Koh, H.-J.; Jang, K.; Lee, J.-D.; Choi, J.; Yang, C.-S. The targeted delivery of the c-Src peptide complexed with schizophyllan to macrophages inhibits polymicrobial sepsis and ulcerative colitis in mice. *Biomaterials* **2016**, *89*, 1.
- (86) Yamada, H.; Loretz, B.; Lehr, C.-M. Design of Starch-graft-PEI Polymers: An Effective and Biodegradable Gene Delivery Platform. *Biomacromolecules* **2014**, *15* (5), 1753.

- (87) Chin, S. F.; Mohd Yazid, S. N. A.; Pang, S. C. Preparation and Characterization of Starch Nanoparticles for Controlled Release of Curcumin. *International Journal of Polymer Science* **2014**, *2014*, 8.
- (88) Chen, C.-K.; Wang, Q.; Jones, C. H.; Yu, Y.; Zhang, H.; Law, W.-C.; Lai, C. K.; Zeng, Q.; Prasad, P. N.; Pfeifer, B. A. et al. Synthesis of pH-Responsive Chitosan Nanocapsules for the Controlled Delivery of Doxorubicin. *Langmuir* **2014**, *30* (14), 4111.
- (89) Kyzas, G. Z.; Siafaka, P. I.; Lambropoulou, D. A.; Lazaridis, N. K.; Bikiaris, D. N. Poly(itaconic acid)-Grafted Chitosan Adsorbents with Different Cross-Linking for Pb(II) and Cd(II) Uptake. *Langmuir* **2013**, *30* (1), 120.
- (90) Fernández, R.; Ocando, C.; Fernandes, S. C. M.; Eceiza, A.; Tercjak, A. Optically Active Multilayer Films Based on Chitosan and an Azopolymer. *Biomacromolecules* **2014**, *15* (4), 1399.
- (91) Zhi, J.; Wang, Y.; Luo, G. Adsorption of diuretic furosemide onto chitosan nanoparticles prepared with a water-in-oil nanoemulsion system. *Reactive and Functional Polymers* **2005**, *65* (3), 249.
- (92) Liu, H.; Chen, B.; Mao, Z.; Gao, C. Chitosan nanoparticles for loading of toothpaste actives and adhesion on tooth analogs. *Journal of Applied Polymer Science* **2007**, *106* (6), 4248.
- (93) Bodnar, M.; Hartmann, J. F.; Borbely, J. Preparation and Characterization of Chitosan-Based Nanoparticles. *Biomacromolecules* **2005**, *6* (5), 2521.
- (94) Hsu, B. B.; Hagerman, S. R.; Jamieson, K.; Veselinovic, J.; O'Neill, N.; Holler, E.; Ljubimova, J. Y.; Hammond, P. T. Multilayer Films Assembled from Naturally-Derived Materials for Controlled Protein Release. *Biomacromolecules* **2014**, *15* (6), 2049.
- (95) Meng, L.; Huang, W.; Wang, D.; Huang, X.; Zhu, X.; Yan, D. Chitosan-Based Nanocarriers with pH and Light Dual Response for Anticancer Drug Delivery. *Biomacromolecules* **2013**, *14* (8), 2601.
- (96) Lee, Y.; Chung, H. J.; Yeo, S.; Ahn, C.-H.; Lee, H.; Messersmith, P. B.; Park, T. G. Thermo-sensitive, injectable, and tissue adhesive sol-gel transition hyaluronic acid/pluronic composite hydrogels prepared from bio-inspired catechol-thiol reaction. *Soft Matter* **2010**, *6* (5), 977.

- (97) Verheul, R. J.; Slütter, B.; Bal, S. M.; Bouwstra, J. A.; Jiskoot, W.; Hennink, W. E. Covalently stabilized trimethyl chitosan-hyaluronic acid nanoparticles for nasal and intradermal vaccination. *Journal of Controlled Release* **2011**, *156* (1), 46.
- (98) Mahor, S.; Dash, B. C.; O'Connor, S.; Pandit, A. Mannosylated Polyethyleneimine–Hyaluronan Nanohybrids for Targeted Gene Delivery to Macrophage-Like Cell Lines. *Bioconjugate Chemistry* **2012**, *23* (6), 1138.
- (99) Martínez, A.; Fernández, A.; Pérez, E.; Benito, M.; Teijón, J.; Blanco, M. Polysaccharide-based nanoparticles for controlled release formulations. *The Delivery of Nanoparticles. InTech* **2012**.
- (100) Jonassen, H.; Kjøniksen, A.-L.; Hiorth, M. Stability of Chitosan Nanoparticles Cross-Linked with Tripolyphosphate. *Biomacromolecules* **2012**, *13* (11), 3747.
- (101) Domaratzki, R. E.; Ghanem, A. Encapsulation and release of cladribine from chitosan nanoparticles. *Journal of Applied Polymer Science* **2013**, *128* (3), 2173.
- (102) Chaubey, P.; Patel, R. R.; Mishra, B. Development and optimization of curcumin-loaded mannosylated chitosan nanoparticles using response surface methodology in the treatment of visceral leishmaniasis. *Expert Opinion on Drug Delivery* **2014**, *0* (0), 1.
- (103) Janes, K. A.; Fresneau, M. P.; Marazuela, A.; Fabra, A.; Alonso, M. a. J. Chitosan nanoparticles as delivery systems for doxorubicin. *Journal of Controlled Release* **2001**, *73* (2–3), 255.
- (104) Zaki, N. M.; Hafez, M. M. Enhanced Antibacterial Effect of Ceftriaxone Sodium-Loaded Chitosan Nanoparticles Against Intracellular Salmonella typhimurium. *AAAPS PharmSciTech* **2012**, *13* (2), 411.
- (105) Deng, X.; Cao, M.; Zhang, J.; Hu, K.; Yin, Z.; Zhou, Z.; Xiao, X.; Yang, Y.; Sheng, W.; Wu, Y. et al. Hyaluronic acid-chitosan nanoparticles for co-delivery of MiR-34a and doxorubicin in therapy against triple negative breast cancer. *Biomaterials* **2014**, *35* (14), 4333.
- (106) Honary, S.; Ebrahimi, P.; Hadianamrei, R. Optimization of particle size and encapsulation efficiency of vancomycin nanoparticles by response surface methodology. *Pharmaceutical Development and Technology* **2014**, *19* (8), 987.

- (107) Xu, Q.; Guo, L.; Gu, X.; Zhang, B.; Hu, X.; Zhang, J.; Chen, J.; Wang, Y.; Chen, C.; Gao, B. et al. Prevention of colorectal cancer liver metastasis by exploiting liver immunity via chitosan-TPP/nanoparticles formulated with IL-12. *Biomaterials* **2012**, *33* (15), 3909.
- (108) Park, Y.-S.; Park, H.-J.; Lee, J. Stabilization of glabridin by chitosan nano-complex. *J Korean Soc Appl Biol Chem* **2012**, *55* (4), 457.
- (109) Kim, D.-G.; Jeong, Y.-I.; Choi, C.; Roh, S.-H.; Kang, S.-K.; Jang, M.-K.; Nah, J.-W. Retinol-encapsulated low molecular water-soluble chitosan nanoparticles. *International Journal of Pharmaceutics* **2006**, *319* (1–2), 130.
- (110) Kang, Y.; Wang, C.; Liu, K.; Wang, Z.; Zhang, X. Enzyme-Responsive Polymeric Supra-Amphiphiles Formed by the Complexation of Chitosan and ATP. *Langmuir* **2012**, *28* (41), 14562.
- (111) Rees, D. A.; Welsh, E. J. Secondary and Tertiary Structure of Polysaccharides in Solutions and Gels. *Angewandte Chemie International Edition in English* **1977**, *16* (4), 214.
- (112) Florczyk, S. J.; Wang, K.; Jana, S.; Wood, D. L.; Sytsma, S. K.; Sham, J. G.; Kievit, F. M.; Zhang, M. Q. Porous chitosan-hyaluronic acid scaffolds as a mimic of glioblastoma microenvironment ECM. *Biomaterials* **2013**, *34* (38), 10143.
- (113) Gnanadhas, D. P.; Ben Thomas, M.; Elango, M.; Raichur, A. M.; Chakravorty, D. Chitosan-dextran sulphate nanocapsule drug delivery system as an effective therapeutic against intraphagosomal pathogen Salmonella. *The Journal of Antimicrobial Chemotherapy* **2013**, *68* (11), 2576.
- (114) Xie, Y.; Qiao, H.; Su, Z.; Chen, M.; Ping, Q.; Sun, M. PEGylated carboxymethyl chitosan/calcium phosphate hybrid anionic nanoparticles mediated hTERT siRNA delivery for anticancer therapy. *Biomaterials* **2014**, *35* (27), 7978.
- (115) Ramasamy, T.; Tran, T. H.; Choi, J. Y.; Cho, H. J.; Kim, J. H.; Yong, C. S.; Choi, H. G.; Kim, J. O. Layer-by-layer coated lipid-polymer hybrid nanoparticles designed for use in anticancer drug delivery. *Carbohydrate Polymer* **2014**, *102*, 653.

- (116) Chen, Q.; Hu, Y.; Chen, Y.; Jiang, X.; Yang, Y. Microstructure Formation and Property of Chitosan-Poly(acrylic acid) Nanoparticles Prepared by Macromolecular Complex. *Macromolecular Bioscience* **2005**, *5* (10), 993.
- (117) Rolland, J.; Guillet, P.; Schumers, J.-M.; Duhem, N.; Pr  at, V.; Gohy, J.-F. Polyelectrolyte complex nanoparticles from chitosan and poly(acrylic acid) and Polystyrene-block-poly(acrylic acid). *Journal of Polymer Science Part A: Polymer Chemistry* **2012**, *50* (21), 4484.
- (118) Tang, Y.; Zhao, Y.; Li, Y.; Du, Y. A thermosensitive chitosan/poly(vinyl alcohol) hydrogel containing nanoparticles for drug delivery. *Polymer Bulletin* **2010**, *64* (8), 791.
- (119) Davidenko, N.; Blanco, M. D.; Peniche, C.; Becher  n, L.; Guerrero, S.; Teij  n, J. M. Effects of different parameters on the characteristics of chitosan–poly(acrylic acid) nanoparticles obtained by the method of coacervation. *Journal of Applied Polymer Science* **2009**, *111* (5), 2362.
- (120) Yuan, X.-b.; Li, H.; Yuan, Y.-b. Preparation of cholesterol-modified chitosan self-aggregated nanoparticles for delivery of drugs to ocular surface. *Carbohydr Polym* **2006**, *65* (3), 337.
- (121) Li, X.; Chen, M.; Yang, W.; Zhou, Z.; Liu, L.; Zhang, Q. Interaction of bovine serum albumin with self-assembled nanoparticles of 6-O-cholesterol modified chitosan. *Colloids and Surfaces B: Biointerfaces* **2012**, *92* (0), 136.
- (122) Murray, P. J.; Wynn, T. A. Protective and pathogenic functions of macrophage subsets. *Nature Review Immunology* **2011**, *11* (11), 723.
- (123) Park, J. H.; Jin, H. E.; Kim, D. D.; Chung, S. J.; Shim, W. S.; Shim, C. K. Chitosan microspheres as an alveolar macrophage delivery system of ofloxacin via pulmonary inhalation. *International Journal of Pharmaceutics* **2013**, *441* (1-2), 562.
- (124) Sahay, G.; Alakhova, D. Y.; Kabanov, A. V. Endocytosis of nanomedicines. *Journal of Controlled Release* **2010**, *145* (3), 182.
- (125) Jiang, X.; Dausend, J.; Hafner, M.; Musyanovych, A.; R  cker, C.; Landfester, K.; Mail  nder, V.; Nienhaus, G. U. Specific Effects of Surface Amines on Polystyrene Nanoparticles in their Interactions with Mesenchymal Stem Cells. *Biomacromolecules* **2010**, *11* (3), 748.

- (126) Verma, A.; Uzun, O.; Hu, Y.; Hu, Y.; Han, H.-S.; Watson, N.; Chen, S.; Irvine, D. J.; Stellacci, F. Surface-structure-regulated cell-membrane penetration by monolayer-protected nanoparticles. *Nature Materials* **2008**, *7* (7), 588.
- (127) Pruthi, J.; Mehra, N. K.; Jain, N. K. Macrophages targeting of amphotericin B through mannosylated multiwalled carbon nanotubes. *Journal of Drug Target* **2012**, *20* (7), 593.
- (128) Diab, R.; Brillault, J.; Bardy, A.; Gontijo, A. V.; Olivier, J. C. Formulation and in vitro characterization of inhalable polyvinyl alcohol-free rifampicin-loaded PLGA microspheres prepared with sucrose palmitate as stabilizer: efficiency for ex vivo alveolar macrophage targeting. *International Journal of Pharmaceutics* **2012**, *436* (1-2), 833.
- (129) Tabata, Y.; Ikada, Y. Effect of the size and surface charge of polymer microspheres on their phagocytosis by macrophage. *Biomaterials* **1988**, *9* (4), 356.
- (130) He, C.; Hu, Y.; Yin, L.; Tang, C.; Yin, C. Effects of particle size and surface charge on cellular uptake and biodistribution of polymeric nanoparticles. *Biomaterials* **2010**, *31* (13), 3657.
- (131) Gratton, S. E. A.; Ropp, P. A.; Pohlhaus, P. D.; Luft, J. C.; Madden, V. J.; Napier, M. E.; DeSimone, J. M. The effect of particle design on cellular internalization pathways. *Proceedings of the National Academy of Sciences* **2008**, *105* (33), 11613.
- (132) Jiang, W.; KimBetty, Y. S.; Rutka, J. T.; ChanWarren, C. W. Nanoparticle-mediated cellular response is size-dependent. *Nature Nanotechnology* **2008**, *3* (3), 145.
- (133) Zhang, S.; Li, J.; Lykotrafitis, G.; Bao, G.; Suresh, S. Size-Dependent Endocytosis of Nanoparticles. *Advanced Materials* **2009**, *21* (4), 419.
- (134) Iversen, T.-G.; Skotland, T.; Sandvig, K. Endocytosis and intracellular transport of nanoparticles: Present knowledge and need for future studies. *Nano Today* **2011**, *6* (2), 176.
- (135) Huang, J.; Bu, L.; Xie, J.; Chen, K.; Cheng, Z.; Li, X.; Chen, X. Effects of Nanoparticle Size on Cellular Uptake and Liver MRI with Polyvinylpyrrolidone-Coated Iron Oxide Nanoparticles. *ACS Nano* **2010**, *4* (12), 7151.

- (136) Duan, X.; Li, Y. Physicochemical Characteristics of Nanoparticles Affect Circulation, Biodistribution, Cellular Internalization, and Trafficking. *Small* **2013**, *9* (9-10), 1521.
- (137) Rejman, J.; Oberle, V.; Zuhorn, I. S.; Hoekstra, D. Size-dependent internalization of particles via the pathways of clathrin- and caveolae-mediated endocytosis. *The Biochemical Journal* **2004**, *377* (Pt 1), 159.
- (138) Muro, S.; Garnacho, C.; Champion, J. A.; Leferovich, J.; Gajewski, C.; Schuchman, E. H.; Mitragotri, S.; Muzykantov, V. R. Control of Endothelial Targeting and Intracellular Delivery of Therapeutic Enzymes by Modulating the Size and Shape of ICAM-1-targeted Carriers. *Molecular therapy : the Journal of the American Society of Gene Therapy* **2008**, *16* (8), 1450.
- (139) Hutter, E.; Boridy, S.; Labrecque, S.; Lalancette-Hébert, M.; Kriz, J.; Winnik, F. M.; Maysinger, D. Microglial Response to Gold Nanoparticles. *ACS Nano* **2010**, *4* (5), 2595.
- (140) Sau, T. K.; Rogach, A. L. Nonspherical Noble Metal Nanoparticles: Colloid-Chemical Synthesis and Morphology Control. *Advanced Materials* **2010**, *22* (16), 1781.
- (141) Champion, J. A.; Mitragotri, S. Role of target geometry in phagocytosis. *Proceedings of the National Academy of Sciences of the United States of America* **2006**, *103* (13), 4930.
- (142) Doshi, N.; Mitragotri, S. Macrophages Recognize Size and Shape of Their Targets. *PLoS ONE* **2010**, *5* (4), e10051.
- (143) Richards, D. M.; Endres, R. G. Target shape dependence in a simple model of receptor-mediated endocytosis and phagocytosis. *Proceedings of the National Academy of Sciences of the United States of America* **2016**, *113* (22), 6113.
- (144) Mitragotri, S.; Lahann, J. Physical approaches to biomaterial design. *Nature Materials* **2009**, *8* (1), 15.
- (145) Geng, Y.; Dalhaimer, P.; Cai, S.; Tsai, R.; Tewari, M.; Minko, T.; Discher, D. E. Shape effects of filaments versus spherical particles in flow and drug delivery. *Nature Nanotechnology* **2007**, *2* (4), 249.

- (146) Huang, X.; Teng, X.; Chen, D.; Tang, F.; He, J. The effect of the shape of mesoporous silica nanoparticles on cellular uptake and cell function. *Biomaterials* **2010**, *31* (3), 438.
- (147) Meng, H.; Yang, S.; Li, Z.; Xia, T.; Chen, J.; Ji, Z.; Zhang, H.; Wang, X.; Lin, S.; Huang, C. et al. Aspect Ratio Determines the Quantity of Mesoporous Silica Nanoparticle Uptake by a Small GTPase-Dependent Macropinocytosis Mechanism. *ACS Nano* **2011**, *5* (6), 4434.
- (148) Herd, H. L.; Malugin, A.; Ghandehari, H. Silica nanoconstruct cellular toleration threshold in vitro. *Journal of Controlled Release* **2011**, *153* (1), 40.
- (149) Arvizo, R. R.; Miranda, O. R.; Moyano, D. F.; Walden, C. A.; Giri, K.; Bhattacharya, R.; Robertson, J. D.; Rotello, V. M.; Reid, J. M.; Mukherjee, P. Modulating Pharmacokinetics, Tumor Uptake and Biodistribution by Engineered Nanoparticles. *PLoS ONE* **2011**, *6* (9), e24374.
- (150) Yezhelyev, M. V.; Qi, L.; O'Regan, R. M.; Nie, S.; Gao, X. Proton-Sponge Coated Quantum Dots for siRNA Delivery and Intracellular Imaging. *Journal of the American Chemical Society* **2008**, *130* (28), 9006.
- (151) Vadakkan, M. V.; Annapoorna, K.; Sivakumar, K. C.; Mundayoor, S.; Kumar, G. S. Dry powder cationic lipopolymeric nanomicelle inhalation for targeted delivery of antitubercular drug to alveolar macrophage. *International Journal of Nanomedicine* **2013**, *8*, 2871.
- (152) Gbadamosi, J. K.; Hunter, A. C.; Moghimi, S. M. PEGylation of microspheres generates a heterogeneous population of particles with differential surface characteristics and biological performance. *FEBS Letters* **2002**, *532* (3), 338.
- (153) Yhee, J. Y.; Son, S.; Kim, S. H.; Park, K.; Choi, K.; Kwon, I. C. Self-assembled glycol chitosan nanoparticles for disease-specific theranostics. *Journal of Controlled Release* **2014**, *193* (0), 202.
- (154) Yue, Z.-G.; Wei, W.; Lv, P.-P.; Yue, H.; Wang, L.-Y.; Su, Z.-G.; Ma, G.-H. Surface Charge Affects Cellular Uptake and Intracellular Trafficking of Chitosan-Based Nanoparticles. *Biomacromolecules* **2011**, *12* (7), 2440.
- (155) Rigotti, A.; Acton, S. L.; Krieger, M. The Class B Scavenger Receptors SR-BI and CD36 Are Receptors for Anionic Phospholipids. *Journal of Biological Chemistry* **1995**, *270* (27), 16221.

- (156) Patil, S.; Sandberg, A.; Heckert, E.; Self, W.; Seal, S. Protein adsorption and cellular uptake of cerium oxide nanoparticles as a function of zeta potential. *Biomaterials* **2007**, *28* (31), 4600.
- (157) Wilhelm, C.; Billotey, C.; Roger, J.; Pons, J. N.; Bacri, J. C.; Gazeau, F. Intracellular uptake of anionic superparamagnetic nanoparticles as a function of their surface coating. *Biomaterials* **2003**, *24* (6), 1001.
- (158) Limbach, L. K.; Li, Y.; Grass, R. N.; Brunner, T. J.; Hintermann, M. A.; Muller, M.; Gunther, D.; Stark, W. J. Oxide Nanoparticle Uptake in Human Lung Fibroblasts: Effects of Particle Size, Agglomeration, and Diffusion at Low Concentrations. *Environmental Science & Technology* **2005**, *39* (23), 9370.
- (159) Xiao, K.; Li, Y.; Luo, J.; Lee, J. S.; Xiao, W.; Gonik, A. M.; Agarwal, R. G.; Lam, K. S. The effect of surface charge on in vivo biodistribution of PEG-oligocholic acid based micellar nanoparticles. *Biomaterials* **2011**, *32* (13), 3435.
- (160) Nanotubes keep rolling on. *Nature Nanotechnology* **2009**, *4* (8), 465.
- (161) Musyanovych, A.; Dausend, J.; Dass, M.; Walther, P.; Mailänder, V.; Landfester, K. Criteria impacting the cellular uptake of nanoparticles: A study emphasizing polymer type and surfactant effects. *Acta Biomaterialia* **2011**, *7* (12), 4160.
- (162) Brannon-Peppas, L.; Blanchette, J. O. Nanoparticle and targeted systems for cancer therapy. *Advanced Drug Delivery Reviews* **2004**, *56* (11), 1649.
- (163) Sudimack, J.; Lee, R. J. Targeted drug delivery via the folate receptor. *Advanced Drug Delivery Reviews* **2000**, *41* (2), 147.
- (164) Arap, W.; Pasqualini, R.; Ruoslahti, E. Cancer Treatment by Targeted Drug Delivery to Tumor Vasculature in a Mouse Model. *Science* **1998**, *279* (5349), 377.
- (165) Farokhzad, O. C.; Cheng, J.; Teply, B. A.; Sherifi, I.; Jon, S.; Kantoff, P. W.; Richie, J. P.; Langer, R. Targeted nanoparticle-aptamer bioconjugates for cancer chemotherapy in vivo. *Proceedings of the National Academy of Sciences* **2006**, *103* (16), 6315.
- (166) Ehrenberg, M. S.; Friedman, A. E.; Finkelstein, J. N.; Oberdörster, G.; McGrath, J. L. The influence of protein adsorption on nanoparticle association with cultured endothelial cells. *Biomaterials* **2009**, *30* (4), 603.

- (167) Chen, Z.; Xu, R.; Zhang, Y.; Gu, N. Effects of Proteins from Culture Medium on Surface Property of Silanes- Functionalized Magnetic Nanoparticles. *Nanoscale Research Letters* **2008**, *4* (3), 204
- (168) Zahr, A. S.; Davis, C. A.; Pishko, M. V. Macrophage Uptake of Core–Shell Nanoparticles Surface Modified with Poly(ethylene glycol). *Langmuir* **2006**, *22* (19), 8178.
- (169) Nel, A. E.; Madler, L.; Velegol, D.; Xia, T.; Hoek, E. M. V.; Somasundaran, P.; Klaessig, F.; Castranova, V.; Thompson, M. Understanding biophysicochemical interactions at the nano-bio interface. *Nature Materials* **2009**, *8* (7), 543.
- (170) Free, P.; Shaw, C. P.; Levy, R. PEGylation modulates the interfacial kinetics of proteases on peptide-capped gold nanoparticles. *Chemical Communications* **2009**, *0*(33), 5009.
- (171) Storm, G.; Belliot, S. O.; Daemen, T.; Lasic, D. D. Surface modification of nanoparticles to oppose uptake by the mononuclear phagocyte system. *Advanced Drug Delivery Reviews* **1995**, *17* (1), 31.
- (172) Wijagkanalan, W.; Kawakami, S.; Higuchi, Y.; Yamashita, F.; Hashida, M. Intratracheally instilled mannosylated cationic liposome/NFκB decoy complexes for effective prevention of LPS-induced lung inflammation. *Journal of Controlled Release* **2011**, *149* (1), 42.
- (173) Chaubey, P.; Mishra, B. Mannose-conjugated chitosan nanoparticles loaded with rifampicin for the treatment of visceral leishmaniasis. *Carbohydrate Polymer* **2014**, *101*, 1101.
- (174) Zhang, Q.; Su, L.; Collins, J.; Chen, G.; Wallis, R.; Mitchell, D. A.; Haddleton, D. M.; Becer, C. R. Dendritic Cell Lectin-Targeting Sentinel-like Unimolecular Glycoconjugates To Release an Anti-HIV Drug. *Journal of the American Chemical Society* **2014**, *136* (11), 4325.
- (175) Chono, S.; Tanino, T.; Seki, T.; Morimoto, K. Uptake characteristics of liposomes by rat alveolar macrophages: influence of particle size and surface mannose modification. *Journal of Pharmacy and Pharmacology* **2007**, *59* (1), 75.

- (176) Xiong, M. H.; Li, Y. J.; Bao, Y.; Yang, X. Z.; Hu, B.; Wang, J. Bacteria-responsive multifunctional nanogel for targeted antibiotic delivery. *Advanced Materials* **2012**, *24* (46), 6175.
- (177) Jiang, H. L.; Kim, Y. K.; Arote, R.; Jere, D.; Quan, J. S.; Yu, J. H.; Choi, Y. J.; Nah, J. W.; Cho, M. H.; Cho, C. S. Mannosylated chitosan-graft-polyethylenimine as a gene carrier for Raw 264.7 cell targeting. *International Journal of Pharmaceutics* **2009**, *375* (1-2), 133.
- (178) Song, E.-H.; Manganiello, M. J.; Chow, Y.-H.; Ghosn, B.; Convertine, A. J.; Stayton, P. S.; Schnapp, L. M.; Ratner, D. M. In vivo targeting of alveolar macrophages via RAFT-based glycopolymers. *Biomaterials* **2012**, *33* (28), 6889.
- (179) Lin, K.; Kasko, A. M. Carbohydrate-Based Polymers for Immune Modulation. *ACS Macro Letters* **2014**, *3* (7), 652.
- (180) Adler, A. F.; Leong, K. W. Emerging links between surface nanotechnology and endocytosis: Impact on nonviral gene delivery. *Nano Today* **2010**, *5* (6), 553.
- (181) Devadasu, V. R.; Bhardwaj, V.; Kumar, M. N. V. R. Can Controversial Nanotechnology Promise Drug Delivery? *Chemical Reviews* **2012**, *113* (3), 1686.
- (182) Levental, I.; Georges, P. C.; Janmey, P. A. Soft biological materials and their impact on cell function. *Soft Matter* **2007**, *3* (3), 299.
- (183) Beningo, K. A.; Wang, Y.-l. Fc-receptor-mediated phagocytosis is regulated by mechanical properties of the target. *Journal of Cell Science* **2002**, *115* (4), 849.
- (184) Yi, X.; Shi, X.; Gao, H. Cellular Uptake of Elastic Nanoparticles. *Physical Review Letters* **2011**, *107* (9), 098101.
- (185) Sun, W.; Hu, Q.; Ji, W.; Wright, G.; Gu, Z. Leveraging Physiology for Precision Drug Delivery. *Physiological Reviews* **2016**, *97* (1), 189.
- (186) Kaur, I. P.; Singh, H. Nanostructured drug delivery for better management of tuberculosis. *Journal of Controlled Release* **2014**, *184* (0), 36.
- (187) Saraogi, G. K.; Sharma, B.; Joshi, B.; Gupta, P.; Gupta, U. D.; Jain, N. K.; Agrawal, G. P. Mannosylated gelatin nanoparticles bearing isoniazid for effective management of tuberculosis. *Journal of Drug Target* **2011**, *19* (3), 219.

- (188) Pourshahab, P. S.; Gilani, K.; Moazeni, E.; Eslahi, H.; Fazeli, M. R.; Jamalifar, H. Preparation and characterization of spray dried inhalable powders containing chitosan nanoparticles for pulmonary delivery of isoniazid. *Journal of Microencapsulation* **2011**, 28 (7), 605.
- (189) Ohashi, K.; Kabasawa, T.; Ozeki, T.; Okada, H. One-step preparation of rifampicin/poly(lactic-co-glycolic acid) nanoparticle-containing mannitol microspheres using a four-fluid nozzle spray drier for inhalation therapy of tuberculosis. *Journal of Controlled Release* **2009**, 135 (1), 19.
- (190) Nimje, N.; Agarwal, A.; Saraogi, G. K.; Lariya, N.; Rai, G.; Agrawal, H.; Agrawal, G. P. Mannosylated nanoparticulate carriers of rifabutin for alveolar targeting. *Journal of Drug Target* **2009**, 17 (10), 777.
- (191) Hwang, S. M.; Kim, D. D.; Chung, S. J.; Shim, C. K. Delivery of ofloxacin to the lung and alveolar macrophages via hyaluronan microspheres for the treatment of tuberculosis. *Journal of Controlled Release* **2008**, 129 (2), 100.
- (192) Zahoor, A.; Sharma, S.; Khuller, G. K. Inhalable alginate nanoparticles as antitubercular drug carriers against experimental tuberculosis. *International Journal of Antimicrobial Agents* **2005**, 26 (4), 298.
- (193) Kumar, P. V.; Asthana, A.; Dutta, T.; Jain, N. K. Intracellular macrophage uptake of rifampicin loaded mannosylated dendrimers. *Journal of Drug Target* **2006**, 14 (8), 546.
- (194) Moretton, M. A.; Chiappetta, D. A.; Andrade, F.; das Neves, J.; Ferreira, D.; Sarmiento, B.; Sosnik, A. Hydrolyzed Galactomannan-Modified Nanoparticles and Flower-Like Polymeric Micelles for the Active Targeting of Rifampicin to Macrophages. *Journal of Biomedical Nanotechnology* **2013**, 9 (6), 1076.
- (195) Okuda, T.; Kito, D.; Oiwa, A.; Fukushima, M.; Hira, D.; Okamoto, H. Gene Silencing in a Mouse Lung Metastasis Model by an Inhalable Dry Small Interfering RNA Powder Prepared Using the Supercritical Carbon Dioxide Technique. *Biological and Pharmaceutical Bulletin* **2013**, 36 (7), 1183.
- (196) De Backer, L.; Braeckmans, K.; Stuart, M. C. A.; Demeester, J.; De Smedt, S. C.; Raemdonck, K. Bio-inspired pulmonary surfactant-modified nanogels: A promising siRNA delivery system. *Journal of Controlled Release* **2015**, 206 (Supplement C), 177.

- (197) De Backer, L.; Naessens, T.; De Koker, S.; Zagato, E.; Demeester, J.; Grooten, J.; De Smedt, S. C.; Raemdonck, K. Hybrid pulmonary surfactant-coated nanogels mediate efficient in vivo delivery of siRNA to murine alveolar macrophages. *Journal of Controlled Release* **2015**, *217* (Supplement C), 53.
- (198) Garg, T.; Rath, G.; Goyal, A. K. Inhalable chitosan nanoparticles as antitubercular drug carriers for an effective treatment of tuberculosis. *Artificial Cells, Nanomedicine, and Biotechnology* **2016**, *44* (3), 997.
- (199) Smitha, K. T.; Nisha, N.; Maya, S.; Biswas, R.; Jayakumar, R. Delivery of rifampicin-chitin nanoparticles into the intracellular compartment of polymorphonuclear leukocytes. *International Journal of Biological Macromolecules* **2015**, *74* (Supplement C), 36.
- (200) Maya, S.; Indulekha, S.; Sukhithasri, V.; Smitha, K. T.; Nair, S. V.; Jayakumar, R.; Biswas, R. Efficacy of tetracycline encapsulated O-carboxymethyl chitosan nanoparticles against intracellular infections of *Staphylococcus aureus*. *International Journal of Biological Macromolecules* **2012**, *51* (4), 392.
- (201) Kiruthika, V.; Maya, S.; Suresh, M. K.; Anil Kumar, V.; Jayakumar, R.; Biswas, R. Comparative efficacy of chloramphenicol loaded chondroitin sulfate and dextran sulfate nanoparticles to treat intracellular *Salmonella* infections. *Colloids and Surfaces B: Biointerfaces* **2015**, *127* (Supplement C), 33.
- (202) S, E.; T.R, N.; V.K, R.; Baranwal, G.; Biswas, R.; R, J.; S, S. Fucoidan coated ciprofloxacin loaded chitosan nanoparticles for the treatment of intracellular and biofilm infections of *Salmonella*. *Colloids and Surfaces B: Biointerfaces* **2017**, *160* (Supplement C), 40.
- (203) Grumezescu, A. M.; Andronescu, E.; Holban, A. M.; Ficai, A.; Ficai, D.; Voicu, G.; Grumezescu, V.; Balaure, P. C.; Chifiriuc, C. M. Water dispersible cross-linked magnetic chitosan beads for increasing the antimicrobial efficiency of aminoglycoside antibiotics. *International Journal of Pharmaceutics* **2013**, *454* (1), 233.
- (204) Hombach, J.; Hoyer, H.; Bernkop-Schnurch, A. Thiolated chitosans: development and in vitro evaluation of an oral tobramycin sulphate delivery system. *European Journal of Pharmaceutical Sciences* **2008**, *33* (1), 1.

- (205) Kumar, P. V.; Asthana, A.; Dutta, T.; Jain, N. K. Intracellular macrophage uptake of rifampicin loaded mannosylated dendrimers. *Journal of Drug Target* **2006**, *14* (8), 546.
- (206) Maya, S.; Indulekha, S.; Sukhithasri, V.; Smitha, K. T.; Nair, S. V.; Jayakumar, R.; Biswas, R. Efficacy of tetracycline encapsulated O-carboxymethyl chitosan nanoparticles against intracellular infections of *Staphylococcus aureus*. *International Journal of Biological Macromolecules* **2012**, *51* (4), 392.
- (207) Wu, F.; Meng, G.; He, J.; Wu, Y.; Wu, F.; Gu, Z. Antibiotic-Loaded Chitosan Hydrogel with Superior Dual Functions: Antibacterial Efficacy and Osteoblastic Cell Responses. *ACS Applied Materials & Interferfaces* **2014**, *6* (13), 10005.
- (208) Gupta, P. K.; Asthana, S.; Jaiswal, A. K.; Kumar, V.; Verma, A. K.; Shukla, P.; Dwivedi, P.; Dube, A.; Mishra, P. R. Exploitation of Lectinized Lipopolymerosome Encapsulated Amphotericin B to Target Macrophages for Effective Chemotherapy of Visceral Leishmaniasis. *Bioconjugate Chemistry* **2014**, *25* (6), 1091.
- (209) Asthana, S.; Jaiswal, A. K.; Gupta, P. K.; Pawar, V. K.; Dube, A.; Chourasia, M. K. Immunoadjuvant chemotherapy of visceral leishmaniasis in hamsters using amphotericin B-encapsulated nanoemulsion template-based chitosan nanocapsules. *Antimicrobial Agents and Chemotherapy* **2013**, *57* (4), 1714.
- (210) Zeng, R.; Wang, Z.; Wang, H.; Chen, L.; Yang, L.; Qiao, R.; Hu, L.; Li, Z. Effect of bond linkage on in vitro drug release and anti-HIV activity of chitosan-stavudine conjugates. *Macromolecular Research* **2012**, *20* (4), 358.
- (211) UNAIDS. AIDS-by-the-numbers. *AIDS-by-the-numbers, Switzerland, Geneva* **2016**.
- (212) Nyamweya, S.; Hegedus, A.; Jaye, A.; Rowland-Jones, S.; Flanagan, K. L.; Macallan, D. C. Comparing HIV-1 and HIV-2 infection: Lessons for viral immunopathogenesis. *Reviews in Medical Virology* **2013**, *23* (4), 221.
- (213) Klasse, P. J. The molecular basis of HIV entry. *Cellular Microbiology* **2012**, *14* (8), 1183.
- (214) Dev, J.; Park, D.; Fu, Q.; Chen, J.; Ha, H. J.; Ghantous, F.; Herrmann, T.; Chang, W.; Liu, Z.; Frey, G. et al. Structural basis for membrane anchoring of HIV-1 envelope spike. *Science* **2016**, *353* (6295), 172.

- (215) Das Neves, J.; Nunes, R.; Rodrigues, F.; Sarmento, B. Nanomedicine in the development of anti-HIV microbicides. *Advanced Drug Delivery Reviews* **2016**, *103*, 57.
- (216) Adlin Jino Nesalin, J.; Anton Smith, A. Preparation and evaluation of stavudine loaded chitosan nanoparticles. *Journal of Pharmacy Research* **2013**, *6* (2), 268.
- (217) Goudanavar, P.; Thandava, K.; Hiremath, D.; Sarfaraz, M. Development and characterization of stavudine loaded nanoparticulate drug delivery system. *BIOINFO Pharmaceutical Biotechnology* **2013**, *2* (1), 24.
- (218) Dev, A.; Binulal, N. S.; Anitha, A.; Nair, S. V.; Furuike, T.; Tamura, H.; Jayakumar, R. Preparation of poly(lactic acid)/chitosan nanoparticles for anti-HIV drug delivery applications. *Carbohydrate Polymer* **2010**, *80* (3), 833.
- (219) Li, Q.; Du, Y.-Z.; Yuan, H.; Zhang, X.-G.; Miao, J.; Cui, F.-D.; Hu, F.-Q. Synthesis of Lamivudine stearate and antiviral activity of stearic acid-g-chitosan oligosaccharide polymeric micelles delivery system. *European Journal of Pharmaceutical Sciences* **2010**, *41* (3–4), 498.
- (220) Giacalone, G.; Fattal, E.; Hillaireau, H. Chitosan nanoparticles for the intracellular delivery of triphosphate nucleotide analogues. *BMC Infectious Diseases* **2014**, *14* (Suppl 2), P75.
- (221) Ramana, L. N.; Sharma, S.; Sethuraman, S.; Ranga, U.; Krishnan, U. M. Evaluation of chitosan nanoformulations as potent anti-HIV therapeutic systems. *Biochimica et Biophysica Acta (BBA) - General Subjects* **2014**, *1840* (1), 476.
- (222) Parker, A. C.; Beenken, K. E.; Jennings, J. A.; Hittle, L.; Shirliff, M. E.; Bumgardner, J. D.; Smeltzer, M. S.; Haggard, W. O. Characterization of local delivery with amphotericin B and vancomycin from modified chitosan sponges and functional biofilm prevention evaluation. *Journal of Orthopaedic Research* **2015**, *33* (3), 439.
- (223) Staedtke, V.; Brahler, M.; Muller, A.; Georgieva, R.; Bauer, S.; Sternberg, N.; Voigt, A.; Lemke, A.; Keck, C.; Moschwitzer, J. et al. In vitro inhibition of fungal activity by macrophage-mediated sequestration and release of encapsulated amphotericin B nanosuspension in red blood cells. *Small* **2010**, *6* (1), 96.

- (224) Vyas, S. P.; Khatri, K. Liposome-based drug delivery to alveolar macrophages. *Expert Opinion on Drug Delivery* **2007**, *4* (2), 95.
- (225) Nagle, A. S.; Khare, S.; Kumar, A. B.; Supek, F.; Buchynskyy, A.; Mathison, C. J. N.; Chennamaneni, N. K.; Pendem, N.; Buckner, F. S.; Gelb, M. H. et al. Recent Developments in Drug Discovery for Leishmaniasis and Human African Trypanosomiasis. *Chemical Reviews* **2014**, *114* (22), 11305.
- (226) Agrawal, A. K.; Gupta, C. M. Tuftsin-bearing liposomes in treatment of macrophage-based infections. *Advanced Drug Delivery Reviews* **2000**, *41* (2), 135.
- (227) Ickowicz, D. E.; Farber, S.; Sionov, E.; Kagan, S.; Hoffman, A.; Polacheck, I.; Domb, A. J. Activity, Reduced Toxicity, and Scale-Up Synthesis of Amphotericin B-Conjugated Polysaccharide. *Biomacromolecules* **2014**, *15* (6), 2079.
- (228) Falk, R.; Grunwald, J.; Hoffman, A.; Domb, A. J.; Polacheck, I. Distribution of amphotericin B-arabinogalactan conjugate in mouse tissue and its therapeutic efficacy against murine aspergillosis. *Antimicrobial Agents and Chemotherapy* **2004**, *48* (9), 3606.
- (229) Kagan, S.; Ickowicz, D.; Shmuel, M.; Altschuler, Y.; Sionov, E.; Pitusi, M.; Weiss, A.; Farber, S.; Domb, A. J.; Polacheck, I. Toxicity mechanisms of amphotericin B and its neutralization by conjugation with arabinogalactan. *Antimicrobial Agents and Chemotherapy* **2012**, *56* (11), 5603.
- (230) Verma, P.; Ahuja, M. Optimization, characterization and evaluation of chitosan-tailored cubic nanoparticles of clotrimazole. *International Journal of Biological Macromolecules* **2015**, *73*, 138.
- (231) Mura, P.; Mennini, N.; Kosalec, I.; Furlanetto, S.; Orlandini, S.; Jug, M. Amidated pectin-based wafers for econazole buccal delivery: Formulation optimization and antimicrobial efficacy estimation. *Carbohydrate Polymer* **2015**, *121*, 231.
- (232) Rai, V. K.; Yadav, N. P.; Sinha, P.; Mishra, N.; Luqman, S.; Dwivedi, H.; Kymonil, K. M.; Saraf, S. A. Development of cellulosic polymer based gel of novel ternary mixture of miconazole nitrate for buccal delivery. *Carbohydrate Polymer* **2014**, *103*, 126.

- (233) Yao, W.; Jiao, Y.; Luo, J.; Du, M.; Zong, L. Practical synthesis and characterization of mannose-modified chitosan. *International Journal of Biological Macromolecules* **2012**, *50* (3), 821.
- (234) Woodworth, J. S.; Cohen, S. B.; Moguche, A. O.; Plumlee, C. R.; Agger, E. M.; Urdahl, K. B.; Andersen, P. Subunit vaccine H56/CAF01 induces a population of circulating CD4 T cells that traffic into the Mycobacterium tuberculosis-infected lung. *Mucosal Immunology* **2016**, *10*, 555.
- (235) Flannagan, R. S.; Heit, B.; Heinrichs, D. E. Intracellular replication of Staphylococcus aureus in mature phagolysosomes in macrophages precedes host cell death, and bacterial escape and dissemination. *Cellular Microbiology* **2016**, *18* (4), 514.
- (236) Gamazo, C.; Prior, S.; Lecaroz, M. C.; Vitas, A. I.; Campanero, M. A.; Perez, G.; Gonzalez, D.; Blanco-Prieto, M. J. Biodegradable gentamicin delivery systems for parenteral use for the treatment of intracellular bacterial infections. *Expert Opinion on Drug Delivery* **2007**, *4* (6), 677.
- (237) Briones, E.; Colino, C. I.; Millan, C. G.; Lanao, J. M. Increasing the selectivity of amikacin in rat peritoneal macrophages using carrier erythrocytes. *European Journal of Pharmaceutical Science* **2009**, *38* (4), 320.
- (238) Abed, N. Nanocarriers for antibiotics: A promising solution to treat intracellular bacterial infections. *International Journal of Antimicrobial Agents* **2014**, *43* (6), 485.
- (239) Knudsen, N. P.; Olsen, A.; Buonsanti, C.; Follmann, F.; Zhang, Y.; Coler, R. N.; Fox, C. B.; Meinke, A.; D'Oro, U.; Casini, D. et al. Different human vaccine adjuvants promote distinct antigen-independent immunological signatures tailored to different pathogens. *Scientific Reports* **2016**, *6*, 19570.
- (240) Billeskov, R.; Tan, E. V.; Cang, M.; Abalos, R. M.; Burgos, J.; Pedersen, B. V.; Christensen, D.; Agger, E. M.; Andersen, P. Testing the H56 Vaccine Delivered in 4 Different Adjuvants as a BCG-Booster in a Non-Human Primate Model of Tuberculosis. *PLoS ONE* **2016**, *11* (8), e0161217.
- (241) Arora, D.; Sharma, N.; Sharma, V.; Abrol, V.; Shankar, R.; Jaglan, S. An update on polysaccharide-based nanomaterials for antimicrobial applications. *Applied Microbiology and Biotechnology* **2016**, *100* (6), 2603.

- (242) Ueki, A.; Un, K.; Mino, Y.; Yoshida, M.; Kawakami, S.; Ando, H.; Ishida, H.; Yamashita, F.; Hashida, M.; Kiso, M. Synthesis and evaluation of glyco-coated liposomes as drug carriers for active targeting in drug delivery systems. *Carbohydrate Research* **2015**, *405*, 78.
- (243) Kallerup, R. S.; Madsen, C. M.; Schiøth, M. L.; Franzyk, H.; Rose, F.; Christensen, D.; Korsholm, K. S.; Foged, C. Influence of trehalose 6,6'-diester (TDX) chain length on the physicochemical and immunopotentiating properties of DDA/TDX liposomes. *European Journal of Pharmaceutics and Biopharmaceutics* **2015**, *90* (0), 80.
- (244) Basu, A.; Kunduru, K. R.; Abteu, E.; Domb, A. J. Polysaccharide-based conjugates for biomedical applications. *Bioconjugate Chemistry* **2015**, *26* (8), 1396.
- (245) Shilakari Asthana, G.; Asthana, A.; Kohli, D. V.; Vyas, S. P. Mannosylated chitosan nanoparticles for delivery of antisense oligonucleotides for macrophage targeting. *BioMed Research International* **2014**, *2014*, 17.
- (246) Xiao, B.; Laroui, H.; Ayyadurai, S.; Viennois, E.; Charania, M. A.; Zhang, Y. C.; Merlin, D. Mannosylated bioreducible nanoparticle-mediated macrophage-specific TNF- α RNA interference for IBD therapy. *Biomaterials* **2013**, *34* (30), 7471.
- (247) Yao, W. J.; Peng, Y. X.; Du, M. Z.; Luo, J.; Zong, L. Preventative vaccine-loaded mannosylated chitosan nanoparticles intended for nasal mucosal delivery enhance immune responses and potent tumor immunity. *Molecular Pharmaceutics* **2013**, *10* (8), 2904.
- (248) Semple, S. C.; Chonn, A.; Cullis, P. R. Influence of Cholesterol on the Association of Plasma Proteins with Liposomes. *Biochemistry* **1996**, *35* (8), 2521.
- (249) Rui, Y.; Wang, S.; Low, P. S.; Thompson, D. H. Dipalmitoylcholine–folate liposomes: an efficient vehicle for intracellular drug delivery. *Journal of the American Chemical Society* **1998**, *120* (44), 11213.
- (250) Giddam, A. K.; Reiman, J. M.; Zaman, M.; Skwarczynski, M.; Toth, I.; Good, M. F. A semi-synthetic whole parasite vaccine designed to protect against blood stage malaria. *Acta biomaterialia* **2016**, *44*, 295.

- (251) Ghaffar, K. A.; Marasini, N.; Giddam, A. K.; Batzloff, M. R.; Good, M. F.; Skwarczynski, M.; Toth, I. Liposome-based intranasal delivery of lipopeptide vaccine candidates against group A streptococcus. *Acta biomaterialia* **2016**, *41*, 161.
- (252) Kawakami, S.; Wong, J.; Sato, A.; Hattori, Y.; Yamashita, F.; Hashida, M. Biodistribution characteristics of mannosylated, fucosylated, and galactosylated liposomes in mice. *Biochimica et Biophysica Acta (BBA) - General Subjects* **2000**, *1524* (2–3), 258.
- (253) Ashley, C. E.; Carnes, E. C.; Phillips, G. K.; Padilla, D.; Durfee, P. N.; Brown, P. A.; Hanna, T. N.; Liu, J.; Phillips, B.; Carter, M. B. et al. The targeted delivery of multicomponent cargos to cancer cells by nanoporous particle-supported lipid bilayers. *Nature Materials* **2011**, *10* (5), 389.
- (254) Doshi, N.; Mitragotri, S. Designer biomaterials for nanomedicine. *Advanced Functional Materials* **2009**, *19* (24), 3843.
- (255) Hallaj-Nezhadi, S.; Hassan, M. Nanoliposome-based antibacterial drug delivery. *Drug delivery* **2013**, *0* (0), 1.
- (256) Maurin, M.; Raoult, D. Use of aminoglycosides in treatment of infections due to intracellular bacteria. *Antimicrobial Agents and Chemotherapy* **2001**, *45* (11), 2977.
- (257) Noel, S. P.; Courtney, H. S.; Bumgardner, J. D.; Haggard, W. O. Chitosan sponges to locally deliver amikacin and vancomycin: a pilot in vitro evaluation. *Clinical Orthopaedics and Related Research* **2010**, *468* (8), 2074.
- (258) Dhillon, J.; Fielding, R.; Adler-Moore, J.; Goodall, R. L.; Mitchison, D. The activity of low-clearance liposomal amikacin in experimental murine tuberculosis. *Journal of Antimicrobial Chemotherapy* **2001**, *48* (6), 869.
- (259) Li, Z.; Zhang, Y.; Wurtz, W.; Lee, J. K.; Malinin, V. S.; Durwas-Krishnan, S.; Meers, P.; Perkins, W. R. Characterization of nebulized liposomal amikacin (Arikace™) as a function of droplet size. *Journal of Aerosol Medicine and Pulmonary Drug Delivery* **2008**, *21* (3), 245.
- (260) Nastase, S.; Bajenaru, L.; Matei, C.; Mitran, R. A.; Berger, D. Ordered mesoporous silica and aluminosilicate-type matrix for amikacin delivery systems. *Microporous and Mesoporous Materials* **2013**, *182*, 32.

- (261) Xiong, Y. Q.; Kupferwasser, L. I.; Zack, P. M.; Bayer, A. S. Comparative efficacies of liposomal amikacin (MiKasome) plus oxacillin versus conventional amikacin plus oxacillin in experimental endocarditis induced by *Staphylococcus aureus*: Microbiological and echocardiographic analyses. *Antimicrobial Agents and Chemotherapy* **1999**, *43* (7), 1737.
- (262) Jones, P. B.; Parrish, N. M.; Houston, T. A.; Stapon, A.; Bansal, N. P.; Dick, J. D.; Townsend, C. A. A new class of antituberculosis agents. *Journal of Medicinal Chemistry* **2000**, *43* (17), 3304.
- (263) Parrish, N. M.; Ko, C. G.; Hughes, M. A.; Townsend, C. A.; Dick, J. D. Effect of n-octanesulphonylacетamide (OSA) on ATP and protein expression in *Mycobacterium bovis* BCG. *The Journal of Antimicrobial Chemotherapy* **2004**, *54* (4), 722.
- (264) Parrish, N. M.; Houston, T.; Jones, P. B.; Townsend, C.; Dick, J. D. In vitro activity of a novel antimycobacterial compound, N-octanesulfonylacетamide, and its effects on lipid and mycolic acid synthesis. *Antimicrobial Agents and Chemotherapy* **2001**, *45* (4), 1143.
- (265) Dover, L. G.; Bhatt, A.; Bhowruth, V.; Willcox, B. E.; Besra, G. S. New drugs and vaccines for drug-resistant *Mycobacterium tuberculosis* infections. *Expert Review of Vaccines* **2008**, *7* (4), 481.
- (266) Parrish, N. M.; Ko, C. G.; Dick, J. D. Activity of DSA against anaerobically adapted *Mycobacterium bovis* BCG in vitro. *Tuberculosis* **2009**, *89* (4), 325.
- (267) Mosaiab, T.; Boiteux, S.; Zulfiker, A. H. M.; Wei, M. Q.; Kiefel, M. J.; Houston, T. A. A Simple glycolipid mimic of the phosphatidylinositol mannoside core from *Mycobacterium tuberculosis* inhibits macrophage cytokine production. *Chembiochem* **2018**, *19* (14), 1476.
- (268) Pumerantz, A.; Muppidi, K.; Agnihotri, S.; Guerra, C.; Venketaraman, V.; Wang, J.; Betageri, G. Preparation of liposomal vancomycin and intracellular killing of methicillin-resistant *Staphylococcus aureus* (MRSA). *International Journal of Antimicrobial Agents* **2011**, *37* (2), 140.
- (269) Drulis-Kawa, Z.; Gubernator, J.; Dorotkiewicz-Jach, A.; Doroszkiewicz, W.; Kozubek, A. In vitro antimicrobial activity of liposomal meropenem against

- Pseudomonas aeruginosa* strains. *International Journal of Pharmaceutics* **2006**, 315 (1-2), 59.
- (270) Davidsen, J.; Rosenkrands, I.; Christensen, D.; Vangala, A.; Kirby, D.; Perrie, Y.; Agger, E. M.; Andersen, P. Characterization of cationic liposomes based on dimethyldioctadecylammonium and synthetic cord factor from *M. tuberculosis* (trehalose 6,6'-dibehenate)-a novel adjuvant inducing both strong CMI and antibody responses. *Biochimica et Biophysica Acta* **2005**, 1718 (1-2), 22.
- (271) Gubernator, J.; Drulis-Kawa, Z.; Kozubek, A. A simple and sensitive fluorometric method for determination of gentamicin in liposomal suspensions. *International Journal of Pharmaceutics* **2006**, 327 (1), 104.
- (272) Kaale, E.; Govaerts, C.; Hoogmartens, J.; Schepdael, A. V. Mass spectrometric study to characterize thioisoindole derivatives of aminoglycoside antibiotics. *Rapid Communications in Mass Spectrometry* **2005**, 19 (20), 2918.
- (273) Zulfiker, A. H. M.; Hashimi, S. M.; Qi, J.; Grice, I. D.; Wei, M. Q. Aqueous and Ethanol Extracts of Australian Cane Toad Skins Suppress Pro-Inflammatory Cytokine Secretion in U937 Cells via NF- κ B Signaling Pathway. *Journal of Cellular Biochemistry* **2016**, 117 (12), 2769.
- (274) Prior, S.; Gander, B.; Lecaroz, C.; Irache, J. M.; Gamazo, C. Gentamicin-loaded microspheres for reducing the intracellular *Brucella abortus* load in infected monocytes. *Journal of Antimicrobial Chemotherapy* **2004**, 53 (6), 981.
- (275) Korsholm, K. S.; Agger, E. M.; Foged, C.; Christensen, D.; Dietrich, J.; Andersen, C. S.; Geisler, C.; Andersen, P. The adjuvant mechanism of cationic dimethyldioctadecylammonium liposomes. *Immunology* **2007**, 121 (2), 216.
- (276) Karlsen, K.; Korsholm, K. S.; Mortensen, R.; Ghiasi, S. M.; Andersen, P.; Foged, C.; Christensen, D. A stable nanoparticulate DDA/MMG formulation acts synergistically with CpG ODN 1826 to enhance the CD4(+) T-cell response. *Nanomedicine (London, England)* **2014**, 9 (17), 2625.
- (277) Korsholm, K. S.; Hansen, J.; Karlsen, K.; Filskov, J.; Mikkelsen, M.; Lindenstrom, T.; Schmidt, S. T.; Andersen, P.; Christensen, D. Induction of CD8+ T-cell responses against subunit antigens by the novel cationic liposomal CAF09 adjuvant. *Vaccine* **2014**, 32 (31), 3927.

- (278) He, X.-Y.; Liu, B.-Y.; Wu, J.-L.; Ai, S.-L.; Zhuo, R.-X.; Cheng, S.-X. A Dual Macrophage Targeting Nanovector for Delivery of Oligodeoxynucleotides To Overcome Cancer-Associated Immunosuppression. *ACS Applied Materials and Interfaces* **2017**, *9* (49), 42566.
- (279) Jiang, H.-L.; Kang, M. L.; Quan, J.-S.; Kang, S. G.; Akaike, T.; Yoo, H. S.; Cho, C.-S. The potential of mannosylated chitosan microspheres to target macrophage mannose receptors in an adjuvant-delivery system for intranasal immunization. *Biomaterials* **2008**, *29* (12), 1931.
- (280) Sun, H.-K.; Pang, A.; Farr, D. C.; Mosaiab, T.; Britton, W. J.; Anoopkumar-Dukie, S.; Grice, I. D.; Kiefel, M. J.; West, N. P.; Grant, G. D. et al. Thioamide derivative of the potent antitubercular 2-(Decylsulfonyl)acetamide is less active against *Mycobacterium tuberculosis*, but a more potent antistaphylococcal agent. *Australian Journal of Chemistry* **2018**, *71* (9), 716.
- (281) Imbuluzqueta, E.; Lemaire, S.; Gamazo, C.; Elizondo, E.; Ventosa, N.; Veciana, J.; Van Bambeke, F.; Blanco-Prieto, M. J. Cellular pharmacokinetics and intracellular activity against *Listeria monocytogenes* and *Staphylococcus aureus* of chemically modified and nanoencapsulated gentamicin. *Journal of Antimicrobial Chemotherapy* **2012**, *67* (9), 2158.
- (282) Yang, T.-C.; Chou, C.-C.; Li, C.-F. Preparation, water solubility and rheological property of the N-alkylated mono or disaccharide chitosan derivatives. *Food Research International* **2002**, *35* (8), 707.
- (283) Chachuli, S. H. M.; Nawaz, A.; Shah, K.; Naharudin, I.; Wong, T. W. In Vitro Investigation of Influences of Chitosan Nanoparticles on Fluorescein Permeation into Alveolar Macrophages. *Pharmaceutical research* **2016**, *33* (6), 1497.
- (284) Dai, T.; Zhou, S.; Yin, C.; Li, S.; Cao, W.; Liu, W.; Sun, K.; Dou, H.; Cao, Y.; Zhou, G. Dextran-based fluorescent nanoprobe for sentinel lymph node mapping. *Biomaterials* **2014**, *35* (28), 8227.
- (285) Zhao, L.; Zhu, B.; Jia, Y.; Hou, W.; Su, C. Preparation of biocompatible carboxymethyl chitosan nanoparticles for delivery of antibiotic drug. *BioMed Research International* **2013**, 2013.

- (286) Silva, N. C.; Silva, S.; Sarmiento, B.; Pintado, M. Chitosan nanoparticles for daptomycin delivery in ocular treatment of bacterial endophthalmitis. *Drug Delivery* **2013**, *0* (0), 1.
- (287) Danielsen, E. T.; Danielsen, E. M. Glycol chitosan: A stabilizer of lipid rafts in the intestinal brush border. *Biochimica et Biophysica Acta (BBA) - Biomembranes* **2017**, *1859* (3), 360.
- (288) Park, H.; Choi, B.; Hu, J.; Lee, M. Injectable chitosan hyaluronic acid hydrogels for cartilage tissue engineering. *Acta Biomaterialia* **2013**, *9* (1), 4779.
- (289) De Giglio, E.; Trapani, A.; Cafagna, D.; Ferretti, C.; Iatta, R.; Cometa, S.; Ceci, E.; Romanelli, A.; Mattioli-Belmonte, M. Ciprofloxacin-loaded chitosan nanoparticles as titanium coatings: a valuable strategy to prevent implant-associated infections. *Nano Biomedicine and Engineering* **2012**, *4*, 157.
- (290) Masotti, A.; Ortaggi, G. Chitosan micro- and nanospheres: fabrication and applications for drug and DNA delivery. *Mini Reviews in Medicinal Chemistry* **2009**, *9* (4), 463.
- (291) Morrow, B. H.; Payne, G. F.; Shen, J. pH-Responsive self-assembly of polysaccharide through a rugged energy landscape. *Journal of the American Chemical Society* **2015**, *137* (40), 13024.
- (292) Lee, W.-H.; Loo, C.-Y.; Traini, D.; Young, P. M. Nano- and micro-based inhaled drug delivery systems for targeting alveolar macrophages. *Expert Opinon on Drug Deilivery* **2015**, *12* (6), 1009.
- (293) Donati, I.; Stredanska, S.; Silvestrini, G.; Vetere, A.; Marcon, P.; Marsich, E.; Mozetic, P.; Gamini, A.; Paoletti, S.; Vittur, F. The aggregation of pig articular chondrocyte and synthesis of extracellular matrix by a lactose-modified chitosan. *Biomaterials* **2005**, *26* (9), 987.
- (294) Marcon, P.; Marsich, E.; Vetere, A.; Mozetic, P.; Campa, C.; Donati, I.; Vittur, F.; Gamini, A.; Paoletti, S. The role of Galectin-1 in the interaction between chondrocytes and a lactose-modified chitosan. *Biomaterials* **2005**, *26* (24), 4975.
- (295) Yao, W.; Peng, Y.; Du, M.; Luo, J.; Zong, L. Preventative vaccine-loaded mannosylated chitosan nanoparticles intended for nasal mucosal delivery enhance immune responses and potent tumor immunity. *Molecular Pharmaceutics* **2013**, *10* (8), 2904.

- (296) Ting, S. R. S.; Min, E. H.; Escalé, P.; Save, M.; Billon, L.; Stenzel, M. H. Lectin recognizable biomaterials synthesized via nitroxide-mediated polymerization of a methacryloyl galactose monomer. *Macromolecules* **2009**, *42* (24), 9422.
- (297) Shang, Y.; Tamai, M.; Ishii, R.; Nagaoka, N.; Yoshida, Y.; Ogasawara, M.; Yang, J.; Tagawa, Y. Hybrid sponge comprised of galactosylated chitosan and hyaluronic acid mediates the co-culture of hepatocytes and endothelial cells. *Journal of Bioscience and Bioengineering* **2014**, *117* (1), 99.
- (298) Öberg, C. T.; Carlsson, S.; Fillion, E.; Leffler, H.; Nilsson, U. J. Efficient and expedient two-step pyranose-retaining fluorescein conjugation of complex reducing oligosaccharides: galectin oligosaccharide specificity studies in a fluorescence polarization assay. *Bioconjugate Chemistry* **2003**, *14* (6), 1289.
- (299) Page, D.; Roy, R. Optimizing lectin-carbohydrate interactions: improved binding of divalent α -mannosylated ligands towards Concanavalin A. *Glycoconjugate Journal* **1997**, *14* (3), 345.
- (300) Ichikawa, S.; Tatebayashi, N.; Matsuda, A. Synthesis of C-Glycosyl Pyrrolo[3,4-c]carbazole-1,3(2H,6H)-diones as a Scaffold for Check Point Kinase 1 Inhibitors. *The Journal of Organic Chemistry* **2013**, *78* (23), 12065.
- (301) Hauck, D.; Joachim, I.; Frommeyer, B.; Varrot, A.; Philipp, B.; Moller, H. M.; Imberty, A.; Exner, T. E.; Titz, A. Discovery of two classes of potent glycomimetic inhibitors of *Pseudomonas aeruginosa* LecB with distinct binding modes. *ACS Chemical Biology* **2013**, *8* (8), 1775.
- (302) Lin, W.; Zhang, X.; He, Z.; Jin, Y.; Gong, L.; Mi, A. Reduction of azides to amines or amides with zinc and ammonium chloride as reducing agent. *Synthetic Communications* **2002**, *32* (21), 3279.
- (303) Madge, P. D.; Maggioni, A.; Pascolutti, M.; Amin, M.; Waespy, M.; Bellette, B.; Thomson, R. J.; Kelm, S.; von Itzstein, M.; Haselhorst, T. Structural characterisation of high affinity Siglec-2 (CD22) ligands in complex with whole Burkitt's lymphoma (BL) Daudi cells by NMR spectroscopy. *Scientific Reports* **2016**, *6*, 36012.
- (304) Abouelmagd, S. A.; Ku, Y. J.; Yeo, Y. Low molecular weight chitosan-coated polymeric nanoparticles for sustained and pH-sensitive delivery of paclitaxel. *Journal of Drug Targets* **2015**, *23* (7-8), 725.

- (305) Amoozgar, Z.; Park, J.; Lin, Q.; Yeo, Y. Low Molecular-Weight Chitosan as a pH-Sensitive Stealth Coating for Tumor-Specific Drug Delivery. *Molecular Pharmaceutics* **2012**, *9* (5), 1262.
- (306) Sosnik, A.; Imperiale, J. C.; Vázquez-González, B.; Raskin, M. M.; Muñoz-Muñoz, F.; Burillo, G.; Cedillo, G.; Bucio, E. Mucoadhesive thermo-responsive chitosan-g-poly(N-isopropylacrylamide) polymeric micelles via a one-pot gamma-radiation-assisted pathway. *Colloids and Surfaces B: Biointerfaces* **2015**, *136*, 900.
- (307) Holme, K. R.; Hall, L. D. Preparation and characterization of N-[2-(glycosyloxy)-ethyl]chitosan derivatives. *Carbohydrate Research* **1992**, *225* (2), 291.
- (308) Quader, S.; Boyd, S. E.; Jenkins, I. D.; Houston, T. A. Multisite modification of neomycin B: Combined Mitsunobu and click chemistry approach. *Journal of Organic Chemistry* **2007**, *72* (6), 1962.
- (309) Lavertu, M.; Xia, Z.; Serreqi, A. N.; Berrada, M.; Rodrigues, A.; Wang, D.; Buschmann, M. D.; Gupta, A. A validated ¹H NMR method for the determination of the degree of deacetylation of chitosan. *Journal of Pharmaceutical and Biomedical Analysis* **2003**, *32* (6), 1149.
- (310) D'Amelio, N.; Esteban, C.; Coslovi, A.; Feruglio, L.; Uggeri, F.; Villegas, M.; Benegas, J.; Paoletti, S.; Donati, I. Insight into the molecular properties of Chitlac, a chitosan derivative for tissue engineering. *The Journal of Physical Chemistry. B* **2013**, *117* (43), 13578.
- (311) Li, X.; Wu, P.; Cheng, S.; Lv, X. Synthesis and Assessment of Globotriose–Chitosan Conjugate, a Novel Inhibitor of Shiga Toxins Produced by *Escherichia coli*. *Journal of Medicinal Chemistry* **2012**, *55* (6), 2702.
- (312) Wang, X.; Chen, Y.; Dahmani, F. Z.; Yin, L.; Zhou, J.; Yao, J. Amphiphilic carboxymethyl chitosan-quercetin conjugate with P-gp inhibitory properties for oral delivery of paclitaxel. *Biomaterials* **2014**, *35* (26), 7654.
- (313) Zhou, J.; Butchosa, N.; Jayawardena, H. S. N.; Zhou, Q.; Yan, M.; Ramström, O. Glycan-Functionalized Fluorescent Chitin Nanocrystals for Biorecognition Applications. *Bioconjugate Chemistry* **2014**, *25* (4), 640.

- (314) Khan, W.; Kumar, N. Drug targeting to macrophages using paromomycin-loaded albumin microspheres for treatment of visceral leishmaniasis: an in vitro evaluation. *Journal of Drug Targets* **2011**, *19* (4), 239.
- (315) des Rieux, A.; Fievez, V.; Théate, I.; Mast, J.; Pr at, V.; Schneider, Y.-J. An improved in vitro model of human intestinal follicle-associated epithelium to study nanoparticle transport by M cells. *European Journal of Pharmaceutical Sciences* **2007**, *30* (5), 380.
- (316) Ramasamy, T.; Tran, T.; Cho, H.; Kim, J.; Kim, Y.; Jeon, J.; Choi, H.-G.; Yong, C.; Kim, J. Chitosan-Based Polyelectrolyte Complexes as Potential Nanoparticulate Carriers: Physicochemical and Biological Characterization. *Pharmaceutical Research* **2014**, *31* (5), 1302.
- (317) Gao, Y.; Wang, Z.-Y.; Zhang, J.; Zhang, Y.; Huo, H.; Wang, T.; Jiang, T.; Wang, S. RVG-Peptide-Linked Trimethylated Chitosan for Delivery of siRNA to the Brain. *Biomacromolecules* **2014**, *15* (3), 1010.
- (318) Wang, X.; Yang, C.; Zhang, Y.; Zhen, X.; Wu, W.; Jiang, X. Delivery of platinum(IV) drug to subcutaneous tumor and lung metastasis using bradykinin-potentiating peptide-decorated chitosan nanoparticles. *Biomaterials* **2014**, *35* (24), 6439.
- (319) Chen, M. S.; Wu, J. L.; Zhou, L. Z.; Jin, C. Y.; Tu, C. L.; Zhu, B. S.; Wu, F. A.; Zhu, Q.; Zhu, X. Y.; Yan, D. Y. Hyperbranched glycoconjugated polymer from natural small molecule kanamycin as a safe and efficient gene vector. *Polymer Chemistry-Uk* **2011**, *2* (11), 2674.
- (320) He, X.; Shu, J.; Xu, L.; Lu, C.; Lu, A. Inhibitory effect of Astragalus polysaccharides on lipopolysaccharide-induced TNF- α and IL-1 β production in THP-1 cells. *Molecules* **2012**, *17* (3), 3155.
- (321) Wu, N.; Wen, Z. S.; Xiang, X. W.; Huang, Y. N.; Gao, Y.; Qu, Y. L. Immunostimulative Activity of Low Molecular Weight Chitosans in RAW264.7 Macrophages. *Marine Drugs* **2015**, *13* (10), 6210.
- (322) Zheng, B.; Wen, Z. S.; Huang, Y. J.; Xia, M. S.; Xiang, X. W.; Qu, Y. L. Molecular Weight-Dependent Immunostimulative Activity of Low Molecular Weight Chitosan via Regulating NF- κ B and AP-1 Signaling Pathways in RAW264.7 Macrophages. *Marine Drugs* **2016**, *14* (9).

- (323) Qi, L.; Xu, Z.; Jiang, X.; Hu, C.; Zou, X. Preparation and antibacterial activity of chitosan nanoparticles. *Carbohydrate Research* **2004**, 339 (16), 2693.
- (324) No, H. K.; Young Park, N.; Ho Lee, S.; Meyers, S. P. Antibacterial activity of chitosans and chitosan oligomers with different molecular weights. *International Journal of Food Microbiology* **2002**, 74 (1), 65.

Appendices

